Experimental Investigation of the Effects of Hydrogen Addition on the Dynamics of Turbulent Premixed Flames

Taaha Hussain

Submitted in partial fulfilment of the requirements for the degree of
Doctor of Philosophy

Department of Mechanical Engineering
University College London

November 2014

I, Taaha Hussain confirm that the work presented in this thesis is my own. Where information has been derived from other sources, I confirm that this has been indicated in the thesis.

Abstract

With an ever increasing need for the reduction of carbon and nitrogen based emissions, gas turbine technology has evolved over the years. Lean burning (i.e. high air to fuel ratio) has proven to be an effective method in reducing the nitrous oxide emissions. However, these flames are susceptible to combustion oscillations that could lead to excessive heat transfer, oscillatory thermal and mechanical stresses and flame blow-off or flashback.

The addition of hydrogen fuel to turbulent flames has been studied in the past and been reported to have reduced combustion oscillations and nitrous oxide formation, however, there are studies in literature that show combustion oscillations triggered by the addition of hydrogen. This project aimed to further investigate the effects of local hydrogen addition on the dynamics of turbulent lean premixed flames in a model gas turbine combustor. The flames were subjected to controlled reactant mass flow oscillations (created by acoustic speakers) that led to flame surface roll-up, thus causing heat release perturbations (i.e. combustion oscillations). Under these conditions hydrogen fuel was locally added into the flow to study the effects on the response of the flame.

A secondary objective was to develop a laser technique for imaging the laser induced fluorescence of atomic hydrogen in turbulent flames. While earlier studies had only focused on laminar flames, this project concentrated on imaging large sections of turbulent premixed flames which were subjected to acoustic forcing.

The results showed that the local addition of hydrogen reduced the heat release oscillations of the flame under certain operating conditions. The change in the response of the flame was due to the alteration of the flame surface area. While there were benefits of reducing heat release oscillations, the addition of hydrogen to the flame had a negative impact on the nitrous oxide exhaust emissions.

Table of Contents

List of Figures

List of Tables

Nomenclature

Variables:

ϕ – Equivalence ratio

U – Velocity

$u'(f)$ – Magnitude of velocity fluctuation at harmonic frequency f

$u'(f)/\langle U \rangle$ – Normalised velocity fluctuation at harmonic frequency f

Q – Heat release

$Q(f)'$ – Magnitude of heat release fluctuation at harmonic frequency f

$Q(f)'/\langle Q \rangle$ – Normalised heat release fluctuation at harmonic frequency f

S_L – Laminar flame speed

FS – Flame surface area

$FS'/\langle FS \rangle$ – Normalised flame surface area fluctuation

FDF – Flame describing function

PSD – Power spectral density

Subscripts:

A – Measurement in region A

B – Measurement in region B

C – Measurement in region C

Radicals/Molecules:

H – Atomic hydrogen

OH – Hydroxyl

H_2 – Hydrogen

CH_4 – Methane

C_2H_4 – Ethylene

N_2 – Nitrogen

NO_x – Nitrogen oxides

CO_2 – Carbon dioxide

Units:

slpm – Standard litres per minute

nlpm – Normal litres per minute

nm – Nanometres

s – Seconds

S/s – Samples per second

Hz – Hertz

V – Volts

W – Watts

Acknowledgements

The completion of this PhD project would not have been possible without the guidance and encouragement of many people. I would like to express my sincere gratitude to everyone who contributed to the success of this project.

I would like to express my appreciation and thanks to my supervisor Dr Ramanarayanan Balachandran, who has always encouraged my research and allowed me to grow as a researcher. There have been times where we have had a difference of opinion; however, this has all led to insightful discussions and above all a rewarding experience as a research student. I would also like to thank Professor Ian Eames, Professor Nicos Ladomatos, Dr Pavlos Aleiferis and Professor Epaminondas Mastorakos for giving constructive comments and suggestions on the experiments and data.

A thank you to the workshop technicians, Richard, Barry and Neil for helping me constructing the experimental lab; from the welding, to the drilling, to the discussion on the complex designs of the combustion rig. I would like to acknowledge their hard work in making the combustion testing cell a reality. Support from the administrative department, in particular, Charlotte and Gill, was really appreciated and I have enjoyed my times talking to them.

A special thank you to all my lab buddies, Aadil, Mart, Midhat, Baptiste, Priyesh, Elena, Aaron and Anne, for the invaluable support during the development of the testing cell and the writing of the thesis. The completion of the project would not have been possible without the support from these colleagues during experimentation and data analysis. Their insightful and humorous discussions over lunch and chocolate walnut brownies were the best breaks from all the hardships faced down in the laboratory.

During the research project I made quite a few friends in the Dept. of Mechanical Engineering, who have always been there for me for constant

encouragement and support. I would like to thank Isabel, Prasun, Anh, Daniel, Chris, Hollie, Giovi, Sandra, Enea, Echo, Julianah, Ewa, Arien, Salwa and Omar for all the great experiences over the years. From listening to my rants about the PhD project to taking trips to Croatia and Amsterdam which kept me refreshed and energised.

Words cannot express how grateful I am to my mother and father (Mrs. Nafisa Hussain and Dr. Imran Hussain) for all of their sacrifices that they have made on my behalf and their endless love and support. I would like to thank my sister, Sarah, and my brother and sister-in-law, Yahya and Harwa, for all their words of encouragement. I would also like to thank my dear Sakina for her love and kindness. Her support during the writing process was awesome (everything is awesome!), as she always motivated me to strive towards my goal.

Finally, I would like to thank the Department of Mechanical Engineering and the Engineering and Physical Sciences Research Council (EPSRC) for the financial support over the years. Without the financial support the research would not have been possible.

Chapter 1: Introduction

1.1 Background

Advances in combustion are essential for developing gas turbine engines for propulsion and power generation with increased fuel economy and low emissions. Lean burning has proven to be an effective method in drastically reducing the emissions of nitrous oxides (NO_x) in many industrial applications (Smith *et al.* 1986, Keller *et al.* 1994, and Schlegel *et al.* 1996). However, these lean burn systems are susceptible to thermo-acoustic instabilities, commonly known as combustion instabilities (Lu 2005). These phenomena occur in many practical systems such as gas turbines, rocket motors, heating systems and industrial furnaces. The occurrence of such instabilities is problematic because large amplitudes of pressure and velocity fluctuations result in severe vibrations of the combustor walls, excessive heat transfer and thermal stresses to the combustor walls, oscillatory mechanical loads and flame blow-off or flashback. This causes component wear which could lead to deterioration in the engine performance and may cause unacceptable noise levels (Putnam 1971, Blomshield 2001). Structural vibration, when coupled with excessive heat transfer to the chamber, could lead to complete failure of the system. Consequently, significant amount of research has been carried out to understand the processes responsible for the excitation of these instabilities. Although extensive research in this field has been carried out for decades, the prediction and control of instabilities has been proven to be a great challenge. This introductory chapter will give an overview of the causes and characteristics of combustion instabilities.

Combustion stability can be characterised as either static or dynamic (Candel 2002, Bompelly *et al.* 2009). Static stability addresses the phenomena of flame flashback and blow-off, for combustors operating at the lean flammability limit (i.e. the lowest equivalence ratio possible for ignition). Dynamic or thermo-acoustic instability is generally referred to large amplitude pressure oscillations in a chamber

where unsteady combustion takes place. These instabilities are spontaneous and self-excited through a feedback loop between the oscillatory combustion and one or more of the natural acoustic modes of the combustor. This is caused by complex interactions between the flow field, acoustics and heat release fluctuations within the combustion chamber. The large number of mechanisms involved in exciting combustion oscillations, (i.e. turbulence, acoustics, chemical kinetics, vibrations) make it extremely difficult to systematically predict the onset of instability of a particular system (Lu 2005). Although the mechanisms may be extremely complex, the essential processes responsible for initiating combustion instabilities are quite simple. An unsteady combustion process (i.e. unsteady heat release) produces sound. The sound generated would simply radiate away in an open field, however, in an enclosed region (i.e. combustor) the sound could be reflected back from the combustor walls allowing the reflected waves to interact with the combustion process.

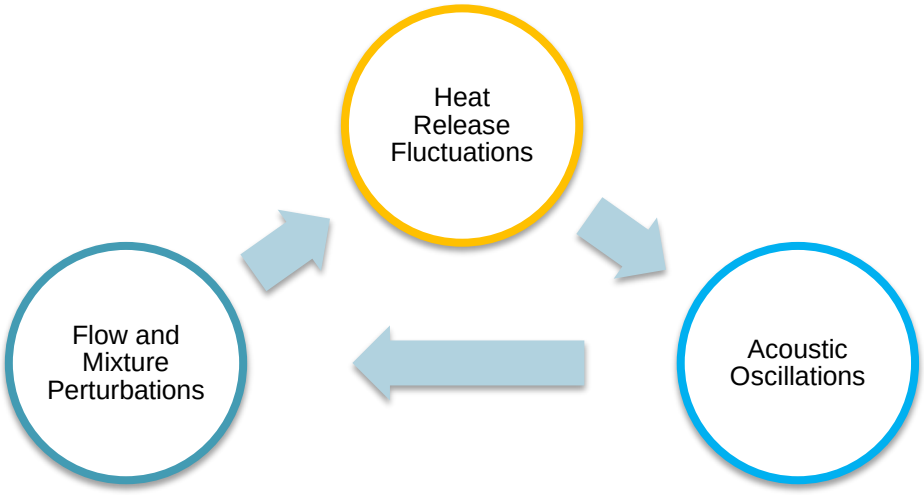

Figure 1.1: Visual representation of the feedback loop responsible for combustion instability. (Adapted from Lu 2005)

The reflected waves can alter the heat release rate either by triggering instability waves in the flame shear layer (Lieuewen 1999), which usually stabilise the flames, causing flame roll-up on the shear layer causing variations in the flame surface; or these waves can travel further upstream through the combustor walls to the air and fuel lines causing fluctuations in the fuel/air mixing, thus affecting the

heat release. These heat release variations in turn affect the acoustics within the chamber thus repeating the process and creating a closed feedback cycle.

The feedback loop for combustion instability can be described by the sequence pictured in Figure 1.1. Initially the presence of mixture and flow inhomogeneity produces an unsteady heat release pulse, creating acoustic waves within the chamber that feed back to the air and fuel lines through the natural modes of the combustor, affecting the local flow and mixture properties (Lu 2005).

The interaction between the acoustic modes of the combustor and the heat release fluctuations can add or remove energy from the acoustic modes. The condition under which heat release fluctuations could amplify the pressure oscillations was first stated by Rayleigh and Strutt (1896):

"If heat be periodically communicated to, and abstracted from, a mass of air vibrating (for example) in a cylinder bounded by a piston, the effect produced will depend upon the phase of the vibration at which the transfer of heat takes place."

The work by Rayleigh described the conditions under which the unsteady heat release added energy to the acoustic field. The statement was first expressed in a mathematical form by Putnam and Dennis (1953) and has now come to be known as Rayleigh's criterion and is defined by the integral below:

$$\int_0^V \int_0^T p(x,t)Q(x,t)dt\,dV \geq \int_0^V \int_0^T \sum_i L_i(x,t)dt\,dV$$

where p is the pressure, Q is the heat release, x is the location, L_i is the acoustic energy lost from the combustor boundaries, T is the period of oscillations, t is the time, and V is the volume including all sections of the system where relevant process occur that affect the growth or decay of the oscillations. The sign of the left hand side (LHS) integral represents the phase difference between the heat release and pressure oscillations. The integral on the right hand side (RHS) represents the cumulative loss of acoustic energy from the system through different processes such as viscous dissipation, radiation and convection of acoustic energy and heat transfer. If the LHS integral is positive, the phase difference between the periodic heat release and pressure oscillations is less than 90° which would cause the

amplification of the pressure oscillations by heat addition, however, if the phase difference is greater than 90°, hence the integral has a negative sign, an attenuation of the pressure oscillations is observed. The difficulty in using this criterion is that the pressure and unsteady heat release are dependent on each other, and the heat release is often part of the solution. However, with experimental data, empirical relationships between the heat and acoustic fluctuations can be extrapolated.

In essence, the growth of combustion instabilities occurs when the energy supplied to the acoustic mode is larger than the energy lost due to damping mechanisms. As the amplitude of the oscillations increases the energy added in and lost per cycle becomes amplitude dependent and the energy lost per cycle rises causing the amplitude of oscillations to increase at a decreasing rate until the equality in Rayleigh's criterion is satisfied. At this point where the energy added to the acoustic field is equal to the energy lost, the magnitude of the oscillations reach a limit-cycle amplitude where there is no further increase in amplitude.

After the discovery of this phenomenon there have been numerous studies on the mechanisms responsible for instabilities and the events occurring due to instabilities. With a wide contribution from several researchers (Schimmer and Vortmeter 1977, Keller *et al.* 1981, Poinsot *et al.* 1987, Bloxsidge *et al.* 1988, Langhorne 1988, Yu *et al.* 1991, Schadow and Gutmark 1992, Lieuwen and Zinn 1998, Bradley *et al.* 1998, Wu *et al.* 2001, Candel 2002, Kulsheimer and Buchner 2002, Balachandran *et al.* 2005, and Cho and Lieuwen 2005) over the years there has been some light shed on the nature and behaviour of unstable flames. All these studies have supported the theory of interactions between the flame and the acoustic mode of the system. Thus, in order to understand the response of flames, it is now generally an accepted rule and a common practice that the analysis of the pressure/velocity and heat release fluctuations within the combustion chamber is carried out. In the following section the combustion dynamics and mechanisms related to combustion oscillations and its amplification/dampening are discussed.

1.2 Combustion theory and literature review

1.2.1 Combustion oscillations

The physical effects and processes that lead to combustion oscillations are numerous, vary in complexity and are difficult to trace. There are several ways in which heat release oscillations may occur due to the parameters of the flame being perturbed (Schimmer and Vortmeter 1977):

i. Oscillatory mass flow of reactants,
ii. Oscillatory mixture/equivalence ratio,
iii. Periodic vortex shedding, generation of turbulence,
iv. Oscillating heat transfer to the combustor, and
v. Fluctuating change of reaction rate by adiabatic compression.

All these influences on the flame characteristics are shown diagrammatically in Figure 1.2. The geometry in this figure is only an example to show some of the mechanisms responsible for combustion oscillations. In this project the experimental work was concerned with i and ii. As discussed earlier, combustion oscillations occur due to the complex interaction between the burner's natural acoustics and the combustion characteristics such as the flow and mixture properties. Combustion oscillations are amplified through a feedback loop between the combustion processes and the acoustic oscillations. This feedback loop is dependent on the system's acoustic characteristics and the operating conditions. Due to the complex coupling between processes, both, experimental and computational studies have been carried out to understand the nature and the fundamental physics behind the driving and damping mechanisms.

1.2.1.1 Driving mechanisms

i. Oscillatory mass flow of reactants:

Mass flow fluctuations of reactants at the inlet of the combustor are caused by acoustic pressure oscillations present in the downstream duct. The fluctuation of the

reactant flow rates has a direct effect on the rate of reaction. The response of premixed flat flames to imposed axial oscillations was studied experimentally and theoretically by Sankar *et al.* (1990) and, Schimmer and Vortmeter (1977). From both the studies it was theoretically noted that if a sound wave was imposed, the flow velocity would increase and decrease periodically with time. As a consequence the flame surface would be displaced upwards or downwards relative to its stable position. However, Schimmer and Vortmeter (1977) suggested that there was no direct relation between the oscillatory heat release caused and the oscillating displacement of the flame surface. If the flame was far away from the burner walls preventing heat transfer away from the flame then there would be no oscillatory change in the reaction rates and hence no change in the heat release rate. However, in an enclosed system the oscillatory change in the position of the flame changes the heat transferred periodically to the system walls, which in turn affects the flame speed, which also has an effect on the flame position, hence, modulating the heat release rate.

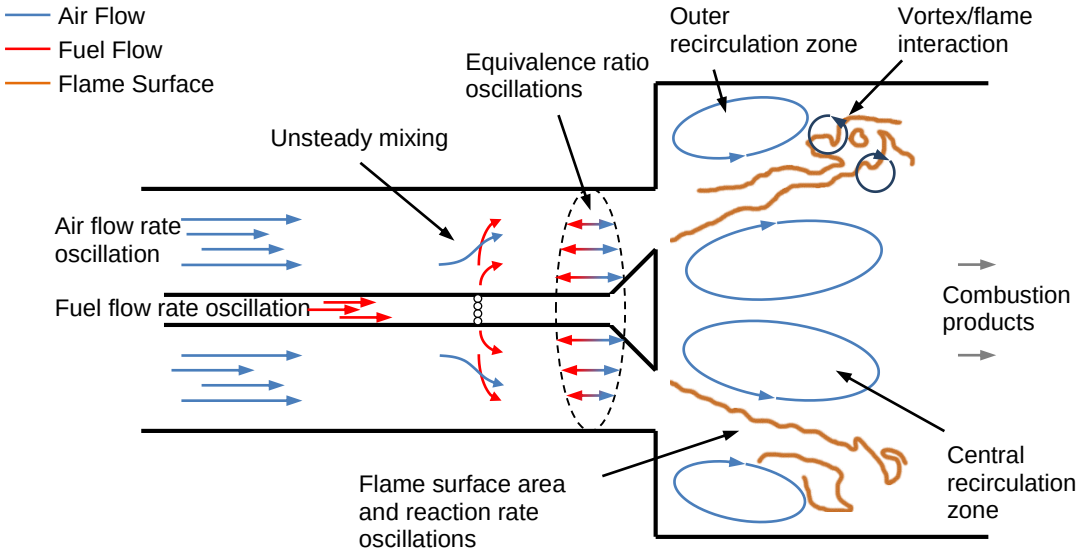

Figure 1.2: Flow and flame processes that cause combustion oscillations in gas turbine combustors. (Adapted from Turns 2006)

The varying reaction rate and the oscillatory velocity of the combustible mixture caused the oscillatory movement of the flame at the burner surface in the

work by Sankar *et al.* (1990). The resulting fluctuation in the production of the exhaust gases causes a fluctuation in the static pressure within the chamber. The periodic expansion of gases within the flame generated velocity perturbations downstream of the flame region. The velocity measurements showed that the perturbations could either be dampened or driven by different local expansion processes in the chamber.

Baillot *et al.* (1992) investigated the response of laminar conical flames subjected to velocity fluctuations at low frequencies. The experimental results were compared to numerical predictions and were in good agreement. It was concluded that the deformation of the flame surface was due to the progressive waves originating at the base and propagating along the flow to the flame front. These conclusions were reinforced with the study by Schuller *et al.* (2002) where it was also suggested that the pressure signal was directly proportional to the flame surface area variation (hence directly proportional to the velocity perturbations).

ii. Oscillatory mixture/equivalence ratio:

Combustor pressure perturbations can propagate to the air and fuel lines modulating the mass flow of reactants and the mixing processes. The heat release rate oscillations experienced at the flame front as a result of the equivalence ratio perturbation could further amplify the combustion oscillations if Rayleigh's criterion is satisfied. Using Figure 1.3 the effect of an oscillatory equivalence ratio at the flame front on the heat release rate can be described (Candel 2002). If, for any reason, the flame produces a cyclic pressure variation the pressure waves can propagate upstream to the fuel lines with a time delay τ_i, causing a cyclic variation of the inlet flow of reactants. Looking at the figure, a positive pressure increase in the combustion zone causes a decrease of the fuel mass flow rate due to the change in the pressure gradient at the exit of the fuel injector. The fall in the amount of reactants entering the flow causes a negative perturbation in the equivalence ratio. This inhomogeneous mixture is convected downstream to the flame zone over a time period, τ_{conv}. The reactive mixture is not consumed immediately when it reaches the flame base as it is not until it reaches the flame front that it is consumed, hence the time lag for a heat release oscillation to occur is denoted by τ_{comb}. With varying amounts of reactants the flame experiences different flame

speeds and hence different heat release rates. As mentioned before, the perturbation of the heat release, if in phase with the pressure oscillations will add energy to the acoustic field thus enhancing or sustaining the oscillatory process. According to Rayleigh's criteria, the maximum driving and sustainment of the oscillations can only be achieved when the total delay experienced is an odd multiple of the half period (Candel 2002):

$$\tau_i + \tau_{conv} + \tau_{comb} = (2n-1)\,T/2 \qquad n = 1, 2, ..$$

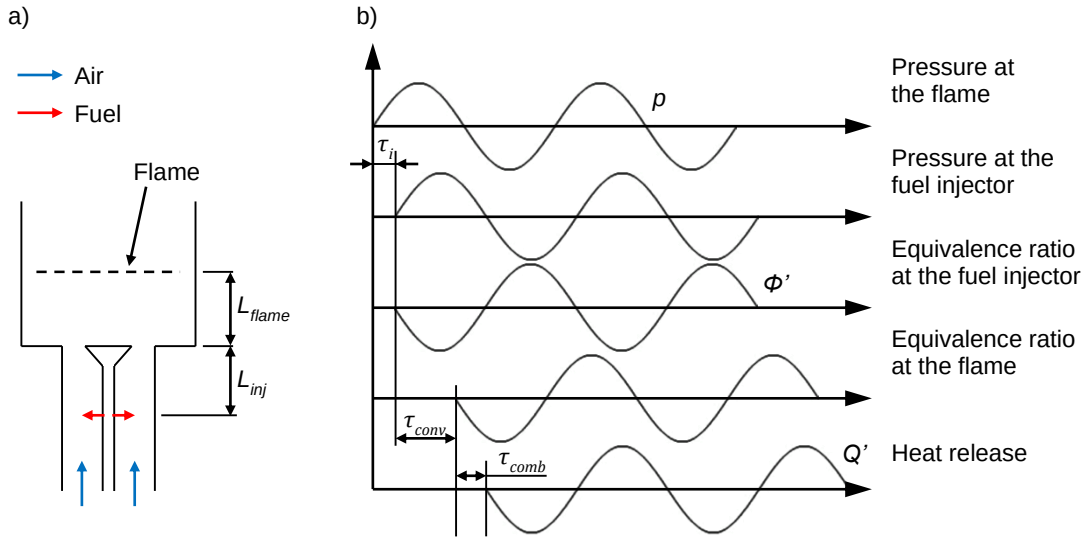

Figure 1.3: Combustion oscillations due to equivalence ratio fluctuation. (a) Commbustion chamber, and (b) the time traces of pressure, equivalence ratio at the fuel injector and flame front, and the resulting heat release fluctuation. (Adapted from Candel 2002)

The pressure oscillations generated by the fluctuating heat release could propagate upstream to the fuel lines and cause further oscillations in the fuel flow rate creating equivalence ratio perturbations; thus creating a closed feedback loop that drives the oscillations.

Cho and Lieuwen (2005) conducted a numerical investigation in to the effects of equivalence ratio oscillations on the response of laminar flames. They observed oscillating flame speeds at the flame front with varying equivalence ratios which altered the flame dynamics. The results showed that the heat release

fluctuation increased with a decrease in the mean equivalence ratio. This phenomenon can be easily understood from the graph in Figure 1.4, which shows a plot of the laminar flame speed versus the equivalence ratio, ϕ, for a laminar premixed methane flame. Experiencing the same amplitude of fluctuation in equivalence ratio at two different mean values can have different effects on the flame speed. From the graph, at a lower mean equivalence ratio the variation in the laminar flame speed is much more compared with a higher mean value. With a larger laminar flame speed variation the flame could experience a higher heat release fluctuation (for further details on the sensitivity of the flame to changes in equivalence ratio refer to Swaminathan and Bray 2011).

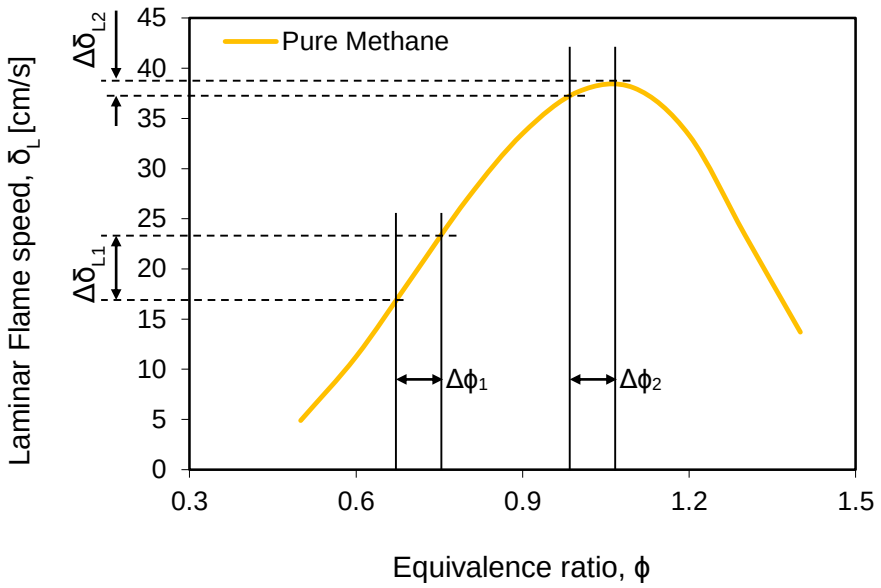

Figure 1.4: The graph shows how the magnitude of fluctuation of the laminar flame speed can vary with varying equivalence ratio, ϕ.

A similar graph was shown by Przemieniecki and Oates (1985) where the chemical reaction time for a hydrocarbon fuel was plotted against the equivalence ratio. Here, the chemical reaction time rose sharply as the equivalence ratio was reduced. Since, the chemical time is inversely proportional to the reaction rate it can be assumed that large variations of the equivalence ratio in lean conditions have a higher impact on the chemical time and hence the reaction rates. This assumption can be confirmed with the findings in the work carried out by Lieuwen *et al.* (1998)

where the flames in a well-stirred reactor experienced a high sensitivity to equivalence ratio oscillations at lean operating conditions.

In an experimental study by Lee *et al.* (2000), on the effect of fluctuating equivalence ratio on the heat release, it was apparent that the results of the equivalence ratio and heat release modulation could be compared quantitatively as there was a strong correlation between the peaks of the modulation. There was a small phase difference which was explained by the convective time between the fuel injection and the flame.

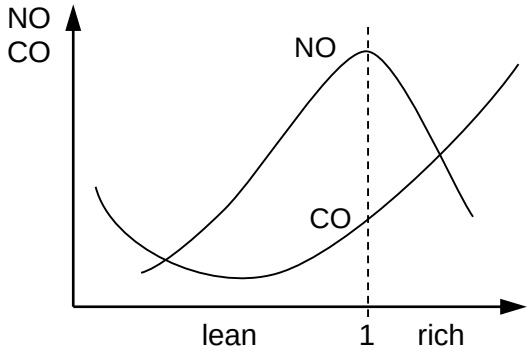

Figure 1.5: Qualitative behaviour of NO and CO vs equivalence ratio (steady-state). (Schrödinger *et al.* 2012)

In a numerical study by Schrödinger *et al.* (2012), the flame response to equivalence ratio oscillations was characterized by the CO and NO flame emissions and the heat release oscillations. The mass fraction of methane at the inflow side was oscillated periodically at varying frequencies and amplitudes. The results showed an increase in the mean values of NO and CO emissions for turbulent flames with increasing amplitudes of equivalence ratio oscillations. These results were explained by the relationship of mean emission of NO and CO to the mean equivalence ratio as shown in Figure 1.5. As the formation of NO and CO increases exponentially when moving from lean to rich mixtures, the oscillation of the equivalence ratio caused greater mean mass fractions of NO and CO.

Other studies (Lieuwen and Zinn 1998, Hathout *et al.* 2000, Birbaud *et al.* 2008, Kim *et al.* 2010, and Hemchandra 2012) came to a similar conclusion that the

heat release rate was affected by the oscillating equivalence ratio experienced at the flame boundary. The reason why it was affected was mainly due to two reasons. First, due to the varying local flame speed as a result of the changing reactant mixture fraction at the flame front, and secondly, the flame speed fluctuations cause the flame surface to wrinkle hence altering the burning area, indirectly affecting the heat release response. The authors have suggested that the fluctuating equivalence ratios could cause large amplitudes of pressure oscillations which may lead to the amplification and sustenance of combustion oscillations.

iii. Periodic vortex shedding:

Under a particular combination of amplitude and frequency of velocity fluctuations the fluid undergoes a fundamental fluid dynamical phenomenon by which the formation of ring-vortex structures appear. The importance of such structures in combustion instability was first identified by Rogers and Marble 1956. In this study high frequency oscillations were observed under “screeching” combustion excited by a transverse acoustic mode. The coupling of the combustor acoustics and the flow generated periodic formation and shedding of vortices. These vortices formed by the roll up of the shear layers between the high and low speed streams in the wake of the rearward facing step and the flame-holder (i.e. bluff-body) in combustors (Keller *et al.* 1981, Poinsot *et al.* 1987, Yu *et al.* 1991, Schadow and Gutmark 1992, Kulsheimer and Buchner 2002, and Balachandran 2005).

The high speed stream consists mainly of a combustible mixture of air and fuel entering the combustion chamber, while the low speed stream is composed of hot combustion products in recirculation zones created by the wake of the dump and flame-holder. As the vortex develops, it entrains hot products around a pocket of combustible mixture creating an interface between the two mixtures, leading to fine scale turbulence (Schadow and Gutmark 1992). Figure 1.6 shows the vortex roll-up occurring and interface between hot products and fresh reactants in a dump combustor. When the vortex reaches the wall there is a sudden breakdown of the swirling flow into small pockets of reactants mixed with hot products. With an increased area of contact between the reactants and products, the intense mixing causes the reactants to ignite, and be rapidly consumed creating a sudden heat

release. The formation and breakdown of these vortices have been identified as a key mechanism in driving combustion oscillations. The sudden heat and expansion of gases creates a pressure wave, and if Rayleigh's criterion is satisfied, it could feedback through the system to further enhance the pressure and velocity perturbations that could cause the formation of vortices at the shear layer and thus the process is repeated.

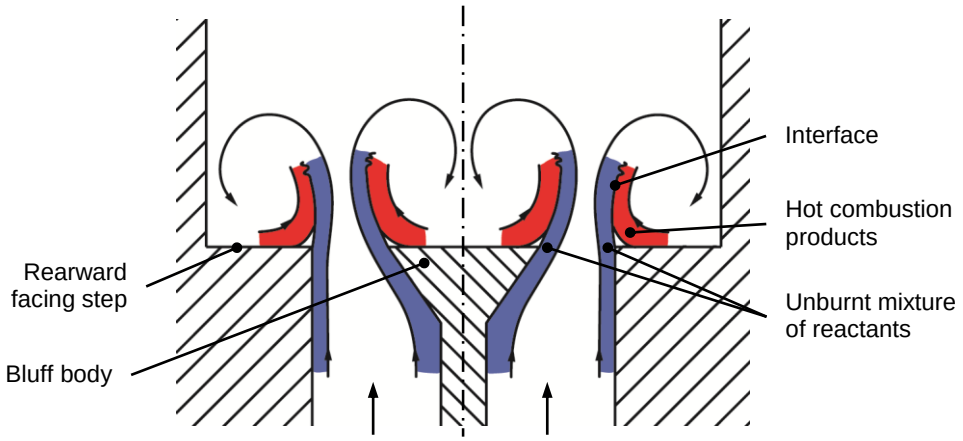

Figure 1.6: Vortex formation in the bluff body combustor. (Adapted from Schadow and Gutmark 1992)

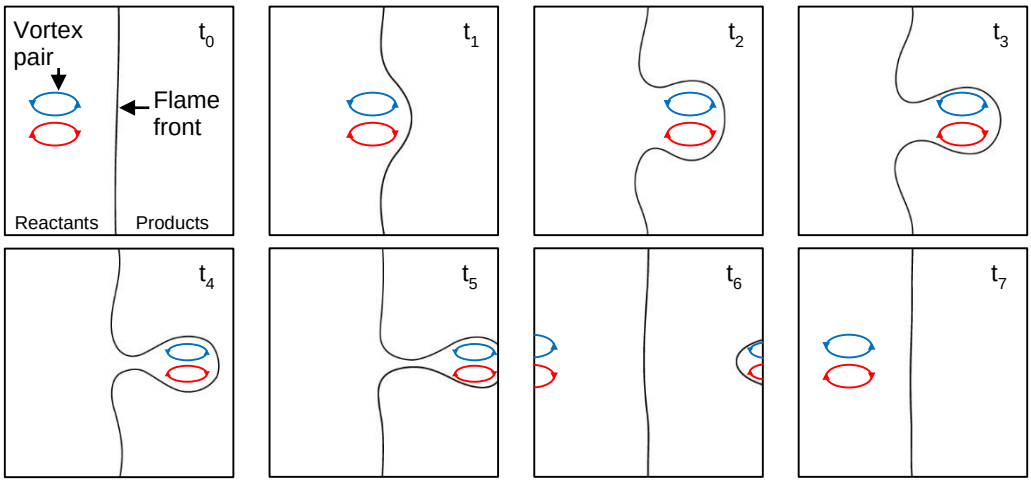

Figure 1.7: Image shows how a counter rotating vortex pair can alter the flame front as it travels through it over time.

The effects of vortex formation on combustion oscillations have been studied extensively over the years (See review Renard *et al.* 2000). From the studies by Poinsot *et al.* (1987) and Ducruix *et al.* (2003), it is evident that the appearance, convection and breakdown of the vortices have a direct impact on the heat release. The studies stated that the flame vortex interaction is one of the most important mechanisms that drives combustion instability. It was indicated that this type of mechanism had two main features; the rapid alteration of the flame front and hence the surface area due to the presence of vortices, and the other is the sudden and significant heat released during the ignition of fresh reactants as the vortex interacts with the wall.

A sketch (based on work done by Mantel and Samaniego 1999, and, Nguyen and Paul 1996) of how a counter rotating vortex pair can alter the flame front while passing through over time is shown in Figure 1.7. The sequence shows that as the vortices pass through, the locally affected flame front becomes more curved thus increasing the flame length and surface area which would have an impact on the concentration of reactants, heat transfer, burning rate and flame speed. A periodic appearance of vortices in the flow would cause the flame surface area to experience a periodic response which could affect the heat release rate.

Schlieren image results shown by Keller *et al.* (1981) and Yu *et al.* (1991) showed that the instability was mainly driven by the periodic formation and destruction of vortices. They observed the formation of vortices in the wake of the rearward facing step (also known as the dump plane) which was due to imposed velocity fluctuations at the inlet duct. A similar conclusion was presented by Schadow and Gutmark (1992) where tests were carried out between non-reacting and reacting flows. Under cold flow forced conditions the acoustics of the non-reacting vortices was low and there was no noticeable feedback between the flow and the acoustic pressure in the chamber. However, this changed when the mixture was ignited and a large cyclic heat release associated with the formation of the vortices occurred.

The PIV (particle image velocimetry) results shown in the work done by Hong *et al.* (2013), indicated that the formation of a large vortex at the edge of a step and its interaction with the flame played a significant role in the instability mechanism. The stability of the combustion process was characterised by the kinematics of the vortex, which, they suggested drove the flame surface and flow

fluctuations. They also observed instances of flow reversal during strong flow oscillations which led to upstream flame propagation (flashback) in some parts of the cycle.

The chemiluminescence, OH and H_2CO PLIF imaging results shown by Balachandran *et al.* (2005) show the non-linearity of the flame response to inlet flow velocity perturbations. The relationship between the flame chemiluminescence, flame surface density and the heat release rate were studied and it was found that the non-linearity observed was solely due to the formation of large coherent vortices which caused the variation of the flame surface by causing it to roll-up. The results showed large variations of the flame surface occurred due to flame surface destruction and the flame-wall interaction as the roll-up grew in size and travelled downstream. Broda *et al.* (1998) also noted similar results and stated that the instability mechanism stems from the significant interaction between the flow disturbances and the flame dynamics.

1.2.1.2 Damping mechanisms

Driving mechanisms of combustion oscillations are always accompanied by damping mechanisms which play an important role in determining the conditions and parameters of combustion instabilities. As mentioned earlier, with the increase in the amplitude of oscillations the energy lost per cycle also rises causing the amplitude of oscillations to increase at a decreasing rate until the equality in Rayleigh's criterion is satisfied, where the energy added to the acoustic field is equal to the energy lost, hence reaching a limit-cycle amplitude. This section provides a brief overview of the mechanisms that damp the oscillations (Lu 2005).

i. Viscous dissipation and heat transfer:

Acoustic waves present in the combustion chamber that are reflected from walls tend to lose energy due to boundary layer losses. Due to the no-slip boundary condition and the temperature boundary condition (i.e. no temperature fluctuation at the wall), the acoustic energy is converted into velocity fluctuations and heat fluctuations. Consequently, the reflected wave has a lower energy compared to the

incident wave. The magnitudes of these losses are dependent on the frequency and viscous or thermal transport timescale. Under higher frequency conditions the magnitude of viscous dissipation and heat transfer increases.

ii. Convection and/or propagation of acoustic energy:

Acoustic energy from the system can be lost due to the convection by the flow or by the propagation of the wave through an open end. The energy lost by the wave is converted to sound energy and can be heard as the 'humming' sound from the combustor. The magnitude of the damping due to the propagation of acoustic waves is scaled with the relation, $(fD/c)^2$, where f is the frequency, D is the diameter of the chamber, and c is the speed of sound. The mean velocity of the flow has a direct impact on the energy of the reflected wave. In an acoustical study (Ingard and Singhal 1975), the authors had shown that the reflection coefficient drastically reduced with the increase in the flow velocity.

iii. Transfer of energy out of resonant frequencies to other frequencies:

Over many years several authors have reported that combustion oscillations are generally composed of several modes at specific frequencies. Several modes exist in the pressure and integrated heat release signal due to the presence of several non-linear mechanisms playing a role in the oscillations, driving at different frequencies (Langhorne 1988, Yu *et al.* 1991, Dowling 1997, Lee *et al.* 2000, Lieuwen and Neumeier 2002, Bellows *et al.* 2007). Mechanisms can cause a transfer of energy from excited frequencies to higher harmonics or sub-harmonics, where it may not be amplified and could be dissipated through viscous and convection/propagation damping mechanisms. Non-linear processes such as vortex formation can cause the transfer of energy from one frequency to another.

1.2.2 Control of combustion oscillations

Gas turbine combustion technology made a shift from non-premixed flames to lean premixed flames in order to reduce nitrogen oxides (NO_x) emissions.

However, this was met with higher sensitivities of flames to acoustic perturbations leading to combustion oscillations. Due to this, strategies must be deployed to reduce the oscillations experienced by the combustor (Candel 2002). Figure 1.8 shows thermo-acoustic interactions that could occur in a combustion chamber due to the mechanisms that were discussed earlier, and the route used for introducing a controller.

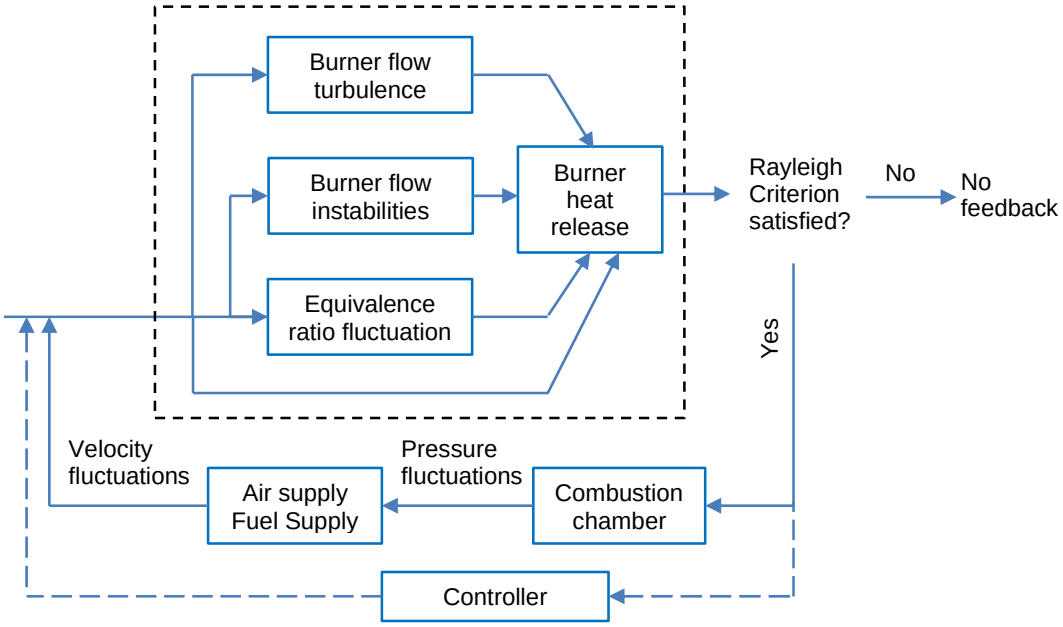

Figure 1.8: Thermo-acoustic interactions experienced in gas turbine combustors. (Adapted from Candel 2002)

To reduce or remove combustion oscillations, the coupling between the acoustic waves and the oscillatory heat release must be disrupted to dampen the oscillations rather than make them grow in amplitude. Control methods can be divided in to two categories; passive control, and active control. Passive control methods (Culick 1988) involve modifications made to the hardware that are fixed in time, which includes the combustion chamber dimensions, inlet and exit configurations, the method of injection and location of the fuel injectors, acoustic dampers, the flame stabilisation method (for example, the design and arrangement of the bluff-body), and other features that can alter the properties of the combustor.

Several studies have been conducted on the overall effects on combustion instability with changes in combustor geometry.

Changes to the duct length can have a significant effect on the pressure oscillations experienced due to the unstable combustion. Schadow and Gutmark (1992) changed the duct length causing a shift in the natural frequency of the combustor; this in turn caused the pressure oscillations to reduce. In a study by Tran *et al.* (2009) the authors aimed to reduce the combustion oscillations by altering the inlet boundary condition by placing a perforated plate. The design of the perforated plate altered the reflection coefficient and prevented the onset of non-linear interactions with incident acoustic waves of high amplitudes.

The disadvantage of applying this method of control is that this method is only effective over a limited range of frequencies and operating conditions. The modifications made to the combustion system can be costly and time consuming. Acoustic liners that are used to remove energy need to be fitted into the combustion system causing space and weight problems.

The second method known as active control introduces another method of interrupting the coupling between the unsteady heat release and pressure oscillations. This method provides a more dynamic approach to controlling oscillations by introducing an actuator that responds to the signals picked up by sensors placed in the combustion chamber (closed-loop controller). The actuator modifies parameters in response to the measured signal. An open-loop active control system does not use a time varying input from the combustion system.

The techniques developed in active and passive control, both, aim to decouple the acoustic and heat release response. This is done by altering the time delay between the pressure oscillation at the flame and the resulting heat release oscillation. This will alter the phase relation between the waves and the amplitude will decay rather than grow in magnitude. (For detailed reviews see McManus *et al.* 1993, Culick 1988, Candel 2002, Dowling and Morgans 2005).

In this project the main objective was to study the effects of the local addition of hydrogen fuel on the heat release of the flame. The results helped understand whether the local addition of hydrogen could be used to control combustion oscillations.

1.2.3 Combustion with secondary fuel addition

Combustion oscillations in practical devices are usually suppressed by controlling one or more of the various mechanisms described earlier. One of the common methods of control is the dynamic creation of a localised richer zone close to the flame base to alter the heat release. This is achieved by localised fuel addition, whereby a secondary fuel injection (also known as pilot injection) is made close to the base of the flame, altering the local equivalence ratio and hence the local flame properties. Changes in the flame dynamics alter the phase relation between the heat release and the acoustic pressure modulation (i.e. altering the Rayleigh criteria).

Numerous studies have been carried out experimentally (Mansour *et al.* 1999, Sattinger *et al.* 2000, Nair and Lieuwen 2003, Emiris and Whitelaw 2003, Pasquier *et al.* 2007, Kang and Kyritsis 2009, Anselmo-Filho *et al.* 2009, Guo *et al.* 2010, Albrecht *et al.* 2010, Galizzi and Escudie 2010, Kim and Hochgreb 2011) and numerically (Bradley *et al.* 1998, Marzouk *et al.* 2000, Robin *et al.* 2008, and Nogenmyr *et al.* 2011) on several types of flames to understand the impact of secondary fuel addition on the burning characteristics of the flame.

In a study by Bradley *et al.* (1998), it was noted that the stability of the flame in a swirl burner was dependent on the flame straining and the strength of the outer recirculation zone. An increase in the flame strain caused the flame to detach from the outer recirculation zones to a location further downstream where it was less stable. It was suggested that the combustion oscillation can be avoided by a localised increase in the equivalence ratio at the flame front. Local fuel injection was recommended to affect this, which would be sufficient to preserve the hot gases in the outer recirculation zones and improve the overall stability.

In the work presented by Emiris and Whitelaw (2003), turbulent natural gas flames were subjected to acoustic oscillations and it was noted that the low-frequency pressure oscillations observed during lean combustion were caused by the local extinction and re-ignition of the flame, thus affecting the flame stabilisation. A small quantity of fuel from the main flow was redirected to a secondary fuel injector placed close to the entrance of the combustion chamber. This improved the overall stability of the combustion process by reducing the amplitude of the pressure

oscillations; however, the improved performance was only achieved within a narrow range of operating conditions.

Marzouk *et al.* (2000) numerically showed with methane/air flames that a secondary fuel injection can have a significant effect on the burning process, including reaction zone broadening, burning rate enhancement, and extension of the flammability limit toward leaner mixtures. The radical concentrations in the flame remained elevated and a history effect was noticed where-by the lean mixture flame propagation was supported by the stream of hot radicals and products created as a result of the previously burnt reactants of a higher equivalence ratio. The spatial radical and temperature gradients produced by the unsteady equivalence ratio mixtures provided the flame with the ability to burn at leaner mixtures (i.e. below the minimum equivalence ratio required for continuous combustion).

Studies (Anselmo-Filho *et al.* 2009 and Haworth *et al.* 2000) have shown that the mean flame angle relative to the flow direction increased as the amount of secondary fuel injection increased. This indicated a higher mean reaction rate which was explained by the appearance of concentration pockets. These pockets contained mixtures of higher equivalence ratio which allowed for higher burning rates, although the global equivalence ratio was the same. The variation in the flame surface density (FSD - the length of flame per unit area or the area of flame surface area per unit volume) and flame curvature was also studied and the results indicated that local fuel addition caused an increase in the flame surface area due to the different localised flame propagation rates due to pockets of leaner and richer mixtures.

In recent work by Albrecht *et al.* (2010), a secondary fuel injector was placed at the flame base and at the combustor dump plane. These were used to introduce localised fuel/air addition to control combustion oscillations; the equivalence ratio of the secondary injection was kept constant while the total equivalence ratio was varied to see the effect on the flame stability. The unstable turbulent natural gas flames were actively controlled by using a periodically ignited premixed flame at the secondary injector exit. This caused a reduction in the pressure oscillations and reduced NO_x emissions. It was stated that the damping effect was mainly achieved by the high jet momentum through the secondary injector. Moreover, the combined injection of fuel and air through the injector prevented the lift-off of the main flame which appeared to be another damping source for pressure oscillations.

Studies carried out numerically and experimentally have led to three main conclusions on spatially non-uniform reactant mixtures due to local fuel addition or pressure oscillations. First, local fuel addition in premixed flames allowed the flame to burn at equivalence ratios lower than its flammability limit. This was due to the effect which was known as the history effect where the flame propagation under lower equivalence ratio (even lower than the flammability limit) could continue burning due to the stream of hot products available from the combustion of the previously higher equivalence ratio mixture (Marzouk *et al.* 2000 and Robin *et al.* 2008). Secondly, there was a significant change in the flame geometry due to the varying flame surface area. The localised increase in ϕ in one region compared to another region in the vicinity caused a difference in the localised burning velocities which in turn stretches flame surface area causing an increase in the reaction rate, hence causing an increase in the heat release rate. This increase in flame surface area caused a change in the local flame structures such as curvature, flame brush thickness and flame surface density (Pasquier *et al.* 2007, Anselmo-Filho *et al.* 2009, Albrecht *et al.* 2010, Galizzi and Escudie 2010, and Kim and Hochgreb 2011). Lastly, secondary fuel addition had a direct effect on the pressure and velocity fluctuations experienced by the flame. This was due to the alteration of the heat release response relative to the pressure/velocity oscillations. Decoupling the acoustics and the heat release would cause a damping effect on the oscillations as stated by Rayleigh's criterion.

The literature presented has shown that secondary fuel injection could be successfully employed to control combustion oscillations; however, these studies have been limited to the same type of fuel being used in the primary and secondary injector. Alternative fuels or gases can be used as additives to alter the phase relation between the heat release and acoustics. As a result, over the years, hydrogen, H_2, has received considerable attention in being a potential solution to controlling flame stability. Hydrogen is well known for being a very clean alternative fuel as there are no CO, CO_2, SO_x and unburnt hydrocarbons, except for NO_x emissions from hydrogen fuel combustion (Ilbas *et al.* 2005 and Mardani and Tabejamaat 2010). As mentioned earlier, under lean conditions, combustion of hydrocarbons are highly susceptible to oscillations. Using a blend of hydrocarbons and hydrogen can significantly improve the overall combustion characteristics by

improving the flame stability and the ignitibility (Schefer *et al.* 2002, Kim *et al.* 2009, Kim, Arghode, Linck and Gupta 2009, and Mardani and Tabejamaat 2010).

Hydrogen (H_2) addition to alter the heat release from the flame has been explored by many researchers; however, the results from these studies were not conclusive. There are many advantages for the above approach. Studies (Dahl and Suttrop 1998, Jackson at al 2003, Guo *et al.* 2005, Cozzi and Coghe 2006, Mandilas *et al.* 2007, Frenillot *et al.* 2009, and El-Ghafour *et al.* 2010) have demonstrated that the addition of H_2 to hydrocarbon gaseous fuel increases the lean limit of operation and can significantly improve the emission performance. This reduces the risk of blow off, a common problem in lean premixed combustors. The increase in the lean flammability limit is caused by higher reaction rates of H_2 (Day *et al.* 2011). This raises the temperature in the reaction zone and hence expands the size of the reaction zone making the recirculation zones smaller, which increases the availability of ignition energy for incoming air/fuel mixture. Reducing the size of the recirculation zone reduces the availability of the relatively cooler gases (compared to the gases in the reaction zone) which leads to an increase in the global temperature, thus enhancing the production of NO_x (Choudhuri and Gollahalli 2003, Ilbas *et al.* 2005, Guo *et al.* 2005, Cozzi and Coghe 2006, Barbosa *et al.* 2007, and El-Ghafour *et al.* 2010). However, under different swirl conditions the size and strength of the recirculation zones can be manipulated as shown in work conducted by Kim *et al.* (2009) to change the peak temperature within the flame to reduce the production of NO_x.

Dahl and Suttrop (1998) reported a reduction in the level of NO_x produced with the addition of H_2 content under certain conditions. Similar findings were reported by Guo *et al.* (2005) and Wicksall and Agrawal (2007) where a reduction of CO_2 and NO was a result of hydrogen addition allowing the flame to burn at ultra-lean conditions, resulting in large reductions in CO_2 and NO emissions. With a high equivalence ratio, the addition of hydrogen caused a decrease in the formation of NO_2 and N_2O. However, for flames closer to the extinction limits, the overall emissions of NO_2 and N_2O, first increased, and then decreased with the increase in the addition of hydrogen. Keeping the global equivalence ratio constant and with increasing H_2 content there was a noticed reduction in the CO production as there was a lower amount of carbon based fuel used (Choudhuri and Gollahalli 2003, Frenillot *et al.* 2009, and Kim *et al.* 2009). The reason for the reduction in the CO

was the increase in H, O and OH mole fraction with the increase in H_2 (Wang *et al.* 2009). Mole fraction of CH_2O and CH_3CHO was reduced leading to lower carbon emissions as the reaction shift towards lower carbon reaction pathways.

Recent work by Barbosa *et al.* (2007) in an industrial type burner reported a reduction in combustion oscillations under some operating conditions. The results presented by Kim, Arghode, Linck and Gupta (2009) showed that the higher combustibility of hydrogen caused higher stability of the flame at both low and high swirl strengths. Similar conclusions were gathered by El-Ghafour *et al.* (2010) where the increase in the flame stability appeared as a significant enhancement in the flame lift off and blowout limits, which can be attributed to the high burning velocity of hydrogen fuel.

However, the results from Wicksall and Agrawal (2007) study in a premixed burner showed that their combustor exhibited strong instabilities with increasing the % of H_2 under stable operation. With H_2 content as high as 40% by volume in CH_4 flames the flame exhibited strong pressure fluctuations or sound levels. Chen (2009) also concluded that the mixing of H_2 to CH_4/air can destabilise the flame. This occurred by altering the characteristics of the flame's dependence of the propagating speed on stretch rate and local instability of propagating flames.

While some studies suggest a promising role for hydrogen enrichment in the development of low-emission combustion technologies, the role of hydrogen addition, particularly its effect on combustion oscillations is poorly understood. Furthermore, the literature in this area is ambiguous. Researchers that have conducted investigations of hydrogen addition within the context of combustion instability have reported contradictory results. This project aims to investigate the addition of H_2 to turbulent premixed ethylene (C_2H_4) and methane (CH_4) flames under varying operating conditions. The operating conditions and different fuels will help in realising that the effects of H_2 addition are dependent on the fuels and operating conditions applied. Self-excited flames will be subjected not only to the addition of H_2, but also to the addition of C_2H_4 and N_2 to show that the response of the flame with the addition of hydrogen is unique.

1.2.4 Atomic hydrogen and its laser induced fluorescence

Atomic hydrogen is highly reactive and diffusive (Law 2006), and plays an important role in combustion chemistry. Measurements of atomic hydrogen concentrations are important in understanding the relationship between the chemistry and transport within flames. The reactivity and diffusivity of the H-atom can have a significant impact on the flame dynamics and shape (Najm and Wyckoff 1997).

In a numerical study carried out by Yoo *et al.* (2009) it was shown that the increase in the concentration of OH molecules in regions of highly curved flames is governed by the preferential diffusion of hydrogen atoms leading to the increase in the reaction rates. The increased production of OH radicals leads to the increase in the overall rate of reaction as there is an increase in the flame speed. In studies conducted by Echekki and Chen (1996) and Najm and Wyckoff (1997) the mechanisms of focusing and defocusing and correlations between the mass fraction of atomic hydrogen and the flame curvature were deduced.

It (Najm and Wyckoff 1997) was computationally shown that the net production of H atoms occurred in the oxidation layer on the products side in regions of positive curvature (i.e. flame front convex to oncoming reactants), involving reactions, 3, 10, 13, 7 and 2 from Table 1.1. These reactions require H_2 and CH_3, which are supplied by the diffusion of these molecules from the inner layer where they are produced. This diffusion is dominant in locations of positive curvature. These reactants are focused into the oxidation layer due to the positive flame curvature leading to enhanced fluxes and faster reaction rates, hence the expansion of the positively curved flame front. However, the produced H atoms on the products side in regions of positive curvature were suggested to be defocused from the oncoming reactants and readily diffused to regions of negative curvature creating a large concentration of H atoms in those regions (Echekki and Chen 1996). The large concentration of H atoms in negatively curved flame surface caused the local focusing of H atoms on to the oncoming reactants.

These atomic H were then consumed in reactions such as 9, 11, and 12 which enhance the breakdown of CH_4 to CO, leading to an increase in reaction rate and thus creating a corner. With the formation of the corner the flame fronts in close proximity collide thus causing a flame surface annihilation event thus reducing the

level of wrinkling of the flame (the evolution of this flame front is shown in Figure 1.9). A dominant consumer of H atoms is reaction 1, which produces O and OH radicals which is a key chain-branching step in the oxidation layer. The rate of production, consumption and diffusion of the H atoms will determine the overall consumption rate of the methane or other hydrocarbon fuels. Understanding this diffusional focusing and defocusing of atomic hydrogen will help in understanding how the reaction rates can be modified in various locations to change the overall shape of the flame and reduce the heat release oscillations. However, the scope of this project does not cover this analysis but is recommended for future studies into the use of hydrogen fuels.

Reactions			
1.	$H + O_2$	↔	$O + OH$
2.	$O + H_2$	↔	$H + OH$
3.	$H_2 + OH$	↔	$H + H_2O$
4.	$H + O_2 + M$	↔	$HO_2 + M$
5.	$H + HO_2$	↔	$2OH$
6.	$H + HO_2$	↔	$O_2 + H_2$
7.	$OH + CO$	↔	$H + CO_2$
8.	$H + CH_3 (+ M)$	↔	$CH_4 (+ M)$
9.	$H + CH_4$	↔	$CH_3 + H_2$
10.	$O + CH_3$	↔	$H + CH_2O$
11.	$H + H_2CO$	↔	$HCO + H_2$
12.	$H + HCO$	↔	$H_2 + CO$
13.	$HCO + M$	↔	$H + CO + M$
14.	$H + H_3CO$	↔	$H_2 + H_2CO$
15.	$H + H_2CO (+ M)$	↔	$CH_3O (+ M)$

Table 1.1: List of reactions involving the production and consumption of H atoms from the C1 Methane-Air mechanism (Najm and Wyckoff 1997).

The laser induced fluorescence of atomic hydrogen is achieved by using a two-photon excitation scheme (Lucht *et al.* 1983, Kulatilaka *et al.* 2008, and Kulatilaka *et al.* 2009). Single photon excitation of ground state hydrogen requires vacuum ultraviolet excitation wavelengths (i.e. below 122 nm) which are very difficult to achieve as these wavelengths are readily absorbed by air. Hence a two-photon excitation scheme is used at a wavelength of 205.1 nm, which is needed to

excite the hydrogen atoms to the H(n=3) electronic level. In this method the H atoms are excited from the ground $1s^2$ *S* electronic level to the excited $3d^2$ *D* level by two-photon absorption at 205.1 nm (Lucht *et al.* 1983). When the excited atom decays from the n=3 to n=2 state there is an emission of light at a wavelength of 653.6 nm (illustrated in Figure 1.10) which is detected.

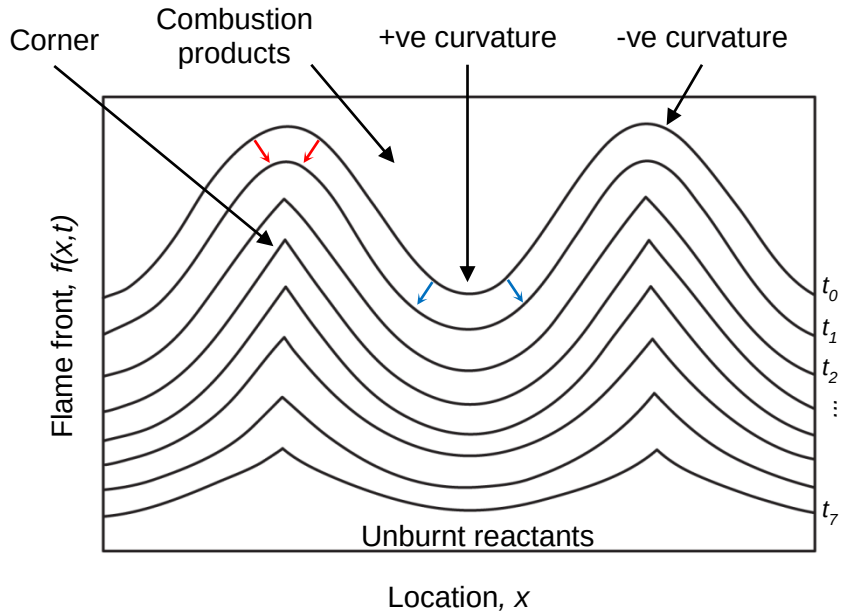

Figure 1.9: Evolution and propagation of an initially sinusoidal flame surface showing the formation of corners (Turns 2006).

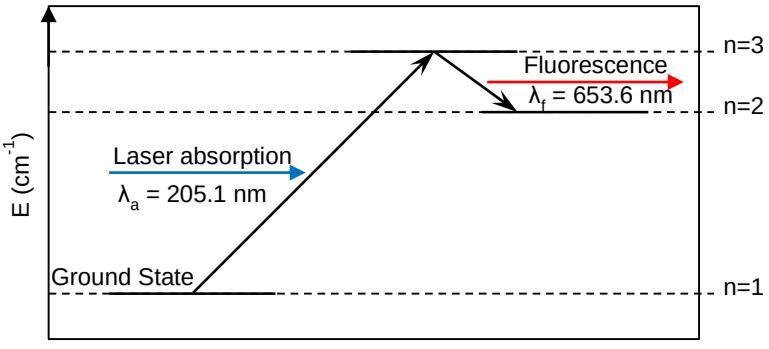

Figure 1.10: Energy level schematic for two photo excited fluorescence. (Adapted from Lucht *et al.* 1983)

Lucht *et al.* (1983) produced the required 205.1 nm excitation beam using an Nd:YAG laser to pump a dye laser operating at 568 nm. The second harmonic of the beam produced by the dye laser (i.e. 284 nm) and the fundamental Nd:YAG laser radiation (i.e. 1064 nm) were combined in a KDP mixing crystal which produced a beam of wavelength 224 nm. The three beams were focused into a Raman shifting cell, which contained H_2 at a pressure of 650 kPa, which produced an output beam of wavelength 205.1 nm which was required to excite the atomic hydrogen.

1.3 Objectives

Numerous studies have been carried out in understanding the mechanisms responsible for the oscillations and significant progress has been made in collecting experimental data and developing computational models in order to predict the onset of combustion instabilities for different systems (Mugridge 1980, Dowling 1995, Mueller *et al.* 1995, Dowling 1997, Mantel and Samaniego 1999, Samaniego and Mantel 1999, Lieuwen 1999, Renard *et al.* 2000, Balachandran 2005, Altay *et al.* 2009). However, the accuracy of the models is uncertain as many assumptions were made as the heat release of the flame cannot be directly measured. The models that have been developed are good in predicting the linear response of the flame to velocity perturbations, however, under high amplitude velocity oscillations the flame undergoes a non-linear response which is caused by the response of the individual mechanisms that play a key role in causing the fluctuation in the heat release.

There were two major objectives of this study. First, was to experimentally investigate the response of lean premixed methane and ethylene turbulent flames with the local addition of hydrogen. The fact that there is limited and ambiguous information on the stability of locally added hydrogen enriched flames makes this investigation highly beneficial for the further development of leaner and cleaner gas turbine technology. The information gathered from the experiments will greatly improve our understanding of how hydrogen fuel could be used to reduce combustion oscillations.

The second objective was to develop a new approach to imaging the laser induced fluorescence of atomic hydrogen in turbulent flames. While earlier studies (Lucht *et al.* 1983, Kulatilaka *et al.* 2008 and Kulatilaka *et al.* 2009) have only focused on laminar flames, this project attempted to image large sections of atomic hydrogen in turbulent flames which were subjected to combustion oscillations. This will show how changes were brought about in the flame shape with the addition of hydrogen fuel and how combustion oscillations influenced the appearance of atomic hydrogen within the flame. The results generated from these experiments will be beneficial in developing combustion models which can predict the onset of instability in certain systems.

1.4 Outline of the thesis

This dissertation focuses on the effects of local hydrogen addition on the dynamics of combustion within a model gas turbine combustor. The experiments studied how the periodic mass-flow/velocity fluctuations of the reactants had an impact on the heat release rate of turbulent premixed flames. The study also looked at the appearance of atomic hydrogen in the flame using a novel laser based technique. The results are detailed in depth to understand the global flame characteristics.

Chapter 2 describes the experimental apparatus – the combustion chamber and the different features that allow the investigation of different types of flames. The acoustic, optical and laser based measurement techniques/equipment used in the study are discussed in detail. The methods of data analysis are also presented, which describe the ways in which the relevant information on the flame response is extracted from the experimental data.

In chapter 3 the cold flow velocity within the combustion chamber is presented. Data and images on how the flow is altered with acoustic forcing are shown. Chapters 4 and 5 discuss the response of a fully and imperfectly premixed ethylene and methane flames subjected to controlled velocity oscillations and how the response is affected by the local addition of hydrogen fuel. The dynamics of these flames are described by the use of OH* chemiluminescence and with phase-locked images of the spatial distributions of OH and H radicals and the corresponding flame front.

Chapter 6 presents the imperfectly premixed ethylene flames under self-excitation (i.e. the velocity perturbations, hence the combustion oscillations are not controlled), and aims to validate the results obtained in chapter 5. The final chapter summarises the main findings of the project and concludes with possible further work that could be carried out to aid the findings of this study.

Chapter 2: Experimental setup and data analysis

2.1 Design of the combustor

To understand the flame dynamics under excited and enriched conditions a combustor was designed and developed. The design was adapted from Balachandran (2005) and certain modifications were made. The design of the combustor had to fulfil five main requirements:

i. To include provisions for attaching speakers and pressure transducers to create and record acoustic oscillations.
ii. To allow several modes of primary fuel delivery into the flow.
iii. A design which would allow the addition of secondary fuel close to the inlet of the combustion chamber.
iv. The combustion chamber must be optically accessible for the laser and imaging systems.
v. For the geometry to be modular to allow for controlled acoustic forcing as well as self-excitation conditions of the flame.

The design of the combustor had to take all these requirements in to account. The construction of the combustor can be described using three main sections, i) the plenum and the duct, ii) the bluff-body, and iii) the combustion zone, which are labelled in Figure 2.1. The description of the sections detail how each of the five requirements influenced the design of the combustor.

i) The plenum and duct

The plenum is the main chamber of the combustor with an inner diameter (ID) of 100 mm and length 200 mm. This was constructed from several sections of

aluminium parts with divergent and convergent cross sections at the inlet and exit of the plenum which prevented any flow separation during the expansion and contraction of the gas. The air and primary fuel lines are connected to the base of the plenum, where the flow was streamlined using a section of honeycomb mesh placed as a flow straighter.

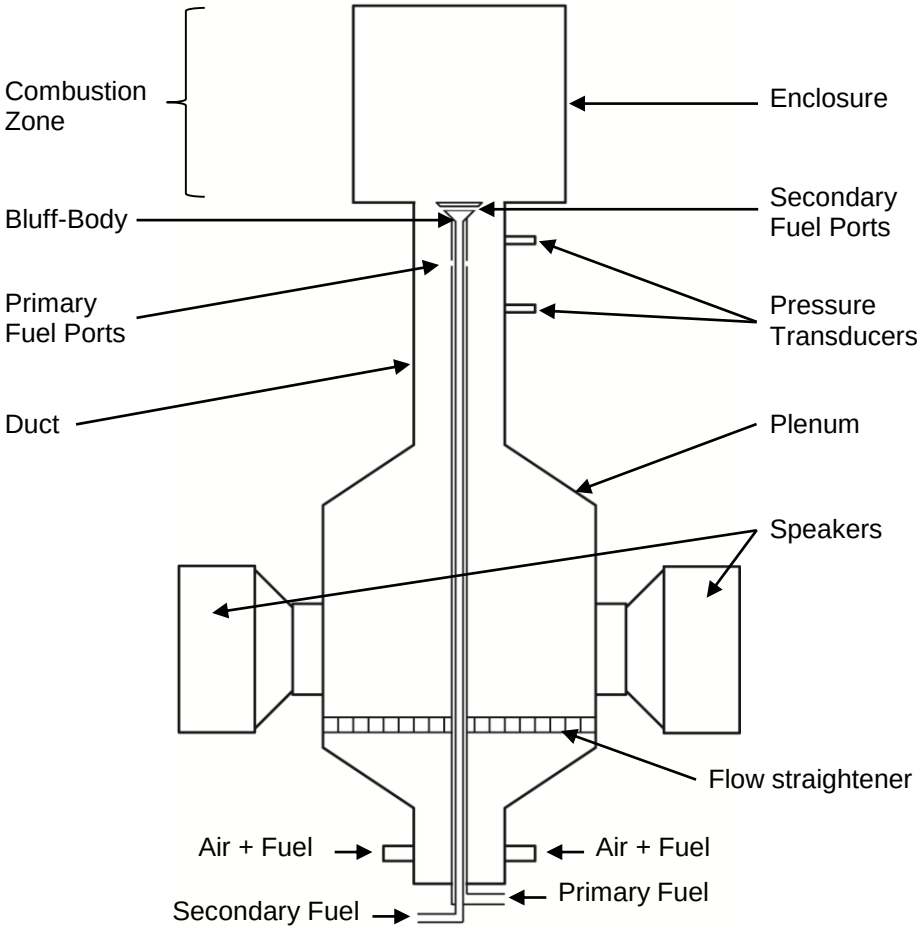

Figure 2.1: Shows the schematic of the combustor assembly.

The plenum provided a provision for attaching four orthogonally placed, speakers, rated at 60 W, along the circumference and at a location 100 mm downstream of the plenum exit. A TTi 60 MHz Arbitrary waveform generator was used to generate a known sinusoidal wave of varying frequencies and amplitudes. The sinusoidal waves were amplified and distributed to the speakers using a power

amplifier. The modulation of the output from the speakers provided the necessary controlled acoustic perturbations for velocity/mass flow fluctuations during experiments. This method of generating velocity fluctuations at the inlet of the combustion chamber shall be referred to as 'forced' conditions, while 'unforced' will refer to cases where the speakers were switched off. Velocity fluctuations as high as 80% of the mean axial velocity was achieved at particular forcing frequencies. The duct above the plenum had an ID of 35 mm and had provisions for placing pressure transducers used to characterise the burner's acoustic response and to measure the velocity oscillations in the flow. These designs fulfil the first requirement, allowing the generation and measurement of pressure/velocity perturbations, thus creating mass flow perturbations in the flow, which was important for this study.

ii) The bluff-body

A bluff-body is a flame-holding device typically in the form of a "vee gutter" with the tip of the V facing upstream. Turbulent flames were stabilised in the wake of the bluff-body, where strong recirculation zones were present. There was a central recirculation zone (CRZ) created by the bluff-body and the two outer recirculation zones (ORZ) created by the step in the combustor (shown in Figure 1.2 in Chapter 1). The recirculation zones consisted of burnt products at nearly adiabatic temperature (Turns 2006). The products recirculated towards the base of the flame where they provided energy and intermediate reactants that ignited the fresh air/fuel mixture, and form shear layers for flame stabilisation. It is the strength and characteristics of the shear layers and recirculation zones that give the flame its shape.

The bluff-body used in this project was conical in shape and had a diameter of 25 mm giving a blockage ratio of 50%. The primary fuel could either be mixed completely with the air before entering the combustor, and this mode of mixing shall be referred to as a fully premixed mixture; or it can be locally injected into the air flow through the primary fuel ports on the bluff-body (shown in Figure 2.2); this mode of local primary fuel introduction will be referred as an imperfectly premixed mixture. The primary fuel ports consisted of six holes of diameter 0.25 mm placed circumferentially on the main fuel pipe, 50 mm below the inlet of the combustion chamber. The bluff-body also provided ports for secondary fuel injection. These

ports included six 2 mm openings placed 2 mm below the base of the combustion zone. The secondary fuel injection introduced a local equivalence ratio variation in the flame which could cause the response of the heat release fluctuation to change.

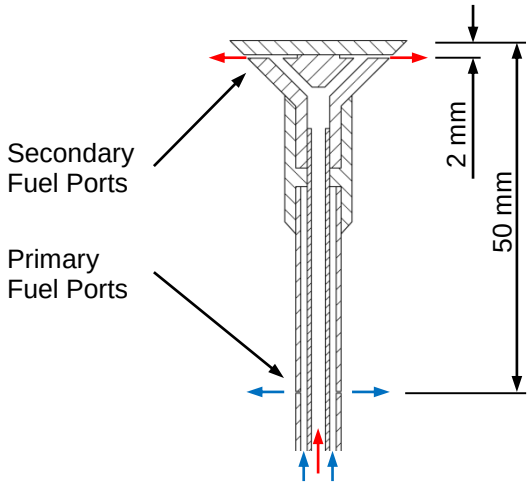

Figure 2.2: Sectional view of the bluff-body, showing the primary and secondary fuel ports.

iii) The combustion chamber

The combustion zone is the region where the flammable mixture ignited and the flame stabilised on the shear layers created by the recirculation zones. The flame was enclosed using a UV fused silica quartz cylinder of ID 70 mm and length 100 mm. This prevented any local equivalence ratio fluctuations due to air entrainment from the surrounding. The fourth design condition was to allow optical access of the flames. The quartz provided the optical access needed for the lasers, cameras and other optical equipment. The length of the quartz enclosure was selected to be small so that its resonant frequency was much higher than the frequency of forcing. This reduced the interference from the acoustics of the downstream geometry on upstream forcing. For the current study, the forcing frequency was varied between 20 to 450 Hz while the fundamental frequency of the downstream duct was around 860 Hz (estimated using the resonant frequency function for a closed cylinder), hence the resonant effects of the downstream geometry were minimised.

Part of the project required the self-excitation of flames. This was achieved by a detachable 200 mm long stainless steel tube that was placed on top of the quartz, increasing the total height of the enclosure to 300 mm. The increase in length caused the acoustic waves generated by the flame to reflect, amplify and feed back to the air/fuel supply within the chamber which caused perturbations in the air flow leading to self-imposed combustion oscillations.

2.2 Experimental methods and instrumentation

2.2.1 Acoustics and flow rate measurements

To characterise the burner's acoustic response and to measure the velocity fluctuations in the flow, two Kulite high-sensitivity pressure transducers (Model XCS-093 with sensitivities of 4.2857x10-3 mV/Pa) were used. The signal from the pressure transducers were amplified using a Flyde Micro Analogue amplifier with a 400 kHz sampling rate. The amplified signal was digitised using a data acquisition (DAQ) system with an analogue to digital convertor. The DAQ system used here was a National Instruments PCI 6010 card with 16 bits resolution and an input voltage range of ±5 V with the capability of recording 250 kS/s. In order to reduce the distortion of the signals, each channel was recorded at a high sampling frequency of 10,000 Hz and over a time series lasting 2 seconds.

The air was supplied from a central system at a constant pressure of 6 bars. The fuel and other diluents were supplied from commercially available cylinders fitted with appropriate pressure regulators, supplying the gas at constant pressure of 5 bars. The volume flow rates of air and the different fuels were measured using Red-Y Smart digital mass flow meters at a constant room temperature of approximately 20°C. The measurement ranges varied from 40 - 450 normal litres per min (nlpm – measured at 0°C and 1 atm) for air, 0 – 60 nlpm for methane and ethylene, 0 – 20 nlpm for hydrogen and 0 – 50 nlpm for nitrogen, with an accuracy of ± 1.5% of the full scale reading and ± 0.5% of the reading. Figure 2.3 shows an image of the control panel set up to control the flow rates of the gases fed in to the combustor. The panel consisted of five mass flow controllers that were monitored using a computer. The controllers were calibrated and programmed to allow the flow

and measurement of different gasses such as air, nitrogen, methane, ethylene, hydrogen, carbon dioxide etc. The volume flow rate for each device was displayed on the LCD panel.

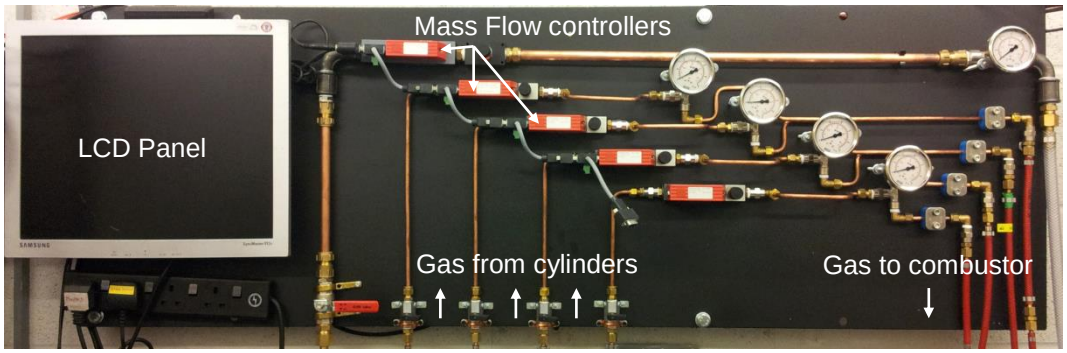

Figure 2.3: Photographic image of the control panel used to regulate and monitor the flow of reactants to the combustion chamber.

2.2.2 Chemiluminescence

Optical light detection and its analysis forms one of the fundamentals of diagnostic techniques used in analysing a flame. The advantage of such techniques is its ability to be non-intrusive (i.e. no use of physical probes in the combustion chamber) that could affect the combustion dynamics and its ability to define several characteristics of the flame. The measurement of the heat release rate is extremely important in understanding the flame chemical dynamics, however, this quantity is extremely difficult to measure if not impossible. Techniques have been developed over the years that can give a qualitative indication of the flame's heat release rate (Price *et al.* 1969, Langhorne 1988, Ratner *et al.* 2002, Lauer and Sattelmayer 2008). A widely used measurement technique is known as chemiluminescence, which involves the formation of excited radicals from chemical reaction, Eq. (2.1), in the flame and the spontaneous emission of light/photon through the loss of energy to reach its ground state Eq. (2.2), (Ballester and Armingol 2010).

$$A + B \rightarrow R^* + others \qquad \text{– Eq. 2.1}$$

$$R^* \rightarrow R + hv \qquad \text{– Eq. 2.2}$$

Where '*' denotes the excited state of the radical R, and hv is the energy released with the photon. The formation of these excited radicals occurs in a particular region within the combustion zone. Figure 2.4 illustrates the regions formed during fully premixed combustion (Turns 2006).

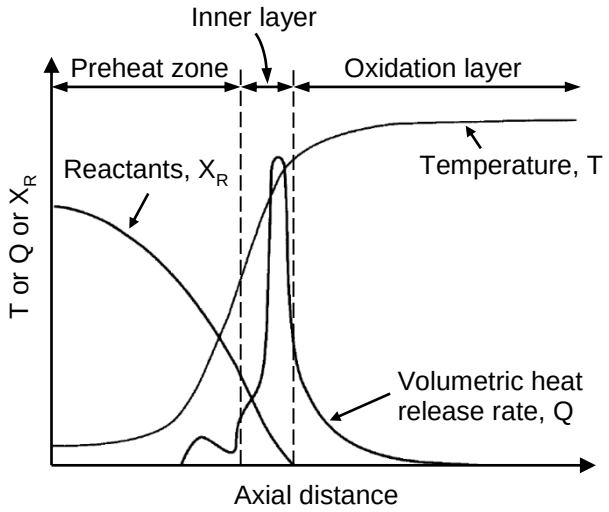

Figure 2.4: Shows the different reaction zones during fully premixed combustion and the change in reactant concentration, X_R, heat release rate, Q, and temperature, T, with axial distance. (Adapted from Turns 2006)

In the 'preheat zone' the reactants breakdown in to different radicals due to the heat transfer to the reactants from the combustion chamber. The 'Inner layer' is where the bulk of the chemical reactions take place and most of the heat is released in this zone. In this zone the chemically excited species are formed that cause chemiluminescence. The oxidation layer is where the chemistry is dominated by slow radical recombination reactions with the ultimate formation of CO_2. The correlation of chemiluminescence with the heat release rate is based on the understanding that an increase in the chemical reactions will lead to the further production of chemically excited radicals with an increase in the release of heat.

This technique was qualitatively employed in the mid-80s by Price *et al.* (1969) where by the noise generated by turbulent premixed ethylene/air flames was correlated to the optical intensity measurements of the free radicals C_2* generated during the chemical reactions. The study showed a linear correlation between the

mean chemiluminescence intensity of C_2* and the volume flow rate of combustible mixture. Lawn (2000) investigated the use of OH* for the correlation with the heat release rate. The author concluded that the RMS value of the fluctuating component of the radiation intensity is likely to be proportional to the mean of the heat release rate. Many authors have reported a linear increase in the mean chemiluminescence intensity with increasing fuel-flow rate, and a decreasing intensity with increasing air excess ratio (Haber *et al.* 2000 and Hardalupas and Orain 2004).

The main radicals that contribute to the chemiluminescence emitted from the hydrocarbon flame are OH*, CH*, C_2* and CO_2*. The accepted reaction pathways for these radicals are shown in Table 2.1 (Krishnamachari and Broida 1961, Porter *et al.* 1967, Becker *et al.* 1969, and Ballester and Armingol 2010).

Radical	**Reaction**		**Wavelength (nm)**
OH*	R1:	$CH + O_2 \rightarrow CO + OH^*$	308.9
	R2:	$H + O + M \rightarrow OH^* + M$	
	R3:	$OH + OH + H \rightarrow OH^* + H2O$	
CH*	R4:	$C_2H + O_2 \rightarrow CO_2 + CH^*$	431.4
	R5:	$C_2H + O \rightarrow CO + CH^*$	
C_2*	R6:	$CH_2 + C \rightarrow C2^* + H_2$	516.5
CO_2*	R7:	$CO + O + M \rightarrow CO_2^* + M$	350-600

Table 2.1: The table lists the formation routes of excited radicals and their corresponding emission wavelengths. (Ballester and Armingol 2010)

The light emitted by the radicals are mostly narrow band in the case of OH*, CH* and C_2*, however, CO_2* is emitted over a broad wavelength spectrum. In order to determine the adequacy of the radicals as indicators of heat release the chemical kinetics of the combustion must be understood. Figure 2.5 shows a simplified reaction pathway for the combustion of methane, CH_4 (Najm *et al.* 1998). HCO has been considered as an excellent flame marker and it correlates well with the heat release and burning rates. However, capturing the chemiluminescence of HCO is extremely difficult as the intensity of the radical is very low.

Under turbulent combustion there have been conflicting observations due to the unsteady nature of the burning characteristics of turbulent flames. Unsteady

flame curvature and high strain affect the measurements of several radicals making it inadequate for interpreting the heat release rate. Several authors have stated that the use of OH* chemiluminescence as an indicator was acceptable under unsteady strain rates but it was inconsistent and insensitive to the variations in large unsteady curvature (Nori and Seitzman 2007, Nori and Seitzman 2008, Lauer and Sattelmayer 2010). CO_2* was also suggested to have a complicated dependence on the curvature and flow history making it a less adequate marker for the flame's heat release rate (Najm *et al.* 1998). It was concluded that CH*, and C_2* were not reliable indicators of the turbulent heat release rate because their appearance in the flame was not an indicator for the pathway of carbon oxidation for the main portion of carbon.

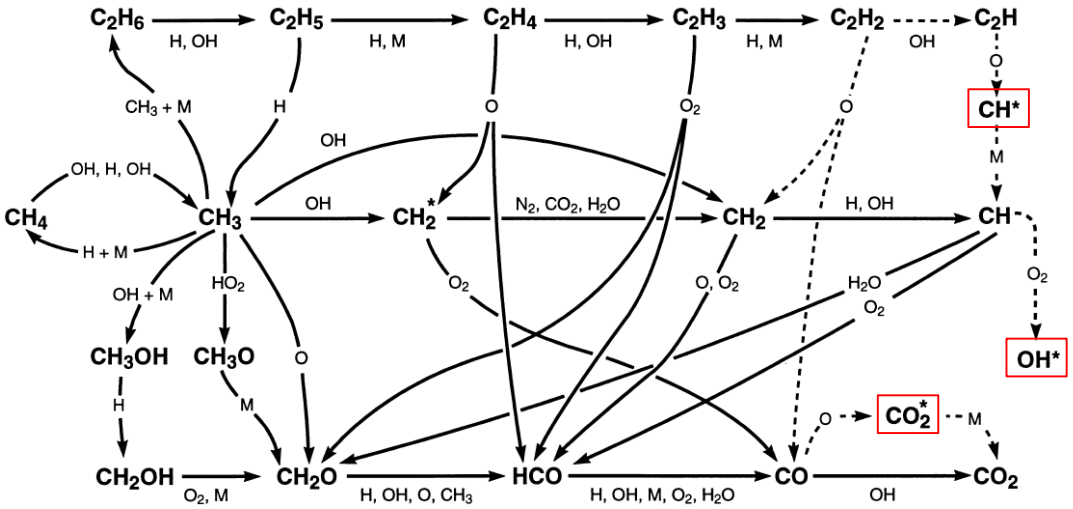

Figure 2.5: Reaction pathway for a freely propagating premixed methane flame. (Najm *et al.* 1998)

The study by Haber *et al.* (2000) showed the relationship between the heat release rate, determined by the CH* chemiluminescence, and the fuel-flow on a Bunsen burner. The results validated the findings by Najm *et al.* (1998) that CH* was not a good indicator of the heat release rate in all flame environments. CH* chemiluminescence failed to capture a decrease in the sensible enthalpy change of the gases through the flame, however, OH* chemiluminescence did capture this decrease. Lauer and Sattelmayer (2010) stated that the chemiluminescence could

be used to monitor the integral heat release of turbulent flames if an empirical correlation between chemiluminescence and heat release can be obtained.

Although chemiluminescence signals of radical species vary with different types of flames they are generally used as an indicator of the integral heat release rate. The downside of such measurements is its inability to capture a spatial variation in the heat release of the flame due to it being a line of sight integration technique. To improve the accuracy and to obtain a spatial variation of the heat release; laser induced fluorescence imaging techniques are being applied to correlate with the heat release rate and study the flame structure (Broda *et al.* 1998, Ikeda *et al.* 2000, Balachandran *et al.* 2005, and Ayoola *et al.* 2006). This technique gives an insight in to the flame appearance and flame height and could be used to find the local distribution of radicals within the flame on a 2D plane.

OH* chemiluminescence has generally been accepted as a heat release indicator for methane and ethylene flames (Najm *et al.* 1998, Haber *et al.* 2000, Balachandran 2005). This study encompassed the use of global emission of OH* chemiluminescence to obtain the heat release oscillations and the flame describing function of the different flames. However, it must be noted that an assumption was made that the use of OH* chemiluminescence, to determine the heat release oscillations, is valid for methane and hydrogen, and ethylene and hydrogen mixture based flames.

The chemiluminescence was detected by line of sight integrating detectors known as a photo-multiplier tube (PMT). This detector was chosen due to its ability to capture the chemiluminescent light at an extremely high frequency. This was good for self-excited or forced flame conditions where the integrated light of the modulating flame was captured quite well. The PMT was fitted with a convex lens which focused the entire flame on to the collection window. For the detection of OH* chemiluminescence the PMT was fitted with an interference filter with a centre wavelength of 307 nm and a bandpass of ±10 nm.

2.2.3 Planar laser induced fluorescence (PLIF)

In recent years laser probing techniques have gained considerable interest in the use for various combustion diagnostic applications. It offers detailed knowledge of the underlying physical and chemical mechanisms of combustion

processes. There are several advantages of using laser techniques over physical probing methods, which have been used in the past to study and characterize combustion phenomena. Combustion processes are easily affected by physical probes due to their intrusion in the combustion chamber. This physical intrusion could inherently affect the combustion process either by disturbances in the flow field, or act as a thermal source or as a catalyst to alter the fundamental processes involved with the combustion. In several applications where the flame is stabilised on the shear layers created by recirculation zones, physical probes could affect this layer and cause a change in the shape of the flame and in some cases act as a flame-holder itself.

A further disadvantage of using physical probes is that in severe experimental environments physical probes must be physically robust. These probes cannot perform measurements in several localised regions simultaneously. Due to these factors the probes' spatial and temporal resolution is reduced and there are concerns of reliability and survivability or the probes at high temperature and pressure environments. Laser diagnostics for combustion studies are of considerable interest due to their remote and non-intrusive character, unlimited temperature capability, and the potential for simultaneous temporal and spatial measurements.

As with achieving a good spatial resolution a high temporal response can be achieved with continuous lasers, however there are disadvantages. Compromises are made either in both space and time scales to achieve adequate signal levels. One major disadvantage to using lasers is that the test rig must have optical access by incorporating windows in the design. This could make sophisticated geometries, such as an annular gas turbine combustor extremely challenging to design with optical access due to the high temperatures and pressures. Although, laser techniques have a better spatial resolution compared to physical probing there is a lack of resolution in all three spatial coordinates to resolve the finer scales in turbulent combustion. For instance, resolutions of 100 μm or less are often required to resolve the Kolmogorov micro-scales and the flamelet thicknesses in certain regimes of turbulent combustion. Although there are certain disadvantages of using laser techniques for studying combustion, the advantages outweigh the disadvantages.

Laser induced florescence (LIF) is an important laser imaging technique used for qualitative and quantitative measurements of the flame characteristics. Planar laser induced fluorescence (PLIF) is a common technique performed by expanding the laser beam in to a laser sheet used to image a 2-D plane of a flame. Laser induced fluorescence works on the principle of selectively exciting atomic or molecular species with a laser at specific wavelengths to a higher energy state. The excitation of the species is followed by a spontaneous emission of a photon (light) when the excited atom or molecule decays back to its ground state. It is this spontaneous emission, or also known as fluorescence, that is captured on a CCD camera. Its intensity can be used to make quantitative or relative comparisons between different types of flames.

Chemical species such as OH, H and O, are considered chain carriers as these species contribute to the majority of the forward fuel consumption reactions as shown in the earlier Figure 2.5. Concentration enhancements or reductions of these species can significantly alter the flame propagation and heat release rates. The concentrations of these species can be affected by several parameters such as the strain-rate, which modifies the convective transport along the normal and tangential directions to the flame, and flame curvature. In a study by Mueller *et al.* (1995) it was shown that the strain-rate history effects could play an important role in altering the flame structure. It was argued in a study by Echekki and Chen (1996) that the concentration of the faster diffusing species can be highly susceptible to flame curvature by a mechanism known as focusing and defocusing (described by Law 1988), while the heavier and slower reacting species are more susceptible to unsteady strain-rates. Focusing/defocusing occurs when reactants or heat is transferred to/from the oncoming stream of reactants. The understanding of the sensitivity of various species to flame roll-up has not been fully understood due to the lack of experimental investigations into the localised and spatial distribution of chain carrier species. In this study an attempt is made in using laser diagnostics to qualitatively show the variation in the concentrations of OH and H species under varying flame roll-up conditions.

Hydroxyl (OH) PLIF: It has been shown in several studies (Najm *et al.* 1998, Haber 2000, Ratner *et al.* 2002, Balachandran *et al.* 2005, Turns 2006), that the majority of the chemical pathways (refer to Figure 2.5) in the combustion

process are dependent on the concentration of the hydroxyl (OH) group radical. Hence there would be a significant concentration of OH radicals at the flame front.

Studies with LIF for certain molecules like OH and CH have shown that the concentration of the species is directly proportional to the fluorescence signal level (Nguyen and Paul 1996). Imaging OH radicals using PLIF provides spatial localisation and determination of flame structure and motion which cannot be determined using chemiluminescence. This allows the examination of the physical processes responsible for the oscillatory response of the flame.

For the laser induced fluorescence of OH radicals a beam of a wavelength approximately 283 nm was needed. To achieve this, a combination of a pump and dye laser were used. The pump laser was an Nd:YAG laser (NanoPIV Litron Laser – marked Laser 1 in Figure 2.9), which was capable of producing a 532 nm beam with a pulse energy of 180 mJ and a pulse width of 5 - 6 ns. The dye laser (marked as Dye Laser 1 in Figure 2.9), was pumped by Laser 1 and was fitted with dye cells containing Rhodamine 6G dye and a frequency doubler. When the dye was fluoresced by the 532 nm beam it created a beam of wavelength 566 nm which is passed through a frequency doubling crystal, thus allowing the output wavelength to be tuned around 283 nm in order to pump the Q1 (6.5) transition of the $A^1 \sum - X^2 \prod(1,0)$ band. The excitation of OH radicals can occur at different excitation wavelengths/bands; however, this particular excitation wavelength/band was selected as the fluorescence observed here was less susceptible to changes in pressure and temperature. This will make the comparison between different flames more comparable as the flames can be burning at different temperatures. The fluorescence of OH radicals occurred at a wavelength of approximately 310 nm. This was captured using the UV-intensifier fitted camera (Camera 1) with a UV 100 mm f/2.8 Cerco lens and a combination of UG 11 and WG 305 Scott glass filters to allow the appropriate light in to the camera.

Phase locked OH PLIF images were used to generate 2-D plane images of the flame. These images were processed using gradient and threshold filters to determine the edge of the flame front. The raw images were corrected using the shot-to-shot variation in the laser intensity and beam profile. The relative intensity between the images was assumed to be related to the relative OH radical concentrations between different types of flames. An example of an instantaneous OH PLIF image is shown in Figure 2.6; it provides valuable information on the

shape of the flame and the relative spatial distribution of OH radicals within the flame.

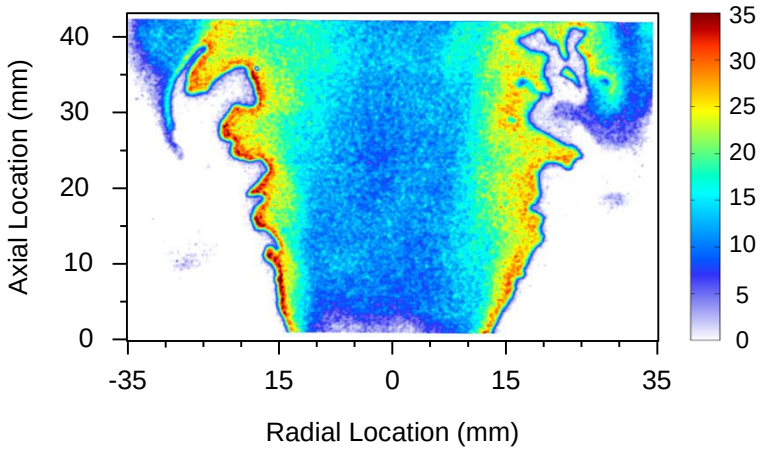

Figure 2.6: Example of an instantaneous raw OH PLIF image captured for imperfectly premixed ethylene flames.

Atomic Hydrogen (H) PLIF: As discussed in Chapter 1, atomic hydrogen is highly reactive and diffusive, and can play an important role in altering the combustion process. In this study no attempt will be made in making quantitative assessments of the radicals within the flame, however, a qualitative approach will be applied to analyse the flame. Information on the relative local concentrations will be gathered from the varying spatial intensities; however, actual concentrations will not be determined.

The method of mixing beams of varying wavelengths in a Raman shifting cell has been done in the past (Lucht *et al.* 1983); however, in this study a different approach was taken. Similar to the OH laser system setup a combination of pump and dye laser was used to produce the 205.1 nm beam required for the excitation of atomic hydrogen. The second Nd:YAG laser (LPY Litron laser marked as Laser 2) is a single shot laser capable of producing a 532 nm beam with a pulse energy of 1400 mJ with a pulse with of 5 – 6 ns. The beam was directed to a dye laser (Dye Laser 2) which used a dye, Rhodamine 101, which produced a beam around 615 nm when fluoresced. This beam was converted using a combination of a frequency doubler and tripler crystals to a wavelength of approximately 205.1 nm, which was needed to excite the hydrogen atoms within the flame. Fluorescence at 656 nm from

atomic hydrogen was collected using an f/1.2 50 mm Nikkor lens with an interference filter of centre wavelength (CW) 656 nm fitted on the visible intensifier connected camera (Camera 2). The camera exposure was set to a short time interval of 0.3 μs to reduce the interference from natural chemiluminescence of the flame.

To make sure that it was atomic hydrogen fluorescence that was being captured by the camera, the wavelength of the excitation beam was shifted by 0.1 nm which resulted in no fluorescence being detected. Also, to make sure that there were no spontaneous emissions from other radicals present due to the energy of the beam used, a simple experiment was setup to obtain H PLIF images of two types of flames using three different energy levels.

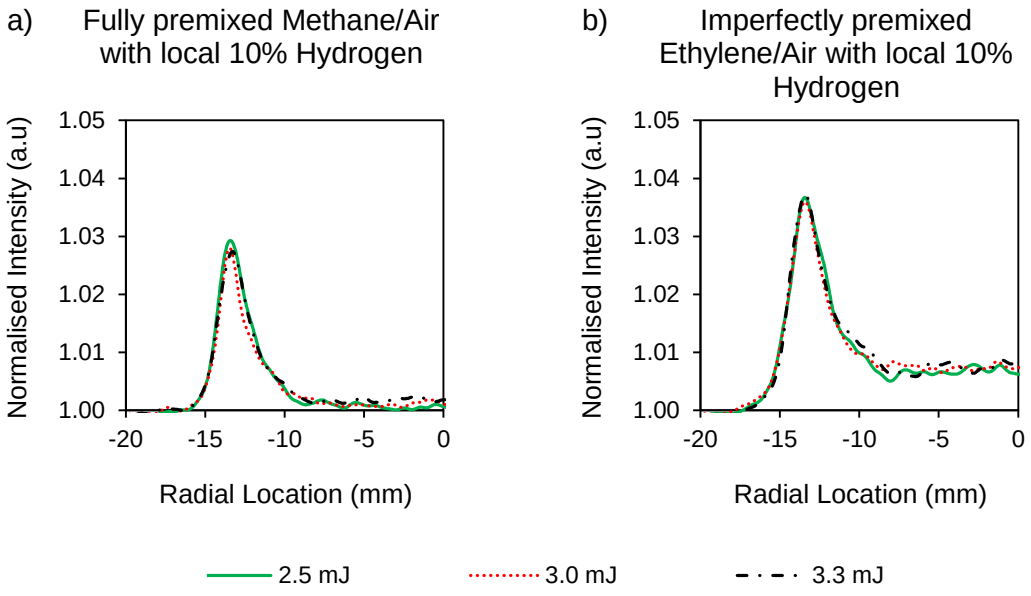

Figure 2.7: Plots of the normalised H PLIF intensity obtained for (a) fully premixed methane with 10% hydrogen flames, and (b) imperfectly premixed ethylene with 10% hydrogen flames, at three energy levels.

The two flames used were, fully premixed methane/air with the local addition of 10% (by volume) hydrogen and imperfectly premixed ethylene/air with local 10% (by volume) hydrogen addition. The three energy levels used were 2.5 mJ, 3.0 mJ and 3.3 mJ. The images obtained were averaged and the line profile of the intensity

at a certain height on the image was extracted and normalised to obtain the following plots in Figure 2.7 (a) and (b). The plots show the typical profile of the intensity of H PLIF of half of the flame at the same height from the base, at the three energy levels. It can be seen that the profiles obtained at the three energy levels for both the flames are nearly identical. The maximum difference between the peaks for both plots, Figure 2.7 (a) and (b), are 6.9% and 3.3%, respectively.

2.2.4 Particle image velocimetry (PIV)

Particle image velocimetry (PIV) is a laser technique used to capture the motion of a flow. It is used to capture instantaneous velocity and other properties of a flow field. PIV is based on the scattering of laser light from tracer particles seeded within the flow. The light reflected from these particles is captured with a camera on a sequence of frames and is used to track the particles as it moves along in the flow. The displacement of the particles is determined from the evaluation of the PIV recordings.

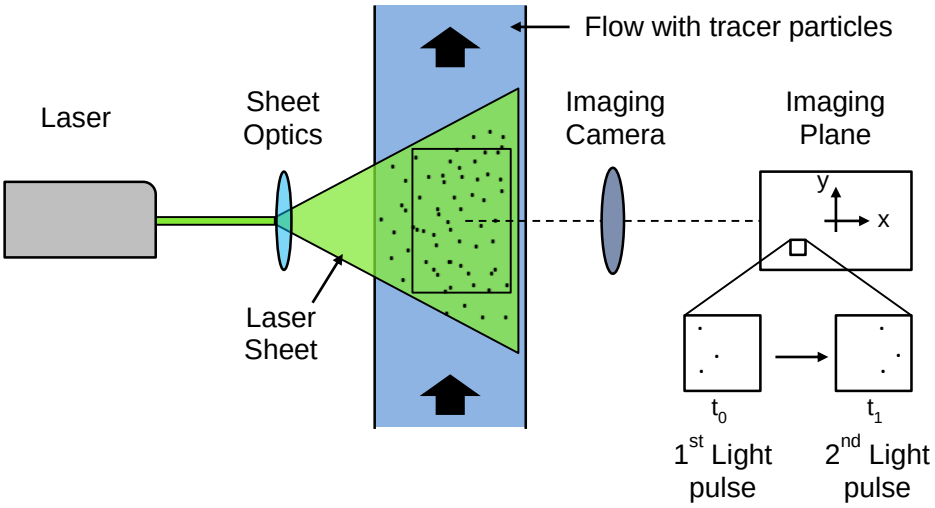

Figure 2.8: Illustration of a simple PIV setup.

A basic experimental setup is shown in Figure 2.8, it consists of a dual pulse laser, a double-shot camera and some optics to direct and convert the laser beam in to a light sheet. The flow was seeded with tracer particles (in this case olive oil)

generated from a particle seeder. The two beams from the laser are made in to a sheet using a combination of optics and were then directed to pass through the flow. Depending on the approximate flow velocity the delay between the two laser-pulses was chosen to be 25 µs to allow for an adequate displacement of the particles between the two illuminations. These illuminations were captured using a double-shot camera fitted with a 50 mm f/1.2 Nikkor lens.

In order to generate velocity vectors of the flow the two images were divided into small subareas called interrogation windows (32 x 32 pixels). The size of the window was selected such that all the particles within this area moved homogeneously with the same velocity. Using an FFT correlator the illuminations of the particles within the flow were detected on both frame and a single vector was generated using the distance calculated and knowing the time delay between each image.

PIV was used in this study to investigate the cold flow characteristics such as the velocity and turbulence, at different operating conditions. Changes in the turbulence could affect the mixing properties of the air and fuel thus affecting the combustion processes. Maintaining the same level of turbulence between the flames was important as the study was focused on understanding the fuel effects rather than the flow effects. PIV was also used to show how the flow changes with acoustic forcing. The flow pattern, at different phase angles of the acoustic forcing are presented to show how the periodic alteration of the recirculation zones and shear layers can affect the flame shape.

2.2.5 Laser tomography

Laser tomography is similar to PIV in the sense that it relies on the illumination of tracer particles seeded in the flow. However, the objective of this technique is not to obtain velocity vectors but to identify the boundary between the reactants and burnt products within the flow to generate a 2-D contour of the unburnt air/fuel mixture in the combustion chamber. These images were used to extract the flame front of the flames during the self-excitation tests. This system was preferred to the OH PLIF system as it is a high speed laser and camera system capable of capturing the unburnt flow structure at a frequency of 3000 Hz. The system included a Pegasis laser (Laser 3 in Figure 2.9) capable of pulsing 532 nm

beams at a maximum of 10,000 Hz and a Photron camera capable of capturing images at a maximum rate of 20,000 frames per second (fps). More details on the technique are presented in Chapter 6.

2.2.6 Optical systems setup

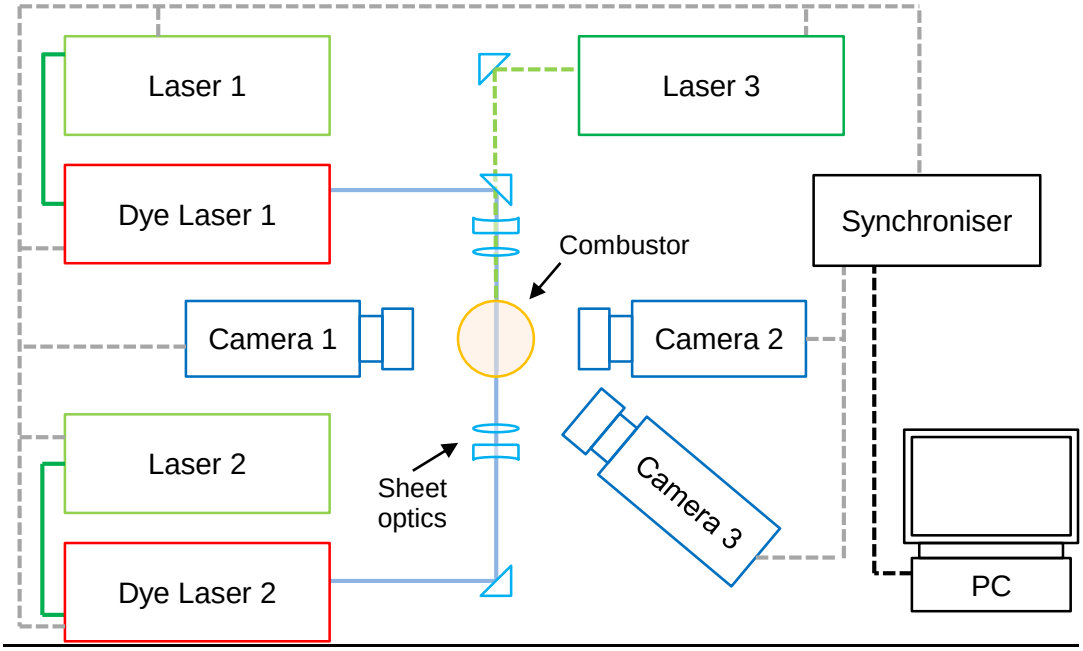

Laser 1: Litron Nano PIV Output: 532 nm	Camera 1: UV Intensified CCD camera Lens: f/2.8 Cerco 100 mm
Laser 2: Litron LPY Output: 532 nm	Camera 2: Visible Intensified CCD camera Lens: f/1.2 Nikkor 50 mm
Laser 3: Pegasus Output: 532 nm	Camera 3: Photron High speed camera
Dye Laser 1: Hydroxyl (OH) PLIF Dye: Rhodamine6G Output: 283 nm	Dye Laser 2: Atomic Hydrogen (H) PLIF Dye: Rhodamine 101 Output: 205 nm

Figure 2.9: Layout of the combustion testing cell, showing the laser, camera and PMT arrangements.

Figure 2.9 shows the layout of the equipment and combustion rig in the testing cell. For the laser based imaging, the beams for OH PLIF and laser tomography were made in to a thin collimated light sheet of 50 mm height, while the

beam for H PLIF was 7.5 mm high, using a combination of a plano-concave and a biconvex lens. The images for PLIF and PIV were phase-locked using the input signal for driving the acoustics speakers. Figure 2.10 shows a plot of how the laser and camera triggers were timed using the reference signal (i.e. the input signal to the acoustic speakers). The laser and camera pulse delays were introduced to shift to other phases to be imaged. For shot-to-shot variations in the energy of the laser beam, photodiodes were placed to record the intensity of each beam simultaneously with the imaging.

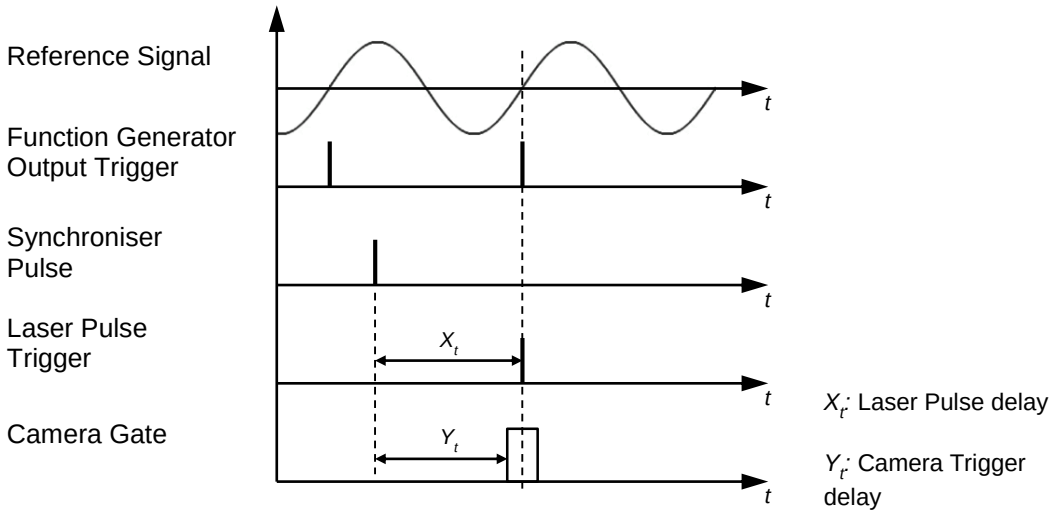

Figure 2.10: Plots for the laser and camera trigger pulses relative to the reference signal.

2.2.7 Exhaust emission composition

The composition of the burner exhaust gas was analysed by measuring the percentage concentration of CO_2 and the parts per million (ppm) of NO_x chemical species using an exhaust gas analyser rack (Horiba MEXA 9100 HEGR). A stainless steel probe of inlet diameter 25 mm was held 120 mm downstream of the bluff-body on the central axis. This probe allowed the flow of exhaust gas to the analyser, where the gas sample was first filtered for particulates, and water vapour was allowed to condense. Readings of exhaust gas composition by the analyser

were recorded through LabView on a PC via an output interface from the analyser control unit.

2.2.7.1 CO_2 measurements

CO_2 measurements were carried out using the method of non-dispersive infrared absorption. The degree of infrared absorption by the CO_2 gas molecule was directly proportional to the level of concentration of CO_2 molecules in the gas sample (assuming mixture pressure and temperature being constant).

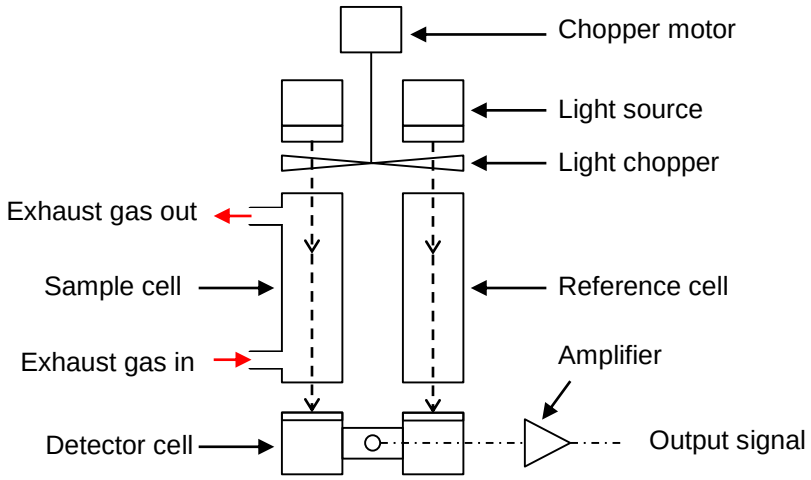

Figure 2.11: Shows the schematic of the detecting equipment used for analysing the exhaust gas for CO_2.

The method in which the CO_2 analyser (Horiba AIA-120) operated can be explained from Figure 2.11, which shows a schematic of a basic detector system. A light source of a particular wavelength was made to pass simultaneously through two gas cells placed parallel to each other. One cell contained the sample gas to be measured and the other cell contained an infrared-inactive gas as a reference. The infrared beams passed through the gas cells and were collected at the exit by detector cells. The intensities of the beams were compared and an output signal related to a CO_2 concentration look-up table was produced. The signal was then amplified and sent through to the computer to be recorded (for detailed information refer to Hellier 2013).

2.2.7.2 NO_x measurements

The NO_2 analyser (Horiba CLA-150) measured the concentration of NO_2 species using a method involving the formation of excited radicals from chemical reactions and the spontaneous emission of light/photon through the loss of energy to reach its ground state (chemiluminescence). The sample gas was passed through a heated catalyst causing it to dissociate according to the following chemical reaction:

$$NO_2 + C = NO + CO$$

The gas was then reacted with ozone (O_3) where 10% of the NO_2 formed was in an electronically excited state NO_2*:

$$NO + O_3 = NO_2^* + O_2$$

Where '*' denotes the excited state of the molecule NO_2. This excited molecule rapidly decayed to its ground state with the spontaneous emission of light:

$$NO_2^* = NO_2 + hv$$

Where h is the plansk constant and v is the frequency. A photomultiplier tube measured the chemiluminescence of the reaction which was proportional to the amount of NO_2 present in the gas sample. The analyser unit was fitted with a vacuum pump so that the above reactions could take place in a chamber with reduced pressure conditions. This minimized the collisions between excited NO_2* radical species and other molecules prior to their decay and hence reducing the interference that could occur due to the presence of other molecular species in the gas mixture.

2.3 Data analysis

2.3.1 Flow analysis

As mentioned earlier, pressure transducers were placed in the combustor to measure the velocity perturbations. The pressure signals from the transducers were analysed using the two-microphone technique to calculate the normalised velocity fluctuation, $u'/\langle U \rangle$, at the inlet to the combustion chamber. This technique was based on the relationship of the pressure wave propagation and its speed of propagation. The speed of propagation is the speed at which the wavefront of an acoustic signal travels through a medium (in this case air), relative to the speed of light. This speed can be influenced by a mean or fluctuating flow. The relationship between the pressure and the flow was used to calculate the normalised velocity fluctuation, $u'/\langle U \rangle$; for a detailed explanation and list of calculations please refer to Seybert and Ross (1976).

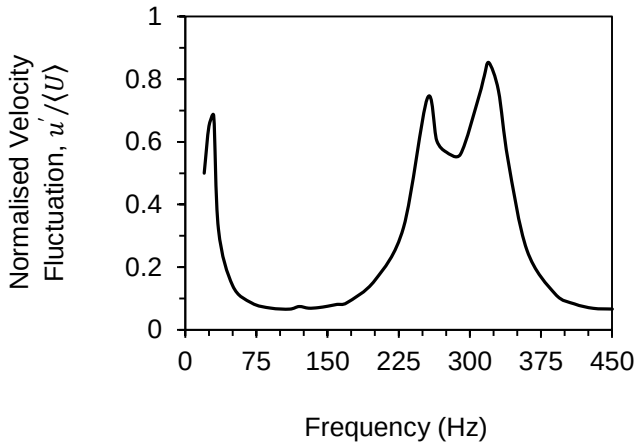

Figure 2.12: Frequency response of the combustor subjected to acoustic forcing.

With the speaker, amplifier and function generator, and combustor geometry configuration the arrangement was tested to understand at which forcing frequencies were large velocity fluctuations at the entrance to the combustion zone achieved. With a constant air flow rate of 250 slpm the flow was perturbed at a fixed input voltage to the speakers and the frequency was varied from 20 to 450 Hz in steps of 10 Hz. Figure 2.12 shows the response of the combustor and it can be

seen that the maximum velocity perturbations occurred at frequencies of 30, 255 and 315 Hz. During forcing conditions the flames were studied under these three forcing frequencies as large magnitudes of velocity fluctuations were needed.

Particle image velocimetry was performed to gather information on the flow field within the combustion chamber. The flow field analysis was only done on cold flow with varying quantities of air volume flow rate and under forced conditions to show the development of the counter rotating vortex pair.

The processing of the PIV images was performed using Insight^{TM} 3G; a software that used FFT (Fast Fourier Transform) to locate the particles and track them from image to image. The images were first adjusted for distortion, background and were calibrated using a known target placed in the combustion chamber. The software divided the images into interrogation windows of 32 pixels by 32 pixels. Locating and comparing the two images that were imaged with a time interval of 25 µs (Figure 2.13 (a)) and averaging over a hundred vector fields generated an average vector field as shown in Figure 2.13 (b). The vector field was used to gather several parameters of the flow.

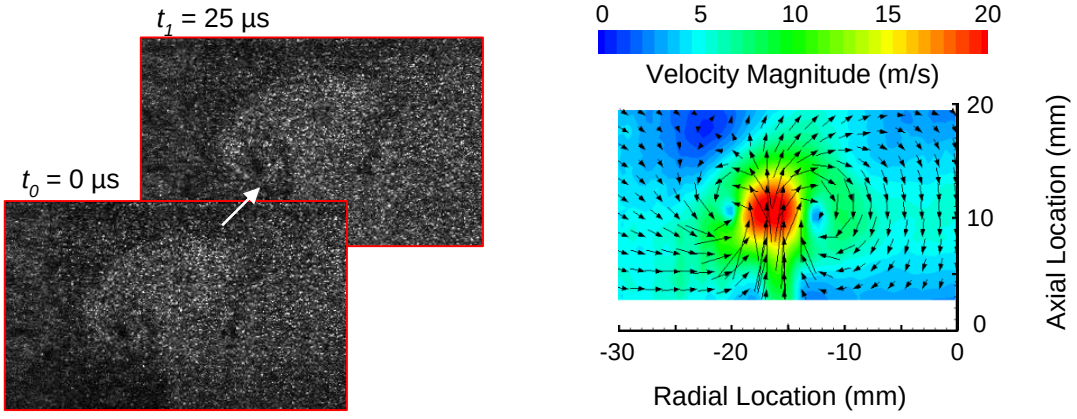

(a) (b)

Figure 2.13: Shows (a) two instantaneous PIV images, which were processed with a series of images to produce (b) an averaged contour plot of the velocity magnitude and the vector field.

The velocity magnitude and turbulence were calculated and values were extracted at heights of 5, 10, and 15 mm from the base of the combustion chamber.

The velocity gradient was also computed to visually see the regions where the flow experienced large amounts of shear, as these regions were favourable for flame stabilisation.

2.3.2 Global heat release fluctuation

The graph in Figure 2.14 (a) shows that the pressure, p, and OH* chemiluminescence signal had a cyclic response under acoustic forcing. Using a Fast Fourier Transform (FFT) technique the spectral time traces of OH* were analysed to evaluate the complex amplitude of the quantity, $OH^{*\prime}$, at the forcing frequency, f. This value was normalised with the time averaged mean $\langle OH^{*} \rangle$ to obtain $OH^{*\prime}(f)/\langle OH^{*} \rangle$. As mentioned earlier, these normalised values were used to represent the heat release fluctuation, $Q'(f)/\langle Q \rangle$.

Figure 2.14 (b) plots the dependence of the global heat release fluctuation, $Q'(f)/\langle Q \rangle$, on the normalised velocity oscillations, $u'/\langle U \rangle$, for two different forced flames (i.e. imperfectly premixed ethylene and fully premixed methane), measured at two separate instances (i.e. Test 1 and Test 2). The two instances were carried out on different days. The purpose of conducting the experiment twice was to show that the measurements were repeatable. For the imperfectly premixed ethylene there was negligible difference in the readings, and with the fully premixed methane flames the maximum difference was 1.7%. Overall other OH* chemiluminescence tests did not show large differences in the readings.

Using the normalised heat release oscillation quantity, $Q'(f)/\langle Q \rangle$, with the velocity perturbations, $u'(f)/\langle U \rangle$, determined from simultaneous pressure oscillation measurements it was possible to determine the flame describing function, FDF, (also known as flame transfer function, FTF) defined by:

$$FDF(Q,U) = \frac{Q'(f)/\langle Q \rangle}{u'(f)/\langle U \rangle}$$

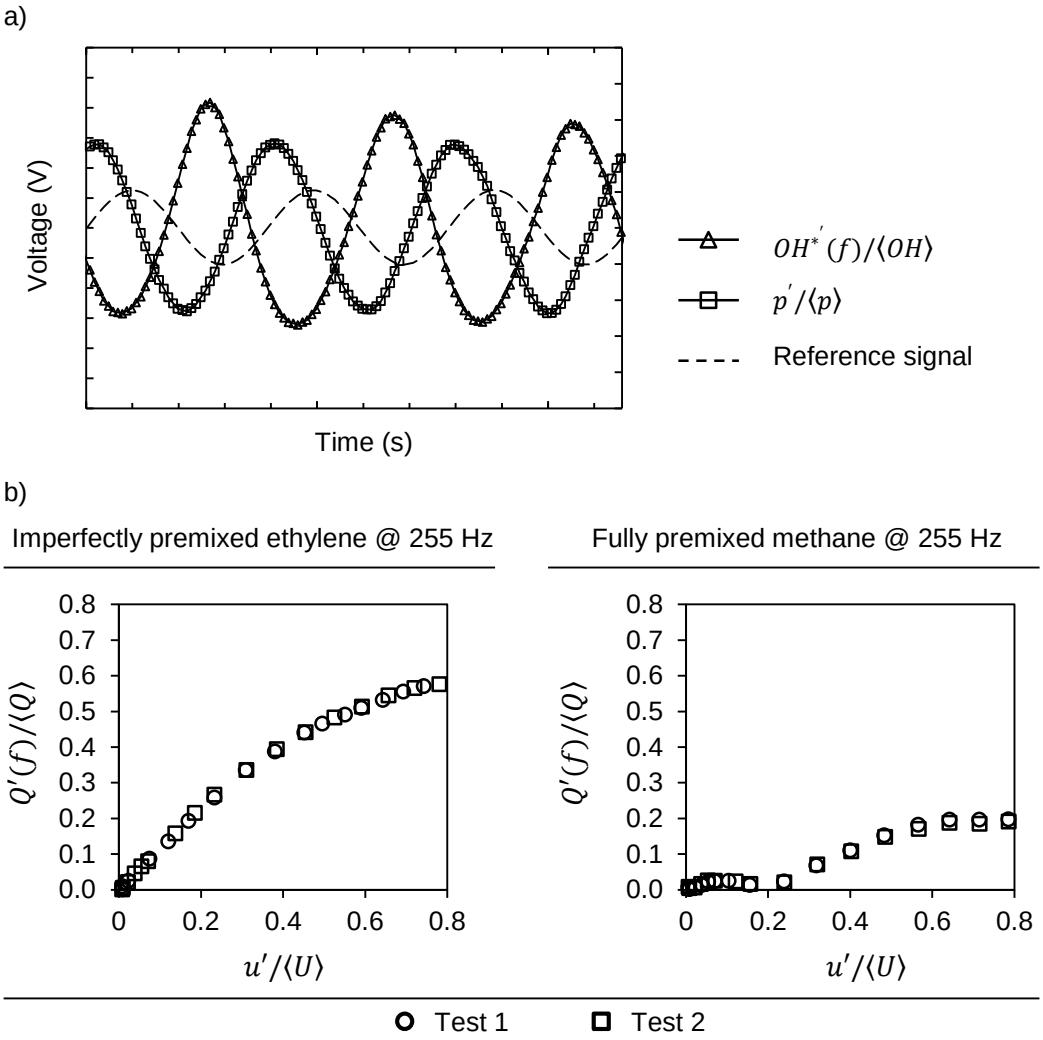

Figure 2.14: (a) Time series of normalised reference signal, acoustic pressure, and OH* chemiluminescence signal during combustion. (b) Shows the dependence of the global heat release (determined from the OH* chemiluminescence), on the normalised velocity perturbations, for two flames measured at two different times (Test 1 and 2), to show the repeatability of the measurements.

2.3.3 Image processing

The raw images of OH and H PLIF were put through several processes before being used to extract information on the flame. The following, lists and details each processing step used to make the images suitable for analysis.

Background noise

The raw PLIF images were initially corrected for background noise. The noise in the background was mainly generated due to the scatter of the laser light in the room and the reflection of the laser light on the quartz cylinder. During experimentation, the flame and flow were switched off and the cameras were used to capture images of the combustion zone with the lasers switched on. One hundred images were captured and averaged to produce an averaged background image as shown in Figure 2.15. A hundred images were captured and averaged to remove any bright spots that may have been captured due to laser light reflecting off dust in the environment. This image shows the laser reflection on the quartz cylinder and a general increase in the background light from one corner of the image. This light was due to the light scatter from the mirrors which directed the 532 nm beams into the dye lasers. Background images were captured for each fuel flow condition and for both OH and H PLIF images. The background images were subtracted from the raw images of OH and H.

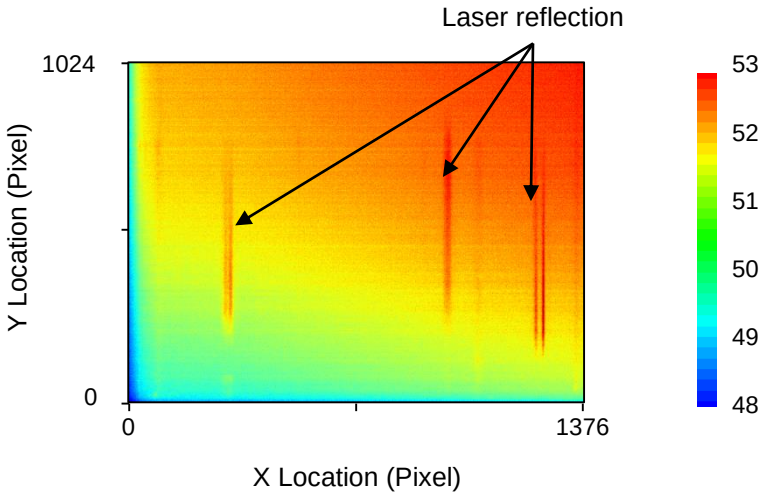

Figure 2.15: Shows an averaged background image captured for OH PLIF image correction.

Beam profile correction

The laser beam from both dye lasers (i.e. OH and H PLIF dye lasers) were not uniform in energy over the entire beam profile. This led to a spatial variation in the fluorescence detected for OH and H PLIF. To correct for the beam energy in-

homogeneities, a beam profile correction technique was applied for all the background subtracted raw images.

Acetone can be fluoresced using the same beam used for OH PLIF. To obtain the OH beam profile, vaporised acetone was fed into the combustion chamber and images were captured of the fluorescence. Assuming that the distribution of the acetone was uniform, the profile of the beam was extracted and inverted to generate the beam profile correction image. This image was then multiplied with all the raw images of the flames to correct for the beam profile.

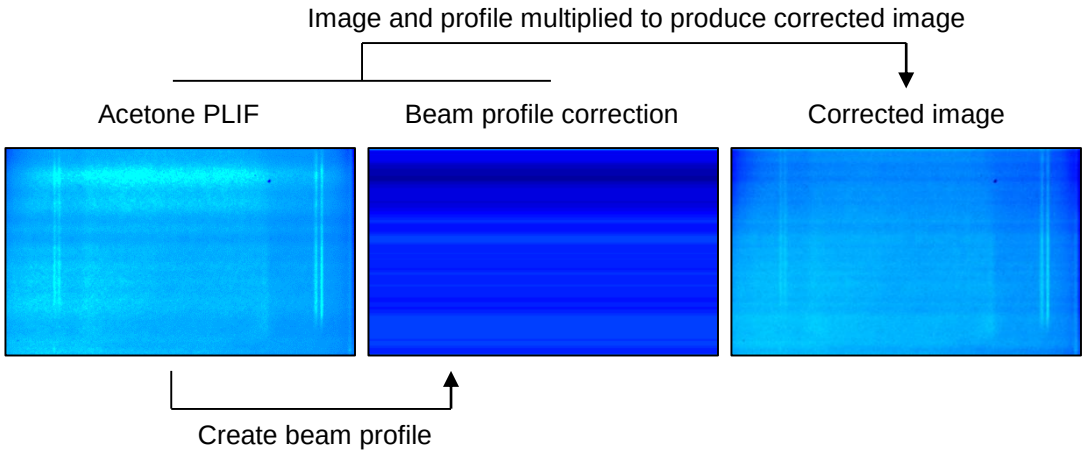

Figure 2.16: Shows the acetone PLIF, the beam profile generated and the corrected image.

The beam profile correction image for H PLIF was created using a laser burn paper. The burn paper was placed in the combustion zone in the path of the beam. Due to the high energy of the laser sheet the burn paper fluoresced and this fluorescence was captured with the cameras giving a line profile of the laser sheet. The burn paper was placed in several positions in the combustion chamber to produce several line profiles. These profiles were extrapolated to produce the beam profile correction for H PLIF.

Shot-to-shot variation

Two photodiodes were placed in the testing area to measure the relative changes in beam energy during PLIF imaging. Using this variation each image was corrected for the fluctuations in the beam energy.

2.3.3.1 Flame boundary and surface area

The images of instantaneous OH PLIF and laser tomography were recorded to obtain the flame boundary and surface area. As mentioned in the previous paragraphs, the raw OH PLIF images were initially corrected for inherent noise; first a background noise subtraction was performed; second, a beam profile correction was applied to account for in-homogeneities in the beam; and finally, the images we corrected for the shot-to-shot variation of the laser beam energy.

To convert the images into binarised images of black and white regions where the black regions show the burnt gas (Figure 2.17) a binarisation algorithms based on Otsu's method was used (Otsu 1979). This method converts the image to a grayscale image and uses an iterative process to calculate a measure of spread for the pixel levels each side of the threshold, i.e. the pixels that either fall in the foreground or background. The measure of spread being calculated is the sum of weighted variances which is referred to as the 'Within Class Variance'. This quantity is calculated for each threshold value applied to the image, and it is the threshold that produces the lowest sum of weighted variances that is selected for identifying the products and reactants in the image. For more details please refer to Appendix A for a simple example and list of formulas used in the Otsu algorithm (Otsu 1979).

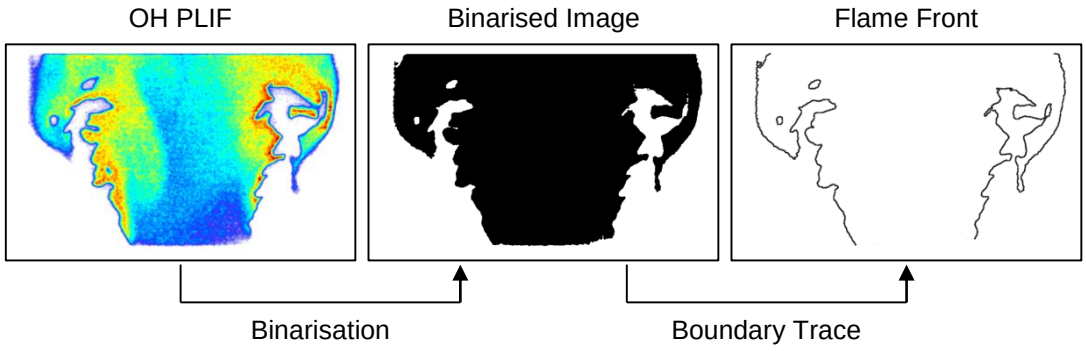

Figure 2.17: Image shows the order of processing steps taken to detect the flame front from an OH PLIF image.

The binarised images were put through a boundary trace function which produced an image of a single pixel thick flame front. The flame front images were revolved around the central axis to produce a 3-dimensional contour of the flame

which, when multiplied by the resolution (55 µm per pixel), gave the flame surface area.

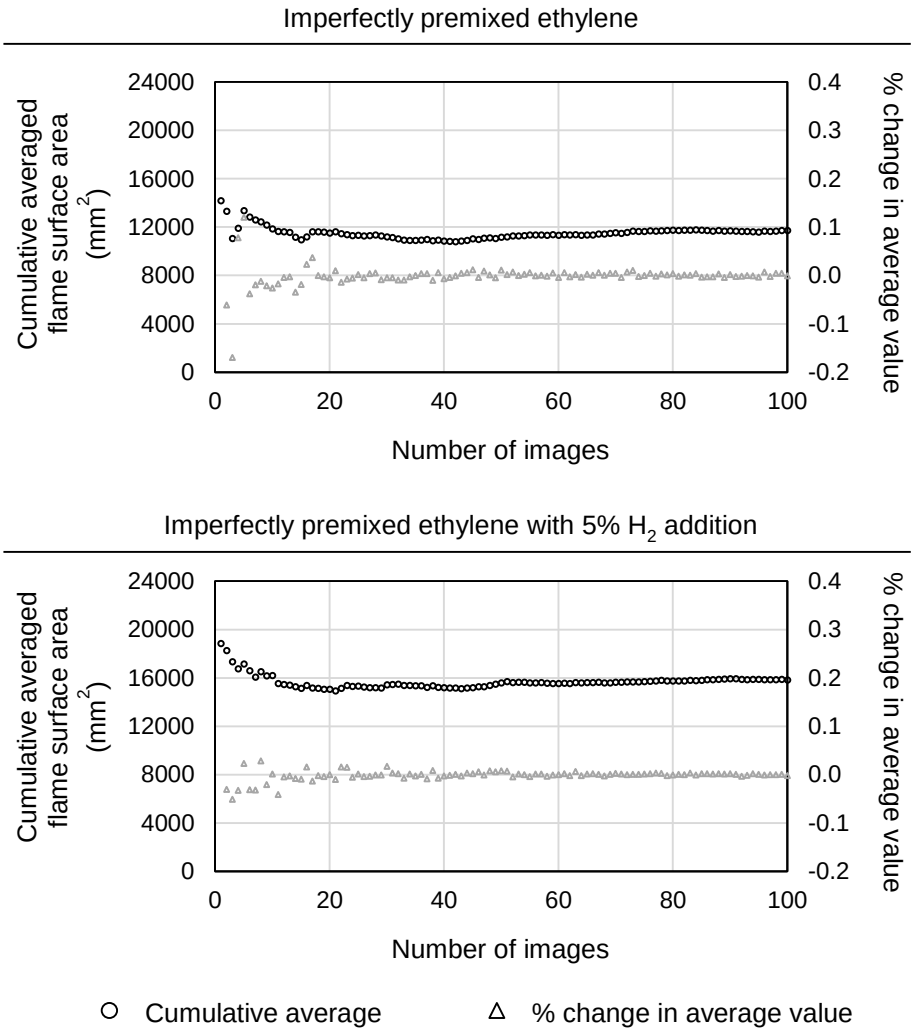

Figure 2.18: Shows the cumulative average of the flame surface area and its percentage change for two types of flames. Flames were forced at f= 255 Hz, and $u'/\langle U\rangle$= 0.4.

For each experimental condition, one hundred images were recorded to generate an average image for each variable (i.e. PLIF intensity and flame surface area). Capturing one hundred images minimised the variation in the average values obtained; which can be deduced from the plots in Figure 2.18. The graphs show the cumulative average of the flame surface area for two different flames, imperfectly

premixed pure ethylene and ethylene/hydrogen flames, acoustically forced and phase locked at 60° and 90°, respectively. The cumulative average fluctuates during the first 20 images but then levelled out. This shows that the data collected from the average images was representative of the flames.

For the imperfectly premixed ethylene flames the threshold value calculated was varied ±10% to see the effects on the final mean flame surface area. The maximum variation was 0.4% and 1.22%, for +10% and -10%, respectively. This shows that the method of calculating the threshold value was robust and it effectively identified the regions of products and reactants.

From these images only the data obtained from the left hand side of the flame was used. Specific regions were specified as Region A, B and C, which are shown in Figure 2.19, where the total flame surface area in these regions were summed up. Region A (2.5 mm to 15 mm from the base) and Region B (25 mm to 40 mm from the base) were chosen specifically to measure the flame surface area of the initial and developed size of the flame roll-up, and how this changed with hydrogen addition. Region C (2.5 mm to 45 mm from the base) measures the entire imaged region which gave an overall view of the changes brought about with the introduction of hydrogen.

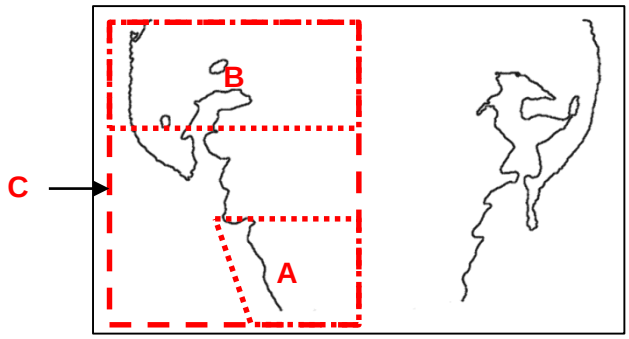

Figure 2.19: Shows the regions A, B and C on a flame front image.

2.3.3.2 Image averages

For visual comparison the OH and H PLIF images were put through the necessary corrections mentioned earlier and then individually averaged. These images provided information on the relative changes in OH and H PLIF signal intensity in the flame at different air and fuel compositions and acoustic forcing. The

signal-to-noise ratio was 2.28 and 1.49 for OH and H PLIF, respectively. The signal of the H PLIF was relatively lower which is why the OH PLIF images were mainly used for the bulk of the analysis. A similar cumulative average analysis was carried out on the OH PLIF signal of the flame and the plot is shown in Figure 2.20. The plot is self-explanatory, showing that the average images created from one hundred images would be representative of the flame.

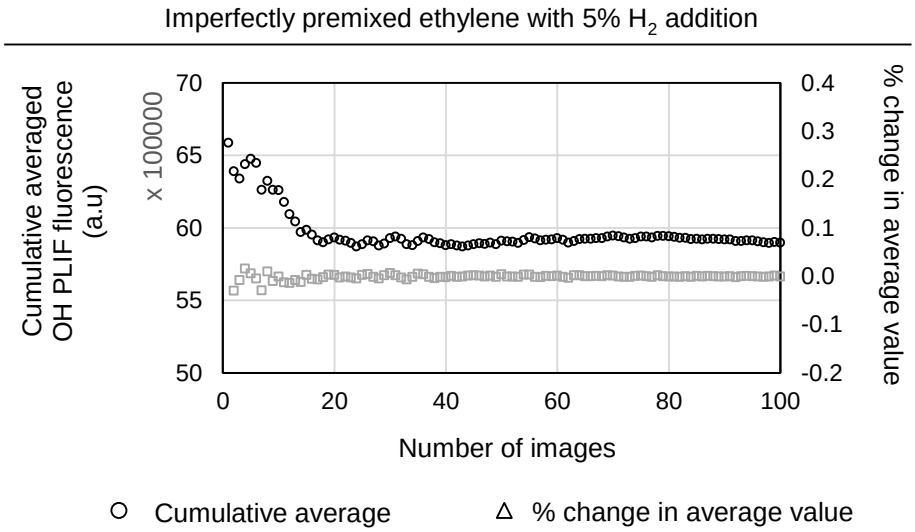

Figure 2.20: Shows the cumulative average and its percentage change of the OH PLIF signal for an imperfectly premixed ethylene flame with 5% H_2 addition, at f= 255 Hz, $u'/\langle U \rangle$= 0.4, and phase 90°.

2.3.3.3 Power spectral density plots

During the testing two signals required further analysis. First, was the signal obtained from the global OH* chemiluminescence and the second was obtained through the flame surface area analysis. The summed up value of the flame surface area in the three regions A, B and C were used to track the change in the quantity with phase during forcing conditions. This data produced a wave as shown in Figure 2.21.

Both these signals were put through fast Fourier transform (FFT) and the power spectral density (PSD) was calculated. This was plotted against the

frequency to provide a breakdown and show the dominant frequencies of oscillations.

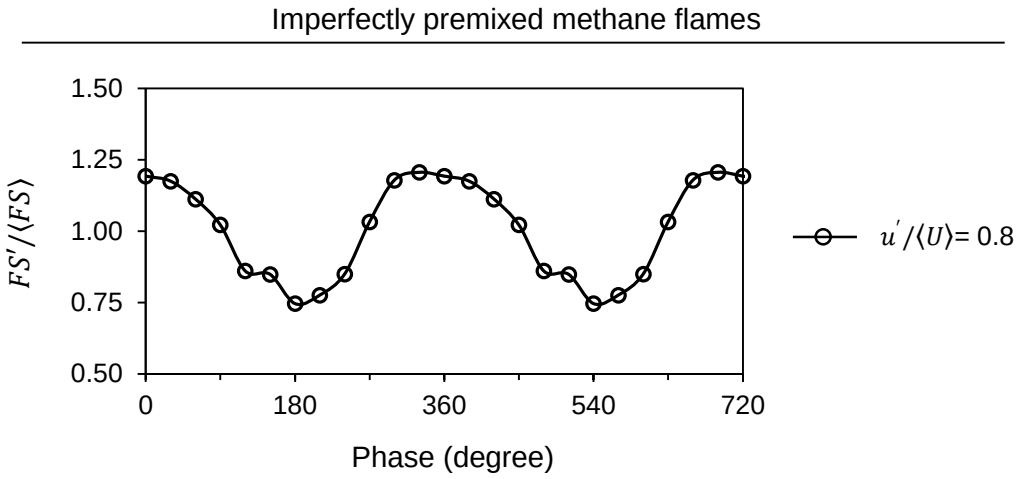

Figure 2.21: Example of a plot of the normalised flame surface area obtained from the boundary images. The data is of an imperfectly premixed methane flame at ϕ_{Global}= 0.70, f= 255 Hz, and $u'/\langle U\rangle$= 0.8.

Chapter 3: Cold flow analysis

3.1 Introduction

Particle image velocimetry (PIV) was used to obtain the velocity fields for the flows within the combustion chamber. Although, the measurements were performed on non-reacting flows it gave an insight in to the formation of recirculation zones and counter rotating vortices created in the wake of the step and bluff-body under unforced and forced operating conditions. As shown in Figure 1.2 in Chapter 1, there were two distinct zones created in the combustion zone due to the presence of a step and bluff-body, namely, the central and outer recirculation zones. The gases in these zones consisted of recirculating hot combustion products which interacted with the fast moving unburnt mixture to create shear layers on which flame stabilisation occurred. The shears layers sustained the flame by creating a flame stabilisation point. Any alteration to these shear layers could alter the burning characteristics such as the flame shape and the heat release response (Zhang *et al.* 2011). As mentioned in Chapter 1, during self-excitation the formation of large scale coherent vortices developed at the entrance of the combustion zone, thus altering the shape of the shear layers, and grew until it collided with the wall to break down in to small scale vortices. The purpose of the chapter is to understand the different flow regions in the combustion zone and how forcing affects these regions.

3.2 Experimental conditions

The experiments conducted using the PIV imaging technique were divided between unforced and forced flow conditions. With the unforced operating conditions the flow field in the combustion chamber was recorded at different air volume flow rates. The range of the volume flow rates used was from 180 to 420 slpm which equated to a range of 6.37 to 14.65 m/s for the bulk air flow velocity. The bulk air flow velocity was calculated using the volume flow rate and the area of

the entrance into the combustion chamber (i.e. the area of the duct at Ø35 mm minus the area of the bluff-body at Ø25 mm). The results obtained show how the axial and radial velocities, and the fluctuation in these quantities changed with increasing air bulk flow velocity under unforced conditions. The results were used to select the single air volume flow rate that would be used throughout the project.

In the second part of the study the air volume flow rate was fixed and the flow was acoustically forced at a forcing frequency of 255 Hz and with a normalised velocity perturbation of approximately 0.8. Phase-locked images were captured for the flow field and are presented in the analysis section.

3.3 Unforced flow field analysis

The initial experiments conducted on the cold and unforced flow was to visualise the flow within the combustion chamber. Figure 3.1 shows an averaged vector flow field and a velocity magnitude contour flood plot for an air flow rate of 250 slpm. The image shows a nearly symmetric flow with the presence of the central recirculation zone (indicated by the red circles). The profiles of the axial velocity, u, its turbulence, u_t, were extracted at heights of 5, 10 and 15 mm which produced the plots in Figure 3.2.

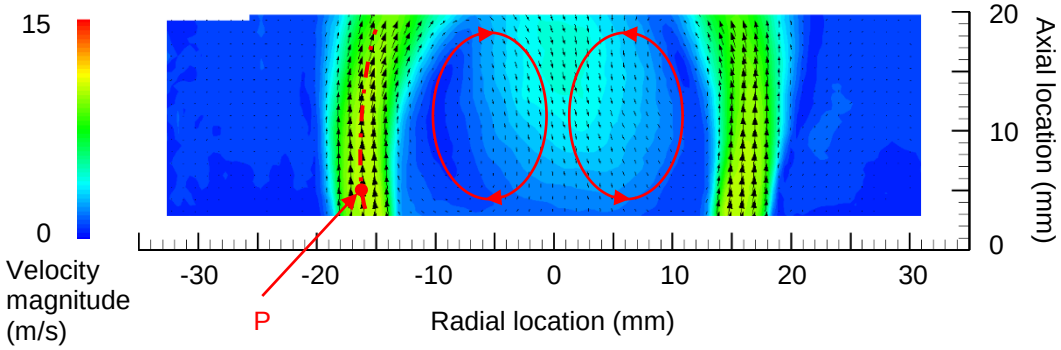

Figure 3.1: Shows the vector and flood plot for the velocity magnitude of the flow field within the combustion zone at an air volume flow rate of 250 slpm.

With increasing axial position the downward axial velocity as well as the peak axial velocity turbulence close to the central axis increased. This indicated that

there could be an increase in the rate of turbulent distortion of the flame surface with an increase in axial position (Kwon *et al.* 1992).

From numerous studies which use bluff-bodies or other bodies to generate recirculation zones (Abdalla *et al.* 1981, Sivasegaram and Whitelaw 1991, Balachandran *et al.* 2005, Birbaud *et al.* 2008, Robin *et al.* 2008, Lee 2009, Tran *et al.* 2009, and Zhang *et al.* 2011), the flame was generally known to stabilise on the shear layer formed in the flow.

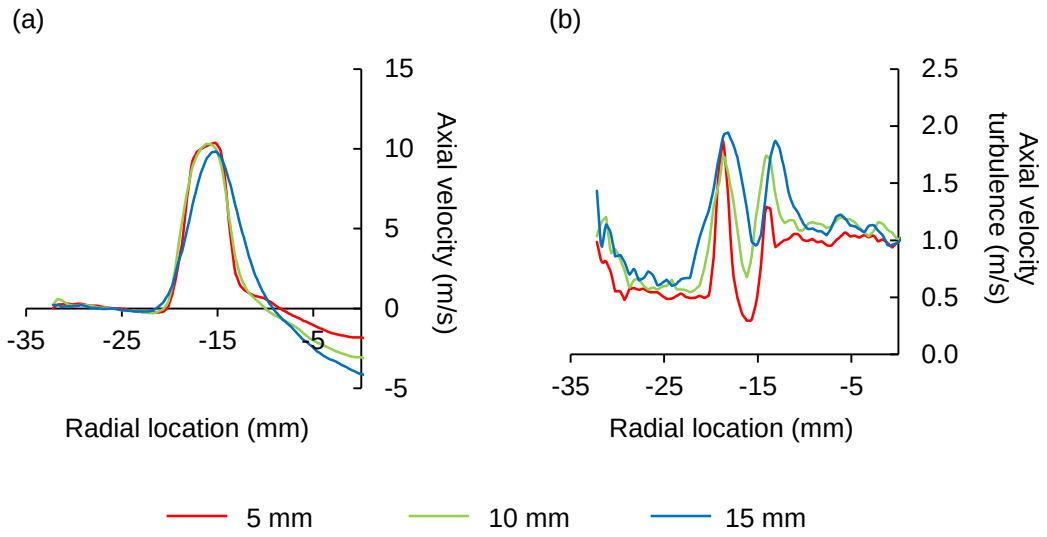

Figure 3.2: Plots of the (a) axial velocity and (b) axial velocity turbulence measured at 5, 10, and 15 mm from the base of the combustion zone.

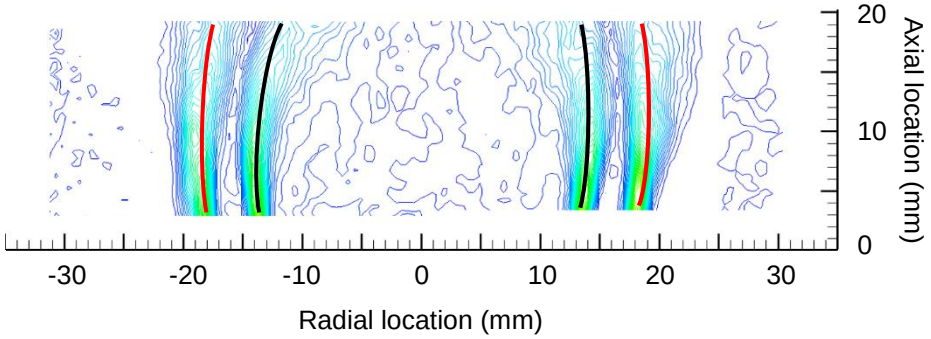

Figure 3.3: Spatial plot of the calculated velocity gradient of the flow in the combustion chamber at an air volume flow rate of 250 slpm.

The shear layer was formed by the interaction between the high velocity jet and the slow moving recirculation zones. In this particular case, with an air volume flow rate of 250 slpm, Figure 3.3, shows the contour lines for the velocity gradient. The inner and outer shear layers are clearly visible in the region of the highest velocity gradient. The inner shear layers are marked with black lines while the out shear layers are marked with red lines. The velocity gradient was highest near the base of the combustion chamber, hence there was a higher level of shear within the flow closer to the base. Although, shear layers provide a location for flame stabilisation, it was not necessary for the flame to stabilise on these layers, and as the shear in the flow reduced moving downstream, it may not provide an optimum stabilisation point for the flame.

The axial and radial velocity turbulence, u_t and v_t, values were extracted on the central axis of the jet entering the combustion chamber at the red point marked 'P' in Figure 3.1. Figure 3.4 shows the plot of u_t and v_t at 5 mm for the bulk air flow velocities that were used.

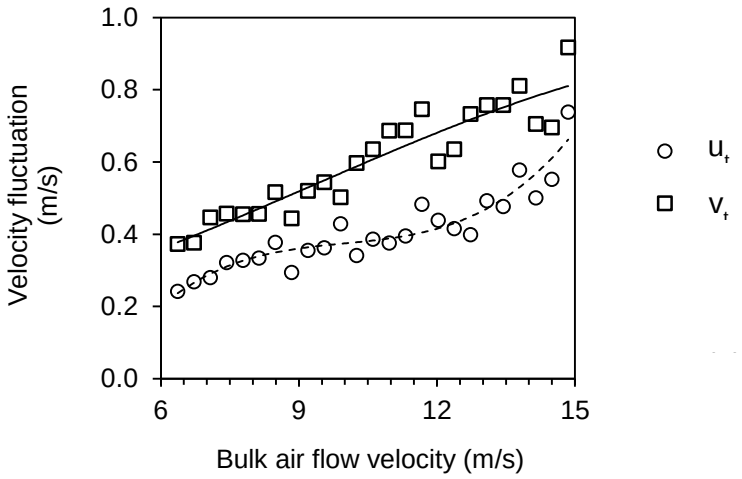

Figure 3.4: Plot shows the axial velocity turbulence, u_t, and radial velocity turbulence, v_t, measured on the central axis of the incoming flow at a height of 5 mm from the combustion zone.

From the graph we can see a steady increase in the axial velocity turbulence, u_t, and radial velocity turbulence, v_t, as the flow rate was increased. The axial velocity turbulence trend line shows a steady increase and then a plateau

before it started to rise again. As the axial velocity turbulence was of interest for the acoustic measurements, the bulk air velocity of 8.84 m/s (i.e. the air volume flow rate of 250 slpm) was selected as the turbulence of the axial velocity lies on the plateau of the trend line, so relatively small additions of fuel flow would have a lower impact on the flow turbulence at the inlet of the combustion zone. This air volume flow rate was selected for all the further cold and hot flow tests.

3.4 Acoustically forced flow analysis

The effects of acoustic forcing on the shear layers in the flow have been studied in detail in the past (Balachandran *et al.* 2005, Kulsheimer and Buchner 2002, Poinsot *et al.* 1987, Yu *et al.* 1991). These studies have shown that under certain forcing frequencies and velocity perturbations the shear layers roll up to form coherent vortex rings, which inherently affected the shape of the flame. In this particular study under a high forcing frequency of 255 Hz and a normalised velocity perturbation of approximately 0.8, the outer and inner shear layers rolled up creating a counter rotating vortex pair. Figures 3.5 and 3.6 show the vector flow field, velocity magnitude and vorticity contour flood plot for the forced flow, in steps of 40°. The images show the how the vortex pair developed at the base of the combustion zone and moved further downstream while increasing in size.

The sequence of images clearly show that the vortices grew in size as it moved downstream. As the large vortices moved out of the imaged area a new vortex pair formed at the base of the combustion chamber and this process repeated for every forcing cycle. Not only that, but there was a clear change in the shear layer formation with the presence of the counter rotating vortex pair.

Figure 3.7 shows the velocity gradient of the flow at a phase angle of 280°, which shows how the gradient profile changed under forcing conditions. The shear layer had clearly been deformed which could alter the shape of the flame in the way represented by the red lines.

The peak axial velocity measured along the central axis of the jet for all phases has been plotted in Figure 3.8. From this graph it can be seen that the axial velocity underwent a periodic variation. The peak velocity achieved was 22.4 m/s and the lowest velocity was 4.4 m/s with a mean velocity of 11.07 m/s, which resulted in an approximate normalised velocity perturbation of 0.81.

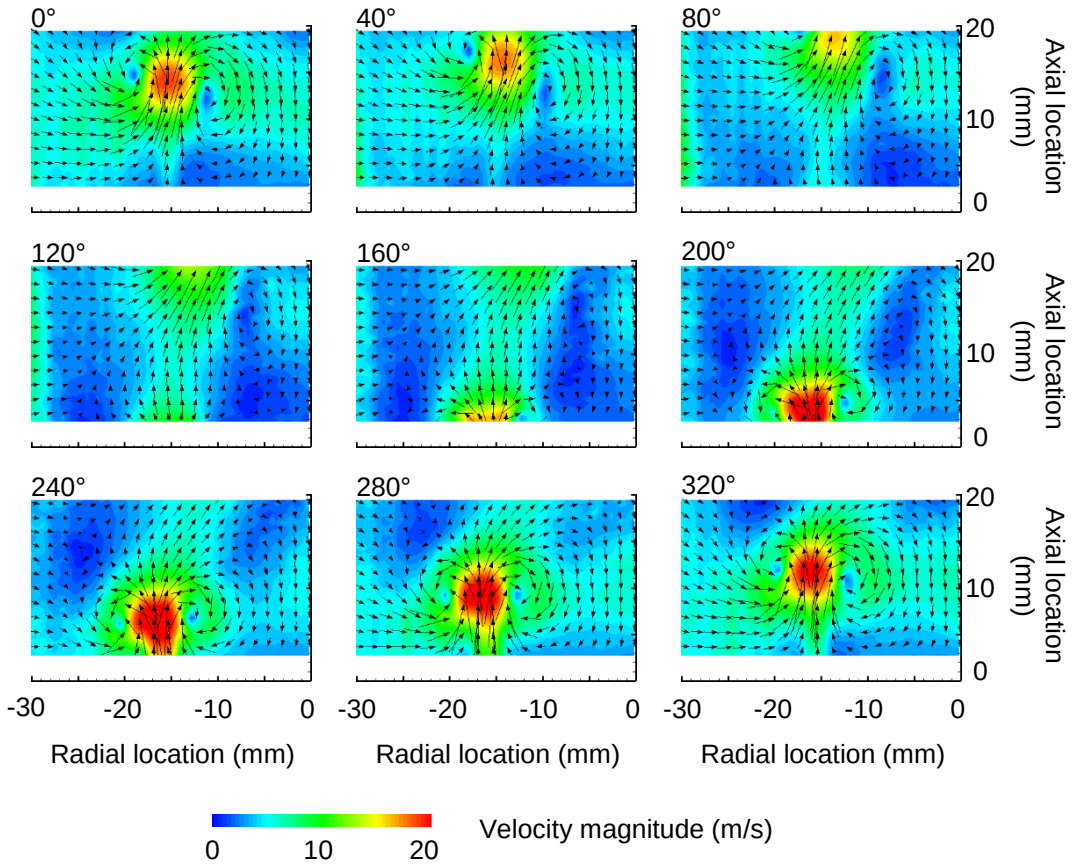

Figure 3.5: Sequence of phase-locked forced flow images in steps of 40° showing the velocity vectors and contour of the velocity magnitude. Images show the development of the counter rotating vortex. Flow conditions: bulk air flow velocity: 8.84 m/s, f= 255 Hz, $u'/\langle U \rangle$= 0.8.

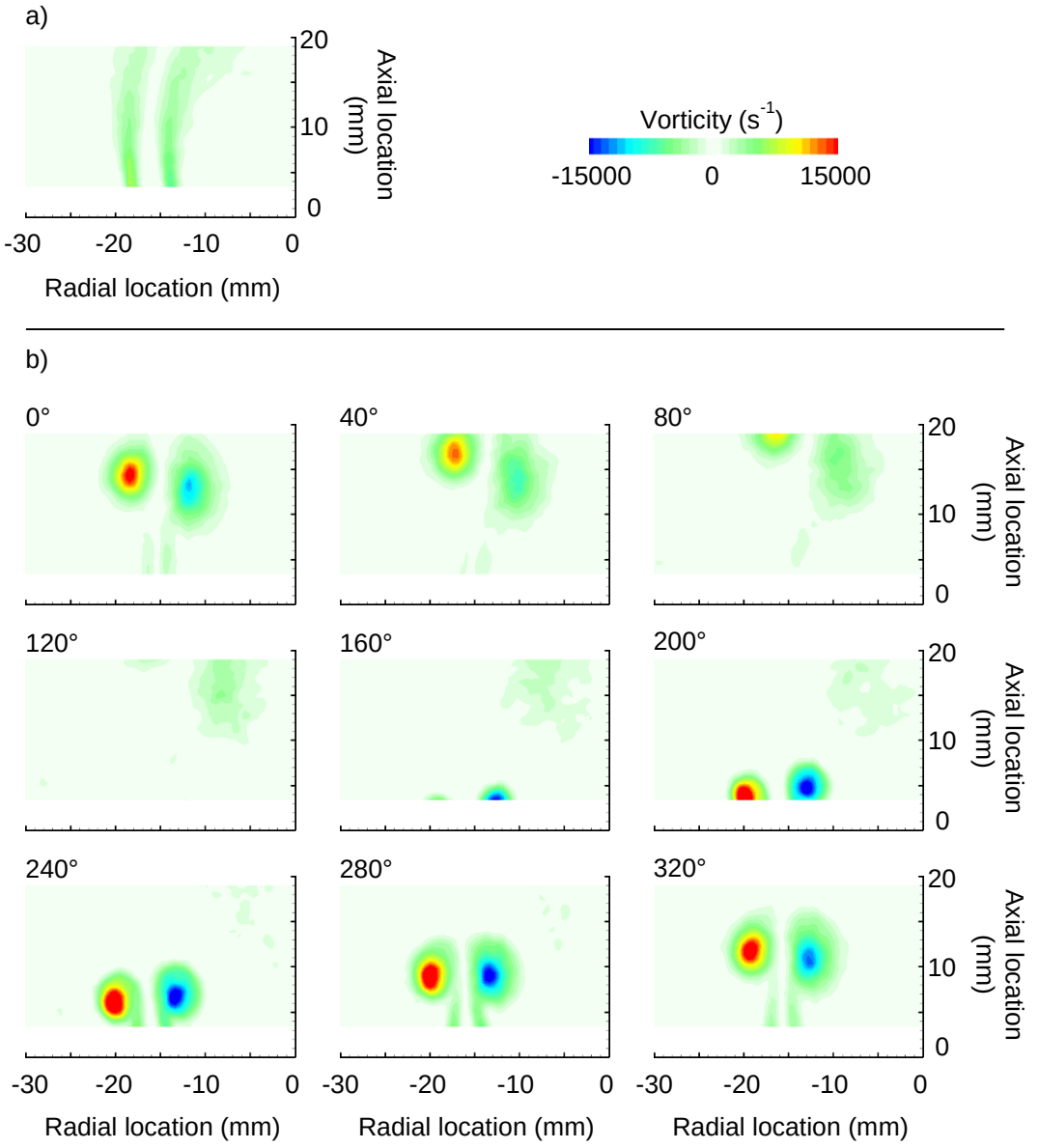

Figure 3.6: Images show the vorticity of the flow, (a) with unforced flow, and (b) under forced conditions. Under forced conditions the sequence of phase-locked images are in steps of 40°. Images show the development of the counter rotating vortex. Flow conditions: bulk air flow velocity: 8.84 m/s, and for forced flow: f= 255 Hz, $u'/\langle U \rangle$= 0.8.

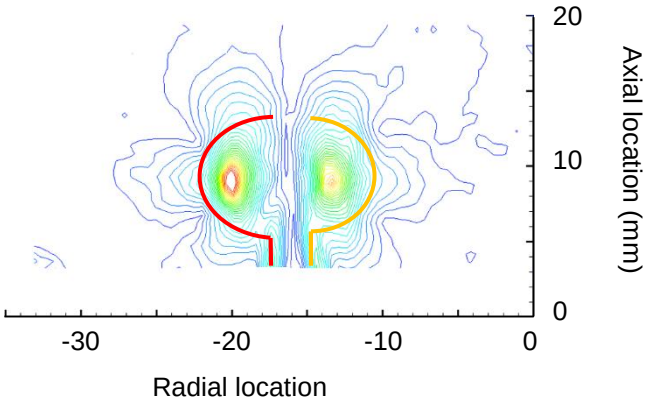

Figure 3.7: Spatial plot of the calculated velocity gradient of the forced flow phase-locked at 280° in the combustion chamber at a bulk air flow velocity of 8.84 m/s, f= 255 Hz, $u'/\langle U\rangle$= 0.8.

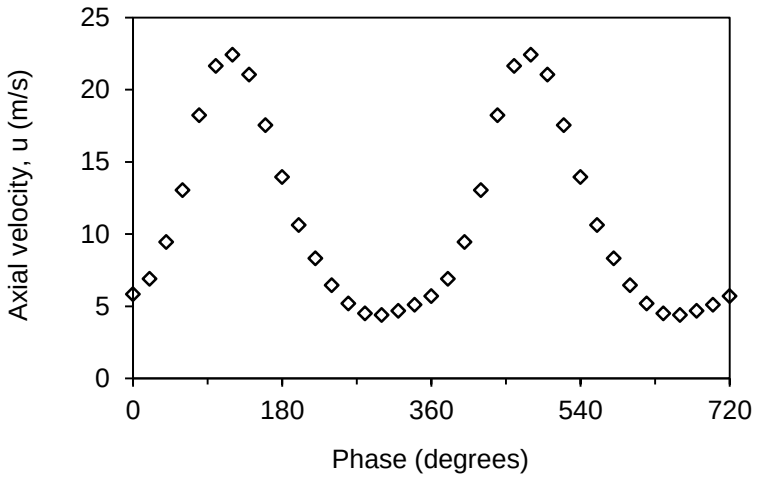

Figure 3.8: Axial velocity oscillation measured at point 'P' in Figure 3.1 during forcing conditions, f= 255 Hz, $u'/\langle U\rangle$= 0.8.

The changes in velocity were the cause for the formation of vortices. The changes in the flow rate of combustible mixture and the complex interactions occurring between the vortices could have a significant impact on the flame dynamics (Balachandran *et al.* 2005, Keller *et al.* 1981, Kulsheimer and Buchner 2002, Schadow and Gutmark 1992), which shall be discussed in the next chapter.

3.5 Summary

The cold flow was studied using the laser based technique, particle image velocimetry where the flow velocity and turbulence was measured for a seeded flow. The purpose of these tests was to gain a basic understanding of the flow in the combustion chamber and observe how the flow was affected by acoustic forcing. The flow was first observed under unforced conditions where the volume flow rate of air was increased from 180 slpm to 420 slpm in steps of 10 slpm.

The flow in the combustion zone created central and outer recirculation zones. The flow in these zones interacted with the oncoming flow to generate shear layers. The spatial velocity gradient of the unforced flow showed the regions where high levels of shearing occurred within the flow. These regions provide a suitable location for flame stabilisation, however, the flame could stabilise elsewhere based on the burning characteristics.

Based on the turbulence plots, the air volume flow rate for the hot flow experiments was chosen to be 250 slpm, as the changes in turbulence at the entrance of the combustion chamber would be minimal with the addition of fuel.

Under forcing conditions the flow entering the combustion chamber underwent velocity/mass flow fluctuations. The sudden increase and decrease in the flow velocity led to the formation of counter rotating vortices in the flow. These vortices caused a deformation in the inner and other shear layers which could potentially alter the shape of the flames during combustion.

Chapter 4: Turbulent ethylene and methane combustion

Leading up to this chapter, the methods of measuring and analysing the experimental data to determine the characteristics of the flame has been detailed. The flow within the combustion chamber was studied using PIV measurements and a suitable air volume flow rate of 250 slpm was chosen based on the velocity fluctuations experienced at the inlet of the combustion zone. Under forcing conditions the flow at the entrance of the combustion zone experienced fluctuating mass/velocity perturbations which created counter rotating vortices in the flow. These vortices caused a distortion to the shear layers created in the flow compared to unforced conditions, at certain frequencies and amplitudes of velocity perturbations.

This chapter will introduce to the reader the flame characteristics within the combustor, obtained from the measurement techniques described in Chapter 2. The flames of pure ethylene and methane were studied under unforced conditions and were subjected to controlled acoustic excitation.

4.1 Imperfectly premixed ethylene combustion

Ethylene, with a molecular composition of C_2H_4, is a highly combustible gas which has a higher flame speed compared to methane gas. At an equivalence ratio of 1.0, ethylene has a laminar flame speed of approximately 68 cm/s (Ravi *et* al. 2014), while methane has a laminar flame speed of 36 cm/s (Selle *et al.* 2011). With a higher flame speed there is a higher flame temperature (Chatterjee 2004) which could lead to higher heat release fluctuations, and may cause self-excited oscillations of the flame. With the current combustor geometry the ethylene flames

were able to achieve a state of self-excitation while the methane flames were unable to produce strong acoustic oscillations for self-excitation. Due to ethylene flames' ability to achieve self-excitation in this experimental setup, and concerns of a possible flame flash back into the combustor duct and plenum, ethylene fuel was only imperfectly premixed with air.

4.1.1 Experimental conditions

Although the study was mainly concerned with acoustically excited turbulent flames it was necessary to understand how and where flame stabilisation occurred in the combustion chamber. The unforced ethylene flames were first studied under varying the bulk air flow velocity and global equivalence ratio, ϕ_{Global}. For each air volume flow rate the global equivalence ratio was varied from 0.6 to 0.8 in steps of 0.05 (except for test number 11).

Test number	Air (slpm)	Bulk air velocity (m/s)	C_2H_4 (slpm)	ϕ_{Global}
1	230.0	8.14	9.7	0.60
2	230.0	8.14	10.5	0.65
3	230.0	8.14	11.3	0.70
4	230.0	8.14	12.1	0.75
5	230.0	8.14	12.9	0.80
6	230.0	8.84	13.7	0.85
7	250.0	8.84	10.5	0.60
8	250.0	8.84	11.4	0.65
9	250.0	8.84	12.3	0.70
10	250.0	8.84	13.1	0.75
11	250.0	8.84	14.2	0.81
12	280.0	9.90	11.8	0.60
14	280.0	9.90	12.7	0.65
15	280.0	9.90	13.7	0.70
16	280.0	9.90	14.7	0.75
17	280.0	9.90	15.7	0.80
18	280.0	9.90	16.7	0.85

Table 4.1: List of experimental flow conditions used for the study of unforced ethylene flames.

As mentioned earlier, the ethylene fuel was imperfectly premixed with the air by it being introduced into the flow through the primary fuel ports located 50 mm upstream from the base of the combustion zone. Table 4.1 shows the test conditions used in the study of unforced imperfectly premixed ethylene flames. The flow conditions described for test number 11 were then studied extensively under forced conditions solely because it was at this flow condition that the flames exhibited self-excitation with a normalised velocity perturbation, $u'/\langle U \rangle$, as high as 0.41, which is later discussed in Chapter 6. The flow conditions for test number 11 will be referred to as the reference case for pure ethylene flames.

4.1.2 Unforced imperfectly premixed ethylene flames

Under imperfectly premixed conditions the ethylene gas was injected into the flow 50 mm from the base of the combustion zone. As discussed previously, the aerodynamic design of the bluff-body and the sudden expansion of the flow in to the combustion chamber caused flow separation leading to the formation of the central and outer recirculation zones. These zones trapped burnt products and acted as reservoirs of energy and radicals which helped to ignite the incoming combustible mixture. Not only did the bluff-body create recirculation zones, but it also promoted turbulent mixing of products and fresh reactants, through the formation of the shear layers (i.e. the interaction of the fast moving un-burnt mixture and slow moving burnt products in the recirculation zones (Behrens 2007)) which gave rise to the ignition of said reactants. During unforced conditions the flame's response was affected by changes in the flow velocity. If the flow velocity at the flame stabilisation point was greater than the local turbulent flame speed it could have led to intermittent local flame extinction which is the first stage to flame blow-off (i.e. flame extinction); (for further details please refer to Kariuki *et al.* 2012). However, if the flow velocity was reduced well under the local flame speed it could have led to the flame propagating upstream leading to flame flashback.

For the first set of tests the effects of varying the inlet bulk air velocities and the equivalence ratio on the unforced flame were studied. Figures 4.1 (a) and (b) show graphs of the same data presented in different ways to simplify and summarise the effects of varying the equivalence ratio and bulk air velocities on the mean heat release rate (determined from the OH* chemiluminescence) of the

turbulent ethylene flames. These plots show that at low equivalence ratios the changes in the mean heat release with variations in bulk air velocity were minimal. However, as the equivalence ratio was increased the changes were significant and non-linear, whilst keeping the bulk air velocity constant. It should also be noted that the flames at a higher equivalence ratio generate a higher mean heat release rate, which was due to the higher amount of combustible gas present in the flow.

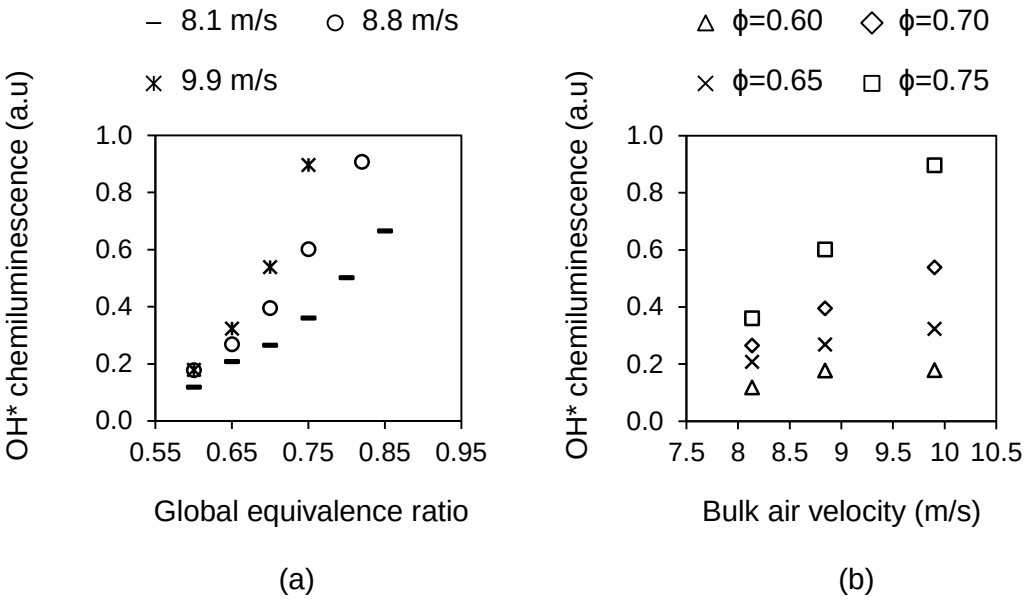

Figure 4.1: Shows the variation of the global mean OH* chemiluminescence for the imperfectly premixed ethylene flames with (a) global equivalence ratio and (b) bulk air velocity.

From the results presented in Chapter 3, with increasing inlet bulk air flow velocity from 8.1 to 9.9 m/s there was an increase in the turbulence magnitude of the stream entering the combustion chamber of approximately 32%. Altering the turbulence can have a direct impact on the size and amount of eddies present, which could affect the wrinkling of the flame front. With increasing turbulence the size of eddies reduce while the number of them increase causing higher wrinkling of the flame surface, hence creating a larger surface area for burning processes to occur (Turns 2006, Li *et al.* 2010). This was most probably why at higher bulk air velocities there was an increase in the mean global heat release rate (Balachandran 2005, Dowlut *et al.* 2012). From a study conducted on the same experimental

combustor (Dowlut *et al.* 2012), PLIF imaging was performed and the data showed a strong correlation between the heat release rates estimates and the flame surface area, FS. The study showed how the changes in the flame surface area due to wrinkling affected the heat release response.

Laser induced fluorescence imaging was conducted on the flames from which several characteristics, such as the OH signal intensity and flame surface area were computed. Figure 4.2 shows an instantaneous OH PLIF image of lean imperfectly premixed ethylene flame for the reference flow conditions. This image shows the flame shape and general location where the flame had stabilised. The flame was primarily anchored on the inner shear layers formed by the central recirculation zone shown in the flow analysis. The outer recirculation zones also provided a stream of radicals and energy to the incoming reactants, however, there was a lower intensity of OH, indicating a lower concentration of reactants and temperature which may possibly be the reason why only intermittent stabilisation of the flame occurred on the outer shear layers during the tests.

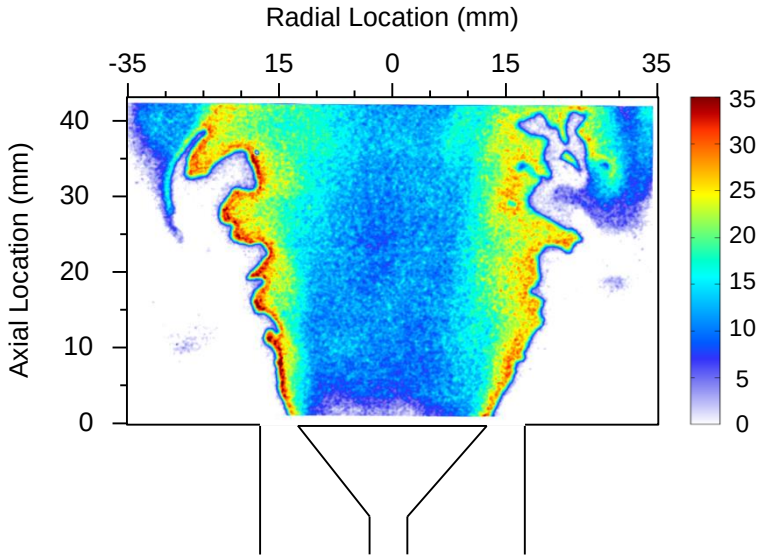

Figure 4.2: Instantaneous OH PLIF image of an unforced imperfectly premixed ethylene flame at a global equivalence ratio of 0.81.

Analysis for the reference for pure ethylene flames is presented in Figure 4.3, which shows an instantaneous OH PLIF with the computed flame front overlaid,

and the averaged OH PLIF intensity and flame front for this flow condition. It shows the axisymmetric nature of the flames in this combustion rig. The averaged OH PLIF image shows a higher fluorescence signal of OH at the flame front on the inner shear layers, which was expected as it was where the flame front and the combustion process occurred. The central recirculation zone was filled with OH radicals which were recirculated and transported towards the oncoming reactants. The averaged flame front (Figure 4.3 (c)) closest to the base of the flame was observed to be more smooth, i.e. it had less wrinkling. However, moving further downstream the averaged flame front image shows a wider flame brush area. The instantaneous OH PLIF and flame front image confirm the fact that the flame was more wrinkled at the top which created a larger flame brush area. The wrinkling of the flame was most likely due to the higher level of turbulence and the increased width of the shear layer downstream of the combustion base as shown in the results presented in Chapter 3. Shown in Behrens (2007), the size of the mixing zone, i.e. the zone where the products and reactants interact, increased further downstream, hence, there was a larger region of where the flame front could develop leading to a higher likelihood of wrinkling.

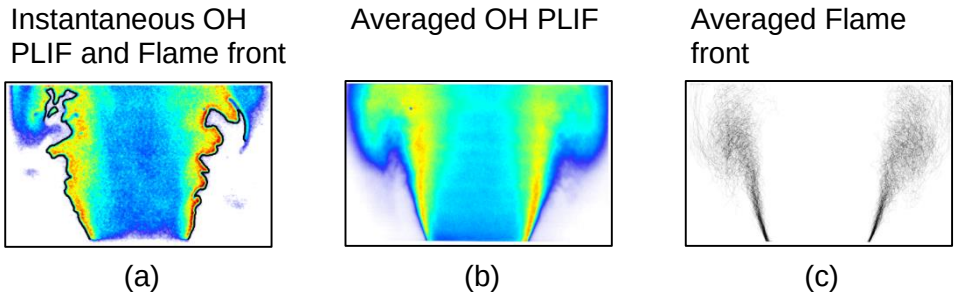

Figure 4.3: Images of the (a) instantaneous OH PLIF with the flame front, the (b) averaged OH PLIF, and (c) averaged flame front for the imperfectly premixed ethylene flame at and global equivalence ratio of 0.81.

4.1.3 Acoustically forced operating conditions

The flow was acoustically excited at the three forcing frequencies of 30, 255, and 315 Hz where high velocity perturbations were achieved. The dynamic

response of the flame was characterised based on how the change in the normalised velocity perturbations affected the global heat release rate determined by the OH* chemiluminescence and the flame shape obtained from PLIF imaging.

As seen in the previous section, the flame stabilised on the inner shear layers with some flame elements on the outer shear layers created by the bluff-body and the rearward facing step. Probably due to a lower temperature in the outer recirculation caused by heat loss to the walls, stabilisation of the flame in the region was not achieved for some conditions.

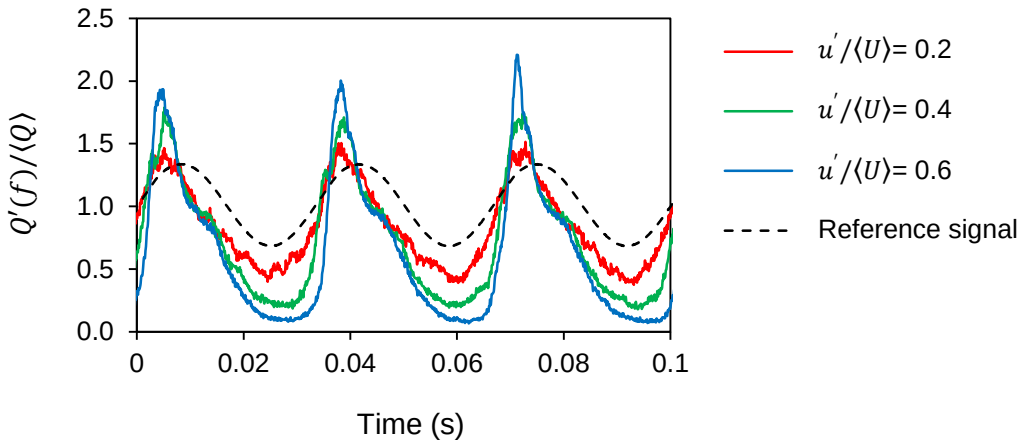

Figure 4.4: Time series of the normalised heat release rate (determined from the OH* chemiluminescence signal) for the imperfectly premixed ethylene flame being acoustically forced at f= 30 Hz and three normalised velocity perturbations of 0.2, 0.4 and 0.6.

Under forcing conditions the reactant mixtures were acoustically perturbed which gave rise to a periodic flame response. Figure 4.4 shows the time series plot of the normalised heat release rate obtained at three normalised velocity oscillations of 0.2, 0.4 and 0.6. The flame underwent a periodic response; however, there were steep rises and falls in the OH* chemiluminescence. The reason why this occurred can be explained by the images of the averaged flame front shown in Figure 4.5, which are phase-locked in steps of 30°. The images show that there were no strong vortical interactions between the flame front and the flow, however, comparing the images at each phase shows that the mean flame surface area experienced large

variations through the cycle. The fluctuation in the OH* chemiluminescence was mainly due to the flame area modulation.

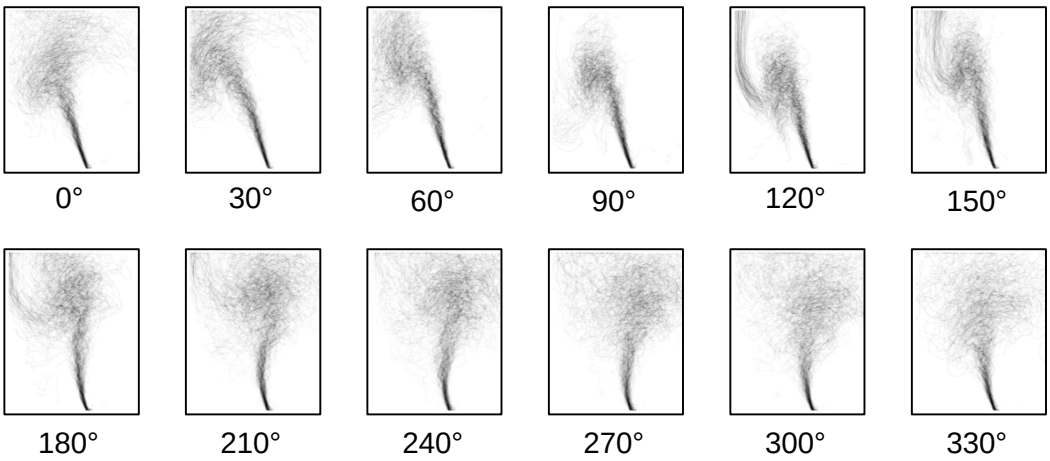

Figure 4.5: Phase-locked averaged flame front (FF) image sequence of 100% ethylene imperfectly premixed, under strong acoustic forcing, $u'/\langle U\rangle$= 0.4, f= 30 Hz.

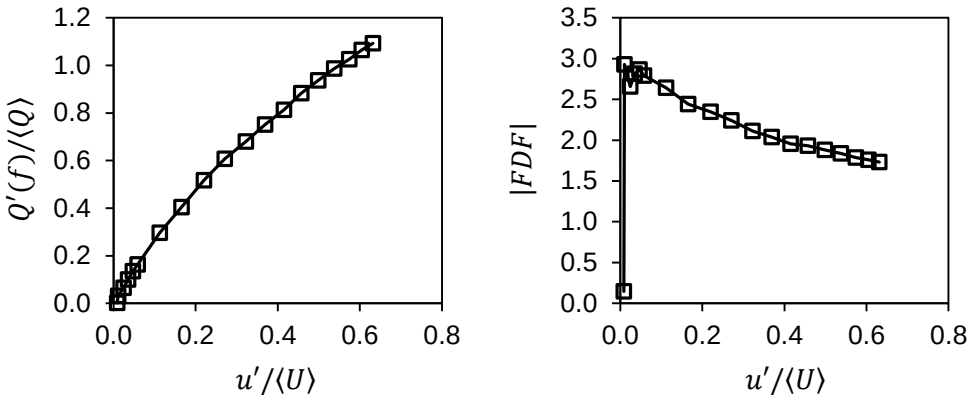

Figure 4.6: The dependence of the global heat release fluctuation and the magnitude of the flame describing function evaluated from OH* chemiluminescence of imperfectly premixed ethylene flames on normalised velocity fluctuations, at a forcing frequency of 30 Hz.

Figure 4.6 shows the dependence of the global heat release fluctuation and the magnitude of the flame describing function, FDF, evaluated from OH* chemiluminescence for the reference ethylene flames at a forcing frequency of 30

Hz. The heat release fluctuation had a close to linear response with increasing $u'/\langle U \rangle$, as there were no strong flame/vortex interactions. A linear trend was also exhibited in the plots for the magnitude of the flame describing function, FDF, between the heat release and the velocity perturbations, which was most likely because there were no strong vortical interactions between the flow and flame which could introduce non-linearity in the flame response (Balachandran 2005).

When the flames were forced under sufficiently large velocity perturbations (higher than 0.2) at higher forcing frequencies (i.e. 255 and 315 Hz), the inner and outer shear layers simultaneously rolled up to create a counter rotating vortex pair which caused the flame surface to roll-up. An example of this roll-up is shown in the instantaneous image presented in Figure 4.7. This outcome was comparable to the flow field response discussed in Chapter 3 where counter rotating vortices formed in the flow which caused an alteration to the shape of the shear layer.

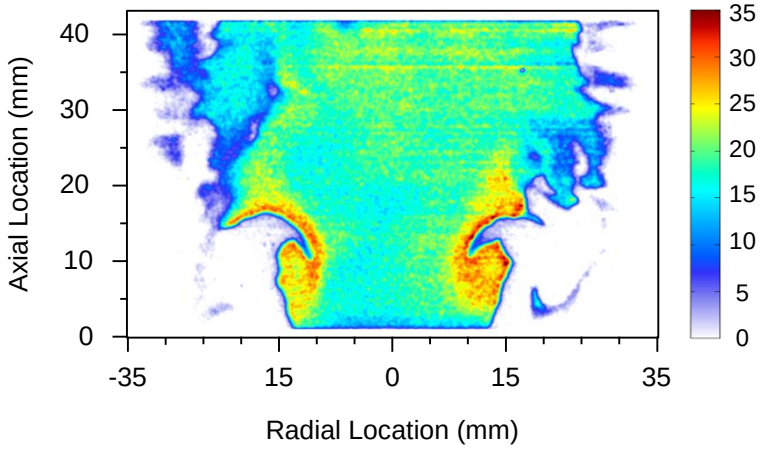

Figure 4.7: Example of an instantaneous OH PLIF image captured for imperfectly premixed ethylene flames under strong acoustic forcing, $u'/\langle U \rangle$= 0.4, f= 255 Hz.

The flame experienced a cyclic response for which a section of the time series of the normalized global OH* chemiluminescence recorded at three magnitudes of normalised velocity perturbations, 0.2, 0.4, and 0.6, at a forcing frequency of 255 Hz is presented in Figure 4.8. The plot clearly shows that the flame had a cyclic response and as $u'/\langle U \rangle$ was increased the peak fluctuation of the global OH* chemiluminescence also increased.

The OH* chemiluminescence was processed to obtain the plots in Figures 4.9 (a) and (b) which show the dependence of the global heat release fluctuation and the magnitude of the flame describing function, FDF, on the normalised velocity perturbations for forcing frequencies 255 and 315 Hz.

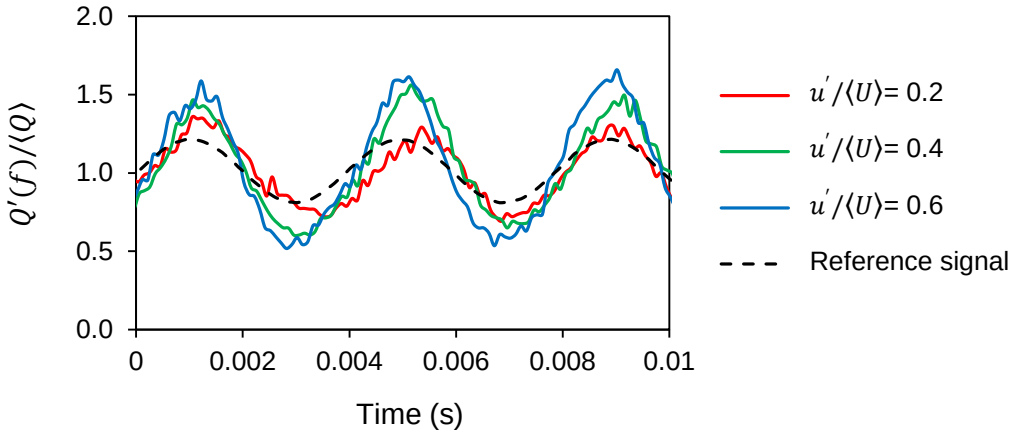

Figure 4.8: Time series of the normalised heat release rate (determined from the OH* chemiluminescence signal) for the imperfectly premixed ethylene flame being acoustically forced at f= 255 Hz and three normalised velocity perturbations of 0.2, 0.4 and 0.6.

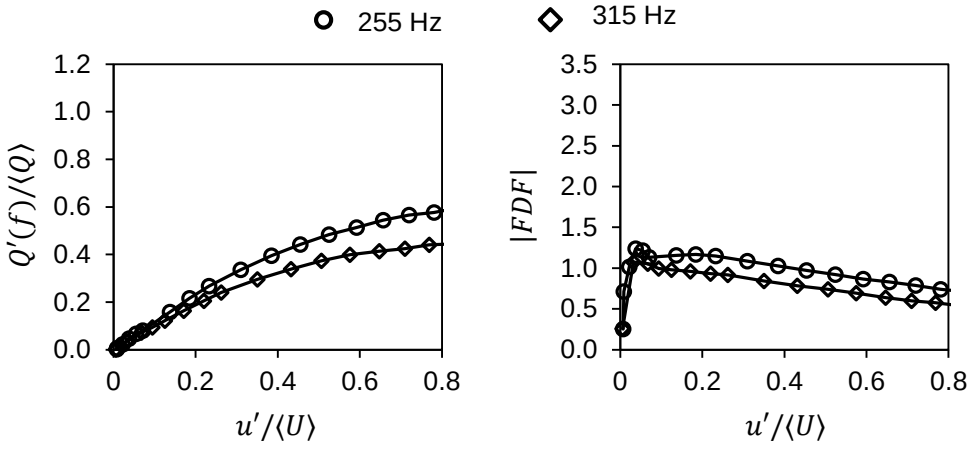

Figure 4.9: The dependence of the global heat release fluctuation and the magnitude of the flame describing function evaluated from OH* chemiluminescence of imperfectly premixed ethylene flames on normalised velocity fluctuations, at forcing frequencies of 255 and 315 Hz.

For both the frequencies, 255 and 315 Hz, similar trends were observed; however, the plots were of different magnitudes. The difference in magnitudes can be explained by the size of the vortex roll-up. At 315 Hz the flame has less time to roll up compared to the flame being forced at 255 Hz. The figure for the global heat release fluctuation (Figure 4.9 (a)) shows that for both the frequencies the flame experienced a linear response from a $u'/\langle U\rangle$ range of 0 to 0.40, while, overall the flame went through a non-linear transition after which the saturation of the normalised heat release fluctuations, $Q'(f)/\langle Q\rangle$, occurred, showing the flame's dependence on the magnitude of $u'/\langle U\rangle$ at the entrance to the combustion zone. Studying the plots of the heat release fluctuation in Figures 4.9, show that as the forcing frequency was increased the magnitude of the normalized heat release modulation reduced indicating that the flame's dynamic response was reliant on the frequency of forcing.

Figure 4.10 shows how the variable $u'/\langle U\rangle$ had an effect on the size of the flame roll-up. The images show the effects on the flame shape with increasing $u'/\langle U\rangle$, from 0.2 to 0.6, at a fixed forcing frequency of 255 Hz. The forced flame images were averaged at phases of 180°, 300° and 420° (60°), which shows how the flame roll-up developed at different forcing phases. The initial growth of the vortex at 180° certainly increased in size as $u'/\langle U\rangle$ was increased. Forced at $u'/\langle U\rangle$=0.2 and 180° the size of the vortices in the flow did not seem to be large enough to distort the shear layers to cause any alterations or roll-up of the flame front. However, as the magnitude of $u'/\langle U\rangle$ was increased the inner shear layer along with the flame front began to curve inwards thus creating an inward flame roll-up; at this point, i.e. 180°, there were negligible flame front occurrences on the outer shear layer to roll-up. During a phase of 180°, in the top half of these images, there was a noticeable loss of flame front as $u'/\langle U\rangle$ increased, indicating flame surface loss either due to the collapse of a previous flame roll-up or due to a process of flame annihilation events (Balachandran 2005). Flame annihilation occurs when two flame surfaces collide, thus igniting all the reactants rapidly between them, leaving no reactants left to burn; hence both flame surfaces are extinguished.

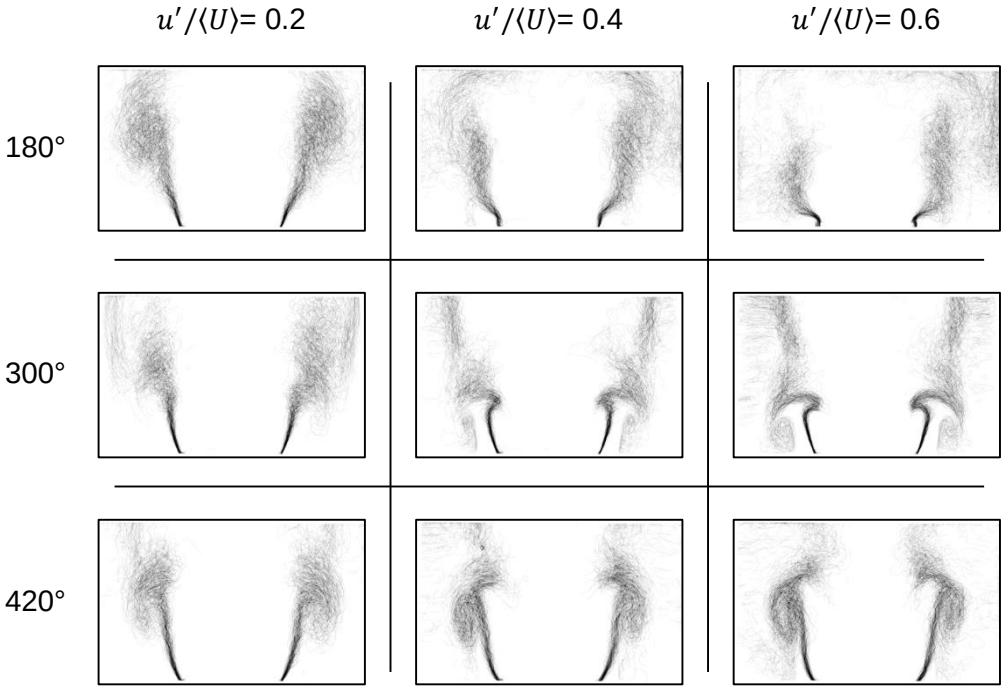

Figure 4.10: Matrix of images showing the effects on the size of the flame roll-up for an imperfectly premixed ethylene flame at three phase-locked angles of 180°, 300° and 420° at three normalised velocity fluctuations of 0.2, 0.4 and 0.6. Flow conditions: ϕ= 0.81, ⟨U⟩= 8.8 m/s, f= 255 Hz.

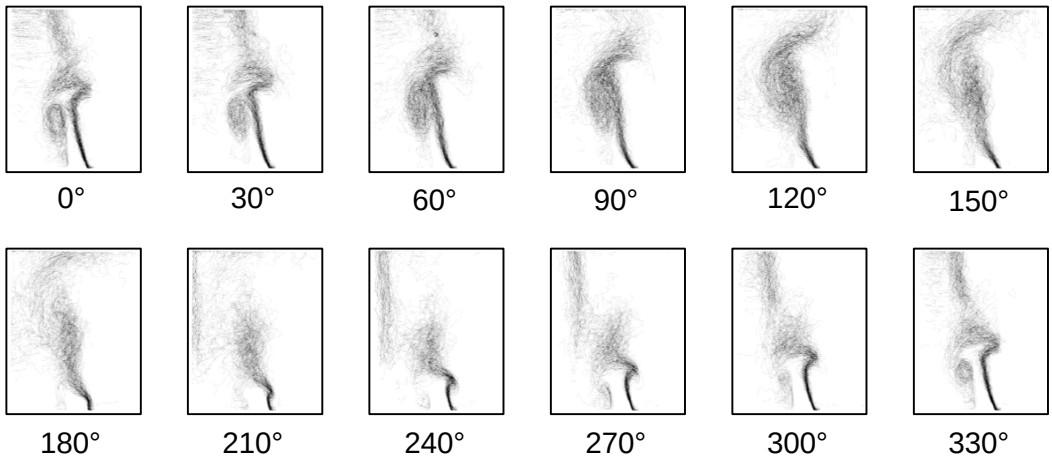

Figure 4.11: Phase-locked averaged flame front (FF) image sequence of pure ethylene imperfectly premixed flames, under strong acoustic forcing, $u'/\langle U\rangle$= 0.4, f= 255 Hz.

Moving from a phase angle of 180 ° to 300° it was observed that the flame roll-up moved downstream while it increased in size (i.e. the flame surface roll-up was greater). With an increase in $u'/\langle U\rangle$, the size of the flame roll-up further increased. At a low $u'/\langle U\rangle$ of 0.2 the flame did not stabilise on the outer shear layers, however as the velocity perturbations were increased flame began to appear on the outer shear layers and there is no doubt that the outer shear layer too, had been deformed, indicated by the presence of a rolled up flame front.

At the phase angle of 420° (60°) the size of the flame roll-up had become quite large. From this instance onwards the size of flame roll-up grew and moved further downstream until it came in contact with the wall of the quartz enclosure which caused a breakup of the flame roll-up. With the collapse of the flame roll-up a new roll-up developed at the base of the combustion zone, thus repeating the cycle. These series of events are better portrayed in Figures 4.11 and 4.12 which show the sequence of phase images (in steps of 30°) at $u'/\langle U\rangle$ of 0.4 and frequencies 255 and 315 Hz, respectively. Comparing these two sequences it is clear that at both forcing frequencies the flame underwent the same phenomenon of flame roll-up due to the inlet velocity perturbations

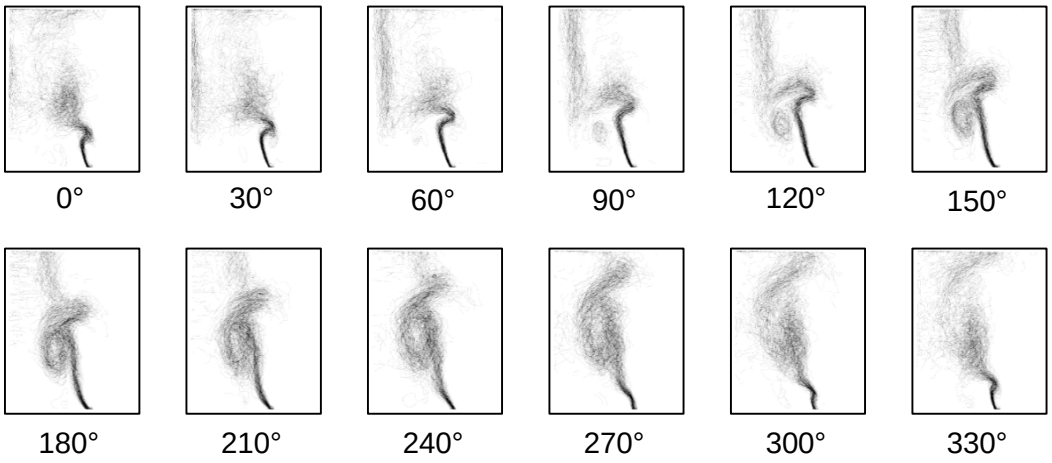

Figure 4.12: Phase-locked averaged flame front (FF) image sequence of 100% ethylene imperfectly premixed, under strong acoustic forcing, $u'/\langle U\rangle$= 0.4, f= 315 Hz.

The flame surface area was measured in the three regions A (2.5 to 15 mm), B (25 to 40 mm) and C (2.5 to 40 mm) mentioned earlier (refer to Figure 2.16 in Chapter 2). The plots for the evolution of the flame surface area in these regions for the reference case for pure ethylene forced flames at 255 Hz are shown in Figure 4.13. Looking at these plots it is immediately noticeable that the difference between $u'/\langle U\rangle$ of 0.2 and 0.4 was significant while the change in the response between 0.4 and 0.6 was minimal.

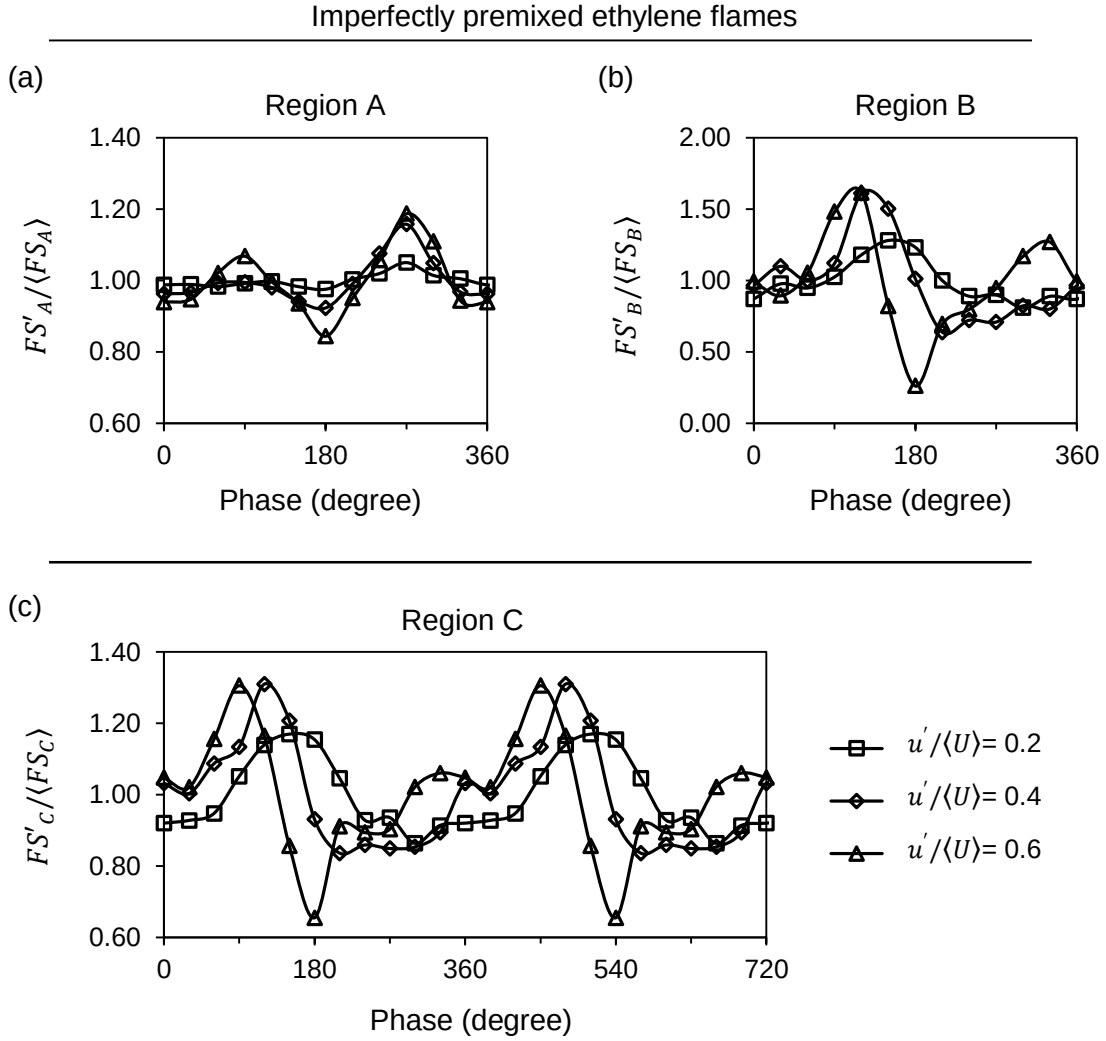

Figure 4.13: Shows the cyclic variation of the normalised flame surface area for the regions (a) A, 2.5 – 15 mm, (b) B, 25 – 40 mm, and (c) C, 2.5 – 40 mm, for imperfectly premixed ethylene flames under forcing conditions, f= 255 Hz.

Studying Region A in Figure 4.13 (a) and the sequence of images in Figure 4.11, the sudden rise in the flame front/surface starting at a phase angle of 180° was due to the initial development of the flame roll-up as shown in the images. The peak of the flame surface plots occurred at 270°, where the flame roll-up was fully developed and was now travelling further downstream. After 270° we see a sharp fall in the flame surface due the flame vortex moving out of the interrogation area, Region A. In Region B (Figure 4.13 (b)), a steep rise in the flame surface occurred from 30° to 120° which was due to the appearance of the flame vortex roll-up in this area. After the phase angle of 120° the roll-up structure collided with the wall causing a sudden break down of the flame roll-up causing a sudden loss of flame surface in this region (represented by the steep drop from 120° to 180° in Region B).

Two major alterations in the flame surface took place during the forced cyclic response of the flame. First was the initial development of the flame roll-up in Region A, and the second was the collapse of the fully developed flame roll-up in Region B. To better understand which of these processes affected the flame the most, the overall cyclic response of the flame surface, i.e. Region C, is shown in Figure 4.13 (c). Here it can be seen that the largest increase and decrease in the flame surface area occurred at the same instance when the flame roll-up collapsed and stabilisation of the flame occurred in Region B. The percentage contribution of the mean flame surface area for regions A and B to region C is approximately 15% and 32%, respectively, for all the values of $u'/\langle U \rangle$. This led to the conclusion that the second event, i.e. the collapse of the flame roll-up in region B was the factor that influenced the cyclic response significantly.

4.2 Methane combustion

This segment is similar to the previous section; however, the primary fuel used in this case was methane. Methane flames, both, imperfectly and fully premixed, were characterised using pressure, chemiluminescence and laser induced fluorescence measurements. The results for unforced and forced methane flames are presented showing the difference in the flame response with the method of fuel mixing (i.e. imperfectly and fully premixed).

4.2.1 Experimental conditions

The tests with methane flames were conducted similar to the ethylene tests. The equivalence ratio and bulk air velocity were varied for the unforced conditions. The table below shows which flow operating conditions at which the unforced flames were studied. Due to the specific laboratory and combustion rig setup the imperfectly premixed methane flames were not tested to see the effects of varying bulk air velocities, however, a reference operating condition for methane was selected and PLIF measurements were carried out for both mixing fuel introductory methods.

Test Number	Air (slpm)	Bulk air velocity (m/s)	CH_4 (slpm)	ϕ_{Global}
1	230.0	8.14	15.7	0.65
2	230.0	8.14	16.9	0.70
3	230.0	8.14	18.1	0.75
4	230.0	8.14	19.3	0.80
5	230.0	8.14	20.5	0.85
6	250.0	8.84	17.1	0.65
7	250.0	8.84	18.4	0.70
8	250.0	8.84	19.7	0.75
9	250.0	8.84	21.0	0.80
10	250.0	8.84	22.3	0.85
11	280.0	9.90	19.1	0.65
12	280.0	9.90	20.6	0.70
13	280.0	9.90	22.1	0.75
14	280.0	9.90	23.5	0.80
15	280.0	9.90	25.0	0.85

Table 4.2: List of experimental flow conditions used for the study of unforced fully premixed methane flames.

For the conditions where methane was used as the primary fuel, only the flames using the flow quantities for test number 7 were studied under acoustic forcing conditions using the imperfectly and fully premixed configurations. This flow was selected to use a similar air flow rate of 250 slpm, and with the current setup of

the fuel lines, fuel flow rates greater than 19 slpm caused high pressures in the lines during imperfectly premixing methane. This flow condition will be used as the reference for methane flames to understand the effects of hydrogen addition on the flame response in the next chapter.

4.2.2 Unforced methane combustion

In the first part of this section the fully premixed flames were studied under varying bulk air velocities and equivalence ratios. Similar to unforced ethylene flames, the methane flame stabilised in the wake of the bluff-body. The flame were anchored on the inner shear layers formed by the central recirculation zone, although, there was absolutely no stabilisation on the outer recirculation zone. This may have been due to a lower flame temperature, thus having less energy in the outer recirculation zones to ignite the oncoming reactants.

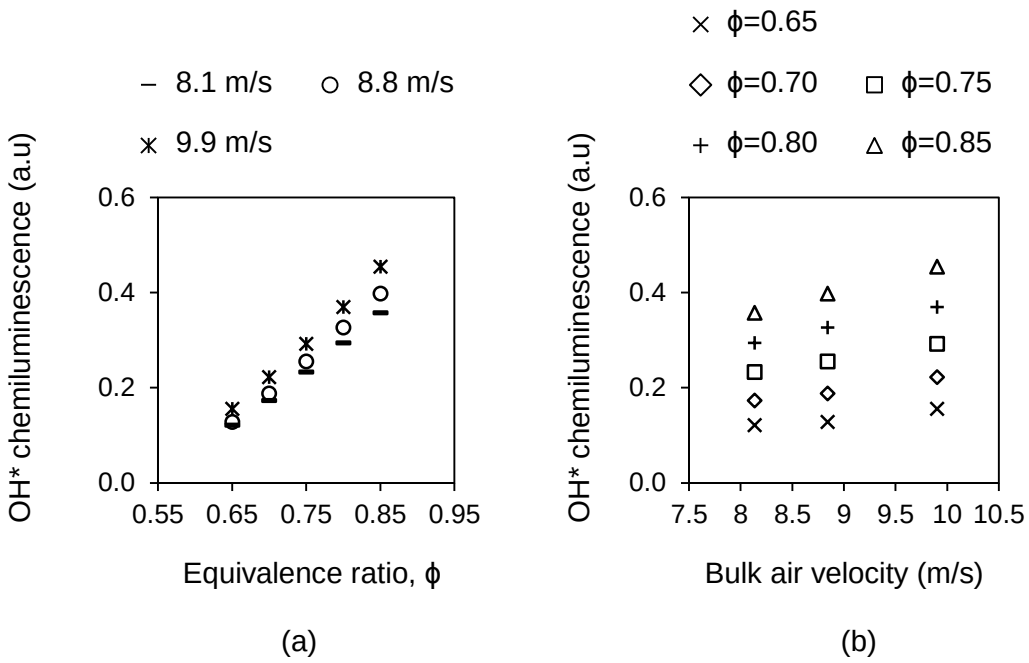

Figure 4.14: Shows the variation of the global mean OH* chemiluminescence for the fully premixed methane flames with (a) equivalence ratio and (b) bulk air velocity.

Figure 4.14 shows the individual effects of varying the bulk air flow velocities and equivalence ratio on turbulent fully premixed methane flames. The graphs show

a linear variation in the mean global heat release rate (determined from the OH* chemiluminescence) with the equivalence ratio and bulk air velocity.

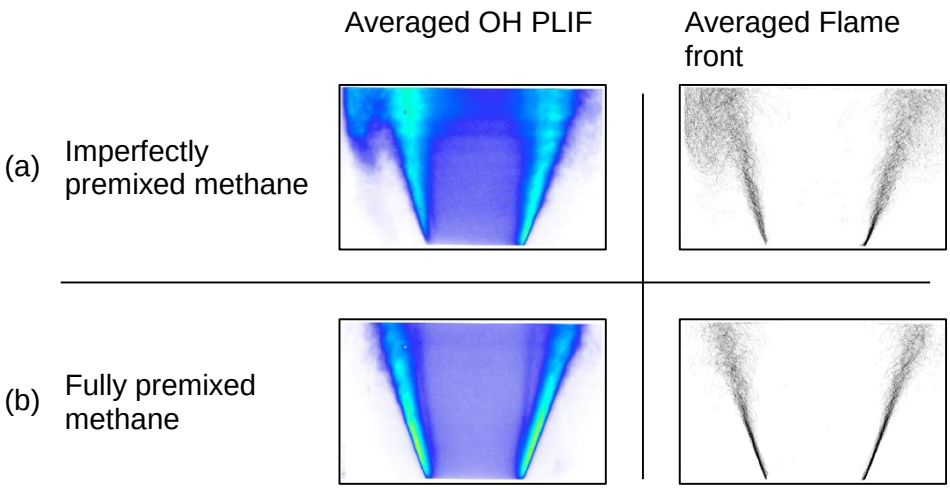

Figure 4.15: Images of the averaged OH PLIF, and averaged flame front for the (a) imperfectly premixed and (b) fully premixed methane flame at and equivalence ratio of 0.70.

Figure 4.15 (a) and (b) show the averaged OH PLIF and flame front images for the imperfectly and fully premixed flames for the reference flow conditions for methane flames. The imperfectly premixed methane flame were slightly asymmetric which could be due to the uneven mixing occurring or the placement of the six primary fuel injection ports 50 mm upstream. However, the flames for the fully premixed mixture were relatively symmetric, indicating a more even distribution of fuel within the mixture. Comparing the images it can be seen that the imperfectly premixed flame was able to weakly stabilise on the outer shear layer while the fully premixed flame had no flame surface above the outer recirculation zone. The images show that the fully premixed flame had a higher fluorescence of OH at the flame front. This may be because of a higher concentration of OH radicals or a higher temperature of the flame. It should be noted that the particular excitation wavelength of OH PLIF that was selected is relatively independent to temperature changes compared to other excitation wavelengths. However, unless temperature measurements are conducted, a conclusion on the radical concentration cannot be made.

4.2.3 Forced turbulent methane flames

The dynamic response of forced imperfectly and fully premixed methane flames, subjected to inlet velocity oscillations are presented in this section. Similar as the previous section, the flow was perturbed at the three forcing frequencies where high velocity perturbations at the entrance to the combustion chamber were achieved, i.e. 30, 255 and 315 Hz. The response of the methane flames was similar to the response of the ethylene flames, with a few exceptions.

The forcing experiments were carried out on the flow configuration of test number 7 in Table 4.2, which was selected as the reference case for methane flames. OH* chemiluminescence was recorded to determine the heat release rate fluctuations, while OH PLIF images were recorded to show the changes in flame shape and OH radical concentration at different forcing conditions.

The response of the imperfectly and fully premixed methane flames at a forcing frequency of 30 Hz was similar to the response of ethylene flames. An overview of the response of the reference methane flames under these conditions can be summed up in Figures 4.16, 4.17 and 4.18. Figure 4.16 shows the normalised data for OH* chemiluminescence obtained at a single forcing $u'/\langle U \rangle$ of 0.4 for both, imperfectly and fully premixed methane flames. The data shows that the flames underwent a periodic response as observed from the OH* chemiluminescence for the flames, however, the peak fluctuation of the imperfectly premixed flames was much more than the fully premixed flames.

The plot and images in Figures 4.17 and 4.18 show how the flame surface of the flames evolved during the forcing. Between the two methods of fuel introduction, the flames showed a notable difference in terms of how the flame shape changed through the forcing cycle. The variation of the flame surface area in Region C (2.5 to 40 mm from the base of the combustion zone), while moving through the forcing cycle for both the flames are shown in Figure 4.17.

The sharp rise and fall of the OH* chemiluminescence for the imperfectly premixed flame can be explained by the rapid and extreme fluctuations in the flame surface area, which is apparent in the images of Figure 4.18. Similarly, the relatively lower fluctuation of the heat release rate for the fully premixed flame can be related to the lower fluctuation of the flame surface area. The images show that for both cases there were no strong vortical interactions between the flame front and

the flow to cause any flame roll-up, and the fluctuation in the OH* chemiluminescence was mainly due to the flame area modulation.

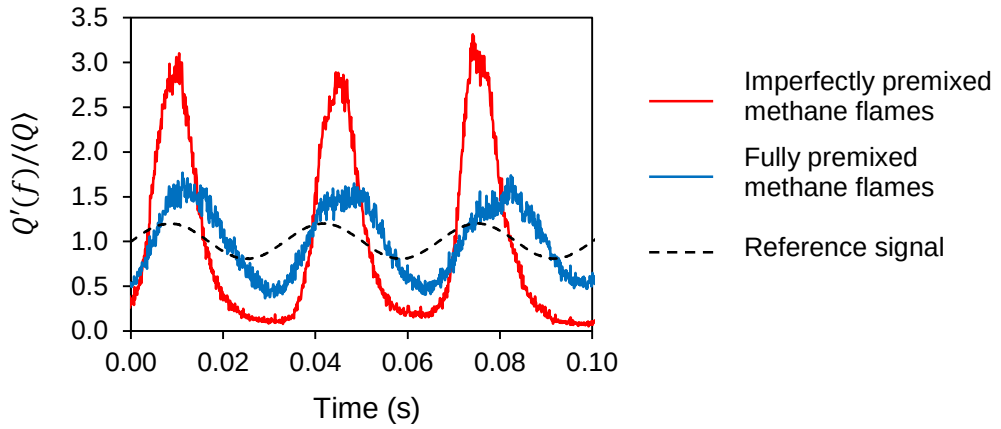

Figure 4.16: Time series of the normalised heat release rate (determined from the OH* chemiluminescence signal) for the imperfectly and fully premixed methane flame being acoustically forced at f= 30 Hz, and $u'/\langle U \rangle$ = 0.4.

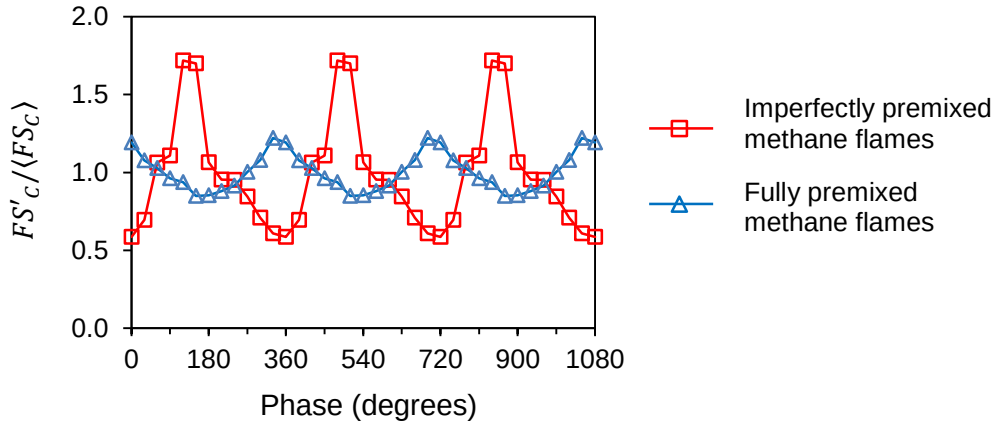

Figure 4.17: Shows the cyclic variation of the normalised flame surface area, $FS'/\langle FS \rangle$, for Region C for imperfectly and fully premixed reference methane flames under forcing conditions, f= 30 Hz, and $u'/\langle U \rangle$= 0.4.

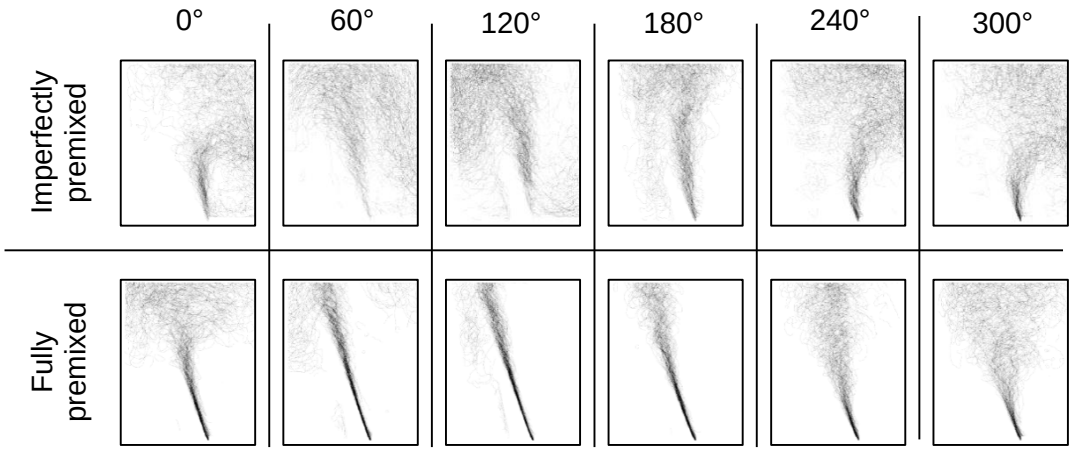

Figure 4.18: Phase-locked images of imperfectly and fully premixed reference methane flames in Region C, in steps of 60°, under forcing conditions f= 30 Hz, and $u'/\langle U\rangle$= 0.4.

This differences in the OH* and flame area oscillation of the fully and imperfectly premixed methane flames was brought about due to the method of fuel mixing. Under forcing conditions, the fully premixed flame would not experience any fluctuations in the global equivalence ratio as both, the air and fuel flow were oscillating. However, with imperfectly premixed flames, the air flow oscillated but the fuel flow did not (as it was a choked flow), which caused a fluctuation of the global equivalence ratio of the mixture entering the combustion chamber. A simple calculation was carried out to plot how the global equivalence ratio oscillated with phase for an imperfectly premixed methane flame; shown in Figure 4.19. The oscillation of the equivalence ratio was calculated using the following equation:

$$Global\ equivalence\ ratio, \Phi = \frac{\dot{m}_f}{\dot{m}_a(1 + Asin(\omega t))} \Big/ \left(\frac{\dot{m}_f}{\dot{m}_a}\right)_{st}$$

Where $\dot{m}_f$ the mass flow of fuel is, $\dot{m}_a$ is the mass flow of air, A is the amplitude of oscillations and the subscript st refers to stoichiometric conditions. The plot shows that the imperfectly premixed flames would experience a steep rise and fall in the equivalence ratio at the flame front. Besides the method of fuel introduction into the flow, the operating conditions between the imperfectly and fully

premixed methane flames are exactly the same (i.e. the global equivalence ratio is constant at 0.70). Thus, it is expected that the oscillations of the equivalence ratio at the flame front of the imperfectly premixed flames was what caused a higher oscillation in the OH* chemiluminescence (Figure 4.16), flame surface area (Figure 4.17) and hence the heat release rate (Figure 4.20 (a)), compared to the fully premixed flames.

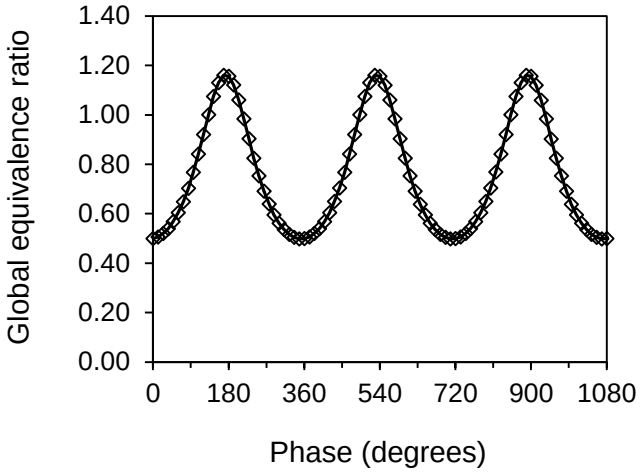

Figure 4.19: Calculated global equivalence ratio oscillation imperfectly premixed reference methane flames at ϕ_{Global} = 0.70, under forcing conditions, f= 30 Hz, and $u'/\langle U\rangle$= 0.4.

Figure 4.20 shows the dependence of the global heat release fluctuation and the magnitude of the flame describing function, FDF, evaluated from OH* chemiluminescence for the reference methane flames. At a forcing frequency of 30 Hz the heat release fluctuation for imperfectly and fully premixed cases had a close to linear response with increasing $u'/\langle U\rangle$ as there were no strong flame/vortex interactions. The magnitude of the heat release rate fluctuation was much lower for the fully premixed methane flames. This was because the fully premixed methane flame experienced a much lower fluctuation in the flame surface area. Linear trends were also exhibited in the plots for the magnitude of the flame describing function. With imperfectly premixed methane flames the magnitude of the FDF saw a linearly decreasing trend with increasing $u'/\langle U\rangle$, however, with fully premixed methane

flames the increase in $u'/\langle U \rangle$ had no effect on the magnitude of the FDF. A constant magnitude of the FDF represents the flame's heat release response increased linearly with increasing $u'/\langle U \rangle$. While the linearly decreasing magnitude shows that the flame is nearing a saturated heat release response, i.e. no further increase in the heat release fluctuation with increasing $u'/\langle U \rangle$.

The methane flames were forced at higher forcing frequencies (i.e. 255 and 315 Hz), and as with the ethylene flames the inner and outer shear layers rolled up simultaneously to create a counter rotating vortex pair causing the flame surface to roll-up. Studying the heat release rate fluctuation plots for both the flames, it can be seen that the magnitude of the heat release fluctuation was much higher at 255 Hz than at 315 Hz which indicates a strong dependence on the forcing frequency. While at 315 Hz there was little difference in the magnitude of the FDF between the two flames, dissimilarities were observed at a forcing frequency of 255 Hz. At this frequency the heat release fluctuation for the imperfectly premixed methane flames showed a comparatively linear response to the fully premixed methane flames. Non-linearity was observed for the fully premixed methane flames at $u'/\langle U \rangle$ of 0.2 and 0.6.

Figures 4.21 and 4.22 show the evolution of the averaged flame surface area in three regions along the forcing cycle in steps of 30°, which are supported by the sequences of phase locked images in Figures 4.23 and 4.24. In Region A for both modes of fuel introduction, there were slight deformations of the flame front however the flame did not develop a counter rotating roll-up at $u'/\langle U \rangle$ of 0.2. Increasing $u'/\langle U \rangle$ further to 0.4 and above, the velocity perturbations were large enough to create larger counter rotating vortices in the flow that caused a flame roll-up leading to large fluctuations of the normalised flame surface area.

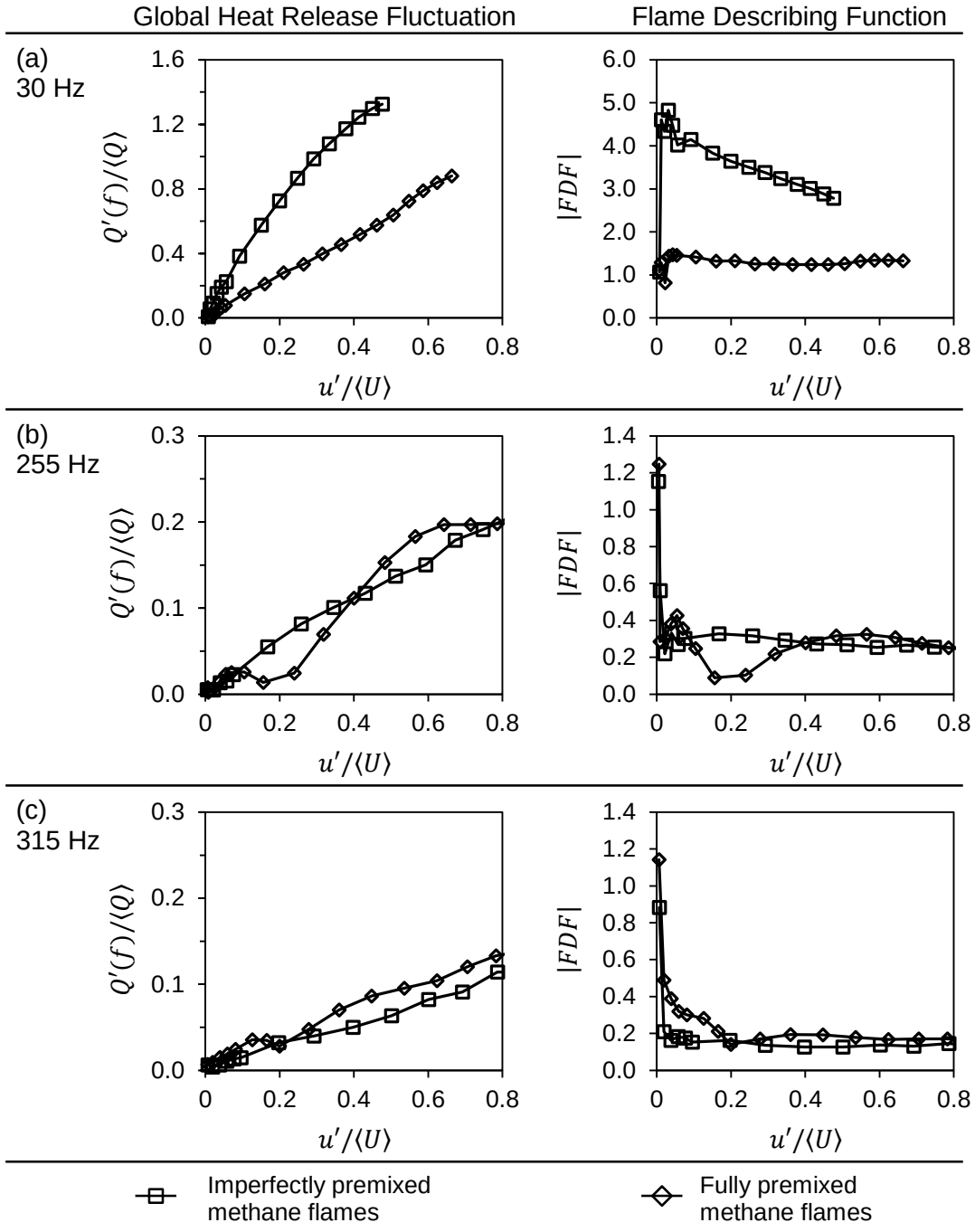

Figure 4.20: The dependence of the global heat release fluctuation and the magnitude of the flame describing function evaluated from OH* chemiluminescence of imperfectly and fully premixed methane flames on velocity fluctuations, at forcing frequencies of (a) 30 Hz, (b) 255 Hz, and (c) 315 Hz.

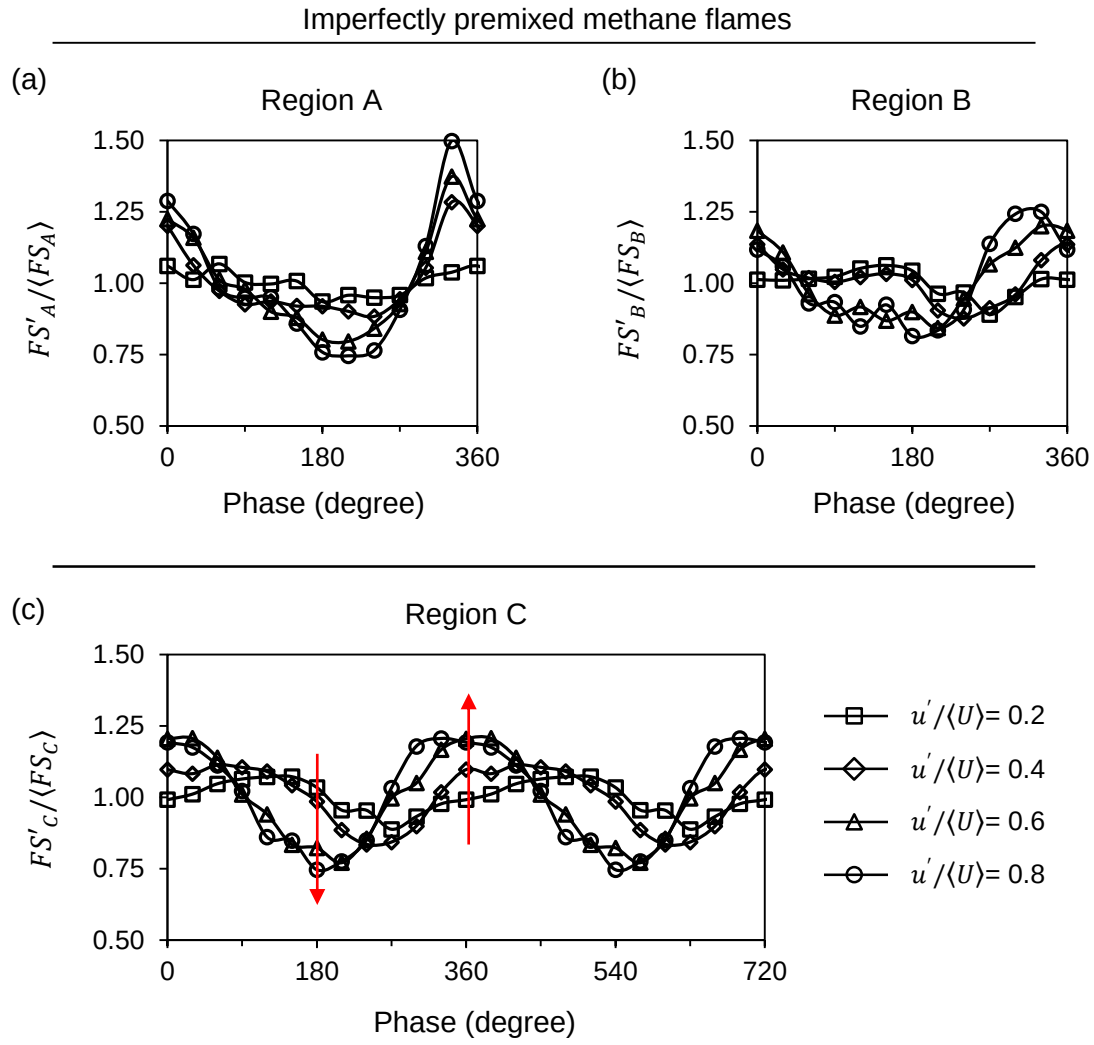

Figure 4.21: Shows the cyclic variation of the normalised flame surface area, $FS'/\langle FS\rangle$, for the regions (a) A, 2.5 – 15 mm, (b) B, 25 – 40 mm, and (c) C, 2.5 – 40 mm, for imperfectly premixed methane flames under forcing conditions, f= 255 Hz.

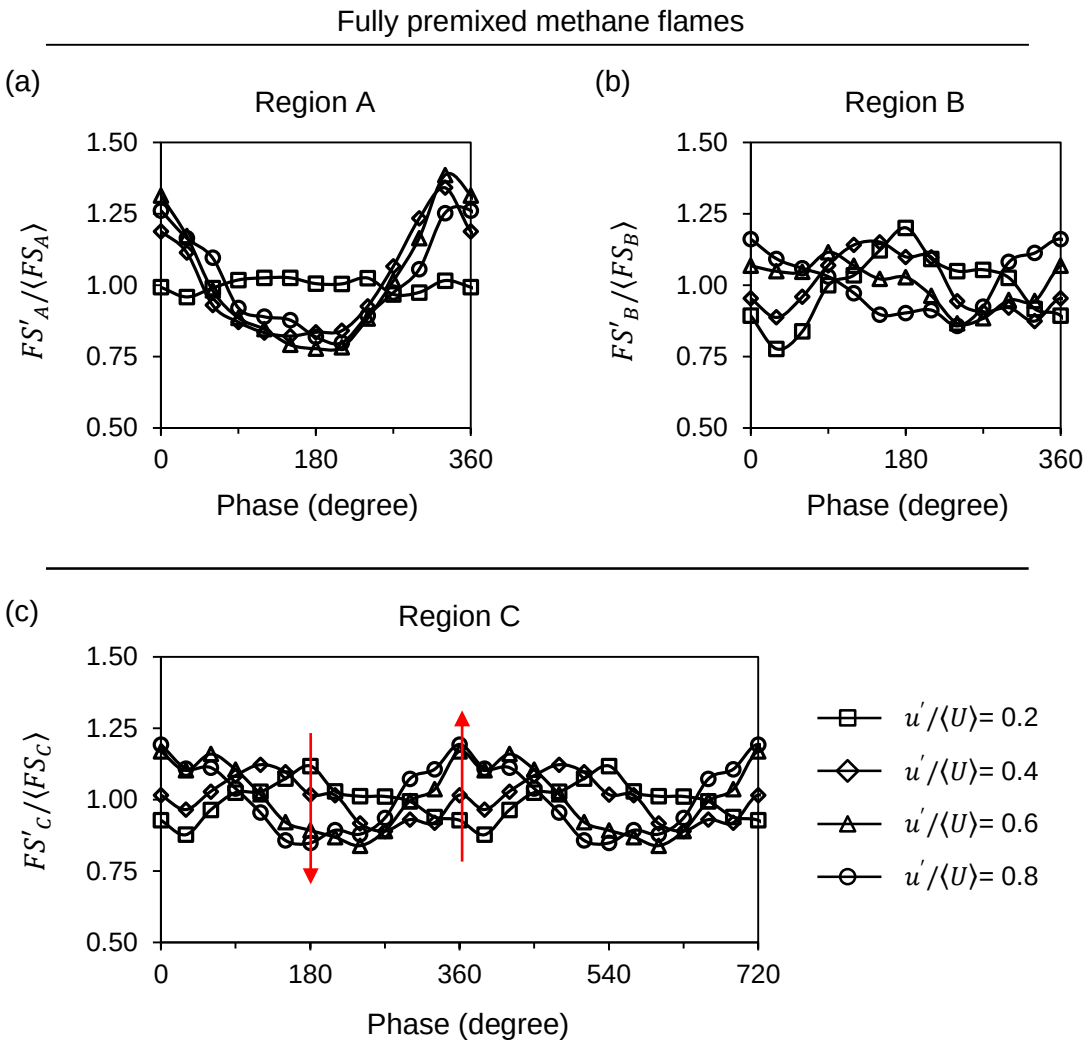

Figure 4.22: Cyclic variation of the normalised flame surface area, $FS'/\langle FS \rangle$, for the regions (a) A, 2.5 – 15 mm, (b) B, 25 – 40 mm, and (c) C, 2.5 – 40 mm, for fully premixed methane flames under forcing conditions, f = 255 Hz.

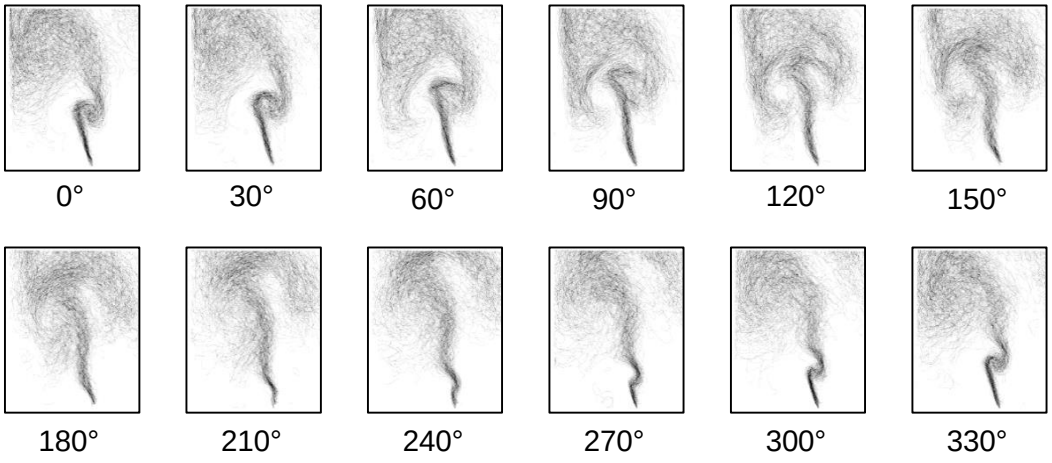

Figure 4.23: Phase-locked averaged flame front (FF) image sequence of imperfectly premixed methane flames, under strong acoustic forcing, f= 255 Hz, and $u'/\langle U \rangle$= 0.4.

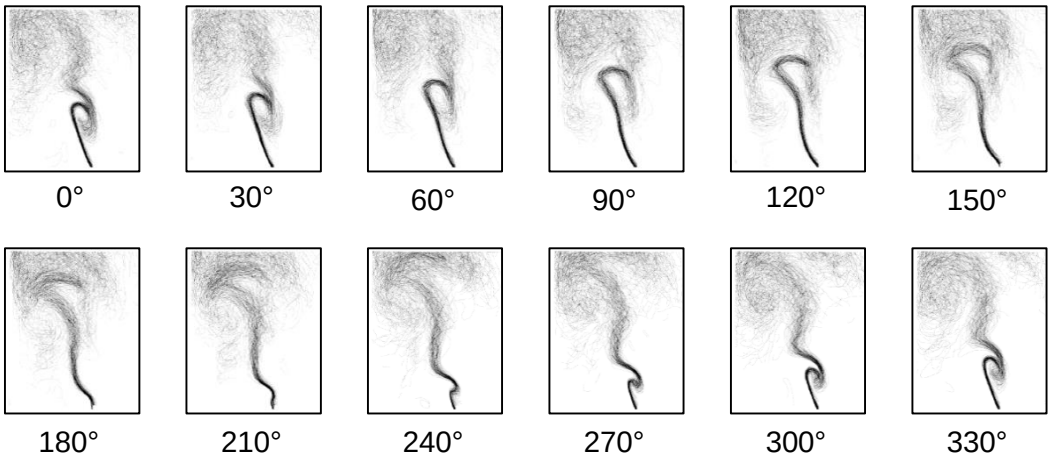

Figure 4.24: Phase-locked averaged flame front (FF) image sequence of fully premixed methane flames, under strong acoustic forcing, f= 255 Hz, and $u'/\langle U \rangle$= 0.4.

For both the methane flames in the Region B there were two significant changes in the flame surface area as the normalised velocity perturbations were increased from 0.2 to 0.8. These changes occurred at 0° (360°) and 180° and were significant enough to be captured in the plot of Region C, indicated by the red arrows in Figures 4.21 (c) and 4.22 (c). At first it seemed that the flame underwent a

phase shift and the formation and destruction of the flame roll-up occurred at different phases along the forcing cycle. However, after further analysis this assumption was incorrect as shown in Figure 4.25, where the images of the averaged flame front at 0° (360°) and 180° with increasing $u'/\langle U \rangle$ are presented for imperfectly premixed methane flames.

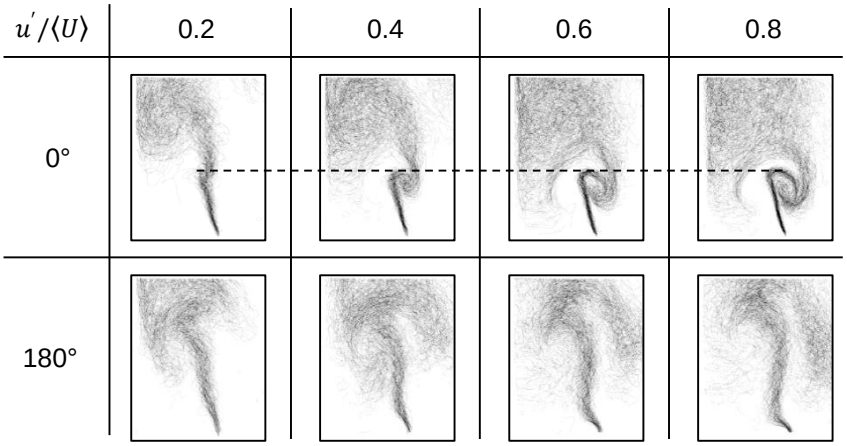

Figure 4.25: Phase-locked averaged flame front (FF) at a phase angle of 0° and 180° for imperfectly premixed methane flames, under increasing velocity perturbations at a fixed forcing frequency of 255 Hz.

The assumption made that the formation and destruction of the flame roll-up occurred at different phases is incorrect, as it can be seen from the images of the flame at 0° in Figure 4.25, that the location where the deformation of the flame front occurred on the inner shear layer (indicated by the dashed line) is the same for all the flames at different $u'/\langle U \rangle$. From the phase locked images at 0° it is clear that the flame surface area increased as the velocity perturbations were increased.

Although the plot for Region C in Figure 4.21 shows a significant reduction in the normalised flame surface area fluctuation at a phase of 180° there is no immediate evidence from the 180° phase images in Figure 4.25. The images show a relatively consistent flame surface area as the $u'/\langle U \rangle$ was increased from 0.2 to 0.8. To aid the understanding of these images, the mean flame surface area of the flames in Region C were normalised against the mean flame surface area of the unforced flame and is shown in Figure 4.26. This plot shows that as the $u'/\langle U \rangle$ was

increased, the mean FS increased as well. With an increasing mean surface area it would explain the reduced $FS^{'}_{C}/\langle FS_{C}\rangle$ in Figure 4.21 (c). This analysis holds true for the fully premixed methane flames as well.

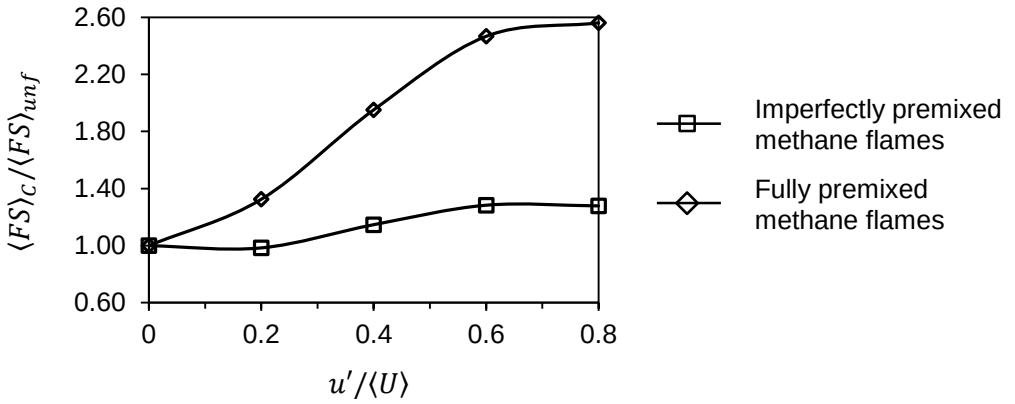

Figure 4.26: Graph of the mean surface area for the acoustically forced imperfectly and fully premixed methane flame normalised against the respective unforced mean surface area with increasing normalised velocity perturbations at a forcing frequency of 255 Hz.

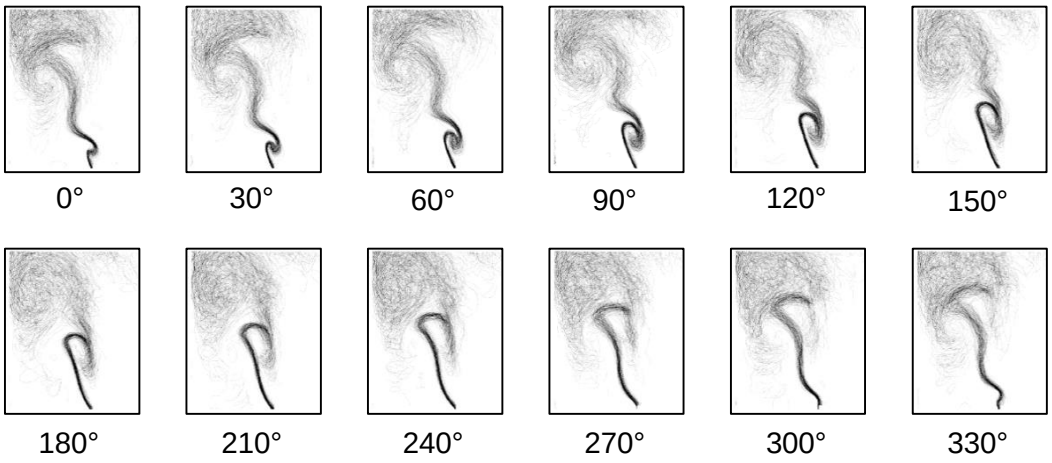

Figure 4.27: Phase-locked averaged flame front (FF) image sequence of 100% methane fully premixed, under strong acoustic forcing, f= 315 Hz, and $u^{'}/\langle U\rangle$= 0.4.

These plots reiterate the fact that the flames had a cyclic response that was governed by the formation of vortices in the flow which caused the flame surface to roll-up leading to variations in the flame surface area and hence the heat release rate. The response of the flames was dependent on the method of how the methane fuel was introduced in to the flow.

At a higher forcing frequency of 315 Hz the flames experienced a similar cyclic response which was mainly due to the formation of vortices and the flame roll-up. The phase evolution of the fully premixed flames at a $u'/\langle U \rangle$ of 0.4 is shown in Figure 4.27.

4.3 Comparison of imperfectly premixed ethylene and methane flames

The flames for imperfectly premixed ethylene and methane were operating under different global equivalence ratios and had different laminar flame speeds (approximately 50 cm/s and 19 cm/s at the equivalence ratio of the reference case of ethylene and methane, respectively), however, some similarities and differences in the trends observed for the heat release and flame surface area fluctuation were observed.

The plots shown in Figure 4.28, show the heat release response of the imperfectly premixed ethylene and methane flames under acoustic excitation. At a low forcing frequency of 30 Hz the heat release fluctuation of the methane flames was much larger than that of the ethylene flames. This can be explained by the large fluctuations in the flame surface area of the methane flames as shown in Figure 4.29. The plot of the normalised flame surface area (Figure 4.29 (a)) shows that the flame surface of the methane flame underwent large fluctuations compared to the ethylene flames. The difference could be due to a number of reasons, such as the difference in the equivalence ratio oscillation experienced at the flame front for each flame. As discussed in section 1.2.1; in cases where the overall equivalence ratio is lower compared to others, the fluctuation in the laminar flame speed would be much higher leading to larger flame surface and heat release oscillations. Also, as the ethylene flame has a higher laminar flame speed the flame may have been more resistive to the changes in the flow. These reasons are only speculative and cannot be proved with the current scope of the project.

As the forcing frequency was increased to 255 and 315 Hz, there was a change in the flames' response, and it can be seen that the heat release oscillation for the ethylene flames was almost three to four times greater than the heat release oscillation of the methane flames. Similarly, the ethylene flames experienced a higher amplitude of oscillation of the flame surface area in two regions, i.e. B and C, shown in Figure 4.30. The initial size of the flame roll-up was much larger for the methane flames indicated by the flame surface fluctuation in Region A and shown by the red arrows on the flame front images at phase 300°. However, the flame surface oscillations in Region B were the major contributor to the overall surface oscillations. So the higher heat release oscillations calculated from the OH* chemiluminescence for the ethylene flames forced at 255 and 315 Hz can be attributed to the larger flame surface fluctuations compared to the methane flames. Despite operating the imperfectly premixed ethylene and methane flames at different equivalence ratios and flame speeds it is interesting to see that the flames' heat release and flame surface oscillation was dependent on the fuel type and on the frequency of forcing.

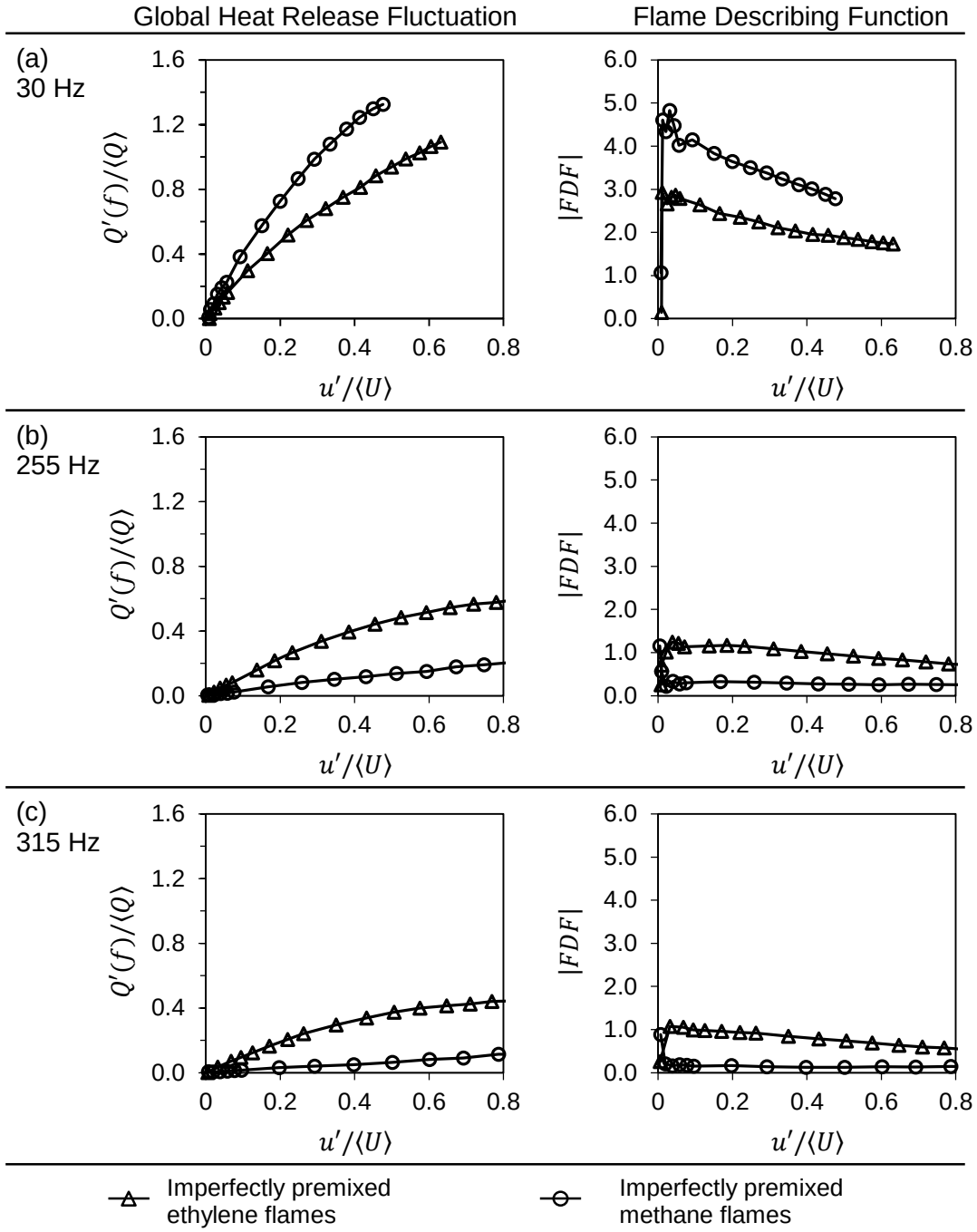

Figure 4.28: The dependence of the global heat release fluctuation and the magnitude of the flame describing function evaluated from OH* chemiluminescence of imperfectly premixed ethylene and methane flames on velocity fluctuations, at forcing frequencies of (a) 30 Hz, (b) 255 Hz, and 315 Hz.

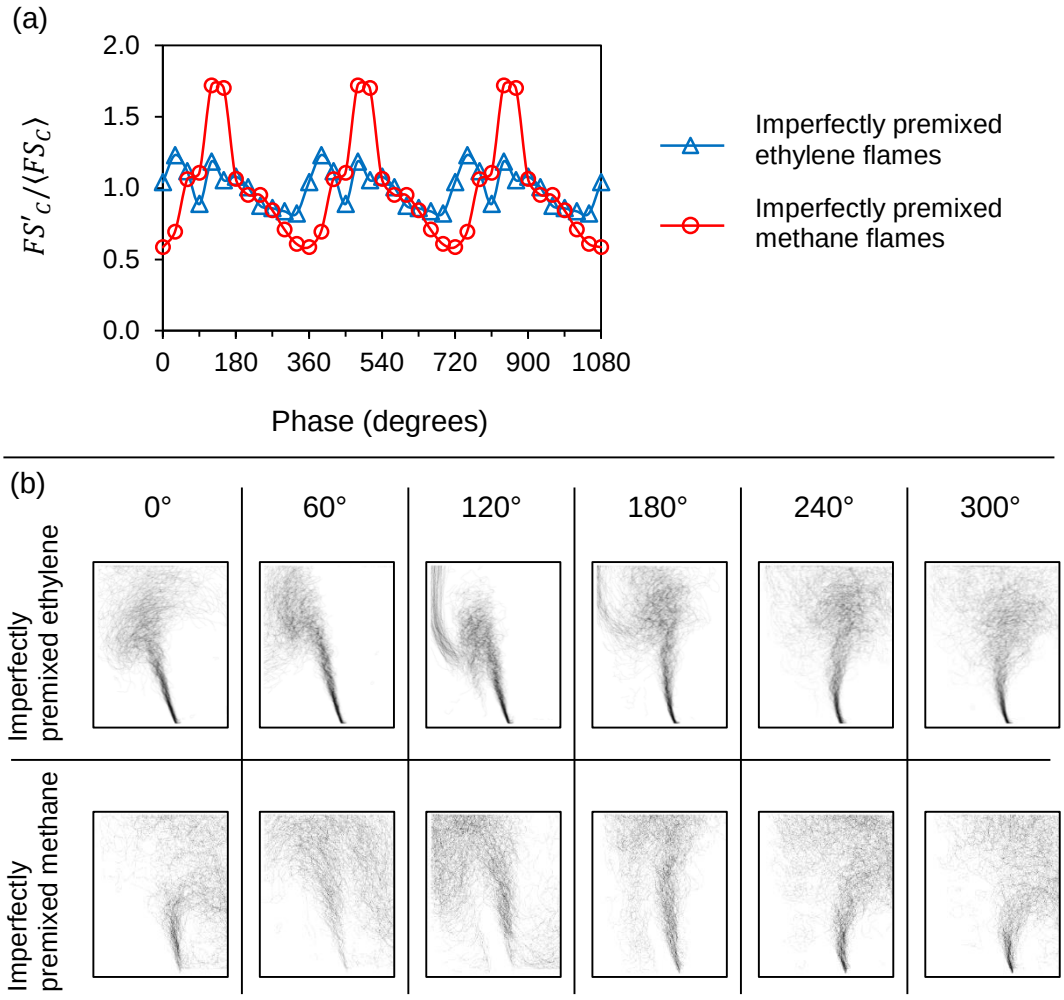

Figure 4.29: Shows the cyclic variation of the (a) normalised flame surface area $FS'/\langle FS \rangle$, in region C, and (b) phase-locked averaged flame front images (in steps of 60°) for imperfectly premixed ethylene and methane flames under forcing conditions, f= 30 Hz, and $u'/\langle U \rangle$= 0.4.

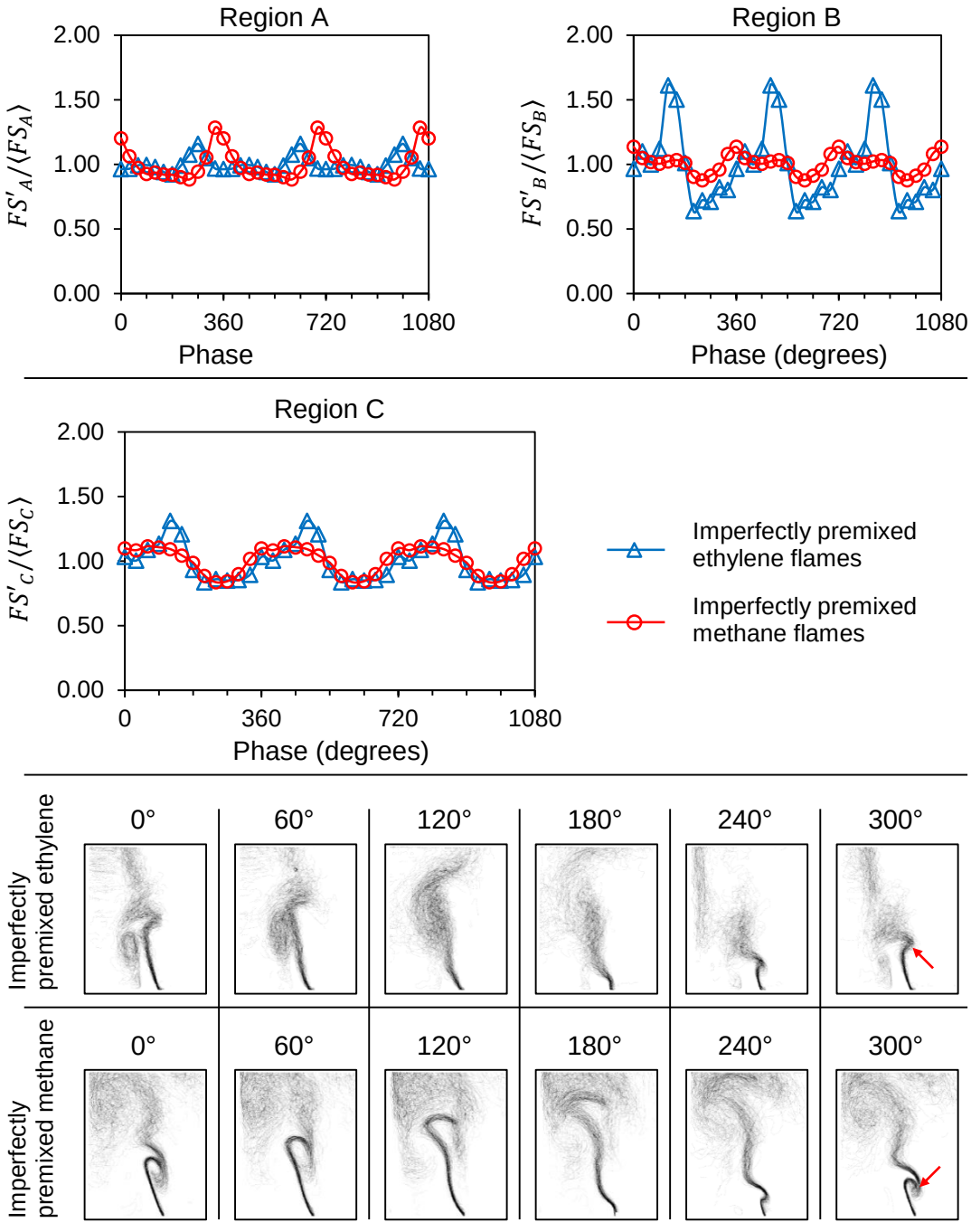

Figure 4.30: Shows the cyclic variation of the normalised flame surface area, $FS^{'}/\langle FS\rangle$, for the regions, A, B, and C; and phase-locked averaged flame front images (in steps of 60°), for imperfectly premixed ethylene and methane flames under forcing conditions, f= 255 Hz, and $u^{'}/\langle U\rangle$= 0.4.

4.4 Summary

The purpose of this chapter was to introduce the turbulent combustion of ethylene and methane flames under unforced and acoustic forcing conditions. The flames were stabilised by a bluff-body placed in the burner and were subjected to inlet velocity perturbations which caused a dynamic response of the flames. The flames were studied using OH* chemiluminescence to determine the heat release rate, and OH PLIF to study the changes in the flame shape and surface area.

The ethylene fuel was imperfectly premixed with the air and the flames mainly stabilised on the inner shear layers. Under acoustic forcing conditions, at low frequencies the flame experienced a flame surface oscillation; however, there were no strong vortical interactions between the flow and the flame front. The relationship between the normalised velocity perturbations and the heat release fluctuation was linear under these test conditions. However, when forced under sufficiently high frequencies (i.e. 255 and 315 Hz) and velocity oscillations the inner and outer shear layers simultaneously rolled up to create a counter rotating vortex pair, thus causing the flame surface to roll-up. This roll-up caused a cyclic variation in the flame surface area and hence the heat release rate.

Similarly, methane flames were tested; however, the fuel was introduced into the flow using two methods, either by imperfectly or fully premixing. Comparing the results of the unforced flames showed that the imperfectly premixed flame was able to intermittently stabilise on the outer shear layers while the fully premixed flame had just stabilised on the inner shear layer. The fully premixed flame had a higher fluorescence of OH at the flame front, either because of a higher concentration of OH radicals or a higher flame temperature.

Under low frequency forcing conditions both the methane flames displayed a linear response between the normalised velocity perturbations and the heat release fluctuations, however, with the imperfectly premixed flame the magnitude of the $Q^{'}(f)/\langle Q\rangle$ was much higher which was due to higher fluctuations experienced in the flame surface area. At higher frequencies of forcing (i.e. 255 and 315 Hz) the flames experienced a similar dynamic response as the ethylene flames as the flame surface rolled up thus causing fluctuations in the heat release oscillations.

Comparing the response of all the flames, of both the fuels under imperfectly premixed conditions, showed that the heat release response and the shape of the

flame is dependent on the velocity oscillations, forcing frequency, fuel type and method of fuel introduction into the flow.

Chapter 5: Local addition of hydrogen to ethylene and methane flames

The combustion characteristics of turbulent ethylene and methane flames were discussed in the previous chapter. The results showed that the oscillations in the flame surface area had a direct correlation with the heat release rate. From the literature survey it was suggested that a local injection of fuel to the inner shear layers of the flame may help in stabilising the flame and thus reducing the heat release fluctuations. The addition of fuel into the inner shear layer was required to increase the local equivalence ratio, thus the local flame speed. As hydrogen is considered a clean fuel and is known to have a high flame speed (Yu *et al.* 1986) it was used to try reduce the combustion oscillations.

This chapter discusses the effects of the local addition of hydrogen on the heat release response of the reference ethylene and methane flames. As mentioned in Chapter 2, the response of the flames were studied using the heat release oscillations (determined from the OH* chemiluminescence), hydroxyl, OH, PLIF and the flame surface area; and in addition to these methods the atomic hydrogen, H, PLIF was also imaged for the hydrogen enriched flames in this chapter.

5.1 Local addition of hydrogen to imperfectly premixed ethylene flames

5.1.1 Experimental conditions

Pure ethylene imperfectly premixed flames were subjected to the local addition of hydrogen through the secondary fuel ports placed 2 mm below the base

of the combustion zone (the method of primary and secondary fuel introduction into the flow is detailed in Chapter 2). The addition of hydrogen was increased in steps, measured by the percentage volume of the fuel mixture. During experimentation the volume flow rate (slpm) of the air was kept constant. Keeping the volume flow rate constant caused negligible changes in the flow turbulence at the entrance of the combustion zone with small increments in the fuel quantities (as discussed in Chapter 3). Table 5.1 shows the flow conditions used in the study of imperfectly premixed ethylene flames with local hydrogen addition. The quantity S_L, is the overall laminar flame speed of the mixture calculated using COSILAB with a modified reaction mechanism established by Nicolle and Dagaut 2006. As the % of H_2 increases the overall flame speed increases as well. These values do not represent the flame speed locally in the flame due to turbulent flow conditions and the localised addition of H_2. However, it does indicate that the addition of H_2 to the mixture does increase the flame speed. These laminar flame speed calculations are purely theoretical and as part of future work, these values should be verified with experimental measurements.

Label	Air (slpm)	Primary		Secondary		ϕ_{Global}	S_L (cm/s)
		C_2H_4 (slpm)	C_2H_4 %	H_2 (slpm)	H_2 %		
0% H_2	250.0	14.2	100.0	0.0	0.0	0.812	53.496
5% H_2	250.0	14.1	95.0	0.7	5.0	0.812	54.153
10% H_2	250.0	13.9	90.0	1.5	10.0	0.811	54.875
20% H_2	250.0	13.6	80.0	3.4	20.0	0.809	56.534
30% H_2	250.0	13.2	70.0	5.7	30.0	0.808	58.523

Table 5.1: Lists the experimental flow conditions under study of the local addition of hydrogen to imperfectly premixed ethylene flames.

5.1.2 Unforced ethylene-hydrogen flames

Hydrogen is known to promote the formation of OH radicals which is a chain initiation and propagation radical (Najm and Wyckoff 1997). The increased formation of the OH radicals promotes a faster breakdown of the fuel molecules. From the OH PLIF images shown in Figure 5.1 (a), it shows that the increase in the

% H_2 had a significant impact on the intensity of the PLIF signal of OH radicals at the inner shear layers and the central recirculation zone. The signal intensity at the shear layers increased with increasing % H_2 which may indicate a faster reaction taking place.

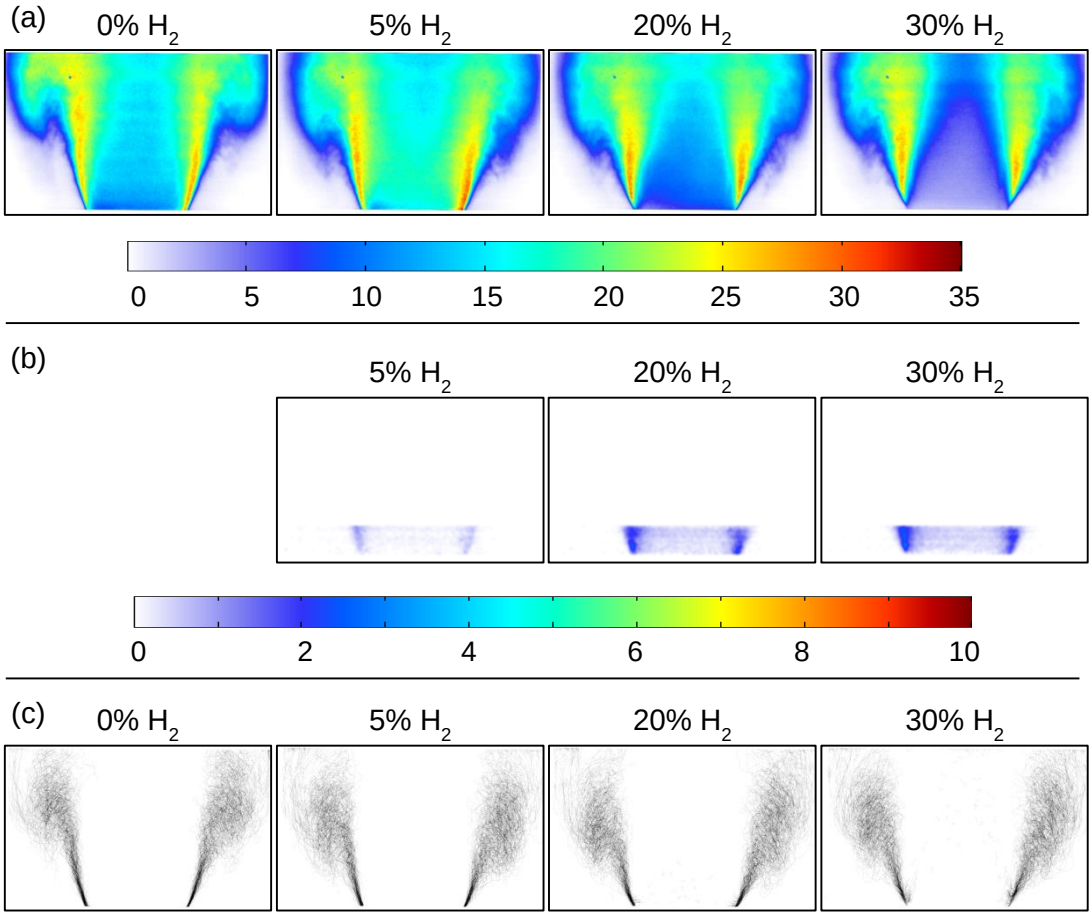

Figure 5.1: Shows the averaged, (a) OH PLIF, (b) H PLIF, and (c) flame front images for the unforced, imperfectly premixed ethylene flames with varying quantities of hydrogen addition (For detailed flow information refer to Table 5.1).

Authors Najm and Wyckoff (1997) and Kee *et al.* (1988) showed that the following chemical reaction was a dominant consumer of atomic hydrogen and a key chain-branching reaction as it produced OH radicals, promoting higher reaction rates as it was controlled by the concentration of OH radicals at the flame front.

$$H + O_2 = OH + O$$

Although the signal of OH PLIF increased at the flame front, the fluorescence in the central recirculation zone reduced significantly with increasing % H_2. There could be several reasons why this reduction of OH radicals occurred. There could have been alterations in the size, position and temperature of the central recirculation zone. However, these possibilities cannot be confirmed due to the limited scope of the current experimental setup.

The local addition of H_2 fuel caused a local increase in the equivalence ratio at the base of the flame. From the H PLIF images in Figure 5.1 (b) there was a notable increase in the intensity of the signal at the lower inner shear layers with the introduction of H_2 fuel. This shows that the H_2 fuel immediately broke down into atomic hydrogen which was then used in the combustion process. The averaged flame front images (Figure 5.1 (c)) show subtle changes in the height and width of the flames with increasing % H_2.

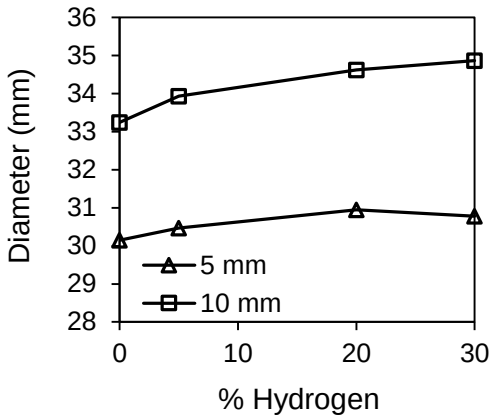

Figure 5.2: Shows the change in the diameter with varying % of hydrogen addition.

The graph presented in Figure 5.2 shows the change in flame diameter at heights of 5 and 10 mm, above the inlet to the combustion zone. With the addition of H_2 to the fuel mixture, the diameter increased; however, there was a non-linear trend observed as the % of H_2 was increased. Between the case with 20% H_2 and 30% H_2 there was very little change in the flame diameter. Besides this, there were

also instances of flame detachment from the lip of the bluff-body with 30% H_2 addition, which have been due to a very high local equivalence ratio.

A brief study on the emissions was also conducted and the parameters that were measured were the NO_x and CO_2 measured in terms of parts per million (ppm) and %, respectively. The plot in Figure 5.3 shows how the NO_x and CO_2 emissions changed with increasing hydrogen fuel content. The results showed that with increasing % H_2 the % CO_2 in the exhaust gases reduced while the NO_x ppm increased. As discussed earlier, Hydrogen is known for being a very clean alternative fuel and can reduce the level of CO and CO_2 in the emissions (Dahl and Suttrop 1998, Wicksall and Agrawal 2007, Guo *et al.* 2005, Choudhuri and Gollahalli 2003, Kim *et al.* 2009). The reduction in the CO_2 was most likely due to the fact that the quantity of ethylene in the flow was reduced by 7%. However, the reduction seemed insignificant to the 200% increase in NO_x ppm. Studies (Barbosa *et al.* 2007, Cozzi and Coghe 2006, Ilbas *et al.* 2005) have shown that the significant rise in NO_x production was a direct result of higher flame temperatures achieved with the addition of hydrogen.

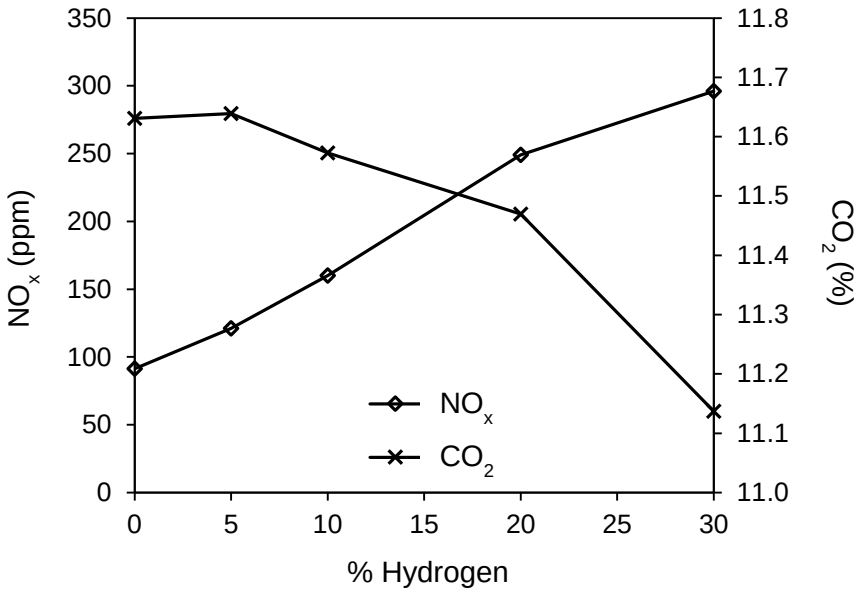

Figure 5.3: The plot shows the change in NO_x (ppm) and % CO_2 emissions with the increase in % hydrogen addition.

5.1.3 Acoustic response of ethylene-hydrogen flames

The dynamic response of forced imperfectly premixed ethylene flames with the addition of hydrogen at varying quantities are presented in this section. At 30, 255 and 315 Hz the flow was acoustically forced to achieve high velocity perturbations. In the previous chapter it was shown how the imperfectly premixed ethylene flames stabilised in the wake of the bluff-body and how they were affected by a continuous imposed sinusoidal perturbation in the flow.

With the addition of hydrogen, the flames experienced a similar periodic response; however, there were noticeable differences in the magnitude of the heat release and flame surface area fluctuation. Figures 5.4, 5.5, 5.6, and 5.7, show the phase-locked images of ethylene flames with 0%, 5%, 20%, and 30% of hydrogen addition, and Figure 5.8 shows the cyclic variation in the normalised flame surface area, $FS^{'}/\langle FS\rangle$, for the regions (a) A, 2.5 – 15 mm, (b) B, 25 – 40 mm, and (c) C, 2.5 – 40 mm, for each case. With the local addition of H_2 via the secondary fuel ports the flame shape changed with increasing % H_2. Comparing the sequence of images, visually it can be seen that a local addition of 5% H_2 caused the initial size of the flame roll-up to reduce (starting from 180°). A local increase of the flame speed due to the addition of hydrogen fuel at the base of the flame could be a possible reason why such a change in the shape occurred. With the increase in flame speed the unburnt gas/fuel mixture was rapidly consumed without having enough time for the flame to roll-up. However, during the cycle, the roll-up still grew in size to an eventual collapse and another roll-up was produced at the base of the flame.

The profile of the overall flame surface oscillation, $FS^{'}_{C}/\langle FS_C\rangle$, (Region C) changed significantly from phase angles of 150° to 240° as the % of H_2 was increased, (Figure 5.8 (c)). The two visible alterations in the flame surface during these phases was the reduced flame roll-up (indicated by the blue arrow) in Region A (i.e. 2.5 mm to 15 mm from the base of the combustion zone), and the retention of flame surface (indicated by the red arrow) in the Region B (i.e. 20 mm to 40 mm from the base of the combustion zone). The percentage contribution of the flame surface area in region A to region C ranged from 16-17% while for region B to C it ranged from 29-35%. Judging from these values and the overall flame surface area fluctuation in Region C (Figure 5.8 (c)), the most significant change in the flame

surface area occurred in Region B. In this region (Figure 5.8 (b)), the size of the vortex roll-up was at its maximum before its collapse into several pockets of burning air/fuel mixture. Due to the collapse there was a loss of flame surface area for the 0% H_2 (pure ethylene) case, however, as the percentage of hydrogen was increased the loss of flame surface in this region reduced. This statement can be verified by the visual inspection of the individual phase-locked images in Figures 5.4, 5.5, 5.6, and 5.7 at a phase of 210°. This revealed that the addition of H_2 appeared to sustain the flame surface in that region which reduced the steep drop in flame surface area from 150° to 270°, shown in Figure 5.8 (c).

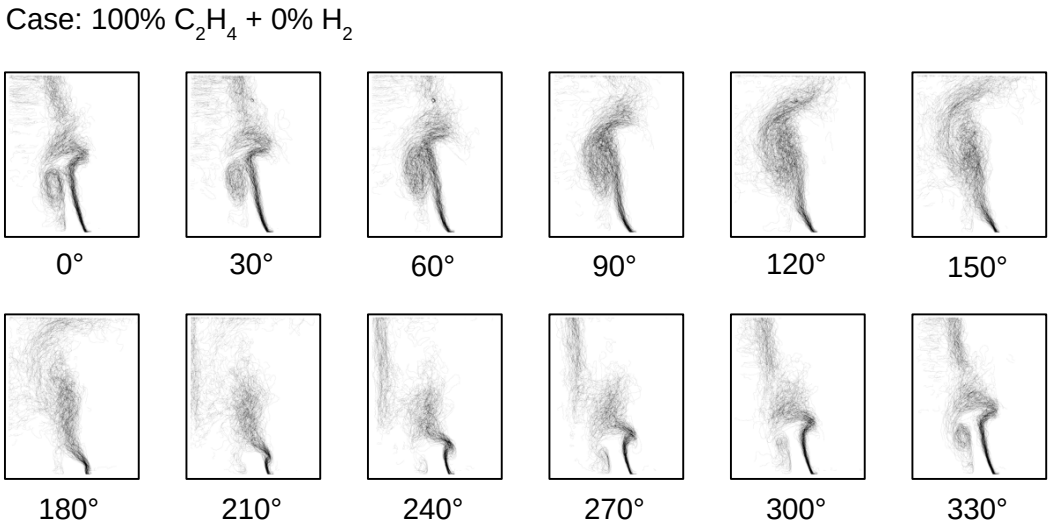

Figure 5.4: Phase-averaged flame front (FF) image sequence of 100% ethylene imperfectly premixed, under strong acoustic forcing, f= 255 Hz, and $u'/\langle U \rangle$= 0.4.

Case: 95% C_2H_4 + 5% H_2

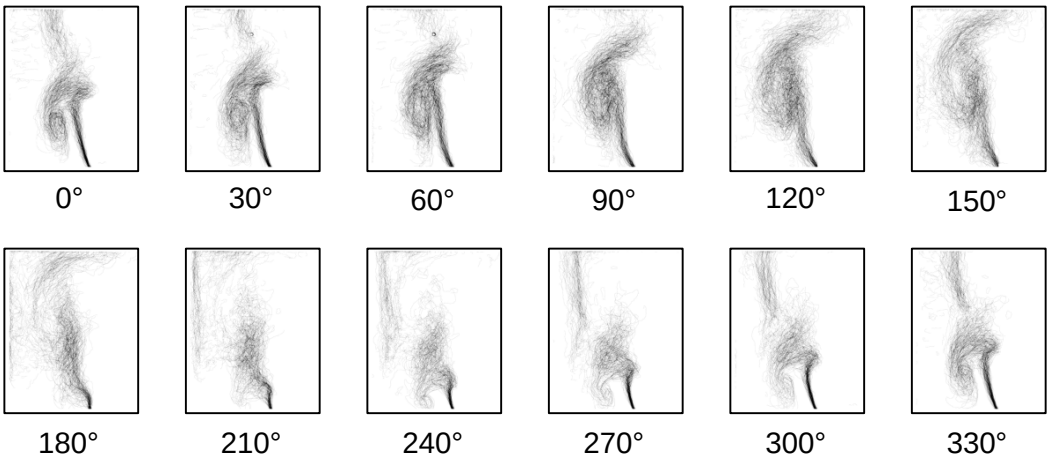

Figure 5.5: Phase-averaged flame front (FF) image sequence of 95% ethylene imperfectly premixed with the local addition of 5% hydrogen, under strong acoustic forcing, f= 255 Hz, and $u'/\langle U\rangle$= 0.4.

Case: 80% C_2H_4 + 20% H_2

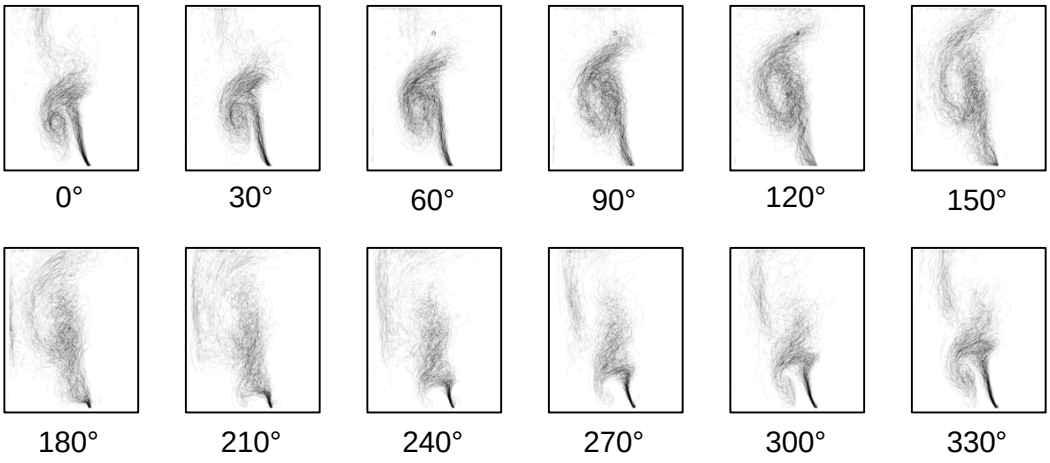

Figure 5.6: Phase-averaged flame front (FF) image sequence of 80% ethylene imperfectly premixed with the local addition of 20% hydrogen, under strong acoustic forcing, f= 255 Hz, and $u'/\langle U\rangle$= 0.4.

Case: 70% C_2H_4 + 30% H_2

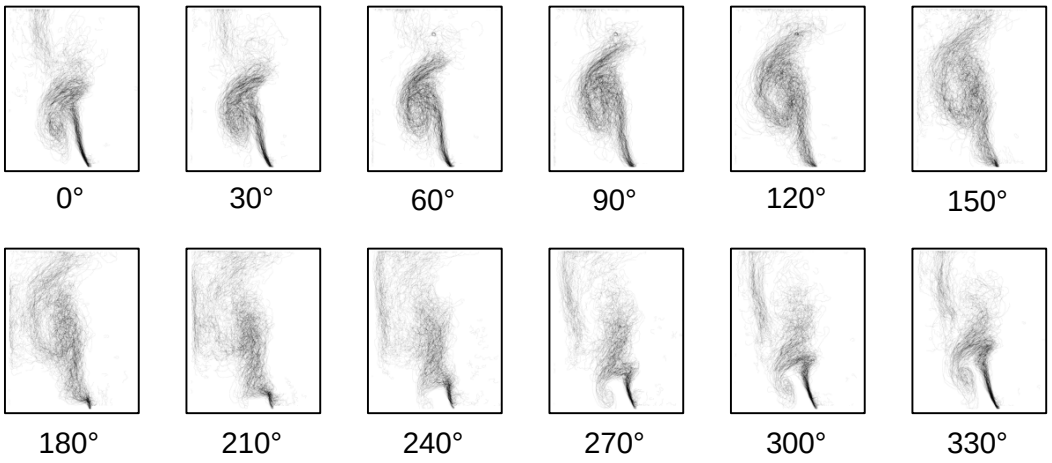

Figure 5.7: Phase-averaged flame front (FF) image sequence of 70% ethylene imperfectly premixed with the local addition of 30% hydrogen, under strong acoustic forcing, f= 255 Hz, and $u'/\langle U\rangle$= 0.4.

The plots in Figure 5.9 (a, b, and c) show the dependence of the global heat release fluctuation and magnitude of the flame describing function, FDF, evaluated from OH* chemiluminescence for the ethylene-hydrogen flames. At a low forcing frequency of 30 Hz the local addition of H_2 caused a slight reduction in the heat release fluctuation, $Q'(f)/\langle Q\rangle$, however, further increasing the quantity of hydrogen caused minimal change in the response. On the other hand at a higher forcing frequency of 255 Hz and 315 Hz, there was a noticeable reduction in the heat release fluctuation with the addition of H_2. This decrease was most likely due to the reduction in the size of the flame roll-up (Region A - Figure 5.8 (a)) and the reduction in the loss of the flame surface in Region B (Figure 5.8 (b)). The magnitude of the FDF reduced with increasing hydrogen content, however, the differences between the 20% and 30% H_2 flames were minor.

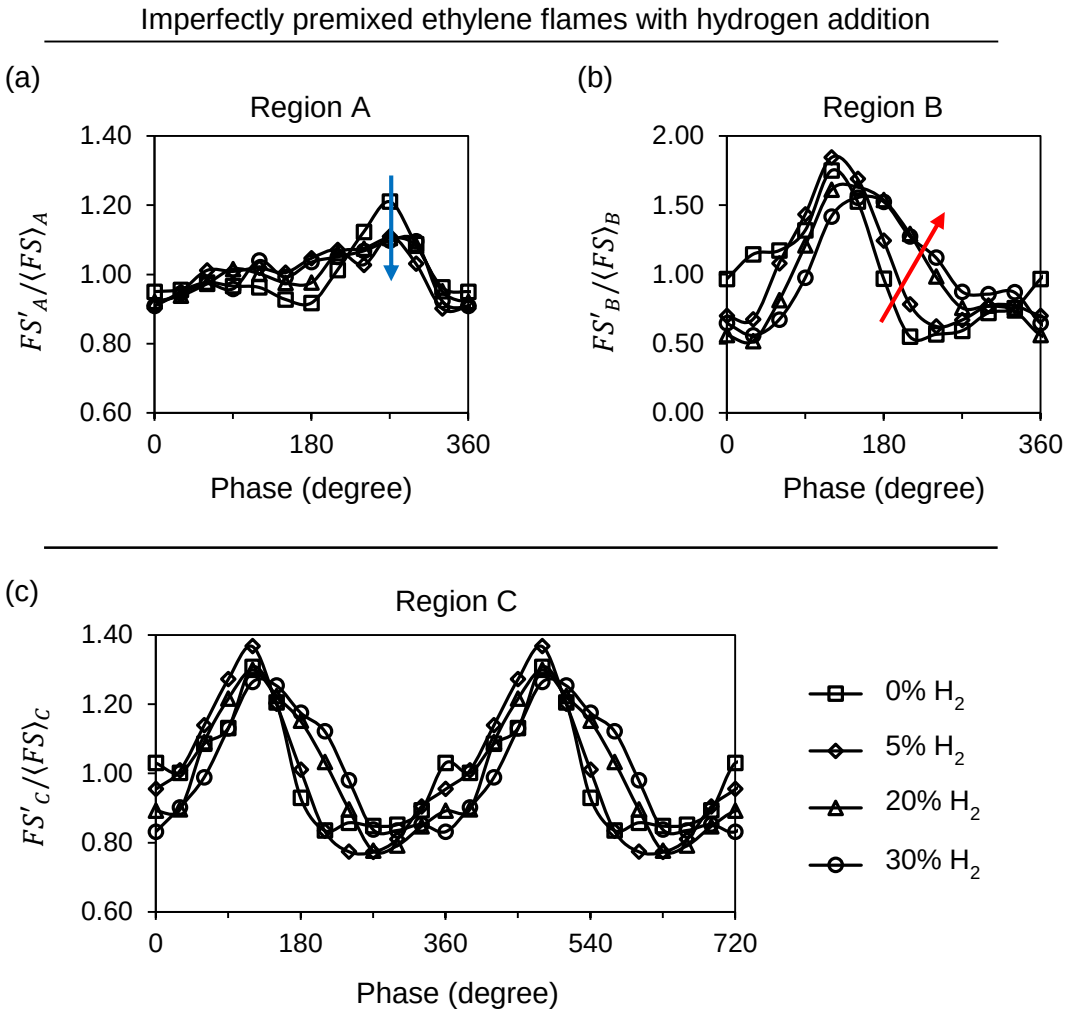

Figure 5.8: Shows the cyclic variation of the normalised flame surface area, $FS'/\langle FS\rangle$, for the regions (a) A, 2.5 – 15 mm, (b) B, 25 – 40 mm, and (c) C, 2.5 – 40 mm, for imperfectly premixed ethylene flames with increasing quantities of hydrogen addition under forcing conditions, f= 255 Hz, and $u'/\langle U\rangle$= 0.4.

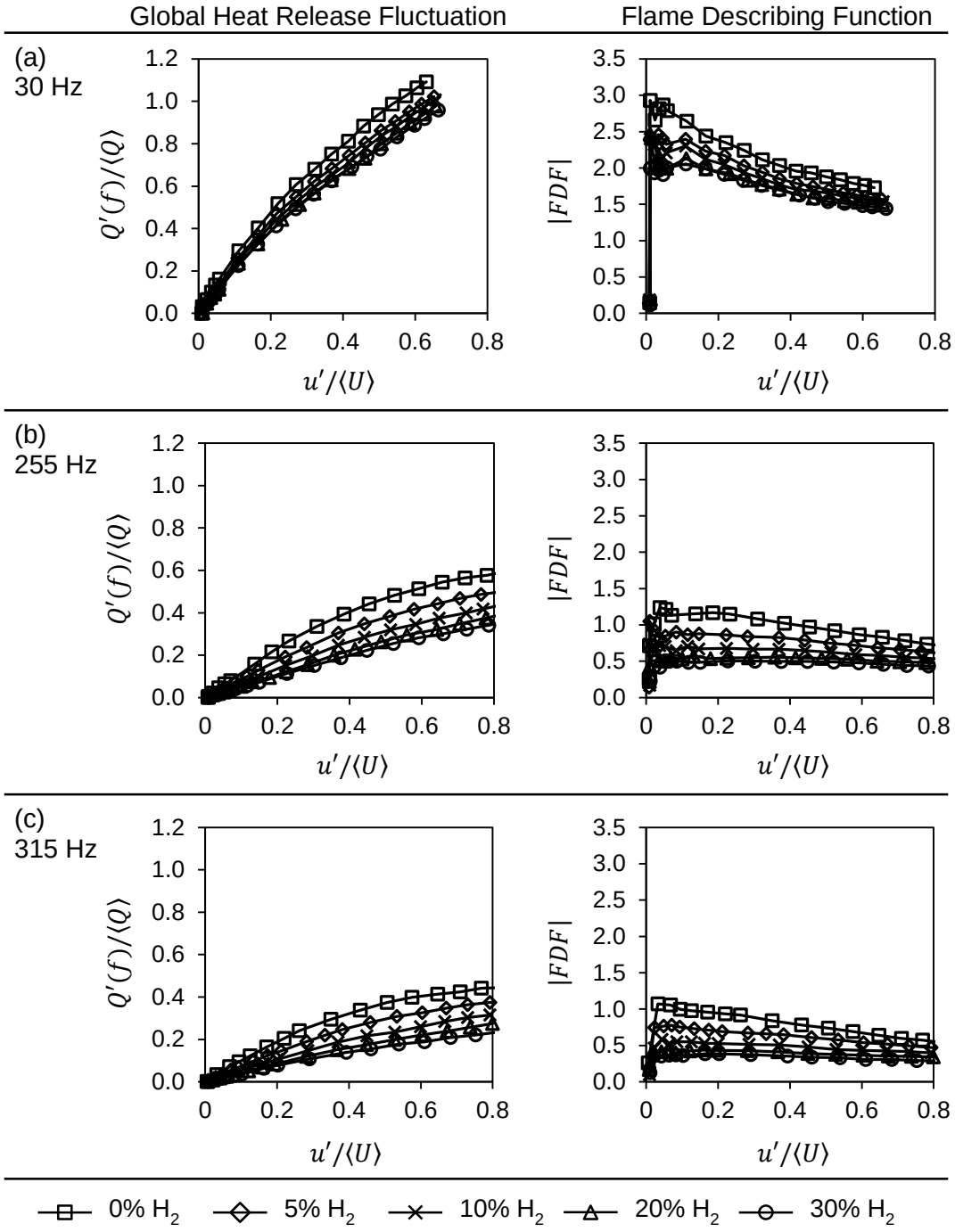

Figure 5.9: The dependence of the global heat release fluctuation and the magnitude of the flame describing function evaluated from OH* chemiluminescence of imperfectly premixed ethylene flames with local addition of hydrogen on velocity fluctuations, at forcing frequencies of (a) 30 Hz, (b) 255 Hz, and (c) 315 Hz.

Hydroxyl, OH, and atomic hydrogen, H, PLIF imaging

Another aspect of the flames that can be qualitatively compared is the intensity of OH and H PLIF of the flames. For clarity the full sequence of the variation of the OH PLIF intensity for the flames are shown in Figures A.3, A.4, A.5 and A.6, in Appendix A. These images show the cyclic variation of the presence of OH radicals in the flame with the addition of varying quantities of hydrogen during acoustic excitation.

The images in Figure 5.10, which show the OH PLIF signal observed for 0% H_2, 5% H_2, 20% H_2, and 30% H_2, phase-locked at 270°, revealed an interesting change in the OH PLIF signal as the percentage of hydrogen was increased. While the flame roll-up reduced in size with increasing the hydrogen content there was a significant reduction in the OH PLIF signal intensity when increasing the % H_2 from 20% to 30%.

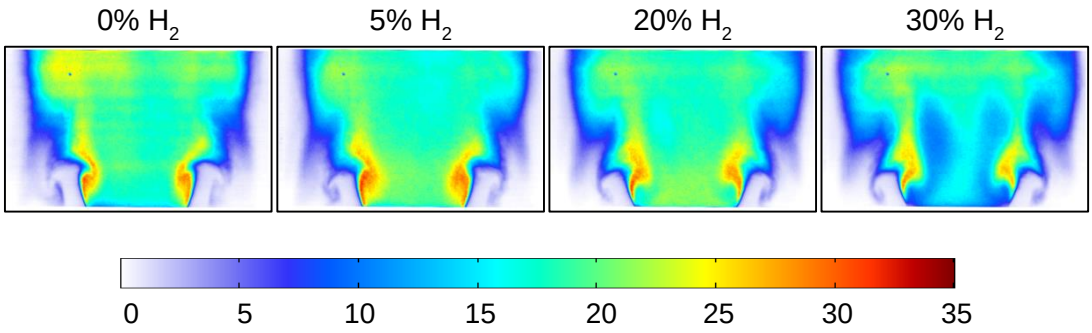

Figure 5.10: Averaged and phase-locked images at 270° of OH PLIF for varying quantities of hydrogen addition to imperfectly premixed ethylene flames, f= 255 Hz, and $u'/\langle U\rangle$= 0.4.

Figure 5.11 shows the variation of atomic hydrogen, H, for the imperfectly premixed ethylene flame with 30% hydrogen addition under forced conditions. The images show that the presence of H had a periodic response. The initial appearance of the flame roll-up occurred from phase 180° to 270° and from the images, it shows that the intensity of the H PLIF signal increased during the initial formation of the flame roll-up. The increased presence of atomic hydrogen in that area might be the reason why there was a reduced size of the flame roll-up.

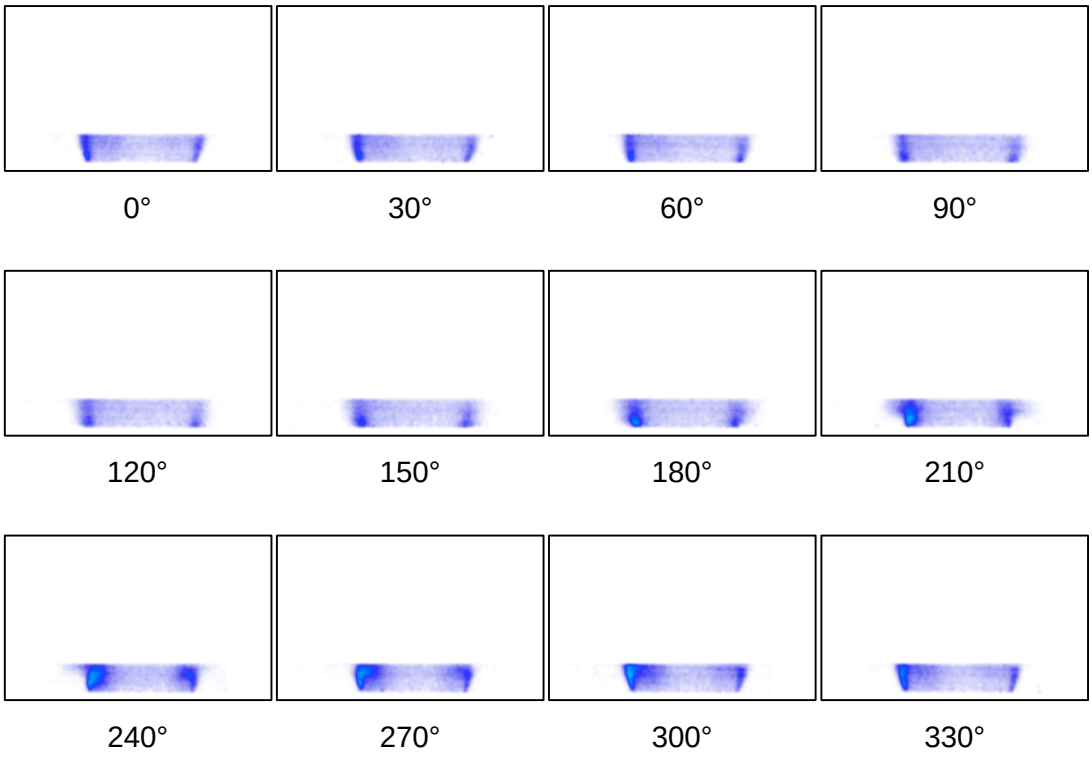

Figure 5.11: Shows the variation of H PLIF signal during acoustic forcing for the imperfectly premixed ethylene flame with 30% hydrogen addition.

5.2 Local addition of hydrogen to methane flames

This section presents the effects of hydrogen addition on imperfectly and fully premixed methane flames and the description of turbulent combustion that was discussed in the previous chapter, but just shows the significant results obtained from the hydrogen addiction, while a lot of the data is shown in the Appendix for reference.

5.2.1 Experimental conditions

The experimental setup described in Chapter 2 was used to study the effects of hydrogen addition on methane flames. Hydrogen was introduced into the flow through the secondary fuel ports, however, two modes of methane mixing were

considered in the study, imperfectly and fully premixed with the air. Table 5.2 shows the list of test conditions used in the study of both imperfectly and fully premixed methane flames with local hydrogen addition. The labels of 0% H_2, 5% H_2 and so on will now refer to the local addition of H_2 to the imperfectly or fully premixed methane flames. The laminar flame speed, S_L, was calculated using the software COSILAB using the GRI mechanism 3.0. The simulations were run similar to ethylene mixtures, so the S_L values shown here are of the overall mixture, and as the % of H_2 increases the laminar flame speed increases as well. In the case of ethylene/hydrogen mixtures, the percentage change in the S_L, going from 0% to 30% H_2 was 10%, while with methane/hydrogen mixtures it is a 30% increase. Although these calculations indicate that the addition of hydrogen increases the laminar flame speed, experimental measurements must be conducted in future work to verify these results.

Label	Air (slpm)	Primary		Secondary		ϕ_{Global}	S_L (cm/s)
		CH_4 (slpm)	CH_4 %	H_2 (slpm)	H_2 %		
0% H_2	250.0	18.4	100.0	0.0	0.0	0.700	21.253
5% H_2	250.0	18.1	95.0	1.0	5.0	0.698	22.231
10% H_2	250.0	17.8	90.0	2.0	10.0	0.696	23.327
20% H_2	250.0	17.1	80.0	4.3	20.0	0.692	25.279
30% H_2	250.0	16.3	70.0	7.0	30.0	0.687	27.706

Table 5.2: Lists the experimental flow conditions under study of the local addition of hydrogen to imperfectly and fully premixed methane flames.

5.2.2 Unforced characteristics of methane-hydrogen flames

Figures 5.12 and 5.13 show the averaged OH and H PLIF, and flame front images for the imperfectly and fully premixed methane cases, respectively. The PLIF testing was carried out for 0% H_2, 10% H_2 and 30% H_2. For both the methods of methane mixing there was a gradual increase in the OH fluorescence intensity at the flame front with the addition of hydrogen, however, at the same time there was a notable change in the OH intensity seen in the central recirculation zone. For

imperfectly and fully premixed methane flames, the flame diameter, at a height of 5 mm, increased around 1 – 2 mm (approximately 3–7% change) with the introduction of hydrogen.

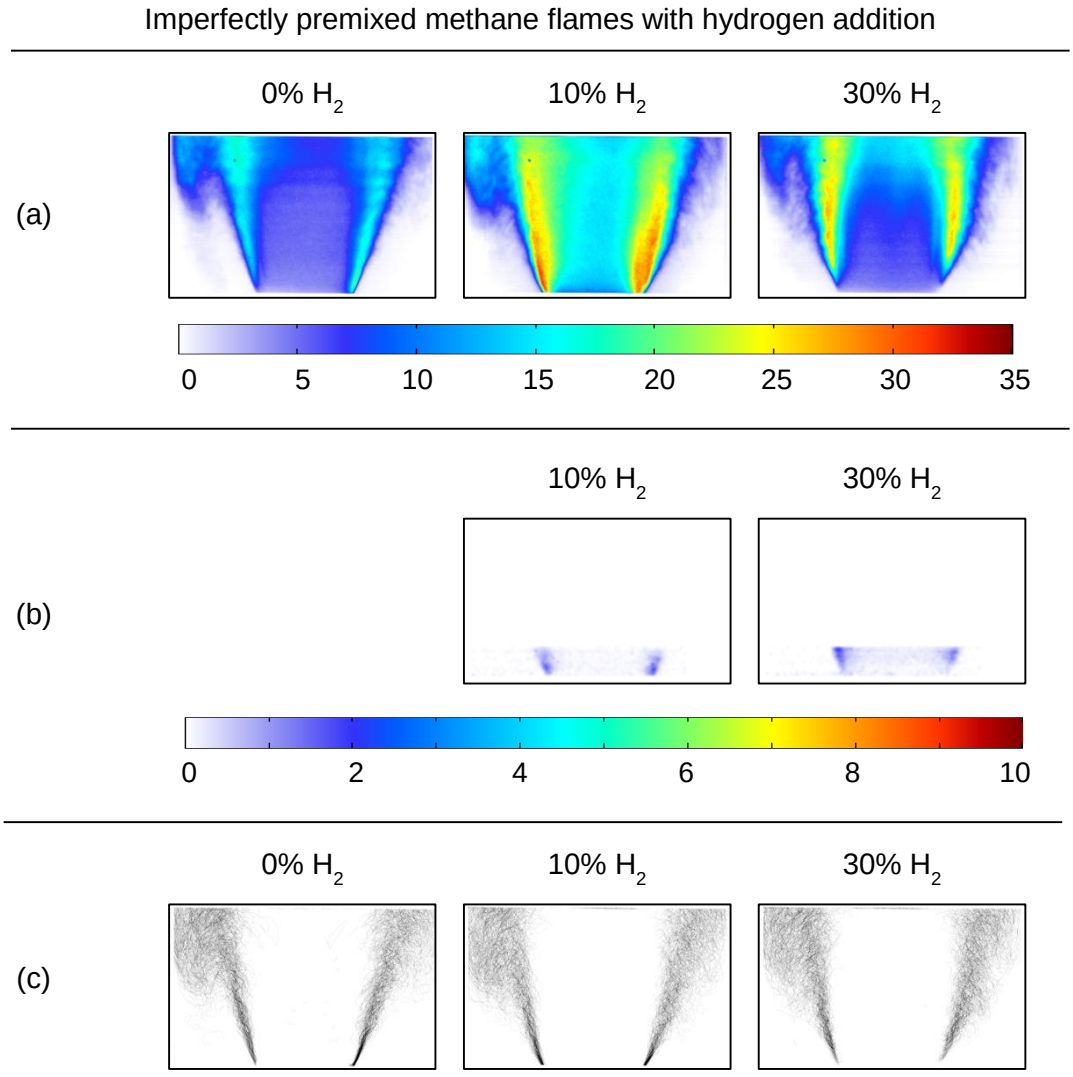

Figure 5.12: Shows the averaged, (a) OH PLIF, (b) H PLIF, and (c) flame front images for the unforced imperfectly premixed methane flames with varying quantities of hydrogen addition (For detailed flow information refer to Table 5.2).

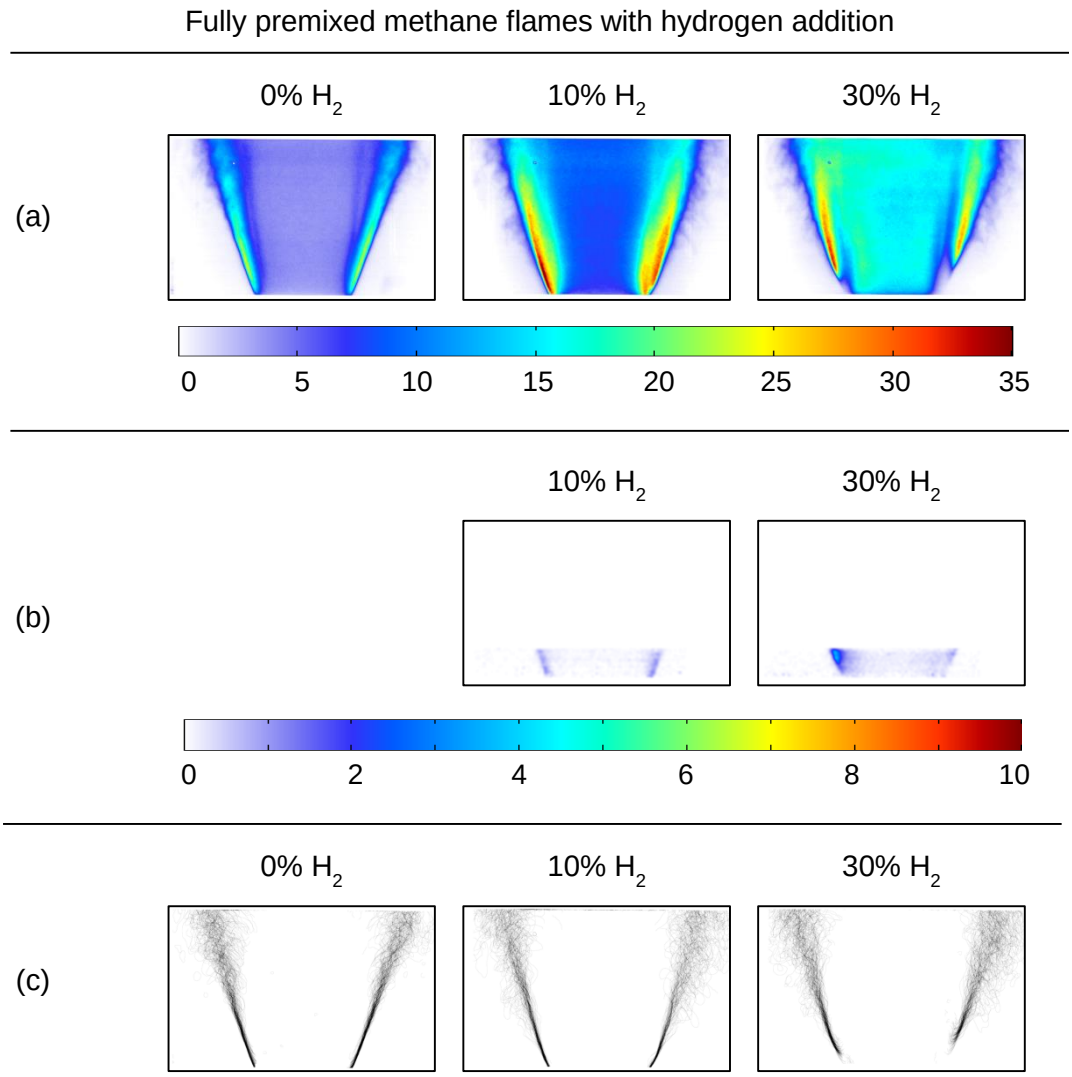

Figure 5.13: Shows the averaged, (a) OH PLIF, (b) H PLIF, and (c) flame front images for the unforced fully premixed methane flames with varying quantities of hydrogen addition (For detailed flow information refer to Table 5.2).

A study on the average NO_x and CO_2 emissions for methane flames with local hydrogen addition was carried out. The data obtained is presented in Figure 5.23, which shows that the results were similar to the plots obtained for ethylene-hydrogen flames. There was a general increase in the NO_x quantity and a decrease in the % CO_2 for both, imperfectly and fully premixed methane flames with increasing % H_2 addition.

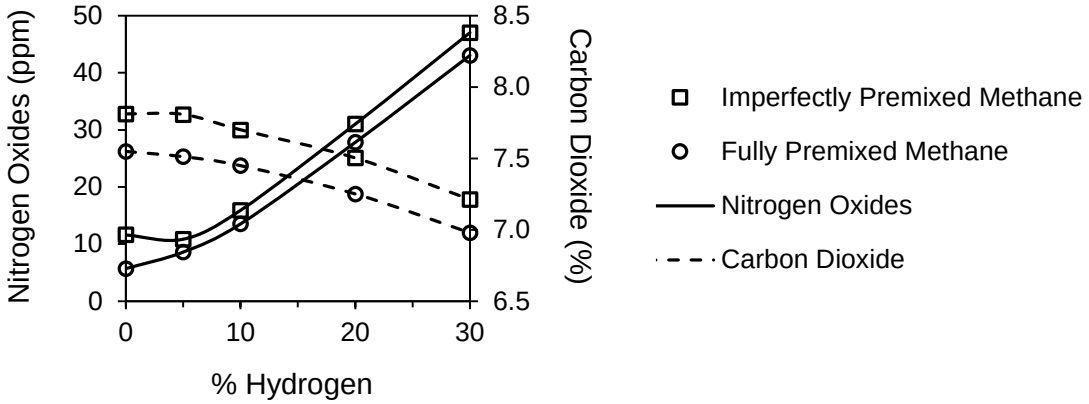

Figure 5.14: The plot shows the change in NO_x (ppm) and % CO_2 emissions with the increase in % Hydrogen addition for imperfectly and fully premixed methane flames.

5.2.3 Dynamic response of methane-hydrogen flames

To study the flame's dynamic response the flow was perturbed at the three frequencies where high velocity perturbations were achieved, i.e. 30, 255 and 315 Hz. Initially, the OH* chemiluminescence was recorded using the PMT device and processed to see how the flames responded at different levels of velocity perturbations. Figures 5.15 and 5.16 show the global heat release fluctuation (determined from the OH* chemiluminescence), and the resulting flame describing function, FDF, for all the cases under study, with imperfectly or fully premixed methane.

At a low forcing frequency of 30 Hz, there was a reduction in the flame response with the increase in the hydrogen addition, whether methane was imperfectly or fully premixed. However, at a forcing frequency of 255 Hz the flames with imperfectly premixed methane had a significant reduction in the heat release response at 20% H_2 and 30% H_2. With fully premixed methane flames the heat release fluctuation increased with the addition of 5% and 10% H_2, compared to the pure methane flames except for when 30% of H_2 was added. Further increasing the forcing frequency had a negative effect, as with any amount of H_2 addition there

was an increase in the heat release fluctuation at high $u'/\langle U \rangle$, for both mixing methods.

In light of the information gathered from the OH* chemiluminescence the PLIF imaging for OH was carried out to extract the flame surface area of the flames. Starting with the imperfectly premixed methane case, Figure 5.17 shows graphs for the normalised flame surface area in the three regions A, B and C, for imperfectly premixed methane flames. The figure contains data of the flames at a forcing frequency of 255 Hz and normalised velocity perturbation of 0.4. For the phase locked images of the flame front for the imperfectly premixed methane flames with 10% and 30% H_2 refer to Figures A.7 and A.8 in Appendix A.The graphs show an apparent change in the $FS'/\langle FS \rangle$ with the addition of hydrogen. In region C (Figure 5.17 (c)) for imperfectly premixed flames, it shows that with the addition of hydrogen there was a reduction in the peak to peak magnitude of the fluctuation and the greatest reduction was achieved with 30% H_2, while with 10% H_2 there was a slight decrease. In Region A with the addition of 10% and 30% H_2, the increase in the FS during the initial flame roll-up formation reduced significantly, thus limiting the peak fluctuation of the FS. While in Region B there were only subtle changes in the peak-to-peak variation and a slight phase shift, which were responsible for the overall reduction in the peak-to-peak fluctuation in Region C. With 30% H_2 addition the slight increase in the normalised FS fluctuation at 180° and reduction at 360° produced a lower rise and fall in the over curve produced for Region C. This was probably the reason why the $Q'(f)/\langle Q \rangle$ reduced with increasing $u'/\langle U \rangle$.

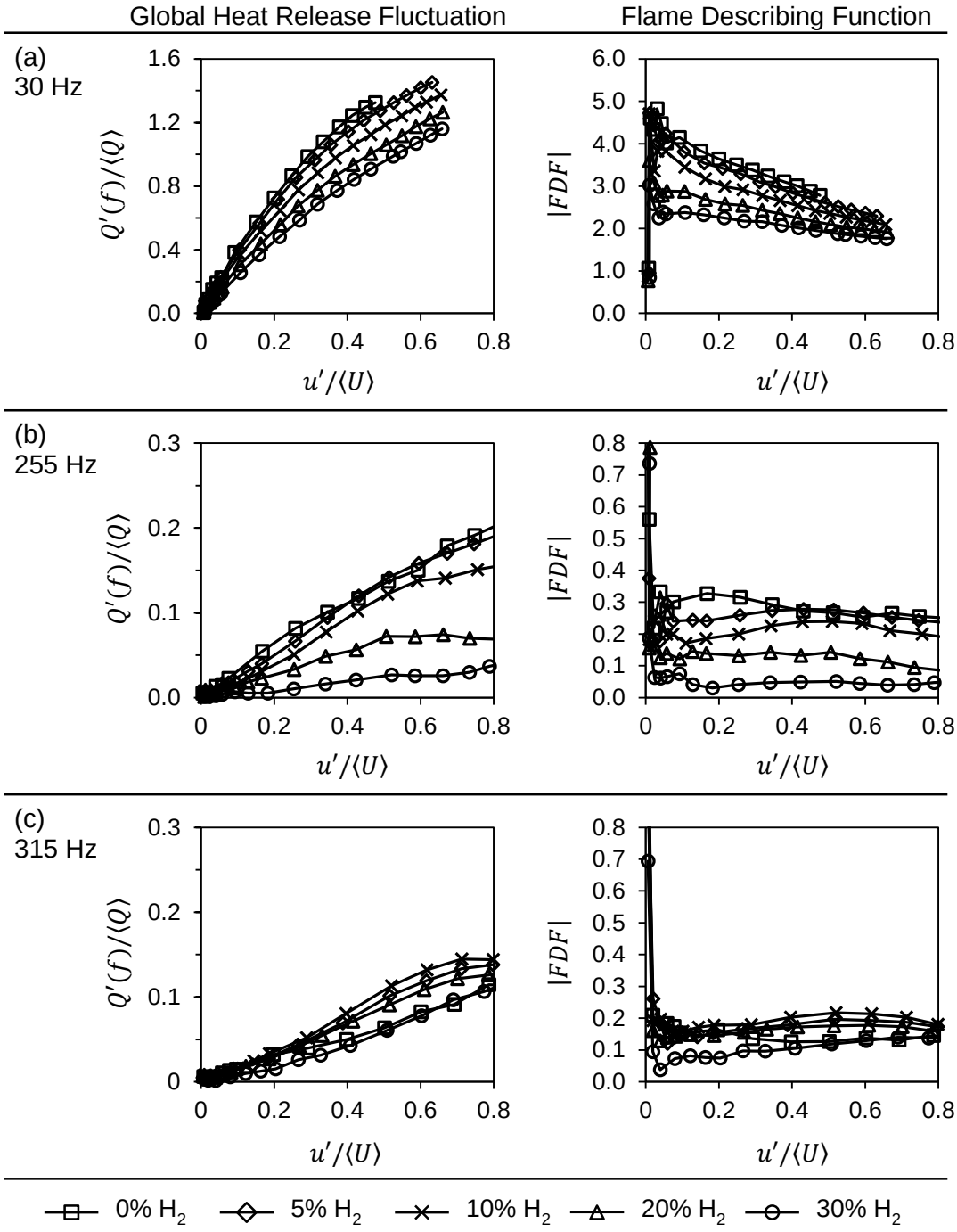

Figure 5.15: The dependence of the global heat release fluctuation and the magnitude of the flame describing function evaluated from OH* chemiluminescence for imperfectly premixed methane flames with the local addition of hydrogen on velocity fluctuations, at forcing frequencies of (a) 30 Hz, (b) 255 Hz, and (c) 315 Hz.

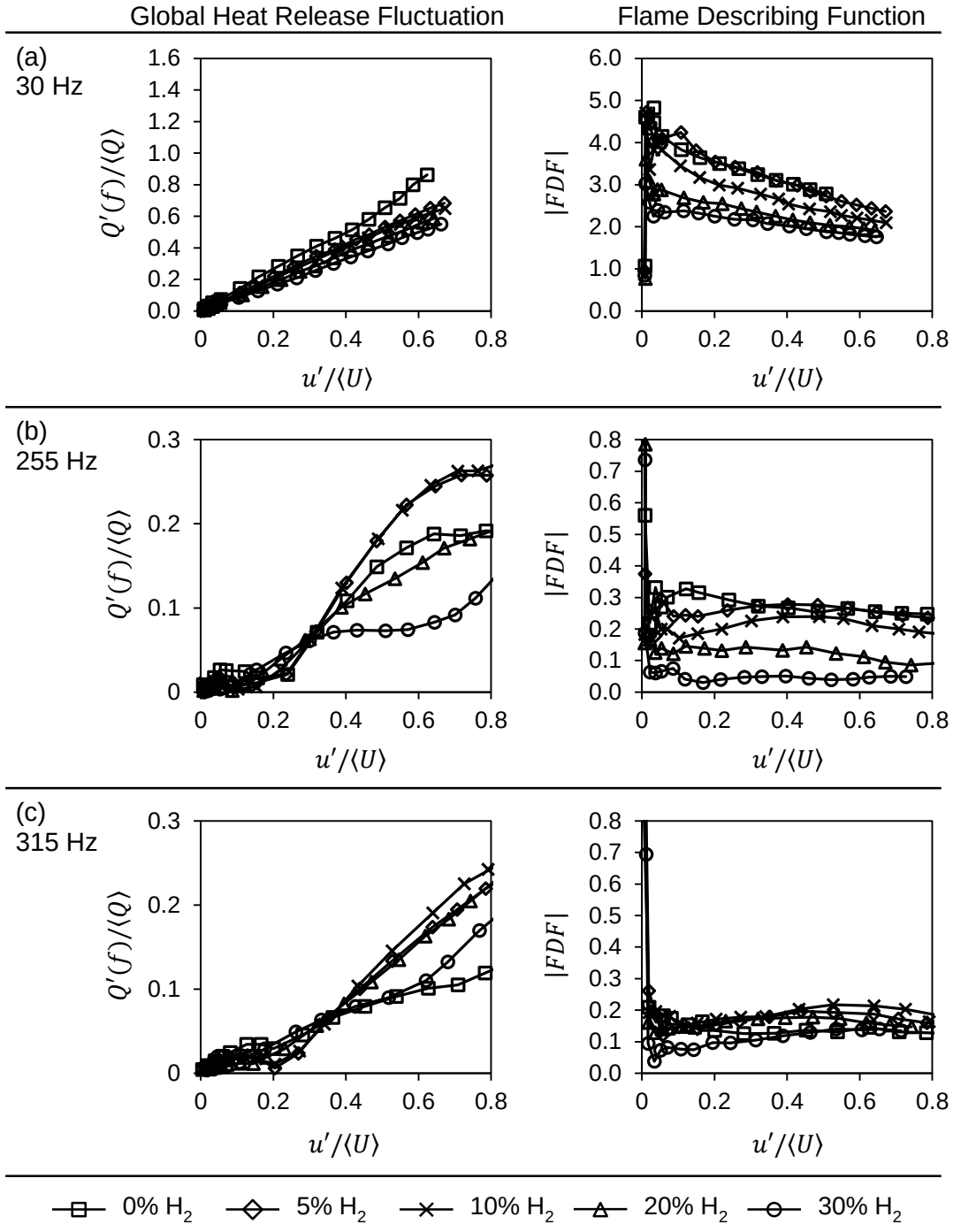

Figure 5.16: The dependence of the global heat release fluctuation and the magnitude of the flame describing function evaluated from OH* chemiluminescence for fully premixed methane flames with the local addition of hydrogen on velocity fluctuations, at forcing frequencies of (a) 30 Hz, (b) 255 Hz, and (c) 315 Hz.

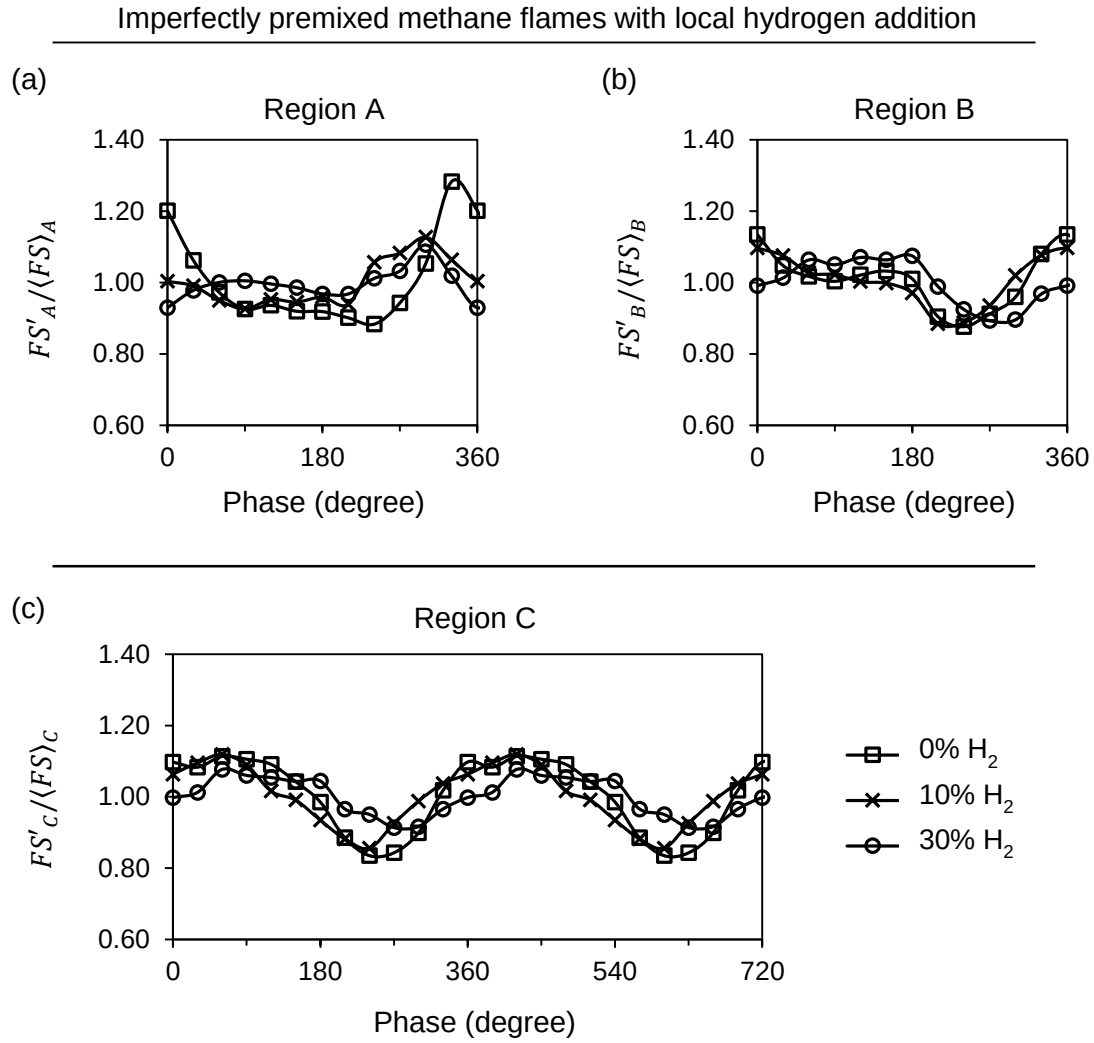

Figure 5.17: Shows the cyclic variation of the normalised flame surface area, $FS'/\langle FS\rangle$, for the regions (a) A, 2.5 – 15 mm, (b) B, 25 – 40 mm, and (c) C, 2.5 – 40 mm, for imperfectly premixed methane flames with increasing quantities of hydrogen addition at f= 255 Hz, and $u'/\langle U\rangle$= 0.4.

The images of the averaged OH PLIF and flame front for 0%, 10% and 30% addition of H_2 at a fixed phase angle of 0° are shown in Figure 5.18 for imperfectly premixed flames. From these images it clearly shows that the addition of H_2 caused a reduction in the size of the flame roll-up (marked in the red circles). Changes in the flame surface oscillations in Region B for 30% H_2, also contributed to the overall reduction in the $FS'_C/\langle FS\rangle_C$, however, with 10% H_2 the oscillations in the FS did not change much compared with the pure methane case. As the flame surface area is

directly related to the heat release rate, the conclusions gathered from the OH* chemiluminescence readings for the heat release verify the findings from the PLIF measurements, that with a 10% addition of H_2 there were only minor changes, however, with an addition of 30% H_2 the fluctuation of the heat release rate reduced as well as the flame surface area.

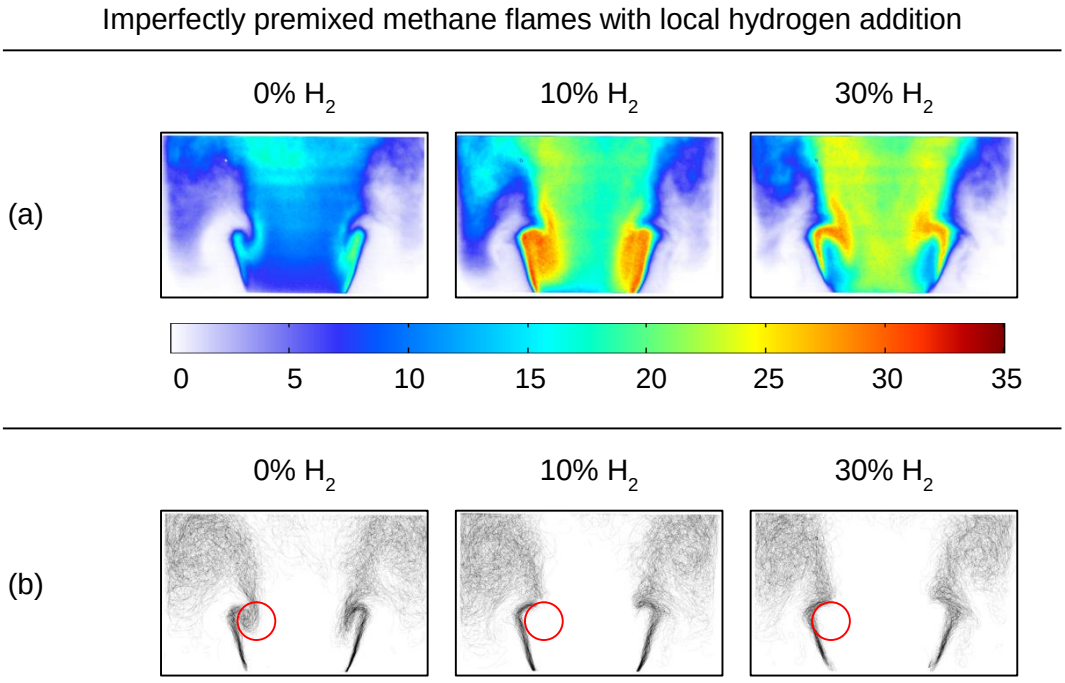

Figure 5.18: Shows the averaged, (a) OH PLIF, and (b) flame front images phase-locked at 0° for the forced imperfectly premixed methane flames with varying quantities of hydrogen addition. f= 255 Hz, and $u'/\langle U\rangle$= 0.4.

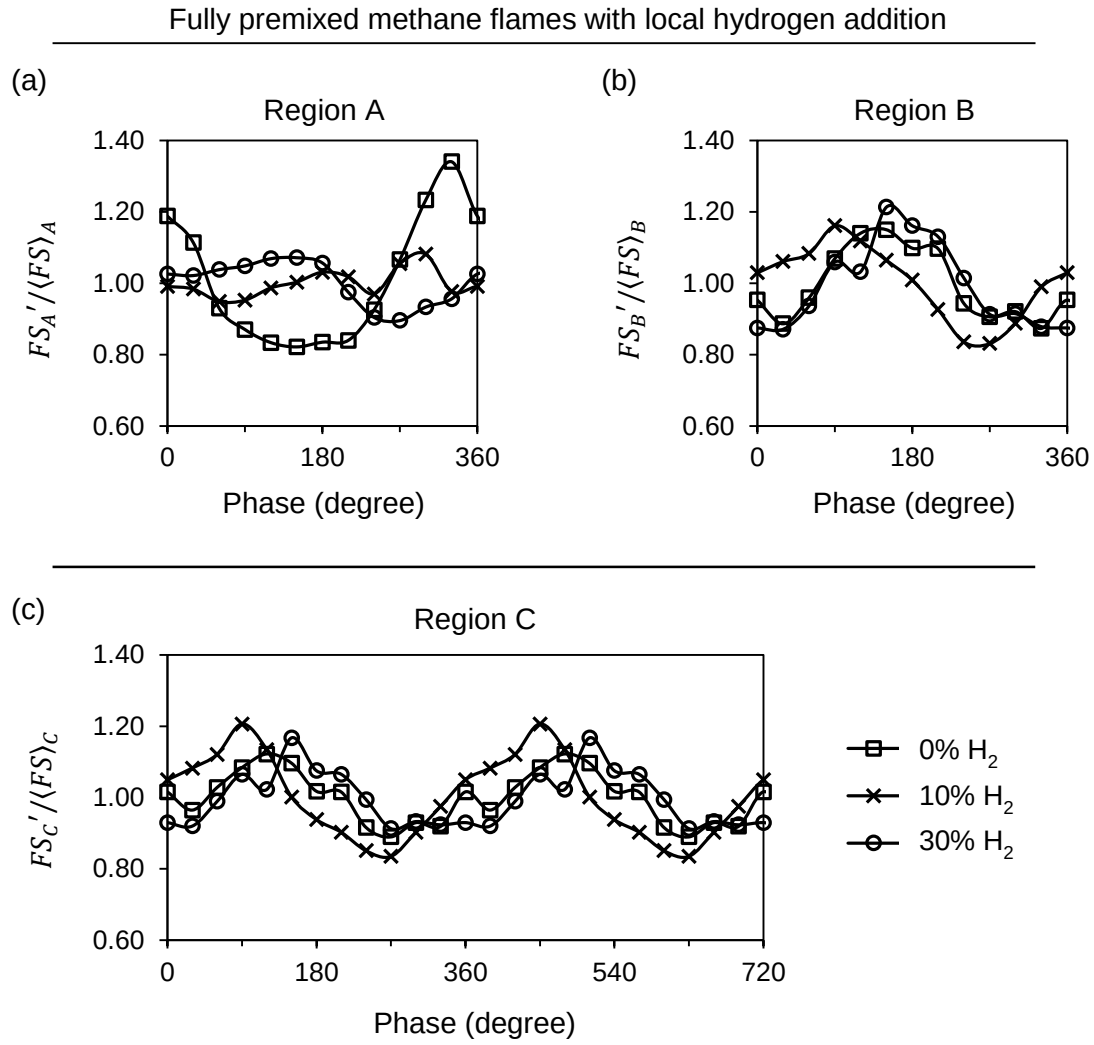

Figure 5.19: Shows the cyclic variation of the normalised flame surface area, $FS'/\langle FS\rangle$, for the regions (a) A, 2.5 – 15 mm, (b) B, 25 – 40 mm, and (c) C, 2.5 – 40 mm, for fully premixed methane flames with increasing quantities of hydrogen addition at f= 255 Hz, and $u'/\langle U\rangle$= 0.4.

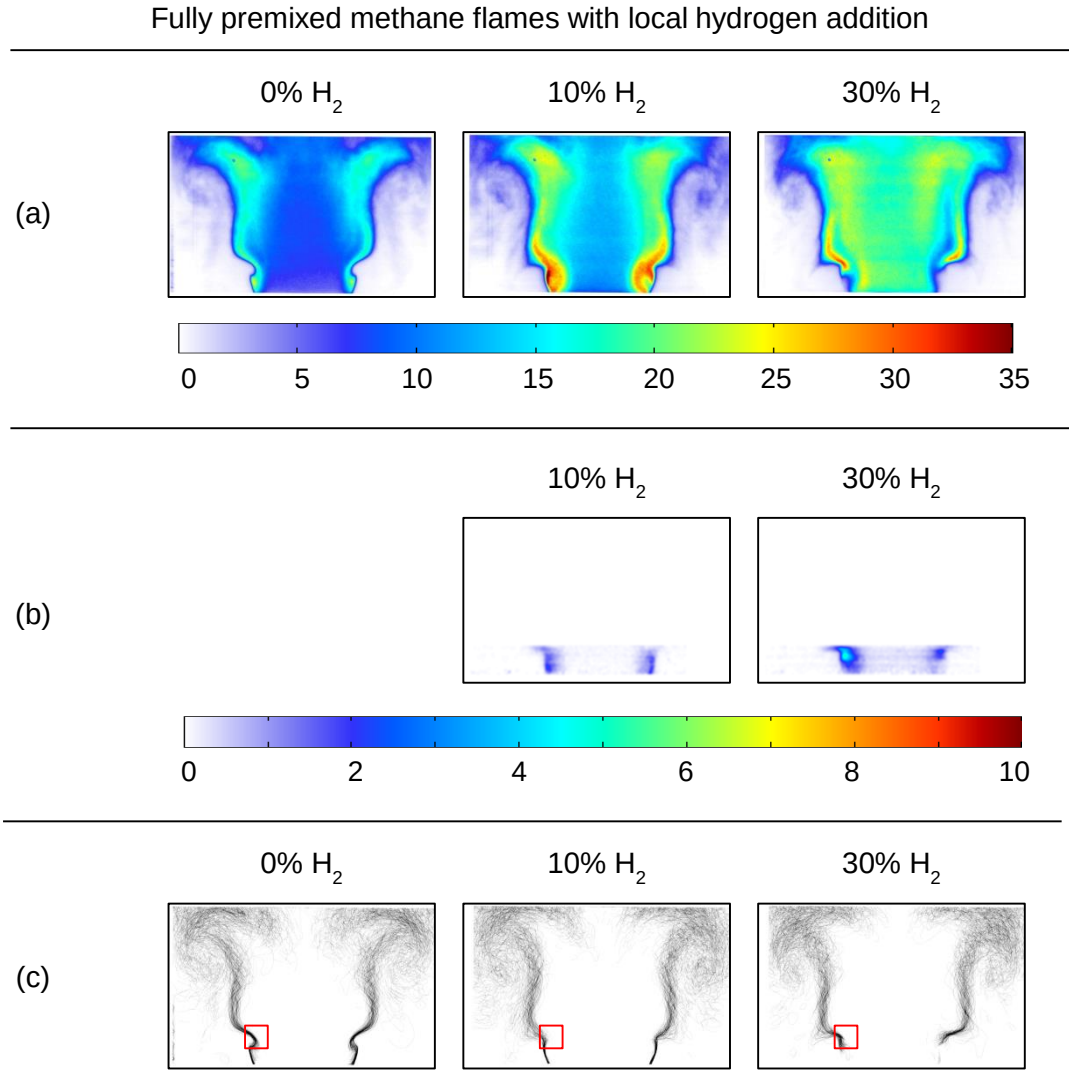

Figure 5.20: Shows the averaged, (a) OH PLIF, (b) H PLIF, and (c) flame front images phase-locked at 240° for the forced fully premixed methane flames with varying quantities of hydrogen addition. f= 255 Hz, and $u'/\langle U\rangle$= 0.4.

Changing the mode of methane introduction into the flow from imperfectly to fully premixed changed the flame's heat release response with additions of H_2 (refer to heat release graphs in Figures 5.16). With fully premixed methane there was an increase in fluctuation with a 5% and 10% addition of H_2 while a reduction occurred only with the addition of 30% H_2. Graphs of regions A, B and C in Figure 5.19 show that H_2 addition did in fact reduce the initial formation of the flame roll-up (Region A).

However, referring to the overall flame surface area fluctuation (Region C), with the addition of 10 % H_2 the flame's surface area response had a slightly larger peak to peak fluctuation.

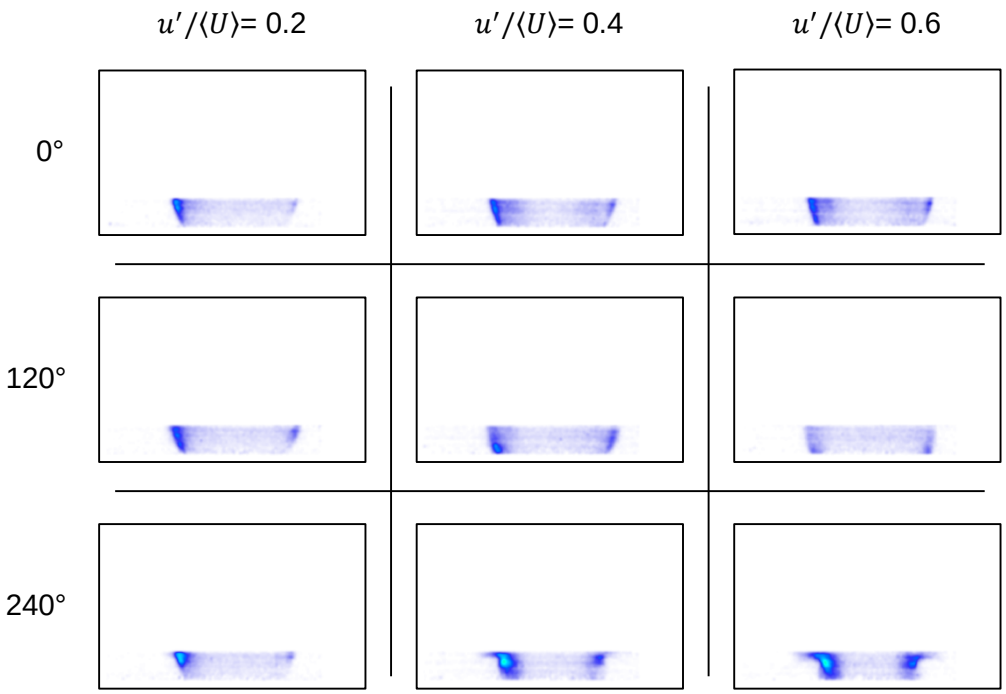

Figure 5.21: Matrix of images showing the effects on the intensity of the H fluorescence for a fully premixed methane flame with 30% H_2 addition at three phase-locked angles of 0°, 120° and 240° at three normalised velocity fluctuations of 0.2, 0.4 and 0.6.

The flame front images shown in Figure 5.20, show that the initial flame roll-up at a phase of 240° was clearly reduced with the addition of hydrogen (marked in red boxes). The H PLIF images (Figure 5.20 (b)) show a large presence of atomic H at the negatively curved flame front during the formation of the flame roll-up which could indicate a faster burning rate at the flame front in this region (Najm *et al.* 1998). As with the ethylene flames, the intensity of atomic hydrogen fluorescence occurred mainly during the initial formation of the flame roll-up (for more images refer to Figure A.9). As stated earlier the intensity of atomic H PLIF was periodic and the greatest fluorescence was observed during the initial formation of the flame

roll-up at the base of the combustion zone. The intensity of the H PLIF fluorescence was affected by the change in the magnitude of the normalised velocity perturbations as shown in Figure 5.21. At $u'/\langle U\rangle$ of 0.2 the fluorescence observed at a phase of 240° was much less than what was observed at $u'/\langle U\rangle$ of 0.4 and 0.6. This indicated that the fluorescence was dependent on the normalised velocity perturbations and the presence of flame roll-up.

With an increase in the velocity perturbations to 0.6, the magnitude of the normalised FS fluctuation increased for 10% H_2 while it decreased for 30% H_2, as shown in Figure 5.22. These results compliment the conclusions gathered from the heat release graphs determined from the OH* chemiluminescence for fully premixed methane flames, that with a low % addition of H_2 there was an increase in the flame surface area fluctuation, and hence the heat release fluctuation. However, with large quantities of H_2 addition (i.e. 30%) there was a steep drop in the heat release perturbation at higher velocity fluctuations. However, this only holds true at a forcing frequency of 255 Hz.

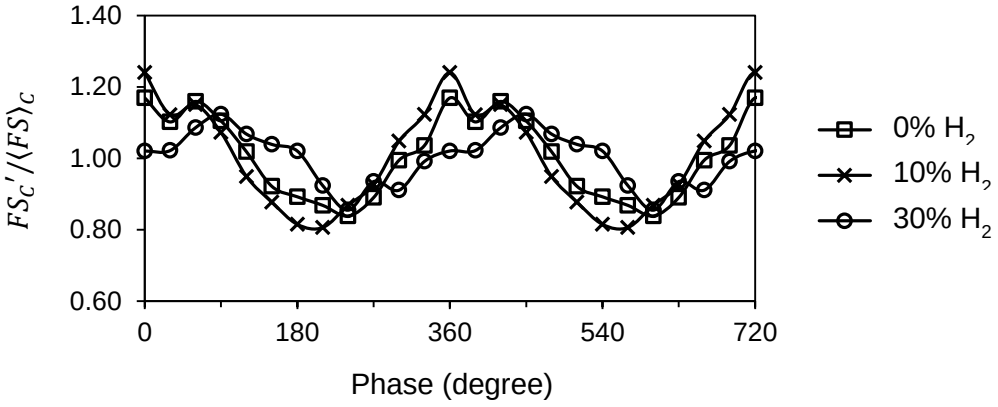

Figure 5.22: Shows the cyclic variation of the normalised flame surface area, $FS'/\langle FS\rangle$, for region C, 2.5 – 40 mm, for fully premixed methane flames with increasing quantities of hydrogen addition at f= 255 Hz and $u'/\langle U\rangle$= 0.6.

Under a higher forcing frequency of 315 Hz, imperfectly and fully premixed methane flames experienced increased heat release oscillations at high $u'/\langle U\rangle$ values with the addition of H_2. Upon close inspection of the flame surface variation in each region it was seen that despite the reduction in the flame surface oscillation

in region A, the overall oscillation increased. Results for imperfectly premixed methane flames with hydrogen addition at a forcing frequency of 315 Hz is shown in Figure 5.23. This indicated that the positive effect of reducing heat release oscillations with the local addition of hydrogen is only applicable under certain operating conditions.

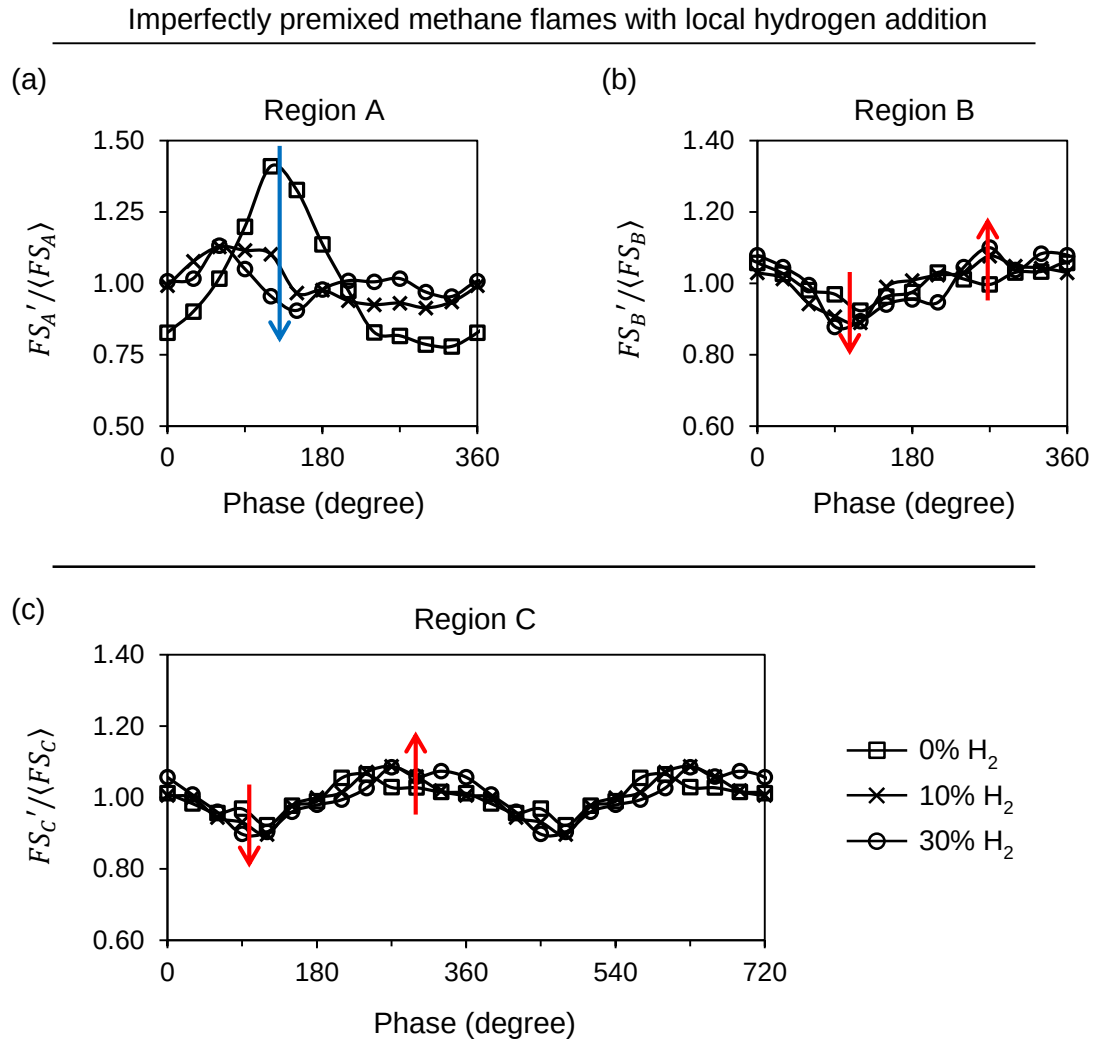

Figure 5.23: Shows the cyclic variation of the normalised flame surface area, $FS'/\langle FS\rangle$, for the regions (a) A, 2.5 – 15 mm, (b) B, 25 – 40 mm, and (c) C, 2.5 – 40 mm, for imperfectly premixed methane flames with increasing quantities of hydrogen addition at f= 315 Hz, and $u'/\langle U\rangle$= 0.4.

5.3 Comparison of ethylene and methane flames with the addition of H_2

Similar to section 4.3, where the flames of imperfectly premixed ethylene and methane flames were compared, this section compares the imperfectly premixed flames with the addition of hydrogen. The data in Chapter 4 showed that both the flames stabilised on, what was assumed to be, the inner shear layers. Figures 5.24 and 5.25 show a comparison of the unforced flames with and without 30% H_2 addition. Several conclusions can be drawn from the images:

- Ethylene flames had a greater OH PLIF signal intensity than methane flames. Either due to a higher concentration of OH radicals or increased flame temperature.
- The addition of hydrogen increased the OH and H PLIF signal near the inner shear layer, for both flames.
- The flame front images show that with a 30% H_2 addition in the ethylene and methane, the flames lifted slightly from the base, and it reduced the flame height.
- The quantity of NOx (ppm) and percentage change in Carbon dioxide in the emissions increased for both flames with the increase in H_2 additions.

To recap from section 4.3; the comparison of the dynamic results of imperfectly premixed ethylene and methane flames showed that the magnitude of the heat release response curves at forcing frequencies of 255 and 315 Hz was higher for the ethylene flames. The dynamic response of the imperfectly premixed flames with the addition of hydrogen is shown in Figure 5.26. Generally with the addition of hydrogen the global heat release oscillation reduced for both base fuel types (i.e. ethylene and methane), however, at a forcing frequency of 315 Hz the response of the methane flames with hydrogen was greater compared to pure methane flames. As shown earlier in Figure 5.23 (c), the oscillation in the flame surface area for imperfectly premixed methane flames increased with hydrogen addition.

Putting aside the heat release response of the flames, a common attribute with the addition of hydrogen to both types of flames was that the initial flame front

roll-up was reduced with any amount of hydrogen added to the flame (Figure 5.27). However, the difference in the flame surface fluctuation in region A, from 0% H_2 to 30% H_2 was larger for methane flames as shown in the plots of $FS'_A/\langle FS_A \rangle$, in Figure 5.28. Suggesting that the addition of H_2 to methane flames had a much greater effect that on ethylene flames.

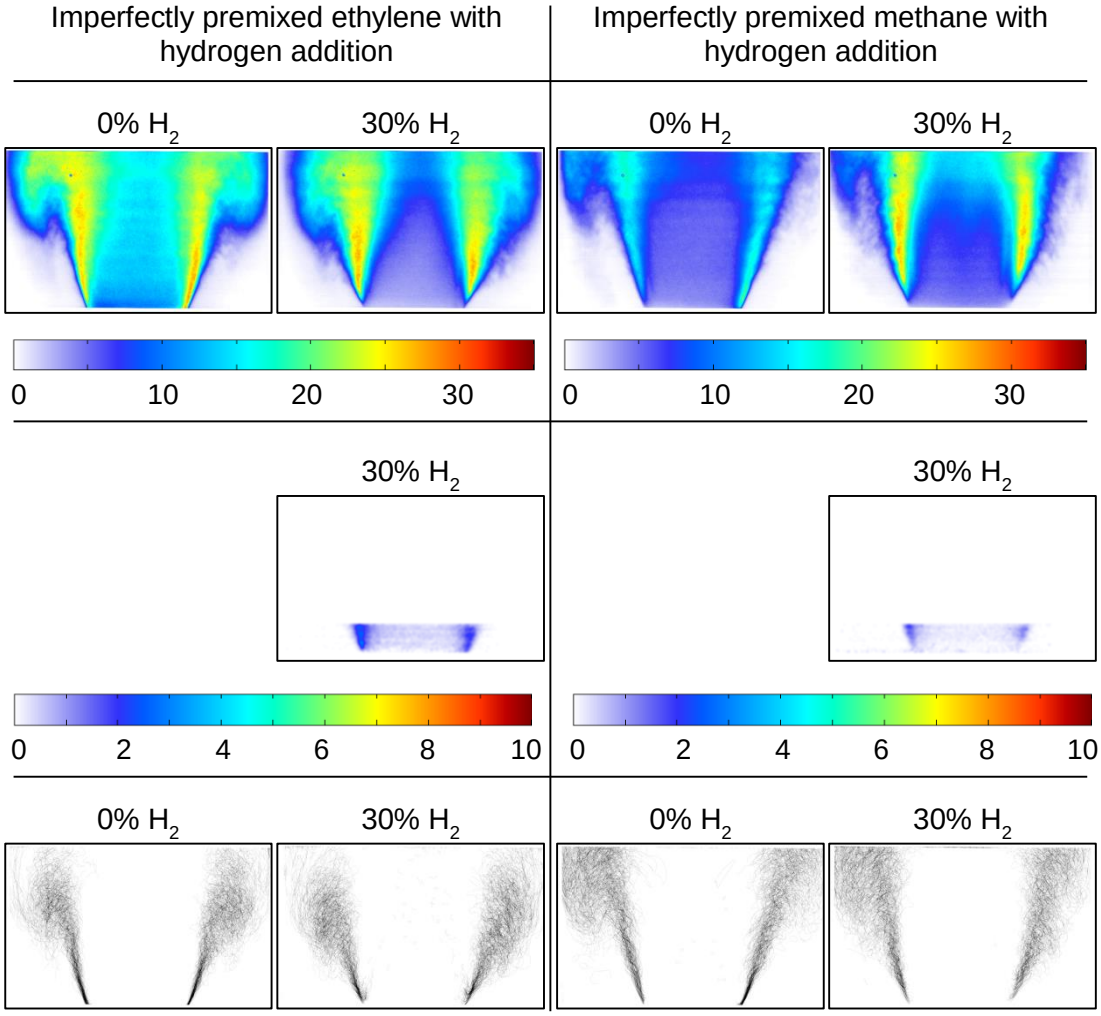

Figure 5.24: Comparison of the averaged OH and H PLIF, and the flame front images of imperfectly premixed ethylene and methane flames with and without the addition of 30% H_2.

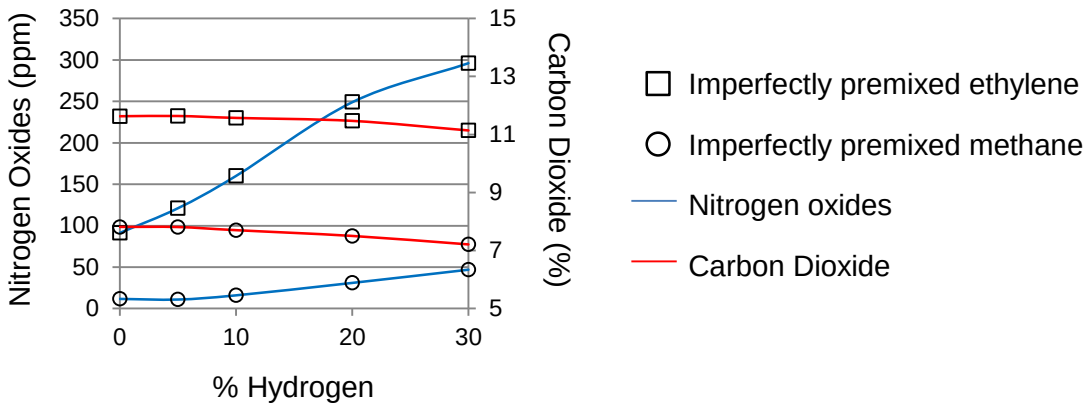

Figure 5.25: The plot shows the change in NO_x (ppm) and % CO_2 emissions with the increase in % Hydrogen addition for imperfectly premixed ethylene and methane flames.

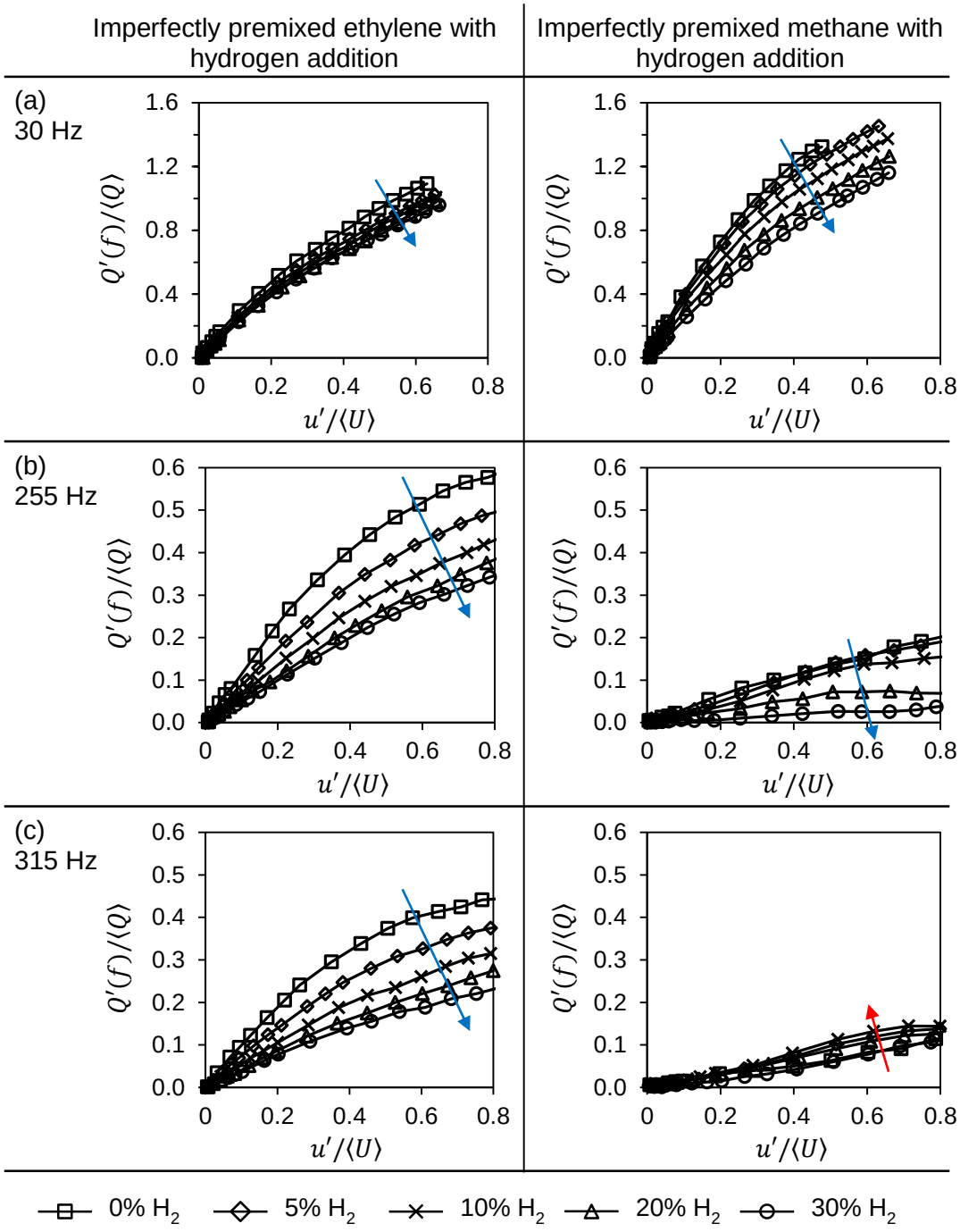

Figure 5.26: The dependence of the global heat release fluctuation evaluated from OH* chemiluminescence on velocity fluctuations, for imperfectly premixed ethylene and methane flames with the addition of hydrogen, at forcing frequencies of (a) 30 Hz, (b) 255 Hz, and 315 Hz.

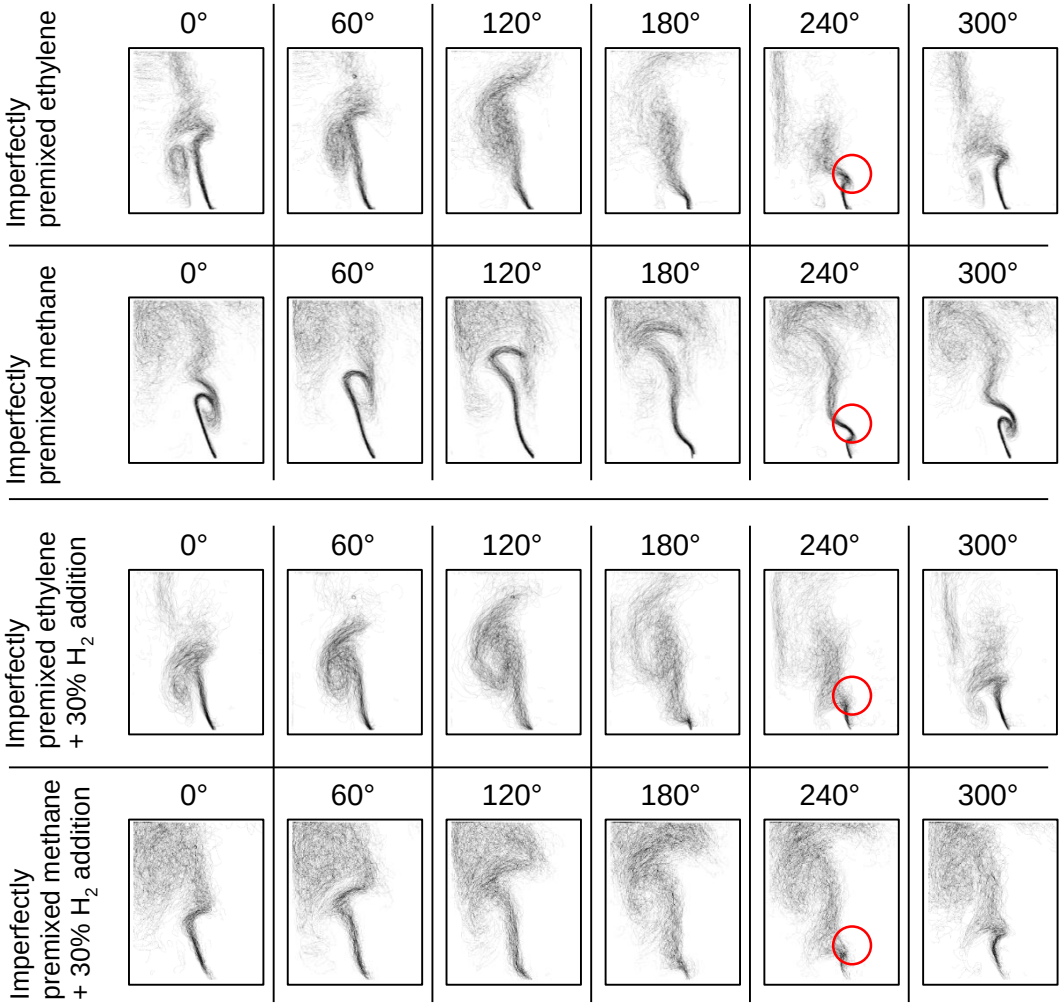

Figure 5.27: Shows the phase-locked averaged flame front images (in steps of 60°), for imperfectly premixed ethylene and methane flames, with and without the addition of 30% H_2, under forcing conditions, f= 255 Hz, and $u'/\langle U \rangle$= 0.4.

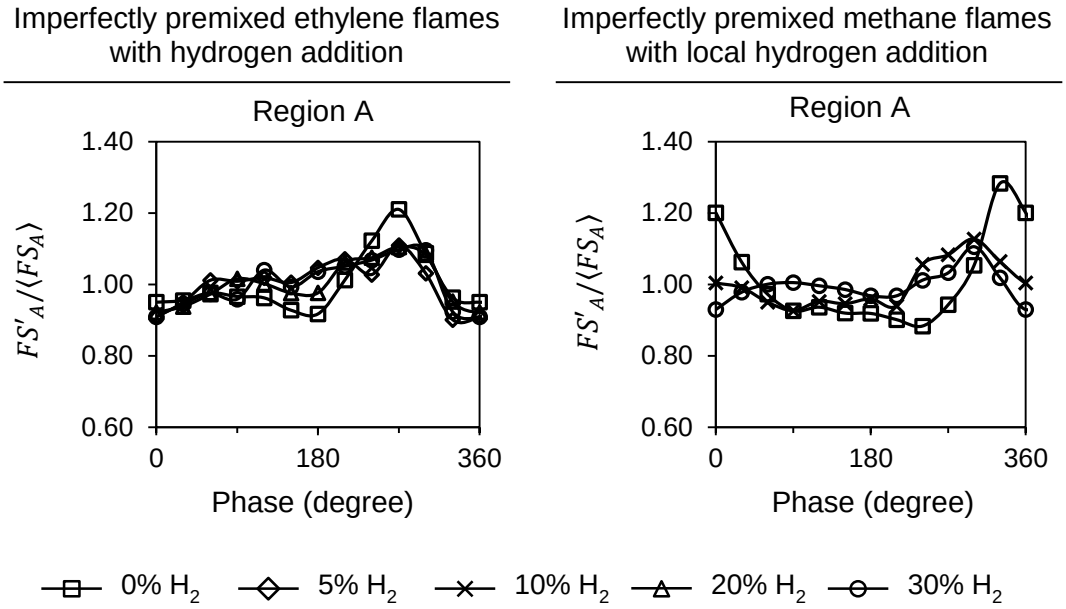

Figure 5.28: Shows the cyclic variation of the normalised flame surface area, $FS'/\langle FS \rangle$, for the region A, 2.5 – 15 mm, for imperfectly premixed ethylene and methane flames with increasing quantities of hydrogen addition at f= 255 Hz, and $u'/\langle U \rangle$= 0.4.

5.4 Summary

This chapter details the effects on the combustion of ethylene and methane flames with the local addition of hydrogen. The first conclusion that can be noted from the results is that, whether the addition of hydrogen decreased or increased the heat release fluctuation, it certainly affected the initial size of the flame roll-up which coincided with the increased presence of atomic hydrogen at the negatively curved flame surface. In the case of imperfectly premixed ethylene, an addition of hydrogen caused a reduction in the heat release response at a forcing frequency of 255 Hz and 315 Hz. With the base fuel set as methane, under imperfectly and fully premixed conditions there were scenarios of increased and decreased heat release oscillations depending on the quantity of hydrogen added and the forcing frequency.

It can be concluded that hydrogen has the potential to alter the combustion characteristics, either positively or negatively depending on the operating conditions. In the next chapter the combustion chamber geometry was altered to

allow the self-excitation of the flames to verify the effectiveness of local hydrogen addition in reducing the combustion oscillations.

Chapter 6: Effects of local hydrogen addition on self-excited flames

One of the main objectives of this study was to understand how the addition of hydrogen had an effect on the heat release rate of the flames and velocity perturbations of inlet flow that went through self-excitation under certain operating conditions. In the previous chapters (Chapter 4 and 5) the response of turbulent ethylene flames with the addition of hydrogen was presented; which showed that the flame shape and its response to acoustic forcing changed as a consequence of the local addition of hydrogen. However, it was only under certain operating conditions that the local addition of H_2 was able to reduce the flame response.

The results presented in this chapter aim to verify the conclusions gathered from the experiments of the forced response. With the current geometry of the combustor, only ethylene flames were able to achieve a state of self-excitation. Due to the possibility of flame flashback during self-excitation under fully premixed conditions, only imperfectly premixed flames were considered. The methodology and the selected flow conditions that were used are listed in section 6.1.

6.1 Experimental methods

6.1.1 Combustor modification and measurement systems

To achieve self-excitation of the flames within the combustion chamber the length of the combustor enclosure was modified. The length was increased from 100 mm to 300 mm to alter the acoustic boundary conditions. During the forced conditions the short enclosure prevented resonance within the combustion

chamber, however, with the increase in the enclosure length the acoustic waves were allowed to resonate causing the self-excitation of the flames.

Due to the no prior knowledge of the frequency at which the flames would self-excite the laser system described in Chapter 2 under the section 'Laser Tomography' was used. This laser and camera system was capable of recording images at 3000 frames per second which helped in observing the flame at varying excited frequencies. In some self-excited test conditions there was a slight shift in the frequency at which the flame was excited, which made the use of this high speed system appropriate. The laser beam was expanded into a laser sheet which was used to highlight the seeded air/fuel mixture entering the combustion chamber. Using these images the boundary of the unburnt flow was produced and hence time-series graphs for the evolution of the flame surface were produced. However, there was a drawback to this method of measurement that must be noted. The air/fuel mixture was seeded with olive oil droplets, which vaporise at high temperatures of approximately 300°C, however, the flow was heavily seeded with droplets until the spacing between the droplets were indistinguishable, which produced images of dense droplet clouds showing the unburnt flow. An assumption was made that these clouds of oil were staggered off from the actual flame front, but since this technique was used for all the flames, the comparative analysis would not be affected. As the oil droplets moved further downstream the loss of droplets due to vaporisation would be large, hence, quantitative measurements for the flame surface area were only carried out in region A (2.5 – 15 mm from the base of the combustion chamber) to limit the errors in the quantitative analysis.

The equipment used in previous tests, i.e. the PMT fitted with the 305 nm bandpass filter and pressure transducers, were used to record the heat release rate and inlet velocity oscillations. To aid the study, a DSLR camera was also used to capture photographic images of the flames to show the differences in overall height and intensity of the flames. The DSLR was set at a fixed position, aperture size, shutter speed, ISO and white balance to allow the comparison of all the images.

6.1.2 Operating conditions

To achieve self-excitation of imperfectly premixed ethylene flames, the volume flow rate of air was kept constant at 250 slpm which resulted in the same bulk air velocity used for the forced conditions. The quantity of ethylene in the flow was increased until the flame could be ignited and stabilised. Once ignited, the enclosure extension was fixed in place, and at low global equivalence ratios there was no self-excitation. The global equivalence ratio of the flame was increased until the flames underwent self-excitation, which was noticed with a sudden change in sound of the flame caused by rapid fluctuations of pressure in the combustion chamber (Wicksall and Agrawal 2007); and this was achieved at a global equivalence ratio, ϕ_{Global}, of 0.812.

To understand the effects of hydrogen on the ethylene flame and see whether other gases could produce the same outcomes a series of tests were planned. To easily illustrate the thought process behind the proposed experiments please refer to Figure 6.1. The figure shows three gases that were locally added to the self-excited flame.

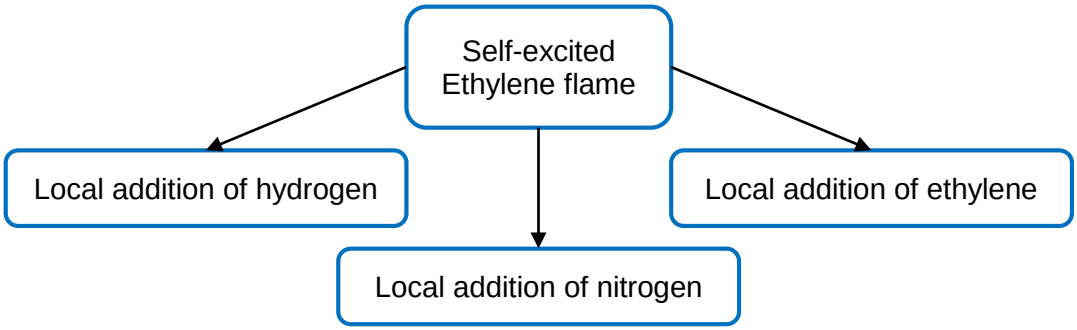

Figure 6.1: Shows the various gases used to study the effects on the combustion oscillations of the self-excited ethylene flames.

Ethylene was used to see whether fuel stratification would reduce heat release oscillations as shown in several studies (Abdalla *et al.* 1981, Robin *et al.* 2008, Kang and Kyritsis 2009, Anselmo-Filho *et al.* 2009, Albrecht *et al.* 2010, Kim and Hochgreb 2011). The addition of an inert gas, nitrogen was considered because it did not add energy to the combustion process. The flame response with the addition of these gases was made comparable by keeping several parameters

constant. The air volume flow rate was fixed at 250 slpm; the input power, calculated from the calorific values of the fuels was kept constant at 13.11 kW. With the local addition of hydrogen; as the quantity of H_2 was increased the momentum ratio between H_2 and the ethylene/air mixture, defined by the following equation, also increased.

$$Momentum\ Ratio = {\rho_{Sec}.{u_{Sec}}^2}\Big/{\rho_{Mix}.{u_{Mix}}^2}$$

In this equation the subscript 'Sec' represents the fuel added from the secondary fuel ports. While 'Mix' represents the air and ethylene mixture, in which the air accounted for 95% of the total mixture flow. With increasing quantities of H_2 the momentum of the gas from the secondary ports increased. With higher momentum the H_2 gas would penetrate the air/ethylene flow more. To keep the level of penetration by each locally added gas (i.e. hydrogen, ethylene and nitrogen) the same, the volume flow rate of ethylene and nitrogen in the secondary fuel ports were calculated and matched with the different quantities of hydrogen added. Tables 6.1, 6.2 and 6.3 list the chosen volume flow rates for each fuel.

Air (slpm)	Primary		Secondary		ϕ_{Global}	Momentum Ratio
	C_2H_4 (slpm)	C_2H_4 %	H_2 (slpm)	H_2 %		
250.0	14.2	100.0	0.0	0.0	0.812	0.00000
250.0	14.1	95.0	0.7	5.0	0.812	0.00065
250.0	13.9	90.0	1.5	10.0	0.811	0.00283
250.0	13.6	80.0	3.4	20.0	0.809	0.01370
250.0	13.2	70.0	5.7	30.0	0.808	0.03799

Table 6.1: Lists the flow rates and % of each fuel used during the local addition of hydrogen to self-excited ethylene flames.

Air (slpm)	Primary		Secondary		ϕ_{Global}	Momentum Ratio
	C_2H_4 (slpm)	C_2H_4 %	C_2H_4 (slpm)	C_2H_4 %		
250.0	14.2	100.0	0.0	0.0	0.812	0.00000
250.0	14.0	98.6	0.2	1.4	0.812	0.00065
250.0	13.8	97.1	0.4	2.9	0.812	0.00283
250.0	13.3	93.6	0.9	6.4	0.812	0.01370
250.0	12.7	89.4	1.5	10.6	0.812	0.03799

Table 6.2: Lists the flow rates and % of each fuel used during the local addition of ethylene (stratification) to self-excited ethylene flames.

Air (slpm)	Primary		Secondary		ϕ_{Global}	Momentum Ratio
	C_2H_4 (slpm)	C_2H_4 %	N_2 (slpm)	N_2 %		
250.0	14.2	100.0	0.0	0.0	0.812	0.00000
250.0	14.2	98.6	0.2	1.4	0.812	0.00065
250.0	14.2	97.2	0.4	2.8	0.812	0.00283
250.0	14.2	94.0	0.9	6.0	0.812	0.01370
250.0	14.2	90.3	1.5	9.7	0.812	0.03799

Table 6.3: Lists the flow rates and % of each fuel used during the local addition of nitrogen to self-excited ethylene flames.

6.2 Experimental results

In each section below, the results for the specific flames are described using the measurement techniques discussed. At the end of the chapter the results are compared and related to the results obtained for the forced flame conditions.

6.2.1 Self-excited ethylene combustion

The self-excitation of imperfectly premixed ethylene flames was achieved at a global equivalence ratio of 0.812. The magnitude of the normalised velocity perturbations was calculated to be 0.41 from the pressure measurements, with the normalised heat release fluctuation calculated to be 0.13 (determined from the OH*

chemiluminescence measured by the PMT). Using fast fourier transform (FFT) the power spectral density (PSD) of OH* chemiluminescence under the self-excited condition was calculated and is shown in Figure 6.2. The dominant self-excitation frequency was found to be 338 Hz. Under these the flow conditions the velocity perturbations caused the roll-up of the flame front. As mentioned before, with the use of high speed imaging the flame front and surface area of the flames were determined and the time-series plot for the flame surface area was created. This data was further processed to extract the PSD plot for the flame surface area to determine the frequency at which the flame surface area fluctuations were taking place.

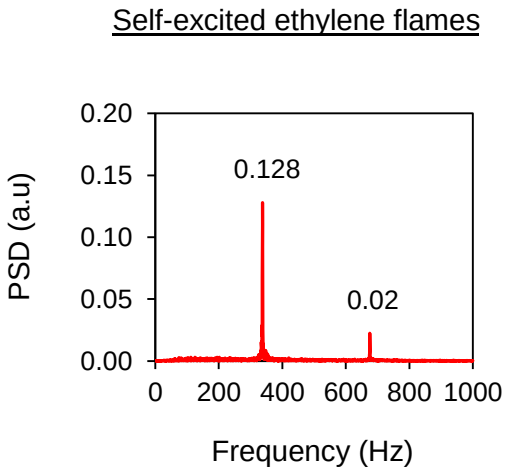

Figure 6.2: Power spectral density of the OH* chemiluminescence for the self-excited imperfectly premixed ethylene flame.

As mentioned before, the flame surface area was only measured in Region A due to the laser technique used. A time series plot for the normalised flame surface area in region A for the self-excited ethylene flame is shown in Figure 6.3 (a). The plot shows large fluctuations in the flame surface area close to the base of the combustor. The time series was processed to obtain the resulting PSD plot shown in Figure 6.3 (b). The frequency of surface area fluctuations was around 340 Hz. As the frequency at with the oscillations for the OH* and FS were occurring was the same, it shows that the heat release rate (determined by the OH* chemiluminescence) was related to the flame surface area.

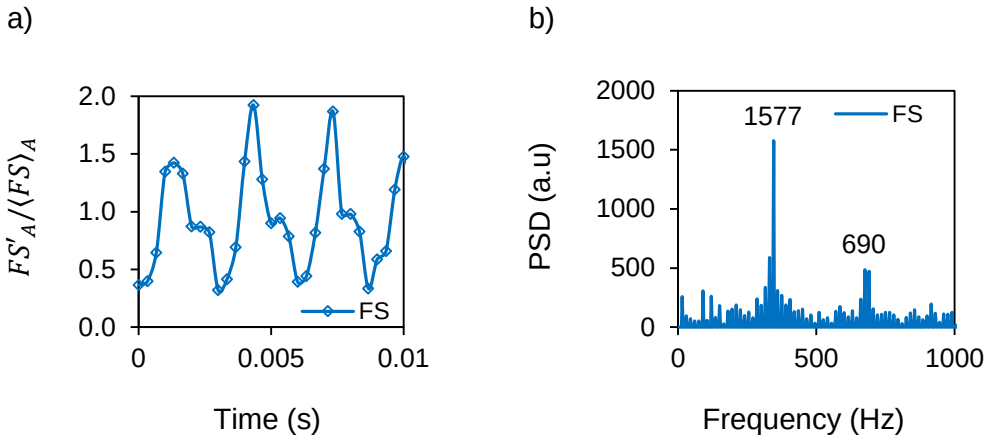

Figure 6.3: (a) Shows a time series plot of the flame surface area for region A determined by laser tomography; which was processed to produce the (b) power spectral density (PSD) plot.

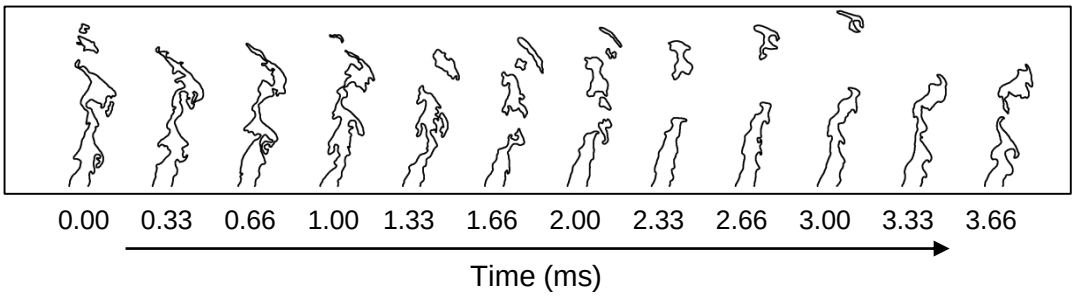

Figure 6.4: Time series evolution of the flame boundary for a turbulent imperfectly premixed ethylene flames.

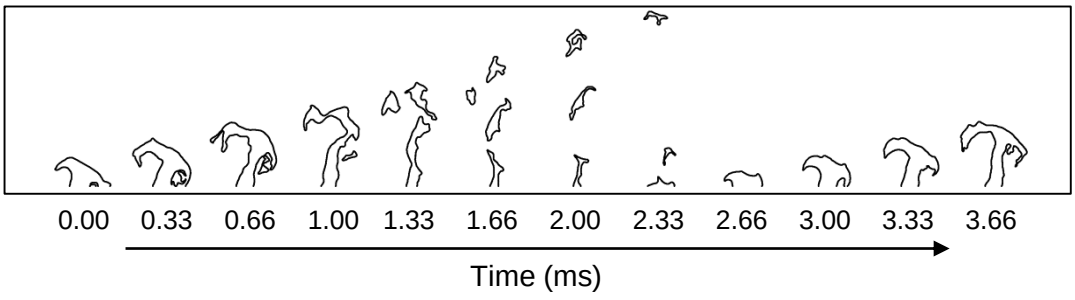

Figure 6.5: Time series evolution of the flame boundary of the self-excited imperfectly premixed ethylene flames.

For visual comparison one side of the evolution of the boundary of the unburnt air/fuel mixture is shown in Figure 6.4, for the turbulent imperfectly premixed ethylene flame at an equivalence ratio of 0.65, while the evolution of the boundary during self-excitation (ϕ = 0.81) is shown in Figure 6.5. The instances of the flame were taken every 0.33 ms and the images show the dramatic change in the flame shape. It must be noted that the timestamps are only relative to the instances of the flame in that particular figure. Comparing the sequence it is apparent, although expected, that the flame exhibited a periodic formation and destruction of the flame roll-up. The peaks of the flame surface area shown in Figure 6.3 (b) occurred due to the flame roll-up approximately at 0.66 ms in Figure 6.5, while the troughs occurred around 2.33 ms in the images.

With the development of flame roll-up during self-excitation, the addition of hydrogen into the flow was employed to validate the controlled forcing tests. From the forcing tests it was clear that hydrogen would be able to reduce the size of the flame roll-up (i.e. the surface area of the roll-up closest to the central recirculation zone), for imperfectly premixed ethylene flames.

6.2.2 Addition of hydrogen to self-excited ethylene flames

With the imperfectly premixed pure ethylene flames in a self-excited state, hydrogen gas was added into the flow using the secondary fuel ports. As discussed earlier the % of hydrogen was increased while the % of ethylene was reduced. Figure 6.6 shows how the normalised pressure, velocity and heat release perturbations were affected with the % increase in hydrogen. In general the addition of H_2 caused a reduction in the perturbations, however, the velocity perturbations reduced to approximately 0.20 after a 10% addition of H_2. Further increasing the H_2 flow to 20% and 30% did not have any significant impact on the velocity fluctuations. Similar results were obtained for the heat release response, where there was no change in the response after the addition of 10% H_2.

The power spectral density plots calculated from the OH* chemiluminescence and flame surface area are shown in Figure 6.7 (a) and (b), respectively. With the PSD plot based on OH* chemiluminescence a significant change only between the tests with 5% H_2 and 10% H_2, which correlates well the information gathered from the plot of the normalised velocity perturbations in Figure

6.6. With the PSD plot based on the FS there was a gradual decrease in the peak fluctuation value. However, from all the plots it was clear that the changes in the OH* and FS between 10%, 20% and 30% H_2 addition were minimal, i.e. around a maximum of 4% difference.

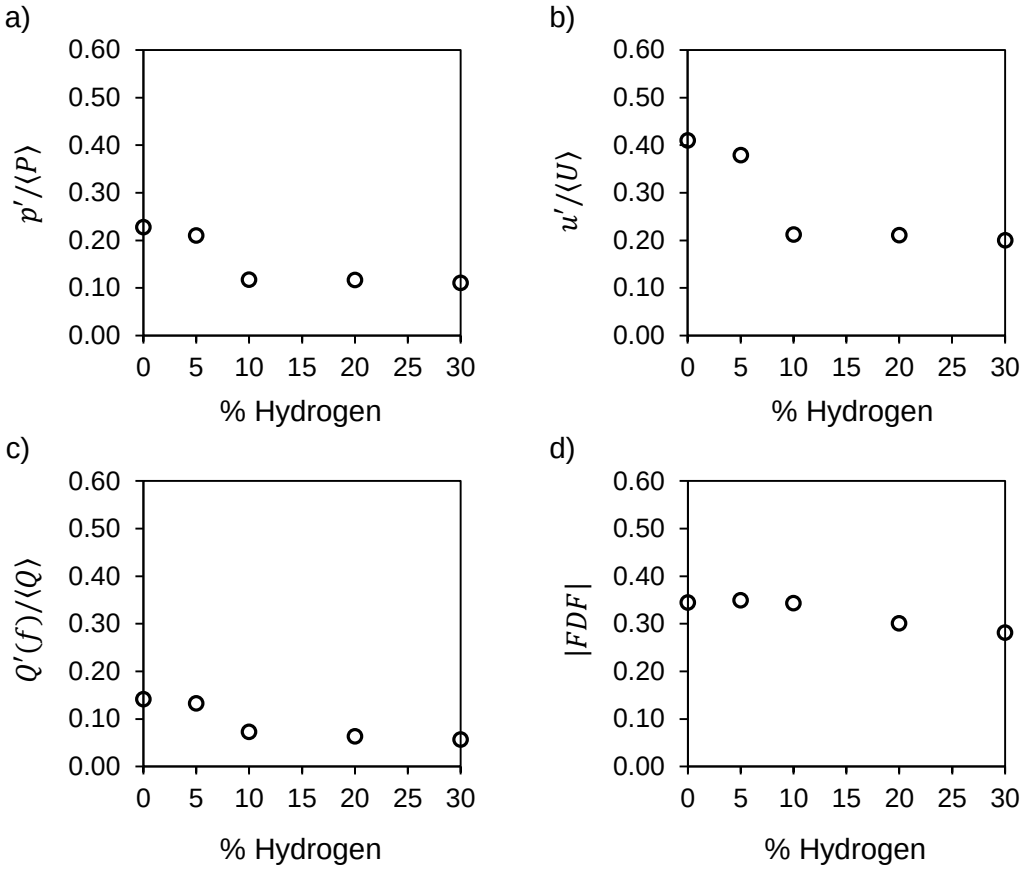

Figure 6.6: Shows the change in the normalised (a) pressure, (b) velocity, (c) heat release perturbations and the magnitude of the flame describing function of self-excited imperfectly premixed ethylene flames with an increase in the local addition of hydrogen.

Studying the images of the flow tomography boundary images for the case with 5% and 20% H_2 in Figure 6.8, it can be seen on the inner boundary that the increase in hydrogen had indeed reduced the surface area of the flame roll-up (i.e. the length of the surface revolved around the central axis). Overall, the addition of H_2 to the ethylene flames helped in reducing the normalised flame surface and

velocity oscillations, which does agree with the statements made in Chapter 5 that the addition of H_2 was beneficial for imperfectly premixed ethylene self-excited flames.

a) Based on OH* chemiluminescence:

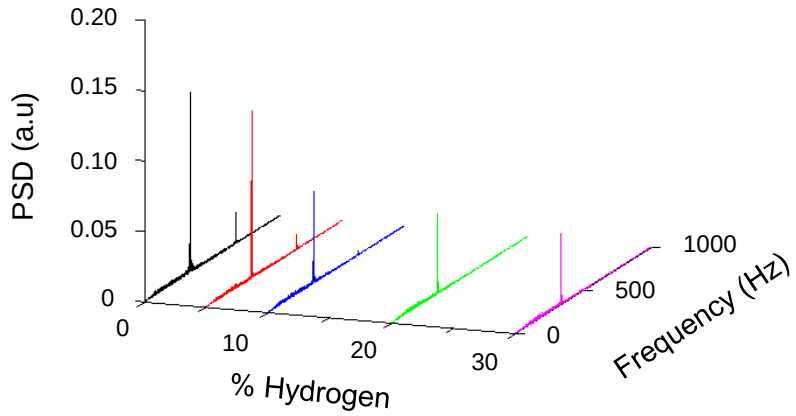

b) Based on Flame surface area:

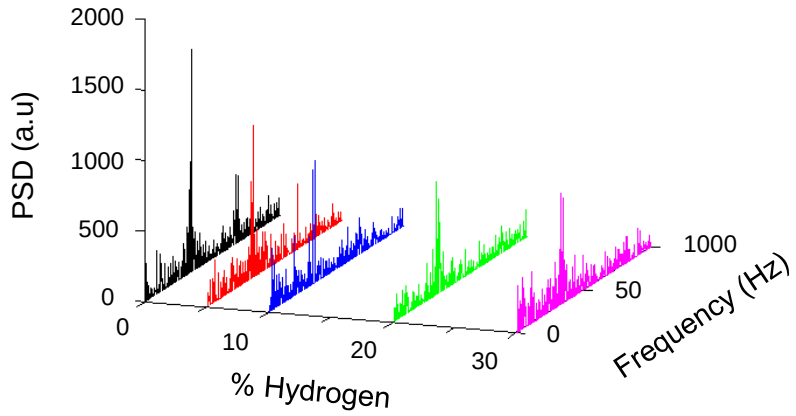

Figure 6.7: Shows the plots for the PSD calculated from (a) the global OH* chemiluminescence, and (b) flame surface area (Region A), for the self-excited flames with 0, 5, 10, 20 and 30% local addition of hydrogen.

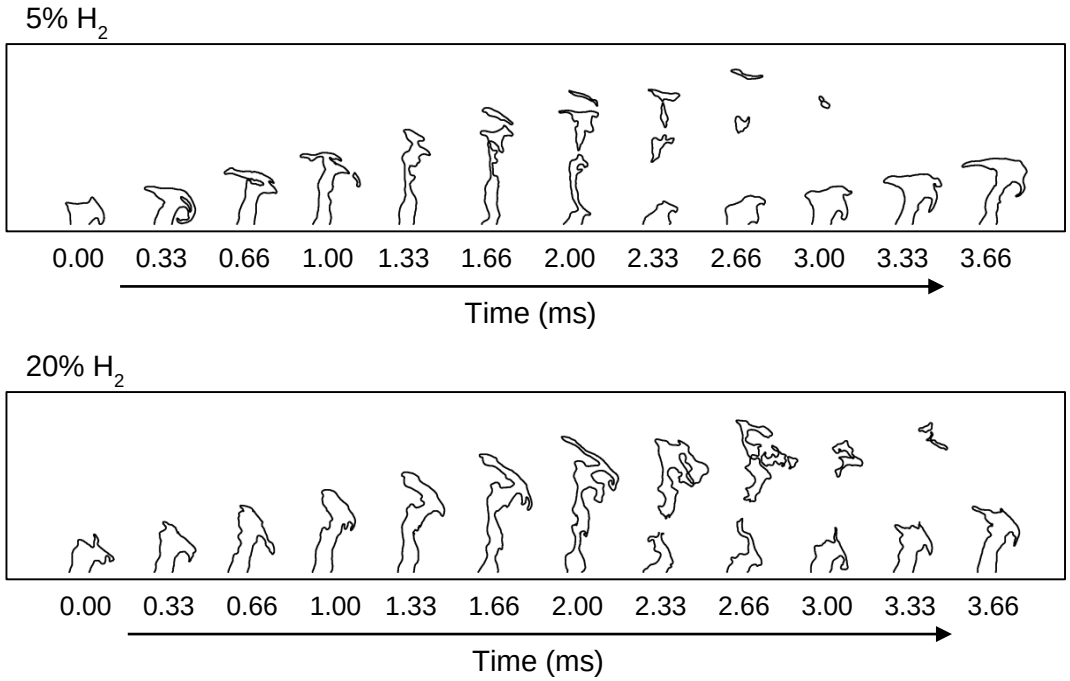

Figure 6.8: The images show the evolution of the flame boundary for the self-excited imperfectly premixed ethylene flames with 5% and 20% local addition of hydrogen.

6.2.3 Stratification of ethylene to self-excited flames

The addition of ethylene was performed to understand whether the method of fuel stratification, whereby a percentage of the primary fuel is siphoned off to be injected locally into the flow, could also be used to reduce the combustion oscillations (Abdalla *et al.* 1981, Kang and Kyritsis 2009, Albrecht *et al.* 2010). During the experiments, with the local addition of ethylene, the flames exhibited yellow soot plumes which represent unburnt hydrocarbons. These were most likely due to poor mixing of the secondary fuel with the oncoming air, creating a locally rich mixture. These plumes caused inaccurate readings of the OH* chemiluminescence from the PMT and caused bright spots in the tomography imaging. Hence, only the changes in the velocity perturbations (Figure 6.9) measured and calculated from the pressure measurements and photographic images (Figure 6.10) are shown.

In the first test, 1.4% of ethylene (by volume) was removed from the primary fuel flow and injected locally through the secondary fuel ports. This local addition increased the normalised velocity perturbations to 0.56, however, further increasing the secondary ethylene fuel flow (and reducing the primary), caused a drop in the velocity fluctuations. With the local addition of ethylene and poor local fuel and air mixing, the flames showed soot formation, as can be seen in Figure 6.10. The soot formation was due to unburnt hydrocarbons which indicated a relatively lower combustion efficiency and higher hydrocarbons in the emissions.

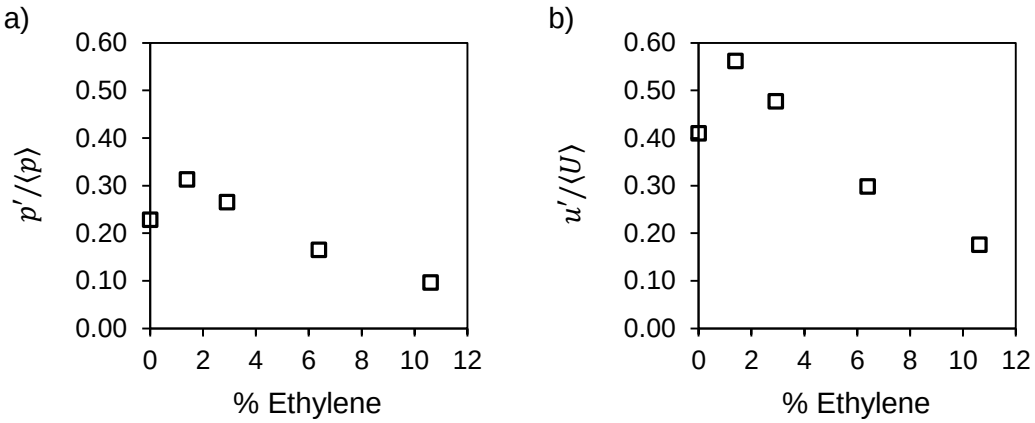

Figure 6.9: Shows the change in the normalised (a) pressure and (b) velocity perturbations of self-excited imperfectly premixed ethylene flames with an increase in the local addition of ethylene.

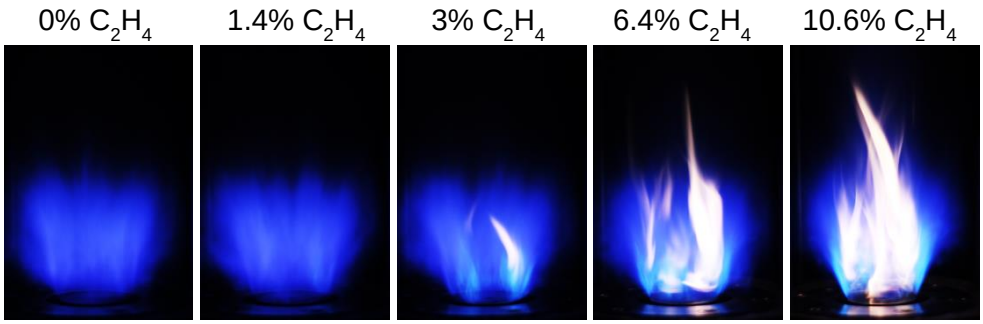

Figure 6.10: Photographic images of the self-excited imperfectly premixed ethylene flame with the local addition of ethylene through the secondary fuel ports.

6.2.4 Addition of nitrogen to self-excited ethylene flames

The local addition of nitrogen to the flame was selected as a control as it did not play a significant role in the combustion process. Although it could lower the flame temperature, the quantities added were minimal to cause a large change.

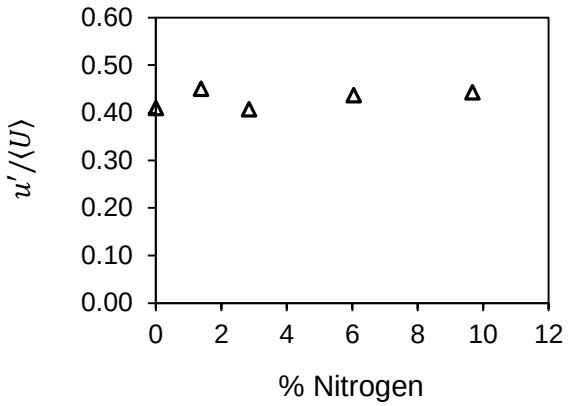

Figure 6.11: Shows the change in the normalised velocity perturbations of self-excited imperfectly premixed ethylene flames with an increase in the local addition of nitrogen.

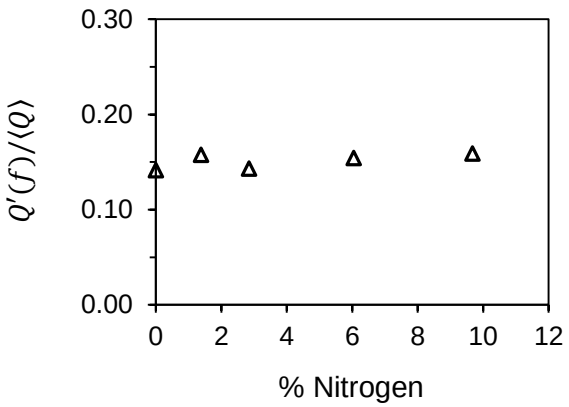

Figure 6.12: Shows the change in the global normalised heat release fluctuations of self-excited imperfectly premixed ethylene flames with an increase in the local addition of nitrogen.

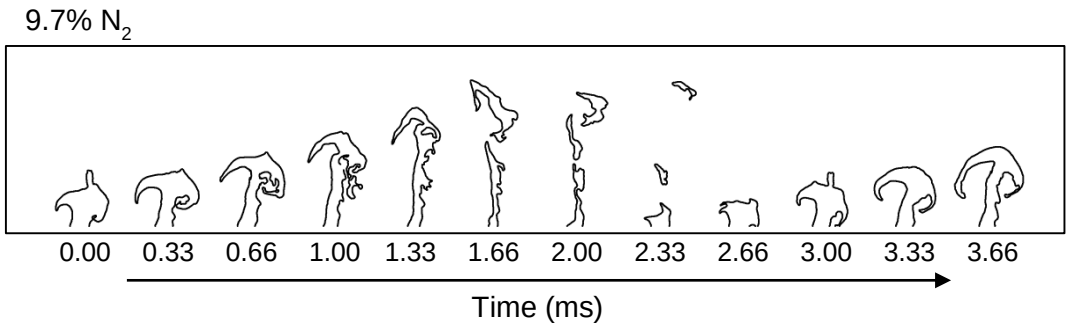

Figure 6.13: The images show the evolution of the flame boundary of the self-excited imperfectly premixed ethylene flames with 9.7% local addition of nitrogen.

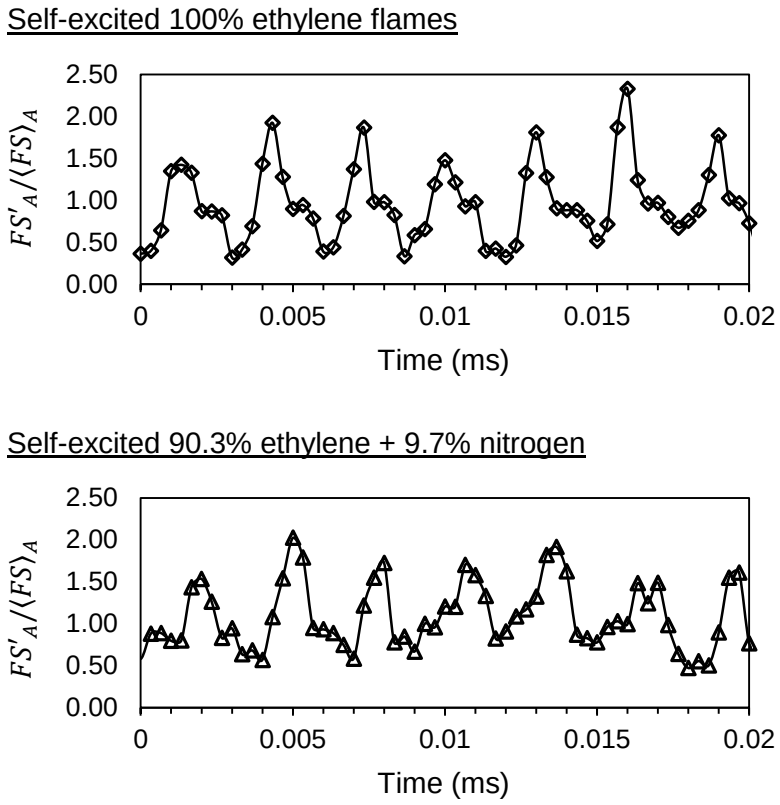

Figure 6.14: Shows the time series plots of the flame surface area for region A determined by laser tomography for pure ethylene and ethylene/nitrogen self-excited flames.

As with previous tests, nitrogen was added into the flow through the secondary fuel ports. The Figures 6.11 and 6.12 summarise the results obtained for all the tests carried out with nitrogen addition and to briefly explain it; nitrogen caused a little increase of the velocity and heat release perturbations in the combustion chamber. The images (Figure 6.13) obtained from the tomography, and the calculated normalised flame surface area in region A (Figure 6.14) clearly confirmed that the addition of nitrogen had a negligible impact on the flame roll-up occurring in the self-excited flames.

6.3 Comparison of the addition of H_2, C_2H_4 and N_2 to self-excited flames

To provide a clear comparison between all the self-excited flames, the following figures (Figure 6.15, 6.16, and 6.17) plot the time series graphs of $p'(f)/\langle P\rangle$, $Q'(f)/\langle Q\rangle$, and $FS'_A/\langle FS_A\rangle$ for all the self-excited flames. In these figures the heat release and flame surface oscillation for stratified ethylene flames was not available due to the presence of the yellow plumes.

The momentum ratio between the secondary fuel and the oncoming primary ethylene fuel and air mixture was calculated to adjust the secondary flow of the gases to match the level of penetration each fuel had into the main flow. Figures 6.18 and 6.19 show the normalised velocity and heat release oscillations for the addition of hydrogen, ethylene and nitrogen to self-excited ethylene flames against the momentum ratio.

These figures summarise the key points from the experimental results and are as follows:

- The self-excited ethylene flames experienced a periodic oscillation of the pressure (velocity), heat release and the flame surface area in region A.
- With the addition of hydrogen there was a reduction of the normalised pressure oscillations (hence the velocity perturbations) of the flow; and a reduction in the heat release. The initial size of the flame roll-up reduced (indicated by the flame surface area in region A) with the addition of H_2.

- There was a negligible difference in the normalised oscillations (pressure, heat release and flame surface area) between the test case of 20% and 30% addition of H_2.
- With the addition of ethylene (i.e. stratification), the normalised pressure and velocity perturbations initially increased (1.4% and 2.9% ethylene in the secondary flow) and then decreased with the increase of % C_2H_4 in the secondary flow.
- The presence of soot with the local addition of C_2H_4 did indicate a lower efficiency and higher hydrocarbons in the emissions.
- The use of C_2H_4 to influence the response of the self-excited flame showed that the reduction in the combustion oscillations achieved with the addition of H_2 was unique.
- With the addition of N_2 there was no noticeable change in the oscillations of the $p'(f)/\langle P \rangle$, $u'(f)/\langle U \rangle$, $Q'(f)/\langle Q \rangle$, and $FS'_A/\langle FS_A \rangle$. Assuming that N_2 gas was inert and did not affect the combustion process, it showed that the change in the response of an excited flame is unique to the addition of fuel.

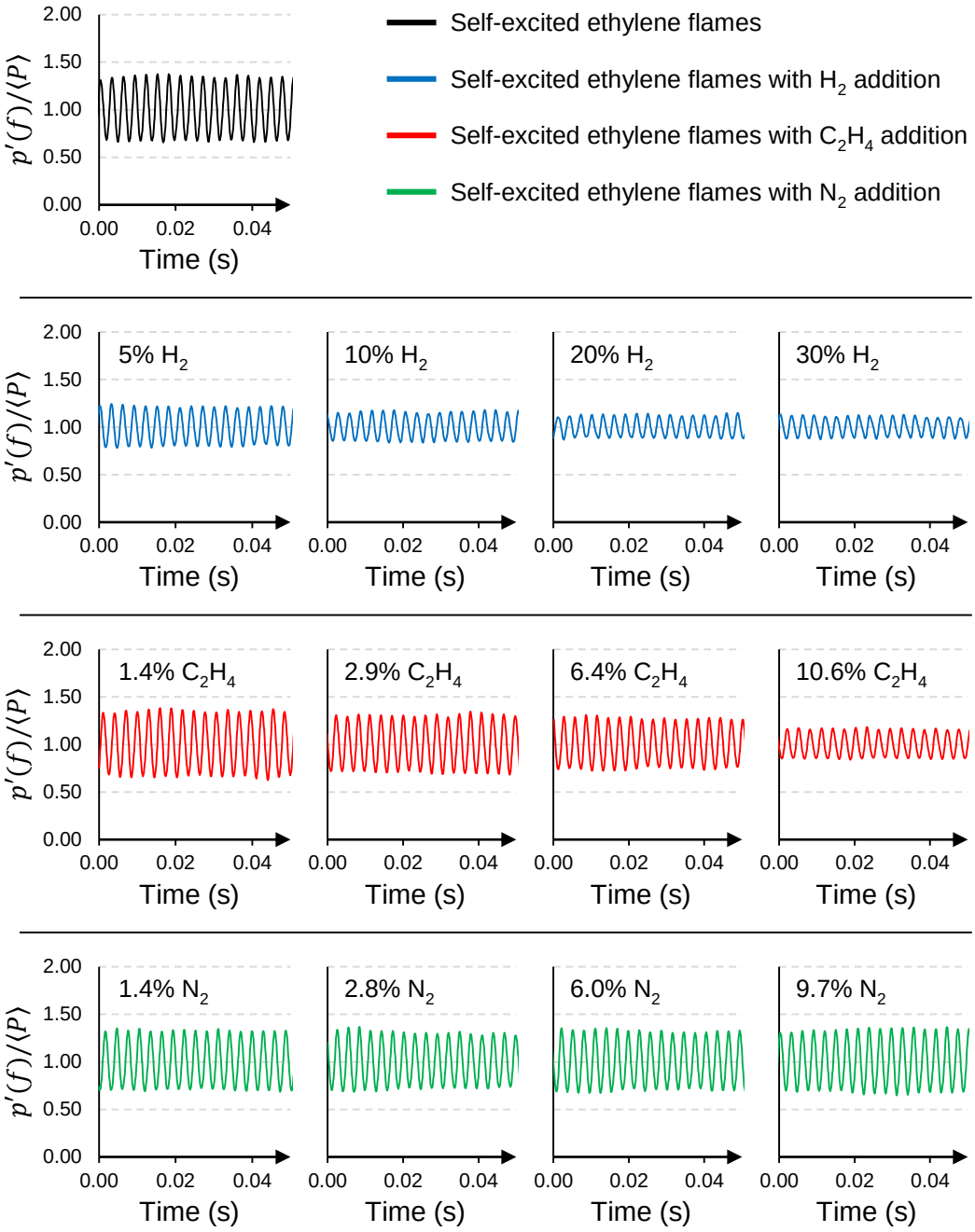

Figure 6.15: Time series plots of the normalised pressure fluctuations measured at the topmost pressure transducer, for the pure ethylene self-excited flames, with the addition of H_2, C_2H_4 and N_2.

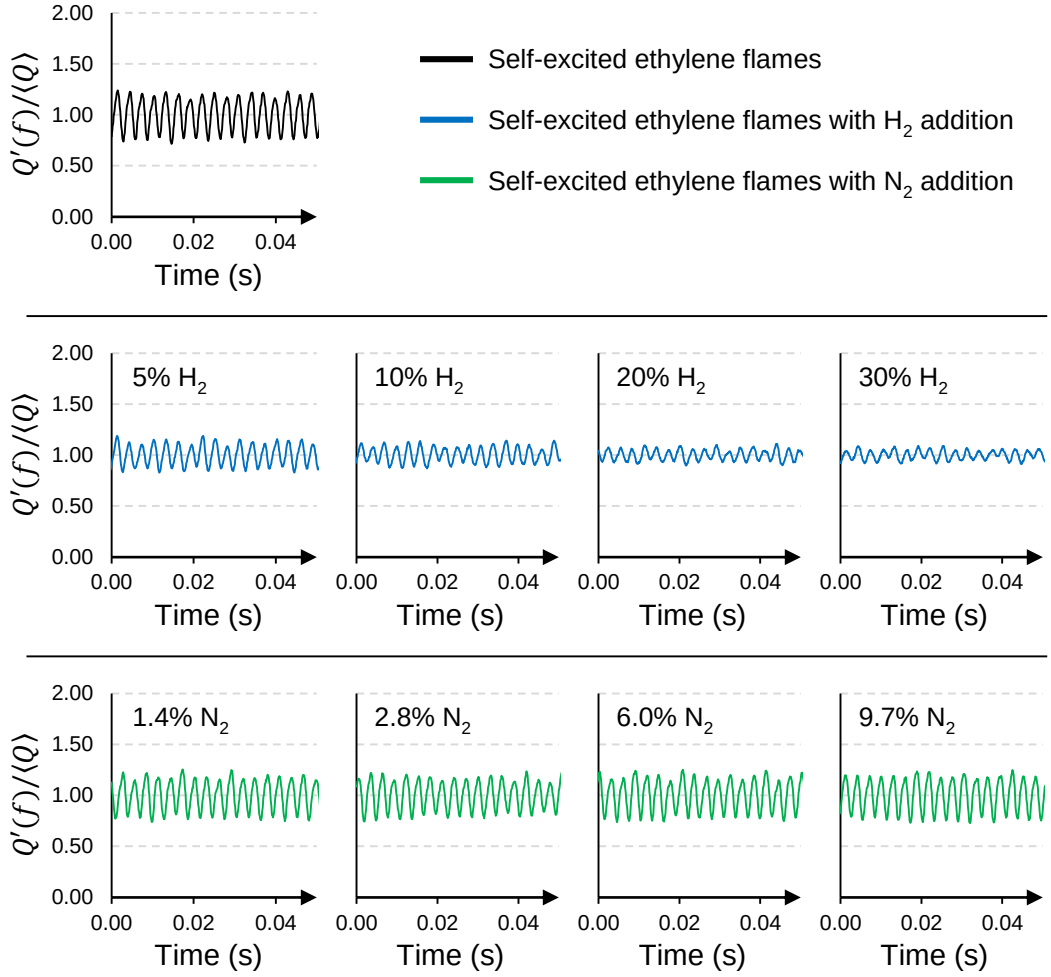

Figure 6.16: Time series plots of the normalised heat release fluctuations evaluated from the OH* chemiluminescence, for the pure ethylene self-excited flames, with the addition of H_2 and N_2.

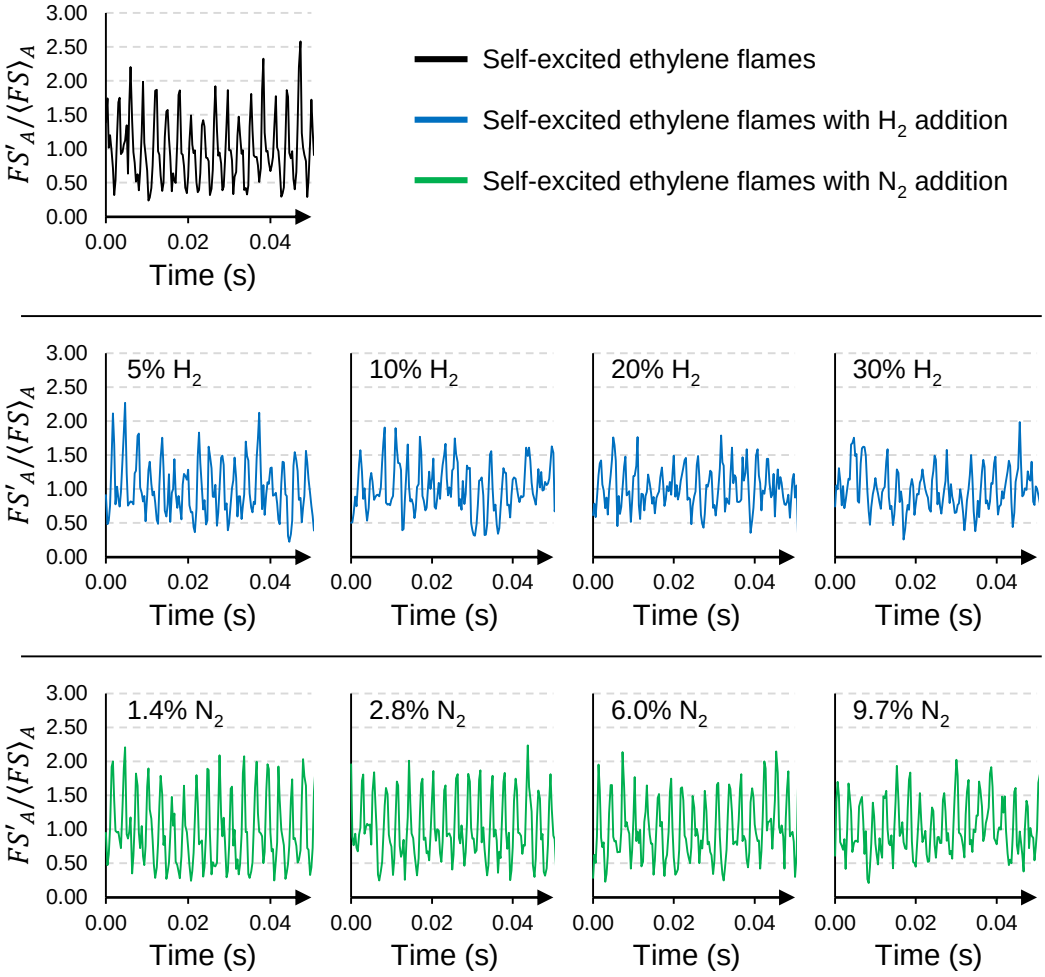

Figure 6.17: Time series plots of the normalised flame surface fluctuation evaluated in Region A, for the pure ethylene self-excited flames, with the addition of H_2 and N_2.

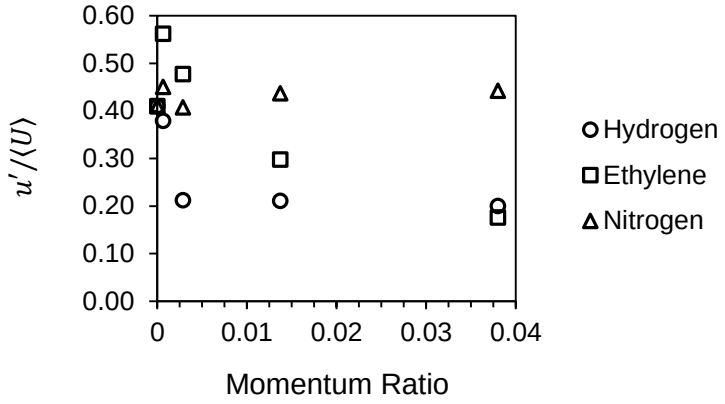

Figure 6.18: Shows the change in the normalised velocity perturbations of self-excited imperfectly premixed ethylene flames with an increase in the momentum ratio of the locally added hydrogen, ethylene and nitrogen gases.

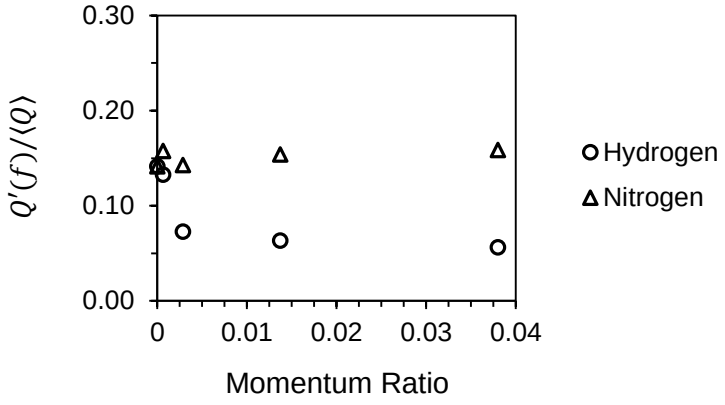

Figure 6.19: Shows the change in the global normalised heat release oscillations of self-excited imperfectly premixed ethylene flames with an increase in the momentum ratio of the locally added hydrogen and nitrogen gases.

6.4 Comparison of self-excited and acoustically forced flames

The purpose of the self-excited experimentation was to verify that the addition of hydrogen has an effect on the combustion response of the turbulent

flames as was seen under controlled (i.e. forced) operating conditions. Figure 6.20 shows the heat release response of the self-excited and forced imperfectly premixed ethylene flames with the addition of hydrogen. The response of the flames is shown for two separate frequencies; self-excitation occurred at approximately 338 Hz and the forced flames presented were at a frequency of 315 Hz. Under the forced conditions it was seen that the addition of hydrogen reduced the heat release oscillations, however, as the percentage of H_2 added was increased, the change in the response reduced. Under self-excitation, the addition of H_2 did reduce the normalised heat release and velocity perturbation. Although the magnitude of the heat release response is different from the forced flames (may be due to the difference in frequencies), the general trend was similar. The self-excited flames with H_2 showed that the addition did indeed reduce the heat release oscillations, and it also showed that there was a limit to how much these oscillations could be reduced (i.e. there was very little change between the addition of 20% and 30% H_2).

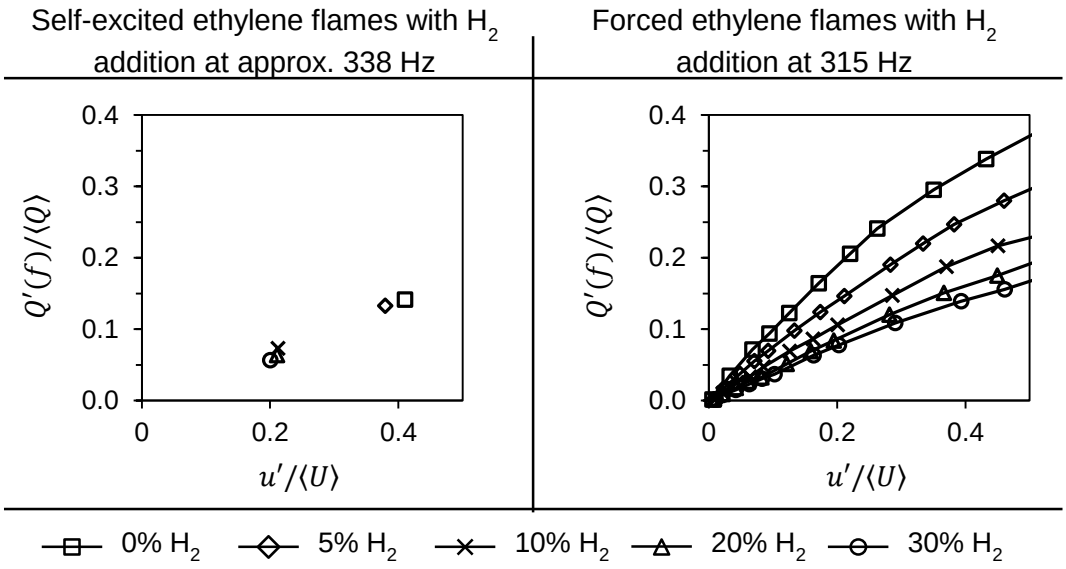

Figure 6.20: The dependence of the global heat release fluctuation (evaluated from OH* chemiluminescence) on velocity fluctuations, for imperfectly premixed ethylene flames with the addition of H_2 under self-excited and forced operating conditions.

Under forced conditions it was seen that with any addition of H_2 there was a change in the initial size of the flame roll-up. Figure 6.21 shows the phase-locked

images of the imperfectly premixed ethylene flames with H_2 addition under forced conditions, and the instantaneous images of the self-excited flames with H_2 addition. The images show that the initial size of the flame roll-up did reduce with the addition of H_2 which would have played a part in the alteration of the heat release response.

From these graphs and images it can concluded that the addition of H_2 has the ability to reduce the heat release oscillations of the imperfectly premixed ethylene flames as demonstrated under forced and self-excited conditions. This ability is unique to H_2 as the addition of C_2H_4 and N_2 did not produce a similar change in the response.

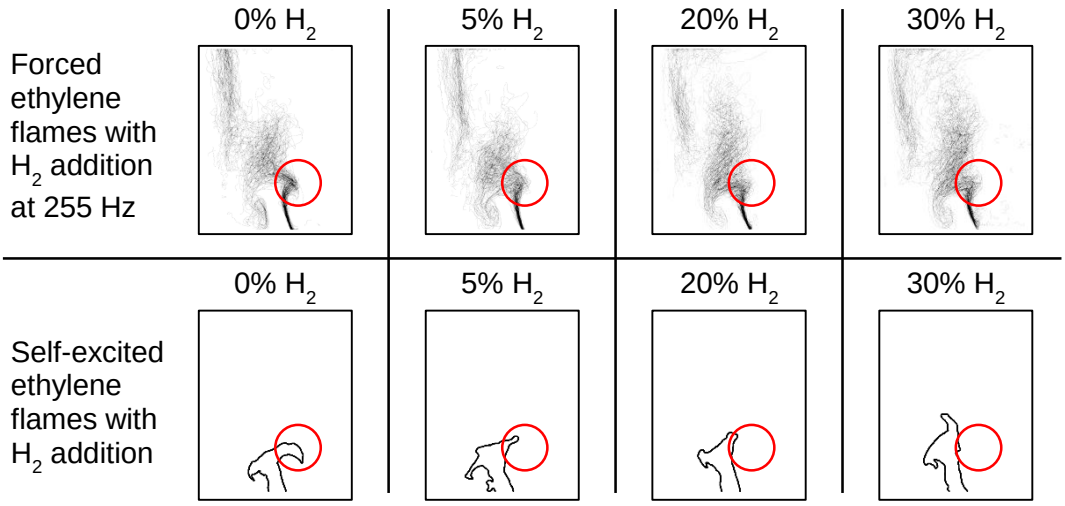

Figure 6.21: Compares the initial development of the flame roll-up of imperfectly premixed ethylene flames with H_2 addition under self-excited and forced operating conditions.

6.5 Summary

The data and figures presented in this section discussed the imperfectly premixed ethylene flames under self-excited conditions. The response of the flame was studied with the local addition of several gasses; which were hydrogen, ethylene and nitrogen. The results showed that the local addition of hydrogen did reduce the size of the flame roll-up, the normalised velocity perturbations and the global heat release oscillations (determined from the OH* chemiluminescence).

Ethylene and nitrogen aided the study, to determine that the response achieved with the addition of H_2 was unique. While H_2 caused a reduction in the $u'/\langle U \rangle$ (from 0.41 to 0.2) and $Q'(f)/\langle Q \rangle$ (from 0.14 to 0.06), N_2 had very little effect and C_2H_4 only caused a reduction at high secondary flow % which led to sooty flames.

The results presented for the addition of hydrogen to a self-excited imperfectly premixed ethylene flame agree with the conclusions gathered from the experiments conducted under forcing conditions. The conclusions stated that the addition of hydrogen would reduce the flame roll-up and hence the heat release oscillations. With the reduction in the heat release oscillations the resulting velocity perturbations were also reduced during the self-excitation study.

Chapter 7: Conclusions and further work

The occurrence of combustion instabilities is problematic in practical applications because the resulting amplitudes of pressure and velocity fluctuations cause severe vibrations, excessive heat transfer and thermal stresses to the combustor walls, oscillatory mechanical loads and flame blow-off or flashback. Based on work published by several authors, a possible method of reducing combustion oscillations was by introducing a secondary fuel into the flow. The main goal of this project was to understand the use of hydrogen as a secondary fuel to reduce or eliminate oscillations of an excited turbulent premixed flame. Many studies had been carried out in the past by other researchers on the use of hydrogen as a control for combustion oscillations; however, the results were inconclusive as some reported a positive outcome with the use of hydrogen while others reported the opposite. Complimentary to this goal was the purpose of developing a unique method to image atomic hydrogen laser induced fluorescence. In the past a handful of research had been done on developing a technique to image these atoms, however, it had been limited to using a laser mixing technique used for point measurements and on laminar flames. In this study the development of a high powered atomic hydrogen PLIF technique was detailed and applied to turbulent flames in a model gas turbine combustor.

7.1 Development of atomic hydrogen laser induced fluorescence

Atomic hydrogen is highly reactive and diffusive and plays an important role in combustion chemistry. The reactivity of the H-atom can have a significant impact on the combustion process. During combustion the H atoms are readily consumed

to produce O* and OH* radicals which are key chain-branching reactants, thus enhancing the reaction rate. However, the presence of atomic H is affected by the flame shape (Najm and Wyckoff 1997) which is why this project involved the development of a unique technique to image these radicals in turbulent flames.

The laser induced fluorescence of atomic hydrogen was achieved by using a two-photon excitation scheme (Lucht *et al.* 1983) at a wavelength of 205.1 nm. When the excited atom decayed from its excited state to the ground state there was an emission of light at a wavelength of 653.6 nm which was imaged (camera and laser system described in Chapter 2).

To ensure atomic hydrogen fluorescence was being detected by the camera, the wavelength of the excitation beam was shifted by 0.1 nm which resulted in no fluorescence being detected. The profile of the fluorescence was also tested at three different beam energy levels with two different types of flames to check that there were no significant spontaneous emissions by other radicals. From the results it was clear that the normalised fluorescence profiles were nearly identical indicating that it was indeed the fluorescence of atomic hydrogen.

7.2 The effects of local hydrogen on turbulent premixed flames

As stated, the main objective was to understand the effects of local hydrogen (H_2) addition on the heat release response and the shape of a turbulent flame. The tests consisted of turbulent premixed ethylene or methane flames subjected to acoustical forcing by loud speakers, which caused the modulation of the mass flow of reactants entering the combustion chamber. This caused the formation of counter rotating vortices in the flow which distorted the flame shape by causing the flame surface to roll up. The formation of the flame roll-up caused a large variation in the flame surface area which had a direct impact on the heat release fluctuation.

In the first set of tests the turbulent flames used the base fuel of ethylene that was imperfectly premixed with the air. Under this condition, with the local addition of hydrogen (H_2) from the secondary fuel ports placed 2 mm below the combustion zone, the flames showed a lower heat release modulation (determined by the OH* chemiluminescence) at the three forcing frequencies that were used (i.e.

30, 255 and 315 Hz). This local addition caused a significant alteration in the initial size of the flame roll-up (quantified by the surface area calculated in Region A). While in Region B the flame surface was sustained with the addition of H_2. The combination of these two changes caused a reduction in the steep fluctuations in the overall flame surface area which was why the fluctuation of the heat release had reduced. Although, the introduction of H_2 into the flow reduced the heat release oscillations, the changes between the flames with high H_2 content (20% and 30%) showed very little difference.

Methane fuel was also used as a base fuel; however, it was either imperfectly or fully premixed with the air. With the local addition of H_2 to the methane flames there were mixed outcomes. For imperfectly premixed methane flames the use of H_2 was beneficial in terms of reducing heat release oscillations only at forcing frequencies of 30 and 255 Hz, while at 315 Hz any addition of H_2 caused a rise in the oscillations.

Similarly, under fully premixed methane conditions the flames showed higher heat release oscillations with any addition of H_2 at a forcing frequency of 315 Hz. However, at a forcing frequency of 255 Hz, the addition of 30% H_2 caused a reduction in the heat release response while lower quantities had a negative effect. Despite the differences in the response of the heat release and flame surface area for all the flames, including ethylene and methane used as a base fuel, with different methods of mixing, the imaging of all the flames showed one similarity. With any amount of H_2 locally injected into the flow, it caused a reduction in the initial size of the flame roll-up causing a reduced fluctuation of the flame surface area in Region A.

The atomic hydrogen, H, PLIF was also performed on these flames and the results showed that with increasing % of H_2 addition the presence of H atoms increased (indicated by the stronger LIF signal). Under forcing conditions the intensity of the LIF signal had a periodic response and the times of increased H PLIF in Region A occurred with the initial formation of the flame roll-up. This increased presence most likely led to higher localised reaction rates at the inner shear layer which helped the flame resist to flame roll-up.

With the observations made during the use of hydrogen during controlled forcing, it was clear that the local addition of hydrogen to the flame could have a beneficial impact on the heat release and flame surface modulation. The

conclusions gathered were put to the test with hydrogen used to reduce the combustion oscillations of self-excited turbulent premixed flames.

7.3 The benefits and consequences of the local addition of hydrogen

The conclusions made from the results for the controlled forcing were validated with tests of local hydrogen addition to self-excited turbulent flames. Imperfectly premixed ethylene flames were made to excite with a modification to the combustor. The dominant frequency of excitation was approximately 338 Hz and the normalised velocity perturbations achieved at the entrance to the combustion zone was 0.41. In addition to using hydrogen to affect the combustion oscillations, ethylene and nitrogen were also used. Ethylene was used to see whether a generally known method of fuel stratification could also be used to reduce combustion oscillations. Being an inert gas, Nitrogen was used as a control to show that it was indeed the addition of a fuel at the inner shear layers that affected the combustion oscillations.

The results showed that H_2 successfully reduced the normalised velocity perturbations to approximately 0.2 and reduced the initial size of the flame roll-up (shown in the images captured by the flame tomography technique used). Although, the differences in the velocity fluctuation and flame roll-up were negligible between H_2 additions of 20% and 30%. The addition of ethylene and nitrogen were not able to match or improve on what the addition of hydrogen achieved; in some cases the combustion oscillations had worsened with an increase in velocity and heat release fluctuations.

Despite the improved flame response with the addition of hydrogen, it does have its drawbacks. Flame emission measurements were conducted and it was shown that with the addition of H_2 there was a significant increase in the production of NO_x while there were minor changes in the CO_2 content. It had been suggested by other researchers that the substantial increase in NO_x was a direct result of a higher flame temperature caused by the addition of hydrogen. In conclusion, while there was a benefit to the use of H_2 in reducing combustion oscillations there was also a negative impact on the combustion emissions.

7.4 Concluding remarks and further research in the area

The project was started off with two key objectives:

- The primary objective was to understand the effects of local hydrogen addition on the dynamic response of turbulent premixed flames, and,
- The secondary objective was to develop a laser diagnostic technique to image the atomic hydrogen PLIF of turbulent premixed flames.

To achieve these objectives, a combustion rig and a laser diagnostic facility was developed. The combustion rig was designed to create bluff-body stabilised flames which could be subjected to controlled acoustic forcing, and with a geometry modification allowed the flames to self-excite.

The study has successfully shown the impact local addition of hydrogen had on bluff-body stabilised turbulent premixed flames. The research has shown the positive and negative aspects of this addition, and provided a base review of how H_2 affected the combustion dynamics. From the findings the following key conclusions can be made:

- The local addition of H_2 in ethylene and methane premixed flames has an effect on the heat release response and the flame shape.
- The addition can have positive or negative effect on the heat release response depending on the method of primary fuel introduction, type of primary fuel and forcing conditions.
- With the addition, irrespective of heat release response, the initial size of the flame roll-up had changed and the increase in the NOx formation was significant.
- The self-excitation tests proved that the change in the response with the addition of H_2 was unique as the addition of C_2H_4 and N_2 showed no benefit to the dynamic response of the flames.

Further research alongside the measurements made in this study is necessary to understand the impact on the combustion chemistry and dynamics during the local addition of fuel to the flame.

The local equivalence ratio in the flow with the addition of hydrogen would be a good start in understanding what the laminar flame speeds are in the region. The

laminar flame speeds could be calculated computationally or simple experiments using a flat flame burner with the use of a PIV system can be set up to determine the laminar flame speed of different fuel mixtures. Understanding the effects on the local flame speed will tie in with the results shown here of the change in the size of the flame roll-up. Additionally a high speed OH PLIF and PIV system could be set up to find the local turbulent flame speed in the region of the flame roll-up and see how this quantity changed with the local addition of hydrogen. Using this data other fuels could be locally added to the flame with the same turbulent flame speed to check if the increase in this key variable was what caused the local addition of H_2 to reduce the combustion oscillations. The addition of 30% H2 to the ethylene and methane flames caused a slightly lifted flame. PIV tests on this case study may show why this occurred.

Another study that could be conducted is on the flame's temperature. Either by means of Rayleigh scattering or OH PLIF measurements (Lee *et al.* 2005, Copeland *et al.* 2007) the temperature of the combustion products could be determined. This combined with emission measurements would validate the increase in the increased in NO_x formation with an increase in the temperature of the combustion products.

Further development of the H PLIF system is required to show the global change in the relative H concentration in the flame during acoustic forcing. The increased presence of these atoms in regions of flame roll-up may assist in understanding the combustion process, which would be beneficial for developing computational models.

Appendix

A.1 Image threshold technique (Otsu Method)

The method below describes how a threshold value was calculated to convert the OH PLIF images into binarised images of black and white regions where the black regions show the burnt gas. The Otsu method converts the image to a grayscale image and uses an iterative process to calculate a measure of spread for the pixel levels each side of the threshold, i.e. the pixels that either fall in the foreground or background. The measure of spread being calculated is the sum of weighted variances which is referred to as the Within Class Variance. This quantity is calculated for each threshold value applied to the image, and it is the threshold that produces the lowest sum of weighted variances that is selected for binarising the image. Below is an example of how the threshold of an image was calculated. The following example was adapted from www.labbookpages.co.uk.

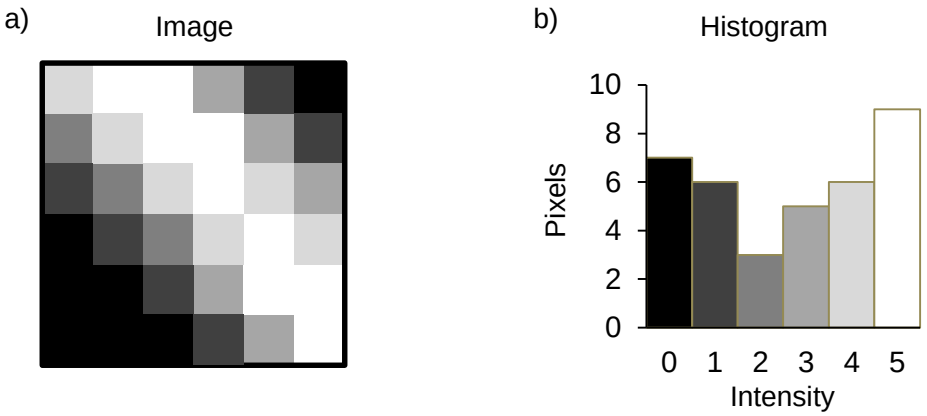

Figure A.1: (a) Shows the 6x6 image used to calculate the threshold, and (b) the histogram showing the number of pixels at each intensity.

In this example the black pixels (intensity 0) will be referred to as the background while the white pixels (intensity 5) will be referred to as the foreground, and there are a total of 6 greyscales used (i.e. intensity ranging from 0 to 5).

To start the calculations, initially a threshold value is selected and the background and foreground pixels are identified. Then the following equations are used to calculate the variables for the background.

$$Weight, W_b = {No.of\ background\ pixels}/{Total\ number\ of\ pixels}$$

$$Mean, \mu_b = {[\sum_{i=0}^{n}(Intensity_n * No.of\ Pixels_n)]}/{Total\ no.of\ background\ pixels}$$

$$Variance, \sigma_b^2 = {\{\sum_{i=0}^{n}[(Intensity_n - \mu_b)^2 * No.of\ Pixels_n]\}}/{Total\ no.of\ background\ pixels}$$

The subscript 'b' represents the variables for the background. These equations are used in the same way to find the variables for the foreground denoted by the subscript 'f'. These values are then used to calculate the 'Within class variance' given by the following equation:

$$Within\ class\ variance, \sigma_W^2 = W_b\sigma_b^2 + W_f\sigma_f^2$$

The threshold value which yields the lowest 'Within class variance' is then selected as the threshold value for that particular image. Below is an example calculation for a threshold value of 2.

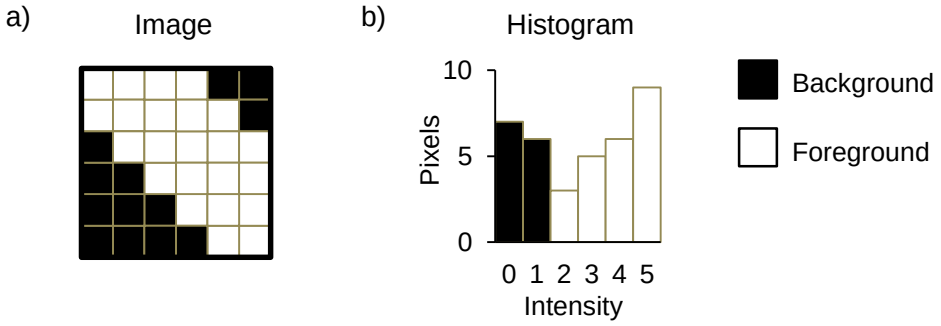

Figure A.2: The resulting (a) Image and (b) histogram using a threshold value of 2.

Background variables:

$$Weight, W_b = {}^{(7+6)}/_{36} = 0.361$$

$$Mean, \mu_b = {}^{(0*7+1*6)}/_{13} = 0.462$$

$$Variance, \sigma_b^2 = {}^{[(0-0.462)^2*7+(1-0.462)^2*6]}/_{13} = 0.249$$

Foreground variables:

$$Weight, W_f = {}^{(3+5+6+9)}/_{36} = 0.639$$

$$Mean, \mu_f = {}^{(2*3+3*5+4*6+5*9)}/_{23} = 3.913$$

$$Variance, \sigma_f^2 = {}^{[(2-3.913)^2*3+(3-3.913)^2*5+(4-3.913)^2*6+(5-3.913)^2*9]}/_{23} = 1.123$$

Once the variables are calculated the 'Within class variance' is found by:

$$Within\ class\ variance, \sigma_W^2 = W_b\sigma_b^2 + W_f\sigma_f^2 = 0.361 * 0.249 + 0.639 * 1.123 = 0.807$$

The variables for each threshold is shown below. In this particular case, the threshold of 3 yields the lowest 'Within class variance' of 0.62, hence that value is chosen as the threshold value for binarising the image.

Threshold = 0

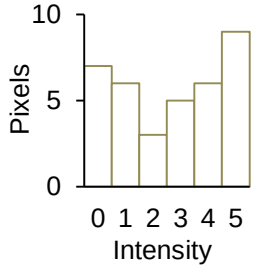

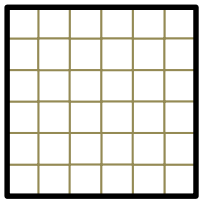

$W_b = 0.00$ $W_f = 1.00$

$\sigma^2 b = 0.00$ $\sigma^2 f = 3.56$

$\sigma^2 W = Wb\,\sigma^2 b + Wf\sigma^2 f = 3.56$

Threshold = 1

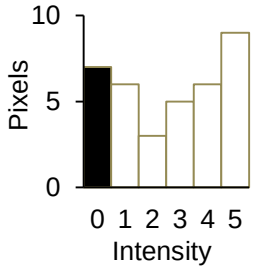

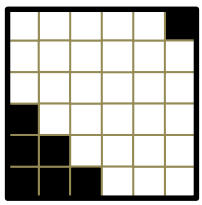

$W_b = 0.19$ $W_f = 0.81$

$\sigma^2{}_b = 0.00$ $\sigma^2{}_f = 2.28$

$\sigma^2{}_W = Wb\,\sigma^2{}_b + Wf\sigma^2{}_f = 1.84$

Threshold = 2

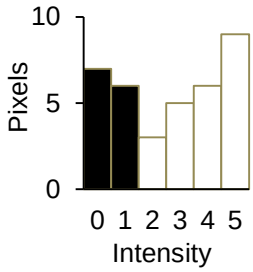

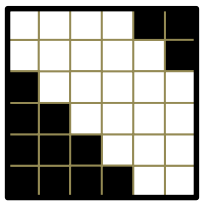

$W_b = 0.36$ $W_f = 0.64$

$\sigma^2{}_b = 0.25$ $\sigma^2{}_f = 1.12$

$\sigma^2{}_W = Wb\,\sigma^2{}_b + Wf\sigma^2{}_f = 0.81$

Threshold = 3

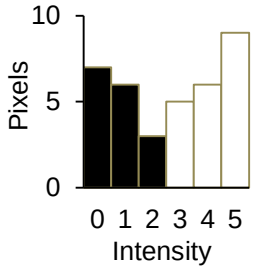

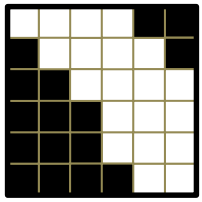

$W_b = 0.44$ $W_f = 0.56$

$\sigma^2{}_b = 0.56$ $\sigma^2{}_f = 0.66$

$\sigma^2{}_W = Wb\,\sigma^2{}_b + Wf\sigma^2{}_f = 0.62$

Threshold = 4

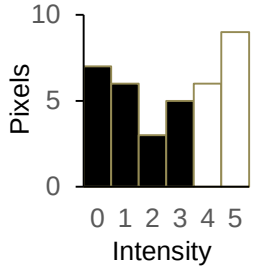

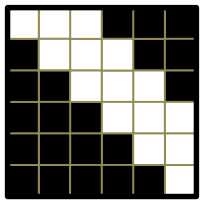

$W_b = 0.58$ $W_f = 0.42$

$\sigma^2{}_b = 1.35$ $\sigma^2{}_f = 0.24$

$\sigma^2{}_W = Wb\,\sigma^2{}_b + Wf\sigma^2{}_f = 0.89$

Threshold = 5

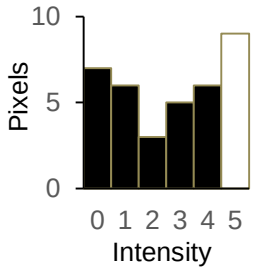

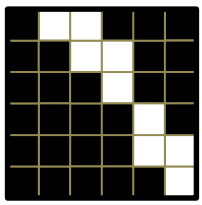

$W_b = 0.75$ $W_f = 0.25$

$\sigma^2{}_b = 2.32$ $\sigma^2{}_f = 0.00$

$\sigma^2{}_W = Wb\,\sigma^2{}_b + Wf\sigma^2{}_f = 1.74$

Reference case: 100% C_2H_4

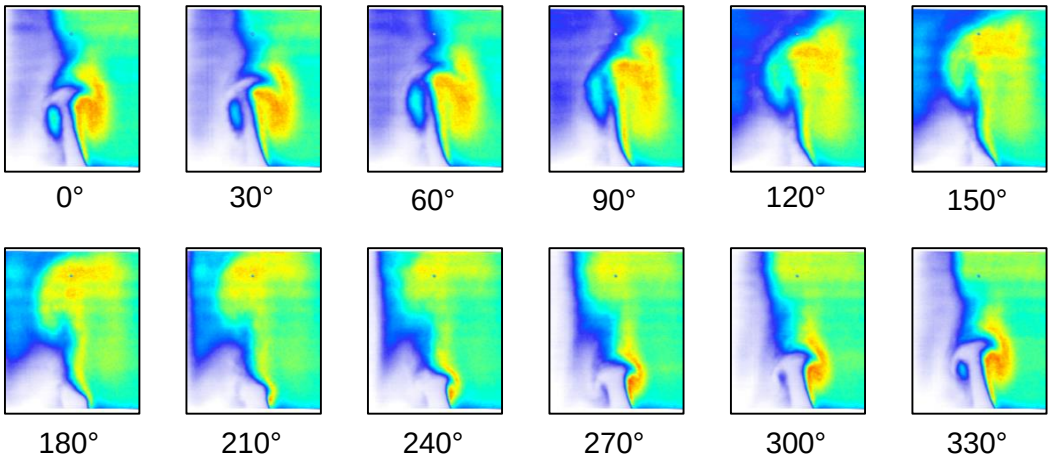

Figure A.3: Phase-locked averaged OH PLIF image sequence of 100% ethylene imperfectly premixed, under strong acoustic forcing, $u'/\langle U \rangle$ = 0.4, f = 255 Hz.

Case: 95% C_2H_4 + 5% H_2

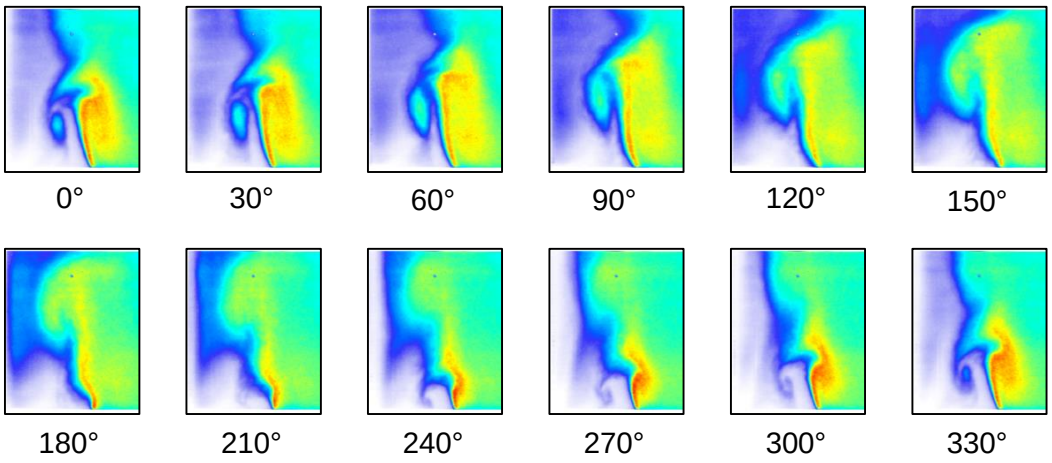

Figure A.4: Phase-locked averaged OH PLIF image sequence of 95% ethylene imperfectly premixed with the local addition of 5% hydrogen, under strong acoustic forcing, $u'/\langle U \rangle$ = 0.4, f = 255 Hz.

Case: 80% C_2H_4 + 20% H_2

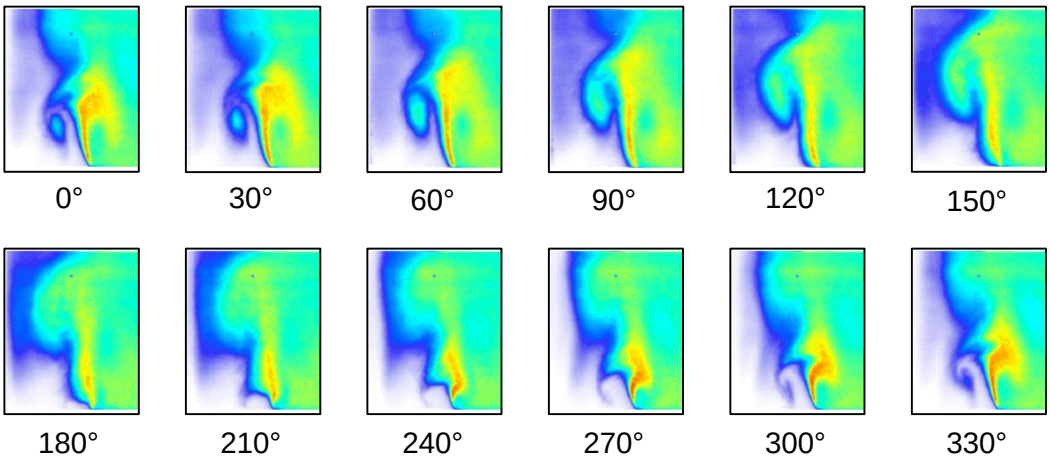

Figure A.5: Phase-locked averaged OH PLIF image sequence of 80% ethylene imperfectly premixed with the local addition of 20% hydrogen, under strong acoustic forcing, $u'/\langle U \rangle$ = 0.4, f = 255 Hz.

Case: 70% C_2H_4 + 30% H_2

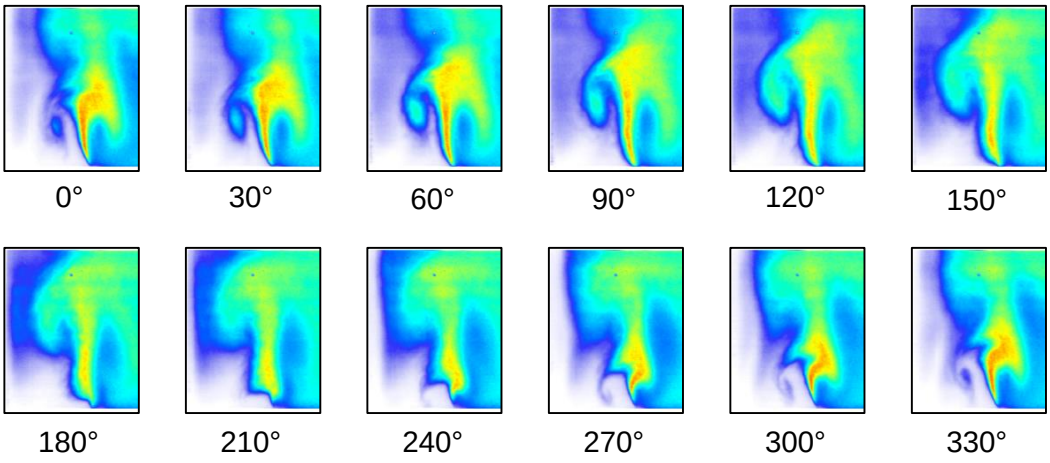

Figure A.6: Phase-locked averaged OH PLIF image sequence of 70% ethylene imperfectly premixed with the local addition of 30% hydrogen, under strong acoustic forcing, $u'/\langle U \rangle$ = 0.4, f = 255 Hz.

Case: Imperfectly premixed 90% CH_4 + 10% H_2

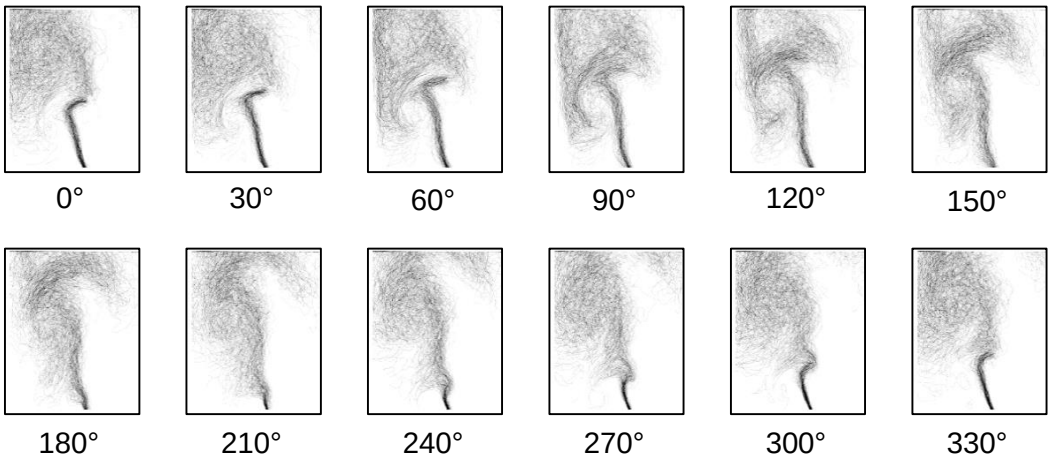

Figure A.7: Phase-locked averaged flame front (FF) image sequence of 90% methane imperfectly premixed with the local addition of 10% hydrogen, under strong acoustic forcing, $u'/\langle U \rangle$ = 0.4, f = 255 Hz.

Case: Imperfectly premixed 70% CH_4 + 30% H_2

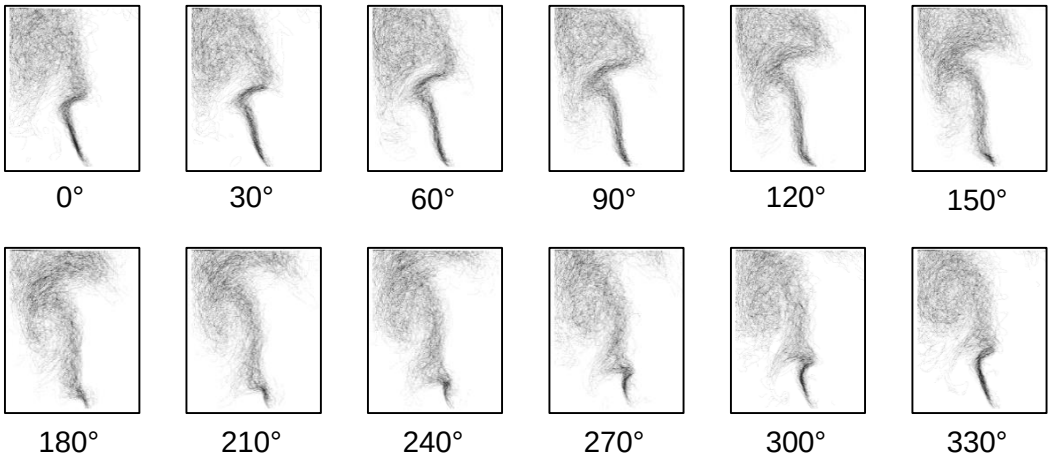

Figure A.8: Phase-locked averaged flame front (FF) image sequence of 70% methane imperfectly premixed with the local addition of 30% hydrogen, under strong acoustic forcing, $u'/\langle U \rangle$ = 0.4, f = 255 Hz.

Case: Fully premixed 70% CH_4 + 30% H_2

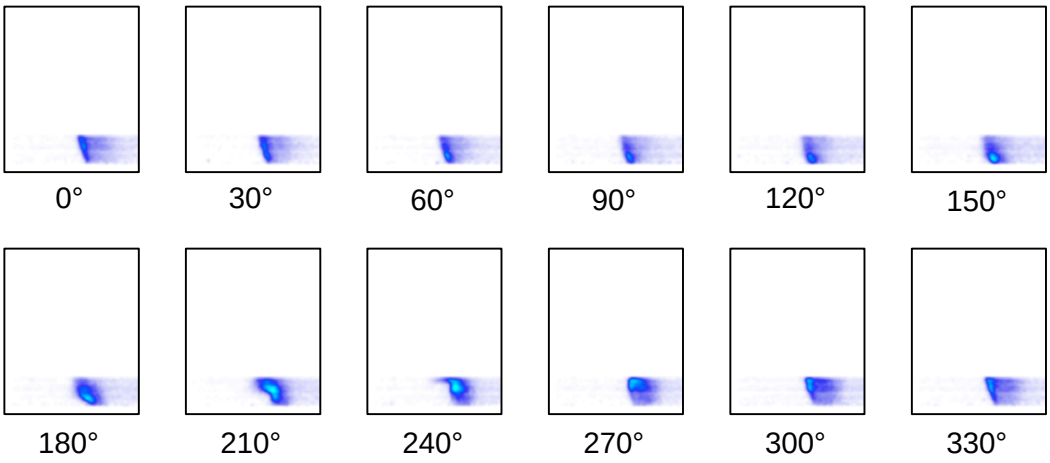

Figure A.9: Phase-locked averaged H PLIF image sequence of 70% methane fully premixed with the local addition of 30% hydrogen, under strong acoustic forcing, $u'/\langle U \rangle$ = 0.4, f = 255 Hz.

List of publications

Hussain, T., Dowlut, A. & Balachandran, R. (2011), “Experimental investigation of response of hydrogen enriched methane flames to acoustic oscillations”, Fifth European Combustion Meeting, Cardiff, Great Britain.

Hussain, T. & Balachandran, R. (2011), “Investigation of the effect of fuel stratification on response of turbulent premixed flames to acoustic excitation”, 18th International Congress on Sound & Vibration, Rio de Janeiro, Brazil.

Hussain, T., Dowlut, A. & Balachandran, R. (2012), “Investigation in to the effect of hydrogen enrichment on the response of turbulent premixed flames subjected to acoustic excitation”, 19th International Congress on Sound & Vibration, Vilnius, Lithuania.

Dowlut, A., Hussain, T. & Balachandran, R. (2012), “Experimental investigation of dynamic response of acoustically forced turbulent premixed CH_4/CO_2/air flames”, 19th International Congress on Sound & Vibration, Vilnius, Lithuania.

Bibliography

Abdalla, A. Y., Ali, B. B., Bradley, D., & Chin, S. B. (1981). Stratified combustion in recirculating flow. *Combustion and Flame*, ***43***, 131–143.

Albrecht, P., Bade, S., Lacarelle, A., Paschereit, C. O., & Gutmark, E. (2010). Instability control by premixed pilot flames. *Journal of Engineering for Gas Turbines and Power*, ***132***, 041501–1–8.

Altay, H. M., Speth, R. L., Hudgins, D. E., & Ghoniem, A. F. (2009). The impact of equivalence ratio oscillations on combustion dynamics in a backward-facing step combustor. *Combustion and Flame*, ***156***, 2106–2116.

Anselmo-Filho, P., Hochgreb, S., Barlow, R. S., & Cant, R. S. (2009). Experimental measurements of geometric properties of turbulent stratified flames. *Proceedings of the Combustion Institute*, ***32***, 1763–1770.

Ayoola, B. O., Balachandran, R., Frank, J. H., Mastorakos, E., & Kaminski, C. F. (2006). Spatially resolved heat release rate measurements in turbulent premixed flames. *Combustion and Flame*, ***144***, 1–16.

Baillot, F., Durox, D., & Prud'Homme, R. (1992). Experimental and theoretical study of a premixed vibrating flame. *Combustion and Flame*, ***88***, 149–168.

Balachandran, R. (2005). Experimental investigation of the response of turbulent premixed flames to acoustic oscillations. University of Cambridge.

Balachandran, R., Ayoola, B. O., Kaminski, C. F., Dowling, A. P., & Mastorakos, E. (2005). Experimental investigation of the nonlinear response of turbulent premixed flames to imposed inlet velocity oscillations. *Combustion and Flame*, ***143***, 37–55.

Ballester, J., & Armingol, T. G. (2010). Diagnostic techniques for the monitoring and control of practical flames. *Progress in Energy and Combustion Science*, ***36***, 375–411.

Barbosa, S., Garcia, M. C., Ducruix, S., Labegorre, B., & Lacas, F. (2007). Control of combustion instabilities by local injection of hydrogen. *Proceedings of the Combustion Institute*, ***31***, 3207–3214.

Becker, K. H., Kley, D., & Norstrom, R. J. (1969). OH* chemiluminescence in hydrocarbon atom flames. In *Twelfth Symposium (International) on Combustion / The Combustion Institute*.

Behrens, A. A. (2007, January). Reacting flow studies in a dump combustor: enhanced volumetric heat release rates and flame anchorability. University of Minnesota.

Bellows, B. D., Bobba, M. K., Seitzman, J. M., & Lieuwen, T. (2007). Nonlinear flame transfer function characteristics in a swirl-stabilized combustor. *Transactions of the ASME*, ***129***, 954–961.

Birbaud, A. L., Ducruix, S., Durox, D., & Candel, S. (2008). The nonlinear response of inverted “V” flames to equivalence ratio nonuniformities. *Combustion and Flame*, ***154***, 356–367.

Blomshield, F. S. (2001). Historical perspective of combustion instability in motors: Case studies. *American Institute of Aeronautics and Astronautics*, *2001-3875*.

Bloxsidge, G. J., Dowling, A. P., & Langhorne, P. J. (1988). Reheat buzz : An acoustically coupled combustion instability. Part 2. Theory. *Journal of Fluid Mechanics*, ***193***, 445–473.

Bompelly, R. K., Lieuwen, T. & Seitzman, J. M. (2009). Lean-blowout and its sensing in the presence of combustion dynamics in a premixed swirl combustor. *47th AIAA Aerospace Sciences Meeting Including The New Horizons Forum and Aerospace Exposition* (Orlando, Florida)

Bradley, D., Gaskell, P. H., Gu, X. J., Lawes, M., & Scott, M. J. (1998). Premixed turbulent flame instability and no formation in a lean-burn swirl burner. *Combustion and Flame*, ***115***, 515–538.

Broda, J. C., Seo, S., Santoro, R. J., G., S., & Yang, V. (1998). An experimental study of combustion dynamics of a premixed swirl injector. In *Twenty-Seventh Symposium (International) on Combustion / The Combustion Institute* (pp. 1849–1856).

Candel, S. (2002). Combustion dynamics and control: progress and challenges. *Proceedings of the Combustion Institute*, ***29***, 1–28.

Chatterjee, P. (2004, July). A computational fluid dynamics investigation of thermoacoustic instabilities in premixed laminar and turbulent combustion systems. Faculty of the Virginia Polytechnic Institute and State University.

Chen, Z. (2009). Effects of hydrogen addition on the propagation of spherical methane/air flames: A computational study. *International Journal of Hydrogen Energy*, ***34***, 6558–6567.

Cho, J. H., & Lieuwen, T. (2005). Laminar premixed flame response to equivalence ratio oscillations. *Combustion and Flame*, ***140***, 116–129.

Choudhuri, A. R., & Gollahalli, S. R. (2003). Characteristics of hydrogen–hydrocarbon composite fuel turbulent jet flames. *International Journal of Hydrogen Energy*, ***28***, 445–454.

Copeland, C., Friedman, J., & Renksizbulut, M. (2007). Planar temperature imaging using thermally assisted laser induced fluorescence of OH in a methane–air flame. *Experimental Thermal and Fluid Science*, ***31***, 221–236.

Cozzi, F., & Coghe, A. (2006). Behavior of hydrogen-enriched non-premixed swirled natural gas flames. *International Journal of Hydrogen Energy*, ***31***, 669–677.

Culick, F. E. C. (1988). Combustion instabilities in liquid-fueled propulsion systems. *California Institute of Technology*, 1–73.

Dahl, G., & Suttrop, F. (1998). Engine control and low-nox, combustion for hydrogen fuelled aircraft gas turbines. *International Journal of Hydrogen Energy*, ***23***, 695–704.

Day, M. S., Gao, X., & Bell, J. B. (2011). Properties of lean turbulent methane-air flames with significant hydrogen addition. *Proceedings of the Combustion Institute*, ***33***, 1601–1608.

Dowling, A. P. (1995). The calculation of thermoacoustic oscillations. *Journal of Sound and Vibration*, ***180***, 557–581.

Dowling, A. P. (1997). Nonlinear self-excited oscillations of a ducted flame. *Journal of Fluid Mechanics*, ***346***, 271–290.

Dowling, A. P., & Morgans, A. S. (2005). Feedback control of combustion oscillations. *Annual Review of Fluid Mechanics*, ***37***, 151–182.

Dowlut, A., Hussain, T., & Balachandran, R. (2012). Experimental investigation of dynamic response of acoustically forced turbulent premixed CH4/CO2/air flames. In *19th International Congress on Sound & Vibration, Vilnius, Lithuania.*

Ducruix, S., Durox, D., & Candel, S. (2003). Combustion dynamics and instabilities: Elementary coupling and driving mechanisms. *Journal of Propulsion and Power*, ***19***, 722-734.

Echekki, T., & Chen, J. H. (1996). Unsteady strain rate and curvature effects in turbulent premixed methane-air flames. *Combustion and Flame*, ***106***, 184–202.

El-Ghafour, S. A. A., El-dein, A. H. E., & Aref, A. A. R. (2010). Combustion characteristics of natural gas–hydrogen hybrid fuel turbulent diffusion flame. *International Journal of Hydrogen Energy*, ***35***, 2556–2565.

Emiris, I., & Whitelaw, J. H. (2003). Control of combustion oscillations. *Combustion Science and Technology*, ***175***, 157–184.

Frenillot, J. P., Cabot, G., Cazalens, M., Renou, B., & Boukhalfa, M. A. (2009). Impact of H2 addition on flame stability and pollutant emissions for an atmospheric kerosene/air swirled flame of laboratory scaled gas turbine. *International Journal of Hydrogen Energy*, ***34***, 3930–3944.

Galizzi, C., & Escudie, D. (2010). Experimental analysis of an oblique turbulent flame front propagating in a stratified flow. *Combustion and Flame*, ***157***, 2277–2285.

Guo, H., Smallwood, G. J., Liu, F., Ju, Y., & Gulder, O. L. (2005). The effect of hydrogen addition on flammability limit and NOx emission in ultra-lean counterflow CH4/air premixed flames. *Proceedings of the Combustion Institute*, ***30***, 303–311.

Guo, H., Tayebi, B., Galizzi, C., & Escudie, D. (2010). Burning rates and surface characteristics of hydrogen-enriched turbulent lean premixed methane-air flames. *International Journal of Hydrogen Energy*, ***35***, 11342–11348.

Haber, L. C. (2000). An investigation into the origin, measurement and application of chemiluminescent light emissions from premixed flames. Virginia Polytechnic Institute and State University.

Haber, L. C., Vandsburger, U., Saunders, W. R., & Khanna, V. K. (2000). An experimental examination of the relationship between chemiluminescent light emissions and heat-release rate under non-adiabatic conditions. In *Active Control Technology for Enhanced Performance Operational Capabilities of Military Aircraft, Land Vehicles and Sea Vehicles*.

Hardalupas, Y., & Orain, M. (2004). Local measurements of the time-dependent heat release rate and equivalence ratio using chemiluminescent emission from a flame. *Combustion and Flame*, ***139***, 188–207.

Hathout, J. P., Fleifil, M., Annaswamy, A. M., & Ghoniem, A. F. (2000). Heat-release actuation for control of mixture-inhomogeneity-driven combustion instability. *Proceedings of the Combustion Institute*, ***28***, 721–730.

Haworth, D. C., Blint, R. J., Cuenot, B., & Poinsot, T. J. (2000). Numerical simulation of turbulent propane–air combustion with nonhomogeneous reactants. *Combustion and Flame*, ***121***, 395–417.

Hellier, P. R. (2013, March). The Molecular Structure of Future Fuels. University College London.

Hemchandra, S. (2012). Premixed flame response to equivalence ratio fluctuations: Comparison between reduced order modeling and detailed computations. *Combustion and Flame*, ***159***, 3530–3543.

Hong, S., Speth, R. L., Shanbhogue, S. J., & Ghoniem, A. F. (2013). Examining flow-flame interaction and the characteristic stretch rate in vortex-driven combustion dynamics using PIV and numerical simulation. *Combustion and Flame*, ***160***, 1381–1397.

Ikeda, Y., Kojima, T., Nakajima, T., Akamatsu, F., & Katsuki, M. (2000). Measurement of the local flamefront structure of Turbulent premixed flames by local chemiluminescence. *Proceedings of the Combustion Institute*, ***28***, 343–350.

Ilbas, M., Yilmaz, I., & Kaplan, Y. (2005). Investigations of hydrogen and hydrogen–hydrocarbon composite fuel combustion and NOx emission characteristics in a model combustor. *International Journal of Hydrogen Energy*, ***30***, 1139–1147.

Ingard, U., & Singhal, V. K. (1975). Effect of flow on the acoustic resonances of an openended duct. *Journal of the Acoustical Society of America*, ***58***, 788–793.

Jackson, G. S., Sai, R., Plaia, J. M., Boggs, C. M., & Kiger, K. T. (2003). Influence of H2 on the response of lean premixed CH4 flames to high strained flows. *Combustion and Flame*, ***132***, 503–511.

Kang, T., & Kyritsis, D. C. (2009). Phenomenology of methane flame propagation into compositionally stratified, gradually richer mixtures. *Proceedings of the Combustion Institute*, ***32***, 979–985.

Kariuki, J., Dawson, J. R. & Mastorakos, E. (2012). Measurements in turbulent premixed bluff body flames close to blow-off. *Combustion and Flame,* **159**, 2589–2607.

Kee, R. J., Miller, J. A., Evans, G. H., & Dixon-Lewis, G. (1988). A computational model of the structure and extinction of strained, opposed flow, premixed methane-air flames. In *Twenty-Second Symposium (International) on Combustion / The Combustion Institute* (pp. 1479–1494).

Keller, J. O., Bramlette, T. T., Barr, P. K., & Alvarez, J. R. (1994). NOx and CO emissions from a pulse combustor operating in a lean premixed mode. *Combustion and Flame*, ***99***, 460–466.

Keller, J. O., Vaneveld, L., Korschelt, D., Hubbard, G. L., Ghoniem, J. A. F., Daily, J. W., & Oppenheim, A. K. (1981). Mechanism of instabilities in turbulent combustion leading to flashback. *American Institute of Aeronautics and Astronautics*, ***20***, 254–262.

Kim, H. S., Arghode, V. K., & Gupta, A. K. (2009). Flame characteristics of hydrogen-enriched methane–air premixed swirling flames. *International Journal of Hydrogen Energy*, ***34***, 1063–1073.

Kim, H. S., Arghode, V. K., Linck, M. B., & Gupta, A. K. (2009). Hydrogen addition effects in a confined swirl-stabilized methane-air flame. *International Journal of Hydrogen Energy*, ***34***, 1054–1062.

Kim, K. T., & Hochgreb, S. (2011). The nonlinear heat release response of stratified lean-premixed flames to acoustic velocity oscillations. *Combustion and Flame*, ***158***, 2482–2499.

Kim, K. T., Lee, J. G., Quay, B. D., & Santavicca, D. A. (2010). Response of partially premixed flames to acoustic velocity and equivalence ratio perturbations. *Combustion and Flame*, ***157***, 1731–1744.

Krishnamachari, S. L. N. G., & Broida, H. P. (1961). Effect of Molecular Oxygen on the Emission Spectra of Atomic OxygenAcetylene Flames. *Journal of Chemical Physics*, ***34***, 1709–1711.

Kulatilaka, W. D., Frank, J. H., & Settersten, T. B. (2009). Interference-free two-photon LIF imaging of atomic hydrogen in flames using picosecond excitation. *Proceedings of the Combustion Institute*, ***32***, 955–962.

Kulatilaka, W. D., Patterson, B. D., Frank, J. H., & Settersten, T. B. (2008). Comparison of nanosecond and picosecond excitation for interference-free two-photon laser-induced fluorescence detection of atomic hydrogen in flames. *Applied Optics*, ***47***, 4672–4683.

Kulsheimer, C., & Buchner, H. (2002). Combustion dynamics of turbulent swirling flames. *Combustion and Flame*, ***131***, 70–84.

Kwon, S., Wu, M. S., Driscoll, J. F., & Faeth, G. M. (1992). Flame surface properties of premixed flames in isotropic turbulence: measurements and numerical simulations. *Combustion and Flame*, ***88***, 221–238.

Langhorne, P. J. (1988). Reheat buzz : An acoustically coupled combustion instability. Part 1. Experiment. *Journal of Fluid Mechanics*, ***193***, 417–443.

Lauer, M., & Sattelmayer, T. (2008). Heat release calculation in a turbulent swirl flame from laser and chemiluminescence measurements. In *14th International Symposium on Applications of Laser Techniques to Fluid Mechanics*.

Lauer, M. & Sattelmayer, T. (2010). On the adequacy of chemiluminescence as a measure for heat release in turbulent flames with mixture gradients. *Journal of Engineering for Gas Turbines and Power*, ***132-8***.

Law, C. K. (2006). Combustion Physics. Cambridge University Press.

Lawn, C. J. (2000). Distributions of instantaneous heat release by the cross-correlation of chemiluminescent emissions. *Combustion and Flame*, ***123***, 227–240.

Lee, H. J. (2009, August). Combustion instability mechanisms in a lean premixed gas turbine combustor. Pennsylvania State University.

Lee, J. G., Kim, K., & Santavicca, D. A. (2000). Measurement of equivalence ratio fluctuation and its effect on heat release during unstable combustion. *Proceedings of the Combustion Institute*, ***28***, 415–421.

Lee, U. D., Oh, K. C., Shin, H. D., & Lee, K. H. (2005). Time-dependent measurements of flame temperature and the OH radical in the unsteady extinction of non-premixed flames. *Combustion and Flame*, ***141***, 186–190.

Li, Z. S., Li, B., Sun, X. S. Z.W.and Bai, & Aldén, M. (2010). Turbulence and combustion interaction: High resolution local flame front structure visualization using simultaneous single-shot PLIF imaging of CH, OH, and CH2O in a piloted premixed jet flame. *Combustion and Flame*, ***157***, 1087–1096.

Lieuwen, T. C. (1999). Investigation of combustion instability mechanisms in premixed gas turbines. Georgia Institute of Technology.

Lieuwen, T., & Neumeier, Y. (2002). Nonlinear pressure-heat release transfer function measurements in a premixed combustor. *Proceedings of the Combustion Institute*, ***29***, 99–105.

Lieuwen, T., Neumeier, Y., & Zinn, B. T. (1998). The role of unmixedness and chemical kinetics in driving combustion instabilities in lean premixed combustors. *Combustion Science and Technology*, ***135***, 193–211.

Lieuwen, T., & Zinn, B. T. (1998). The role of equivalence ratio oscillations in driving combustion instabilities in low NOx gas turbines. In *Twenty-Seventh Symposium (International) on Combustion / The Combustion Institute* (pp. 1809–1816).

Lu, F. K. (2005). Combustion Instabilities in Gas Turbine Engines: Operational Experience, Fundamental Mechanisms, and Modeling, Progress in Astronautics and Aeronautics. (T. C. Lieuwen & V. Yang, Eds.). American Institute of Aeronautics and Astronautics, Inc.

Lucht, J. T. R. P. Salmon, King, G. B., Sweeney, D. W., & Laurendeau, M. (1983). Two-photon-excited fluorescence measurement of hydrogen atoms in flames. *Optics Letters*, ***8***, 365–367.

Mandilas, C., Ormsby, M. P., Sheppard, C. G. W., & Woolley, R. (2007). Effects of hydrogen addition on laminar and turbulent premixed methane and iso-octane–air flames. *Proceedings of the Combustion Institute*, ***31***, 1443–1450.

Mansour, M. S., Chen, Y., & Peters, N. (1999). Highly strained turbulent rich methane flames stabilized by hot combustion products. *Combustion and Flame*, ***116***, 136–153.

Mantel, T., & Samaniego, J. M. (1999). Fundamental mechanisms in premixed turbulent flame propagation via vortex–flame interactions. Part II: Numerical simulation. *Combustion and Flame*, ***118***, 557–582.

Mardani, A., & Tabejamaat, S. (2010). Effect of hydrogen on hydrogen-methane turbulent non-premixed flame under mild condition. *International Journal of Hydrogen Energy*, ***35***, 11324–11331.

Marzouk, Y. M., Ghoniem, A. F., & Najm, H. N. (2000). Dynamic response of strained premixed flames to equivalence ratio gradients. *Proceedings of the Combustion Institute*, ***28***, 1859–1866.

McManus, K. R., Poinsot, T., & Candel, S. M. (1993). A review of active control of combustion instabilities. *Progress in Energy and Combustion Science*, ***19***, 1–29.

Mueller, C. J., Driscoll, J. F., Sutkus, D. J., Roberts, W. L., Drake, M. C., & Smooke, M. D. (1995). Effect of unsteady stretch rate on oh chemistry during a flame-vortex interaction: To assess flamelet models. *Combustion and Flame*, ***100***, 323–331.

Mugridge, B. D. (1980). Combustion driven oscillations. *Journal of Sound and Vibration*, ***70***, 437–452.

Nair, S., & Lieuwen, T. (2003). Acoustic detection of imminent blowout in pilot and swirl stabilized combustors. In *Proceedings of ASME/IGTI Turbo Expo*.

Najm, H. N., Paul, P. H., Mueller, C. J., & Wyckoff, P. S. (1998). On the adequacy of certain experimental observables as measurements of flame burning rate. *Combustion and Flame*, ***113***, 312–332.

Najm, H. N., & Wyckoff, P. S. (1997). Premixed flame response to unsteady strain rate and curvature. *Combustion and Flame*, ***110***, 92–112.

Namer, I., & Schefer, R. W. (1985). Error estimates for Rayleigh scattering density and temperature measurements in premixed flames. *Experiments in Fluids*, ***3***, 1–9.

Nguyen, Q., & Paul, P. H. (1996). The time evolution of a vortex-flame interaction observed via planar imaging of CH and OH. In *Twenty-Sixth Symposium (International) on Combustion / The Combustion Institute* (pp. 357–364).

Nicolle, A., & Dagaut, P. (2006). Occurrence of NO-reburning in MILD combustion evidenced via chemical kinetic modeling. *Fuel*, ***85***, 2469-2478.

Nogenmyr, K.-J., Petersson, P., Bai, X. S., Fureby, C., Collin, R., Lantz, A., Alden, M. (2011). Structure and stabilization mechanism of a stratified premixed low swirl flame. *Proceedings of the Combustion Institute*, ***33***, 1567–1574.

Nori, V. N., & Seitzman, J. M. (2007). Chemiluminescence measurements and modeling in syngas, methane and jet-a fueled combustors. In *45th AIAA Aerospace Sciences Meeting and Exhibit*.

Nori, V. N., & Seitzman, J. M. (2008). Evaluation of chemiluminescence as a combustion diagnostic under varying operating conditions. In *46th AIAA Aerospace Sciences Meeting and Exhibit*.

Otsu, N. (1979). A threshold selection method from gray-level histograms. *IEEE Transactions on Systems, Man, and Cybernetics, **9**,* 62–66.

Pasquier, N., Lecordier, B., Trinite, M., & Cessou, A. (2007). An experimental investigation of flame propagation through a turbulent stratified mixture. *Proceedings of the Combustion Institute*, ***31***, 1567–1574.

Poinsot, T., Trouve, A. C., Veynante, D. P., Candel, S., & Esposito, E. J. (1987). Vortex-driven acoustically coupled combustion instabilities. *Journal of Fluid Mechanics*, ***177***, 265–292.

Porter, R. P., Clark, A. H., Kaskan, W. E., & Browne, W. E. (1967). A study of hydrocarbon flames. In *Eleventh Symposium (International) on Combustion / The Combustion Institute* (pp. 907–907).

Price, R. B., Hurle, I. R., & Sugden, T. M. (1969). Optical studies of the generation of noise in turbulent flames. In *Twelfth Symposium (International) on Combustion / The Combustion Institute* (pp. 1093–1102).

Przemieniecki, J. S., & Oates, G. C. (Eds.). (1985). Aerothermodynamics of Aircraft Engine Components. American Institute of Aeronautics and Astronautics, Inc.

Putnam, A. (Ed.). (1971). Combustion driven ocsillations in industry. American Elsevier Publishers.

Putnam, A. A., & Dennis, W. R. (1953). Organ-pipe oscillations in a flame-filled tube. In *Fourth Symposium (International) on Combustion / The Combustion Institute* (pp. 566–574).

Raezer, S. D., & Olsen, H. L. (1962). Measurement of laminar flame speeds of ethylene-air and propane-air mixtures by the double kernel method. *Combustion and Flame*, ***6***, 227–232.

Ratner, A., Pun, W., Palm, S., & Culick, F. (2002). Comparison of chemiluminescence, or plif, and no plif for determination of flame response to acoustic waves. In *California Institute of Technology*.

Ravi, S., Sikes, T. G., Morones, A., Keesee, C. L. & Petersen, E. L. (2014) Comparative study on the laminar flame speed enhancement of methane with ethane and ethylene addition. *Proceedings of the Combustion Institute,* Article In Press.

Rayleigh, B., & Strutt, J. W. (1896). Theory of Sound, Volume II. MacMillan and Co., Ltd.

Renard, P. H., Thevenin, D., Rolon, J. C., & Candel, S. (2000). Dynamics of flame/vortex interactions. *Progress in Energy and Combustion Science*, ***26***, 225–282.

Robin, V., Mura, A., Champion, M., Degardin, O., Renou, B., & Boukhalfa, M. (2008). Experimental and numerical analysis of stratified turbulent V-shaped flames. *Combustion and Flame*, ***153***, 288–315.

Rogers, D. E., & Marble, F. E. (1956). A mechanism for high-frequency oscillation in ramjet combustors and afterburners. *Jet Propulsion*, ***26***, 456–462.

Samaniego, J.-M., & Mantel, T. (1999). Fundamental mechanisms in premixed turbulent flame propagation via flame–vortex interactions. Part I: Experiment. *Combustion and Flame*, ***118***, 537–556.

Sankar, S. V., Jagoda, J. I., & Zinn, B. T. (1990). Oscillatory velocity response of premixed flat flames stabilized in axial acoustic fields. *Combustion and Flame*, ***80***, 371–384.

Sattinger, S. S., Neumeier, Y., Nabi, A., Zinn, B. T., Amos, D. J., & Darling, D. D. (2000). Sub-scale demonstration of the active feedback control of gas-turbine combustion instabilities. *Transactions of the ASME*, ***122***, 262–268.

Schadow, K. C., & Gutmark, E. (1992). Combustion instability related to vortex shedding in dump combustors and their passive control. *Progress in Energy and Combustion Science*, ***18***, 117–132.

Schefer, R. W., Wicksall, D. M., & Agrawal, A. K. (2002). Combustion of hydrogen-enriched methane in a lean premixed swirl-stabilized burner. *Proceedings of the Combustion Institute*, ***29***, 843–851.

Schimmer, H., & Vortmeter, D. (1977). Acoustical oscillation in a combustion system with a flat flame. *Combustion and Flame*, ***28***, 17–24.

Schlegel, A., Benz, P., Griffin, T., Weisenstein, W., & Bockhorn, H. (1996). Catalytic stabilization of lean premixed combustion: Method for improving NOx emissions. *Combustion and Flame*, ***105***, 332–340.

Schrödinger, C., Paschereit, C. O., & Oevermann, M. (2012). Numerical studies on the impact of equivalence ratio oscillations on lean premixed flame characteristics and emissions. In *Seventh International Conference on Computational Fluid Dynamics*.

Schuller, T., Durox, D., & Candel, S. (2002). Dynamics of and noise radiated by a perturbed impinging premixed jet flame. *Combustion and Flame*, ***128***, 88–110.

Selle, L., Poinsot, T., & Ferret, B. (2011). Experimental and numerical study of the accuracy of flame-speed measurements for methane/air combustion in a slot burner. *Combustion and Flame*, ***158***, 146–154.

Seybert, A. F., & Ross, D. F. (1976). Experimental determination of acoustic properties using a two-microphone random-excitation technique. *Journal of the Acoustical Society of America*, ***61***, 1362–1370.

Sivasegaram, S., & Whitelaw, J. H. (1991). The influence of swirl on oscillations in ducted premixed flames. *Combustion and Flame*, ***85***, 195–205.

Smith, K. O., Angello, L. C., & Kurzynske, F. R. (1986). Design and testing of an ultra-low NOx gas turbine combustor. *American Society of Mechanical Engineers*, *86-GT-263*.

Swaminathan, N., & Bray, K. N. C. (Eds.). (2011). Turbulent Premixed Flames. Cambridge University Press.

Tang, C. L., Huang, Z. H., & Law, C. K. (2011). Determination, correlation, and mechanistic interpretation of effects of hydrogen addition on laminar flame speeds of hydrocarbon–air mixtures. *Proceedings of the Combustion Institute*, ***33***, 921–928.

Tran, N., Ducruix, & Schuller, T. (2009). Damping combustion instabilities with perforates at the premixer inlet of a swirled burner. *Proceedings of the Combustion Institute*, ***32***, 2917–2924.

Turns, S. R. (2006). An Introduction to Combustion: Concepts and Applications, Second Edition. McGraw-Hill International Editions.

Wang, J., Huang, C. Z. Tang, Miao, H., & Wang, X. (2009). Numerical study of the effect of hydrogen addition on methane–air mixtures combustion. *International Journal of Hydrogen Energy*, ***34***, 1084–1096.

Wicksall, D. M., & Agrawal, A. K. (2007). Acoustics measurements in a lean premixed combustor operated on hydrogen/hydrocarbon fuel mixtures. *International Journal of Hydrogen Energy*, ***32***, 1103–1112.

Wu, X., Wang, M., & Moin, P. (2001). Combustion instability due to the nonlinear interaction between sound and flame. In *Annual Research Briefs, Center for Turbulence Research*.

Yoo, C. S., Chen, J. H., & Frank, J. H. (2009). A numerical study of transient ignition and flame characteristics of diluted hydrogen versus heated air in counterflow. *Combustion and Flame*, ***156***, 140–151.

Yu, G., Law, C. K., & Wu, C. K. (1986). Laminar flame speeds of hydrocarbon + air mixtures with hydrogen addition. *Combustion and Flame*, ***63***, 339–347.

Yu, K. H., Trouve, A., & Daily, J. W. (1991). Low-frequency pressure oscillations in a model ramjet combustor. *Journal of Fluid Mechanics*, ***232***, 47–72.

Zhang, Q., Shanbhogue, S. J., Shreekrishna, Lieuwen, T., & O'Conner, J. (2011). Strain characteristics near the flame attachment point in a swirling flow. *Combustion Science and Technology*, ***183***, 665–685.